



HAL
open science

Eu³⁺ ion environment modification by Electron and femtosecond laser irradiation in metaphosphate and polyphosphate glasses

Mohamed Mahfoudhi

► **To cite this version:**

Mohamed Mahfoudhi. Eu³⁺ ion environment modification by Electron and femtosecond laser irradiation in metaphosphate and polyphosphate glasses. Physics [physics]. Université Paris Saclay (COmUE), 2019. English. NNT: 2019SACLX066 . tel-03227516

HAL Id: tel-03227516

<https://theses.hal.science/tel-03227516>

Submitted on 17 May 2021

HAL is a multi-disciplinary open access archive for the deposit and dissemination of scientific research documents, whether they are published or not. The documents may come from teaching and research institutions in France or abroad, or from public or private research centers.

L'archive ouverte pluridisciplinaire **HAL**, est destinée au dépôt et à la diffusion de documents scientifiques de niveau recherche, publiés ou non, émanant des établissements d'enseignement et de recherche français ou étrangers, des laboratoires publics ou privés.



Eu³⁺ ion environment modification by Electron and femtosecond laser irradiation in metaphosphate and polyphosphate glasses

Thèse de doctorat de l'Université Paris-Saclay
préparée à Ecole Polytechnique

École doctorale n°573 : interfaces : approches interdisciplinaires,
fondements, applications et innovations (Interfaces)
Spécialité de doctorat: Physique

Thèse présentée et soutenue à Palaiseau, le 30 septembre 2019, par

Mohamed Mahfoudhi

Composition du Jury :

Gacoin Thierry Professor, École Polytechnique (UMR 7643)	Président
Grégorit Tricot Doctor, Université de Lille (UMR 8516)	Rapporteur
Mohamed Bouazaoui Professor, Université de Lille (UMR 8523)	Rapporteur
Yannick Petit Doctor, ICMCB Bordeaux (UMR 5026)	Examineur
Gavin Mountjoy Doctor, University of Kent (UK)	Examineur
Ollier Nadège Doctor, Ecole Polytechnique (UMR 7642)	Directeur de thèse
Mathieu Lancry Doctor, Université Paris-Sud (UMR 8182)	Invité

Résumé :

Les verres phosphates dopés terres rares (TR) sont des matériaux attractifs en optique en raison de leur basse température de transition vitreuse et de leur grande capacité à dissoudre les ions de terres rares par rapport aux verres silicates. Dans ce travail, nous sommes intéressés à comprendre les mécanismes conduisant aux modifications structurales des verres polyphosphates de zinc et métaphosphates sous différents types d'irradiations afin d'étudier et de contrôler l'environnement des ions dopants RE (ions Eu^{3+} en particulier) et les propriétés de luminescence qui en résultent. Des électrons de 700 KeV et 2.5 MeV (Accélérateur SIRIUS, Laboratoire des Solides Irradiés LSI) ont été utilisés ainsi que des impulsions laser femto seconde (Institut de Chimie Moléculaire et des Matériaux d'Orsay ICCMO) (1030 nm, 250fs, 0.1-5 μJ / impulsion, focalisation 0.6 NA) à faible taux de répétition (10 KHz) et un taux de répétition élevé (500 KHz) conduisant à une accumulation de chaleur dans le dernier cas. Les compositions de verres concernent le mélange de différents ions alcalins et alcalino-terreux (Na, Li, K et Mg), teneurs en Zn ainsi que différents degrés de polymérisation des verres de phosphate.

Après des irradiations électroniques de 2.5 MeV et 700 keV, les spectres Raman ne traduisent aucune évolution significative du réseau vitreux des verres metaphosphates de Na quel que soit la dose alors qu'il existe une légère variation du réseau vitreux dans les verres metaphosphates de Na-Li, Na-Mg et Zn. Cependant, les verres polyphosphates subissent une variation significative de la structure après l'irradiation et la rupture de liaison se produit à forte dose (à partir de 10^8 Gy) avec la création massive des unités du terminal Q^1 . De plus et sous irradiation de 700 keV, la structure semble être modifiés dans un volume plus grand que la profondeur de pénétration des électrons.

En examinant l'environnement local des ions Eu^{3+} , nous avons montré une augmentation importante du rapport d'asymétrie (As) indiquant une diminution significative de la symétrie du site de l' Eu^{3+} où une covalence Eu-O plus élevée. Cet effet est fort dans les verres métaphosphates alcalins alors que la variation du rapport d'asymétrie est moins prononcée dans les verres de phosphate contenant du ZnO, ce qui signifie que la variation locale de la symétrie Eu^{3+} est décorrélée de la variation du réseau vitreux sous irradiation électronique.

La spectroscopie EPR et PL montre la présence de deux types de sites pour les ions divalents Eu^{2+} formés dans des verres métaphosphate et polyphosphates quelles que soient la dose et l'énergie

électronique. Nous avons mis en évidence que la présence de Zn favorise la formation du site de haute symétrie avec une augmentation quasi-linéaire des deux sites avec des doses croissantes. En revanche, une énergie de 700 keV est beaucoup plus efficace pour réduire les ions Eu^{3+} qu'une énergie de 2.5 MeV et la génération d'ions Eu^{2+} est plus importante dans les verres polyphosphates que dans les compositions de métaphosphates.

Concernant les modifications structurales sous irradiation laser femtoseconde avec un faible taux de répétition de 10 kHz, des signes de cristallisation au centre des traces transversales du laser dans des verres métaphosphate de Na et Zn ont été observés quelle que soit l'énergie d'impulsion dans la gamme $1\mu\text{J}$ - $4\mu\text{J}$. A noter que le dopage Eu est nécessaire pour la cristallisation du verre. En revanche, les verres polyphosphates de zinc présentent une évolution structurale similaire à celle observée sous irradiation électronique.

La variation de la symétrie du site de l' Eu^{3+} après l'écriture laser fs dans les verres se comporte différemment de celles rapportées sous irradiation électronique. Ainsi, la diminution de la valeur du rapport d'asymétrie As au centre de la trace laser transversale dans Meta-Na-Eu est en accord avec la tendance de ce verre à cristalliser. Cependant, pour le verre Poly-Zn-Na-Eu, le rapport As souffre d'une légère augmentation identique aux effets d'irradiation électronique. Contrairement à l'irradiation électronique, il n'y a pas de formation d'euporium divalent dans les différents verres de phosphate sous écriture par laser fs.

À partir de ces travaux, nous pouvons dire qu'il est possible de gérer l'environnement de l'euporium dans des verres de phosphate sous irradiation électronique et laser femtoseconde en jouant sur la composition du verre ainsi que sur les conditions d'irradiation comme l'énergie, la dose, la vitesse de balayage et le taux de répétition. En plus, des calculs de dynamique moléculaire sont faites dans ce projet pour mieux comprendre l'évolution de l'environnement local des TR dans les verres phosphates sous irradiation.

Acknowledgements

This thesis would have been incomplete without the support of others.

I would like to express my sincere gratitude to Dr. Nadège Ollier for her valuable supervision and continuous support throughout the development of this research. Her guidance helped me in all the time of research and writing of this thesis.

I would like to thank Dr. Gavin Mountjoy from Kent University and Dr. Matthieu Lancry from Orsay University for their support and their contribution in this work.

I am also grateful to the members of Laboratoire des Solides Irradiés (LSI) in particular Olivier Cavani for their support in overcoming numerous obstacles.

My thanks go to Pr. Ludovic Bellot-Gurlet, Dr. Mélanie Poggie and Dr. Sébastien Marron for their help throughout the experimental part of this study.

I would like to thank all the members of the jury.

I would like to thank my colleagues and friends: Quang, Imen, Uliana, Simone, Pierfrancesco, Karim, Carolina, Rashmi, Seonyoung, Ozlem, Huong... These years of research would have not been the same without their friendship and support.

I am grateful to my parents Salwa and Mokhtar, my siblings Amal, Yathreb and Rahma who have provided me through moral and emotional support in my life no matter how far they are.

I am also grateful to my girlfriend Chaima and my best friend Oussema for their constant mental support.

I would like to thank my other family members and friends who have supported me along the way.

Table of contents

Introduction	11
Chapter 1 Experimental methods	17
1 Photoluminescence spectroscopy	18
1.1 Eu ³⁺ ion spectroscopy	18
1.2 Experimental set up of PL in LSI	19
2 Raman spectroscopy	20
2.1 Quantum theory	21
2.2 Classical theory	22
2.3 Experimental set up	22
3 EPR spectroscopy	23
3.1 Zeeman effect	23
3.2 Experimental set up	25
Chapter 2 Phosphate glasses: elaboration, properties and structure	30
1 Glass samples	31
1.1 Glass composition	31
1.2 Glass synthesis	32
2 Glass structure bibliography	32
2.1 Mixed Alkali effect in phosphate glasses	33
2.2 Zinc containing glasses	34
3 Glass structure by NMR and Raman spectroscopy	36
3.1 Non-doped Metaphosphate glasses	36
3.1.1 Raman spectroscopy	36
3.1.2 NMR spectroscopy	38
3.2 Non-doped polyphosphate glasses	39
3.2.1 Raman spectroscopy	39
3.2.2 NMR spectroscopy	41
3.3 Eu-doped metaphosphate glasses	44
3.4 Eu-doped polyphosphate glasses	45
4 Glass transition temperature	48
4.1 Differential thermal analysis technique DTA	48
4.2 Results and discussion	49
4.2.1 Na vs Mg-Na in metaphosphate glass	50
4.2.2 Rare earth effect	51
5 Density	51

Chapter 3 Molecular dynamics modelling of europium doped and non-doped metaphosphate and polyphosphate glasses	58
1 Rare earth environment in phosphate glasses.....	59
2 Molecular Dynamics method	60
2.1 Molecular Dynamics simulation details	60
2.2 Analysis techniques	62
2.2.1 Partial Pair Distribution Functions.....	62
2.2.2 Accumulated coordination numbers.....	63
2.2.3 Partial and total structure factors	64
3 Molecular dynamic modeling of metaphosphate glasses with medium model (~ 2500 atoms) .	64
3.1 Molecular dynamic modeling of non-doped metaphosphate glasses	64
3.1.1 Image of models: Meta-Na vs Meta-Zn.....	65
3.1.2 Diffraction structure factor	65
3.1.3 Pair distribution function and coordination number	67
3.1.4 M-O correlations	71
3.2 Europium doped metaphosphate glasses.....	73
3.2.1 Image of models: Non-doped and Eu doped glass.....	74
3.2.2 Structure factors.....	75
3.2.3 Pair Distribution Functions and coordination number.....	76
4 Polyphosphate glasses with medium model (~ 2500 atoms).....	80
4.1 Images of models	80
4.2 Diffraction structure factors.....	81
4.3 Pair Distribution Functions and coordination number.....	81
5 Phosphate glasses with big model (~ 25000 atoms)	88
5.1 Images of models	89
5.2 Structure factors.....	91
5.3 Pair distribution function and coordination number	92
Chapter 4 Study of phosphate glasses under electron irradiation	111
1 Electron irradiation conditions (SIRIUS Accelerator).....	112
2 Phosphate glass structure under electron irradiation	114
2.1 Bibliography part (Glass network evolution under irradiation)	114
2.1.1 Generality on glass evolution under irradiation.....	114
2.1.2 Phosphate glasses	115
2.2 Metaphosphate glass structure under 2.5 MeV irradiation.....	116
2.2.1 Alkali and mixed-alkali metaphosphate glasses.....	116
2.2.2 Zinc metaphosphate glasses under irradiation	117

2.3	Polyphosphate glass structure under 2.5 MeV irradiation	119
2.4	Glass structure evolution under 700 keV electron irradiation.....	121
3	Eu ³⁺ ion environment evolution under electron irradiation	125
3.1	Asymmetry Ratio in pristine glasses.....	125
3.2	Asymmetry ratio evolution under 2.5 MeV irradiation.....	126
3.2.1	Energy and dose effect (700 keV vs 2.5 MeV).....	130
3.2.2	Influence of the alkaline ion type.....	132
3.3	⁵ D ₀ → ⁷ F ₀ transition under 2.5 MeV irradiation:	134
3.3.1	Energy shift.....	135
3.3.2	Broadening of the ⁵ D ₀ → ⁷ F ₀ emission band.....	135
3.3.3	Electron energy Effect (700 keV vs 2.5 MeV)	136
3.4	⁵ D ₀ Energy level lifetime	139
4	Eu ³⁺ ion reduction into Eu ²⁺ under electron irradiation	141
4.1	PL spectroscopy analysis	141
4.2	EPR spectroscopy analysis.....	144
4.3	Energy effect: 2.5 MeV vs 700 keV.....	149
Chapter 5: Study of phosphate glasses under IR femtosecond laser irradiation.....		161
1	Experimental methods	162
2	Glass modifications induced by fs-laser (bibliographic part)	164
2.1	Interaction of femtosecond laser pulses with glass materials	164
2.1.1	Photoionization processes	165
2.1.2	Energy relaxation processes.....	165
2.2	Generality on silica:	166
3	Phosphate glass structure under fs laser irradiation at low repetition rate (10 kHz).....	169
3.1	Alkali Metaphosphate glasses	169
3.1.1	Eu-doped Na metaphosphate glass.....	169
3.1.2	Non-doped and Er doped Na metaphosphate glasses:.....	175
3.2	Eu doped zinc metaphosphate glasses	176
3.3	Polyphosphate glasses.....	179
3.3.1	Eu-doped Zinc sodium polyphosphate glass (Poly-Na-Eu-4μJ)	179
3.3.2	Non-doped and Er-doped zinc sodium polyphosphate glasses:	182
4	Phosphate glass structure under fs laser irradiation at high repetition rate (500 kHz).....	183
5	Refractive index changes and optical birefringence at low repetition rate.....	185
5.1	Birefringence:	185
5.2	Refractive index changes.....	185
5.2.1	Generality:	186

5.2.2	Study of refractive index kinetics in Metaphosphate glasses	188
5.2.3	Study of refractive index kinetics in Zinc Polyphosphate glasses:	189
5.2.4	Correlation between defect centers and refractive index changes	191
6	Rare earth environment under fs laser irradiation at low repetition rate.....	194
6.1	Rare earth environment under fs laser irradiation (Bibliographic part)	194
6.2	Photo-Emission micro-spectroscopy:.....	195
6.2.1	Metaphosphate glasses (Meta-Na-Eu and Meta-Zn-Eu).....	195
6.2.2	Polyphosphate glasses (Poly-Zn-Na-Eu)	196
6.3	Asymmetry ratio between $^5D_0-^7F_2$ and $^5D_0-^7F_1$	197
6.4	$^5D_0-^7F_0$ transition:.....	198
6.5	Divalent europium:.....	200
Conclusions and Perspectives		210
Appendix.....		215

Introduction

Phosphate glasses are known as suitable matrix to incorporate large amounts of Rare Earth (RE) and limiting clustering effect contrary to silica. In addition, when compared to silicate glasses, vitreous phosphate materials exhibit relatively high refractive index as well as low glass transition temperature (lower than 450°C). As well, subsequent interest in alkali phosphate glasses stemmed from their high transparency for ultraviolet (UV) light. As a consequence, phosphate glasses are developed for a variety of special applications in the domain of optics, data storage, biomedicine and energy [1–8].

In optics, the RE-doped glasses are potential hosts for amplifiers and laser systems and the spectroscopic properties of the RE ions are strongly affected by their local environment [9,10]. Accurately, the RE properties are defined by the nature and arrangements of the ligands around the rare earth ions which determine the field strength and symmetry. The understanding of the relationship between the structure of host glass and properties of the doping ion is detrimental for the design of materials for definite applications [10].

One way to control the RE environment could be the use of irradiation. In particular, the exposition of RE doped glasses [11–17] to high energy radiation (X-rays, gamma, electron, neutrons and femtosecond laser...) produce various interesting change in their properties which include magnetic, electrical, chemical as well as optical properties. However, they are really dependent on the type of glass matrix and irradiation conditions. In addition, studying the RE environment modification under irradiation in phosphate glasses can be attractive in different fields like nuclear industry (immobilization of high level radioactive waste) where the glass is submitted to internal radiation or in optics or for board space crafts and satellites (containing optical fibers) [11].

In the case of europium ions, many recent works [18–21] show the interest of Eu- doped glasses (aluminosilicate, fluoro-aluminoborate, tellurite, lead phosphate) for phosphors and luminophore applications.

Eu^{2+} is one of the REE used in phosphor materials by emitting light in a broad blue range due to $4f \rightarrow 5d$ transitions, while Eu^{3+} ions exhibit lines narrower in the red range. From the applicative point of view, it can be very attractive to adjust the emission spectra of Eu-doped

phosphors by modifying $\text{Eu}^{2+}/\text{Eu}^{3+}$ relative concentration and site symmetry of each valence state. Different solutions exist to reach this goal: the first one is to produce glasses under reduced atmosphere that mostly affects the $\text{Eu}^{2+}/\text{Eu}^{3+}$ ratio. The second one resides on the use of irradiation [11–13,22].

In addition, the luminescent properties of the Eu^{3+} ions ($4f^6$) used as structural probe have been investigated extensively in many glass systems. Especially, It is possible to obtain information on the local environment via FLN measurements to determine the number of Eu^{3+} sites and via the asymmetry ratio (As) parameter defined as the integrated emission intensity of ${}^5\text{D}_0 \rightarrow {}^7\text{F}_2$ to ${}^5\text{D}_0 \rightarrow {}^7\text{F}_1$. It is a sensitive parameter to characterize the deviation or distortion from centrosymmetric geometry of Eu^{3+} [11-13].

In my thesis work, the central aim is understanding the mechanisms leading to the structural modification of Zn polyphosphate and metaphosphate glasses under electron and femtosecond laser irradiation and to investigate how to control the environment of Eu^{3+} doping ions using irradiation. To reach this goal, we synthesized many glass compositions dealing with different mixing alkaline and alkali-earth ions (Na, Li, K and Mg), different polymerization degree and doped with europium (Eu) and we vary the irradiation conditions (electron energy, laser repetition rate and pulse energy). The glass structure and the RE environment were studied by different experimental techniques: Raman, photoluminescence (PL) and electron paramagnetic resonance (EPR) spectroscopy. In addition, molecular dynamics calculations in unirradiated glasses have been carried out.

The manuscript is divided in to 5 chapters with in addition an introduction, some conclusions and perspectives.

In the first chapter, experimental details including PL, Raman and EPR spectroscopy can be found.

The second part reports the synthesis and chemical compositions of the samples as well as the glass transition temperature and density properties of those glasses. The structure of the different metaphosphate and polyphosphate glasses before irradiation using Raman and NMR spectroscopy are also discussed.

The third chapter concerns the dynamic molecular simulations results. We used two models of 2500 and 25000 atoms to investigate the Eu^{3+} environment and to obtain information about

the interatomic distances, nature of surrounding atoms, coordination numbers and short range structural disorder in the phosphate samples.

The fourth chapter is the main one and concerns the study of the Eu^{3+} environment modification under 2.5 MeV and 700 keV electron irradiation at various doses from 10^5 to over 10^9 Gy. Thus, a first part of this chapter discussed the structural changes of the glass network after irradiation. Then, the main part analyzed the local environment of the Eu^{3+} ion as well as the reduction of Eu^{3+} to Eu^{2+} in phosphate glasses when exposed to high energy electron irradiation.

In chapter five, we analyzed in the first step, the structural modifications in phosphate glasses under femtosecond laser (10 KHz and 500 kHz). Secondly, we discussed respectively the refractive index change and the RE environment modification in metaphosphate and zinc polyphosphate glasses under femtosecond laser writing at a repetition rate of 10 kHz that is a non-cumulative heating regime.

- [1] T.I. Suratwala, R.A. Steele, G.D. Wilke, J.H. Campbell, K. Takeuchi, Effects of OH content, water vapor pressure, and temperature on sub-critical crack growth in phosphate glass, *Journal of Non-Crystalline Solids*. 263 (2000) 213–227.
- [2] J.H. Campbell, T.I. Suratwala, Nd-doped phosphate glasses for high-energy/high-peak-power lasers, *Journal of Non-Crystalline Solids*. 263 (2000) 318–341.
- [3] C. Yamanaka, Y. Kato, Y. Izawa, K. Yoshida, T. Yamanaka, T. Sasaki, M. Nakatsuka, T. Mochizuki, J. Kuroda, S. Nakai, Nd-doped phosphate glass laser systems for laser-fusion research, *IEEE Journal of Quantum Electronics*. 17 (1981) 1639–1649.
- [4] L. Canioni, M. Bellec, A. Royon, B. Bousquet, T. Cardinal, Three-dimensional optical data storage using third-harmonic generation in silver zinc phosphate glass, *Optics Letters*. 33 (2008) 360–362.
- [5] J.C. Knowles, Phosphate based glasses for biomedical applications, *Journal of Materials Chemistry*. 13 (2003) 2395–2401.
- [6] I. Ahmed, M. Lewis, I. Olsen, J.C. Knowles, Phosphate glasses for tissue engineering: Part 1. Processing and characterisation of a ternary-based P₂O₅–CaO–Na₂O glass system, *Biomaterials*. 25 (2004) 491–499.
- [7] B.C. Sales, L.A. Boatner, Lead-iron phosphate glass: a stable storage medium for high-level nuclear waste, *Science*. 226 (1984) 45–48.
- [8] M.I. Ojovan, O.G. Batyukhnova, Glasses for nuclear waste immobilization, *WM*. 7 (2007) 15.
- [9] R. Reisfeld, Radiative and non-radiative transitions of rare-earth ions in glasses, in: *Rare Earths*, Springer, 1975: pp. 123–175.
- [10] H. Ebendorff-Heidepriem, D. Ehrhart, Spectroscopic properties of Eu³⁺ and Tb³⁺ ions for local structure investigations of fluoride phosphate and phosphate glasses, *Journal of Non-Crystalline Solids*. 208 (1996) 205–216.
- [11] H. Ebendorff-Heidepriem, D. Ehrhart, Effect of europium ions on X-ray-induced defect formation in phosphate containing glasses, *Optical Materials*. 19 (2002) 351–363.
- [12] E. Malchukova, B. Boizot, Divalent Europium in β -Irradiated Aluminoborosilicate Glass: Rapid Communications of the American Ceramic Society, *Journal of the American Ceramic Society*. 93 (2010) 4005–4007.
- [13] H. You, M. Nogami, Optical Properties and Valence Change of Europium Ions in a Sol–Gel Al₂O₃–B₂O₃–SiO₂ Glass by Femtosecond Laser Pulses, *The Journal of Physical Chemistry B*. 109 (2005) 13980–13984.
- [14] N. Ollier, R. Planchais, B. Boizot, EPR study of Yb-doped irradiated glasses, *Nuclear Instruments and Methods in Physics Research Section B: Beam Interactions with Materials and Atoms*. 266 (2008) 2854–2858.
- [15] S. Fan, C. Yu, D. He, K. Li, L. Hu, Gamma rays induced defect centers in phosphate glass for radiophotoluminescence dosimeter, *Radiation Measurements*. 46 (2011) 46–50.
- [16] N. Ollier, T. Charpentier, B. Boizot, G. Petite, A structural approach by MAS NMR spectroscopy of mechanisms occurring under β -irradiation in mixed alkali aluminoborosilicate glasses, *Journal of Physics: Condensed Matter*. 16 (2004) 7625–7635.
- [17] J. Qiu, K. Kojima, K. Miura, T. Mitsuyu, K. Hirao, Infrared femtosecond laser pulse-induced permanent reduction of Eu³⁺ to Eu²⁺ in a fluorozirconate glass, *Optics Letters*. 24 (1999) 786.
- [18] M. Sołtys, J. Janek, L. Żur, J. Pisarska, W.A. Pisarski, Compositional-dependent europium-doped lead phosphate glasses and their spectroscopic properties, *Optical Materials*. 40 (2015) 91–96.
- [19] M. Walas, A. Pastwa, T. Lewandowski, A. Synak, I. Gryczyński, W. Sadowski, B. Kościelska, Luminescent properties of Ln³⁺ doped tellurite glasses containing AlF₃, *Optical Materials*. 59 (2016) 70–75.
- [20] N.T. Thanh, V.X. Quang, V.P. Tuyen, N.V. Tam, T. Hayakawa, B.T. Huy, Role of charge transfer state and host matrix in Eu³⁺-doped alkali and earth alkali fluoro-aluminoborate glasses, *Optical Materials*. 34 (2012) 1477–1481.
- [21] H. Bouchouicha, G. Panczer, D. de Ligny, Y. Guyot, R. Ternane, Luminescent properties of Eu-doped calcium aluminosilicate glass-ceramics: A potential tunable luminophore, *Optical Materials*. 85 (2018) 41–47.

- [22] H. Ebendorff, Heidepriem, D. Ehrh, Ultraviolet laser and x-ray induced valence changes and defect formation in europium and terbium doped glasses, *Physics and Chemistry of Glasses Proc. XIX Int. Congr. Glass, Edinburgh*. 43 (2002) 10.

Chapter 1

Experimental methods

Chapter 1 Experimental methods

1	Photoluminescence spectroscopy.....	18
1.1	Eu ³⁺ ion spectroscopy.....	18
1.2	Experimental set up of PL in LSI.....	19
2	Raman spectroscopy.....	20
2.1	Quantum theory.....	21
2.2	Classical theory.....	22
2.3	Experimental set up.....	22
3	EPR spectroscopy.....	23
3.1	Zeeman effect.....	23
3.2	Experimental set up.....	25

1 Photoluminescence spectroscopy

Photoluminescence (PL) corresponds to the emission of light from matter under a photonic excitation (lamp and most of the time laser). A discernible advantage of PL analysis is that it is a simple, non-destructive and versatile technique [1]. Therefore, this technique has been used in our work to investigate the europium environment modification in phosphate glasses under electron and femtosecond laser irradiation.

1.1 Eu^{3+} ion spectroscopy

The electronic configuration of Eu^{3+} ion can be written as $[\text{Xe}] 4f^6$ where 54 electrons are in the same closed shell as the xenon atoms and 6 electrons in the 4f shell. The degeneracy of the $4f^6$ configuration is partly or totally lifted by several perturbation acting on the Eu^{3+} ion: electron repulsion, spin-orbit coupling, the crystal field perturbation and the Zeeman effect (as seen in figure 1) [2].

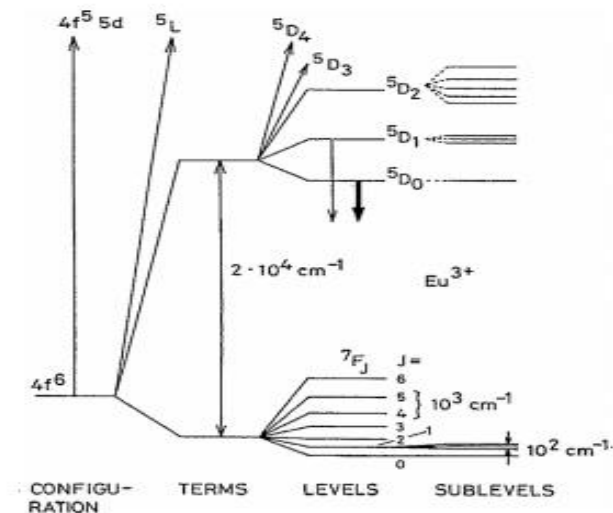


Figure 1 Partial energy diagram of Eu^{3+} ($4f^6$) showing the relative magnitude of the interelectronic repulsion (TERMS), spin-orbit coupling (LEVELS) and crystal-field effects (SUBLEVELS). The downward arrows indicate the excited states $5D_0$ and $5D_1$ from which luminescence occurs [2].

One part of luminescence spectrum of the Eu^{3+} ion is characterized by the transitions $5D_0 \rightarrow 7F_j$ ($j = 0$ to 6) from the $5D_0$ excited state to the J levels of the ground state term $7F_j$. In particular, the most intense emission peak is around 610 nm (electrical dipole transition $5D_0 \rightarrow 7F_2$) that ensuring a red luminescence. The magnetic dipole transition $5D_0 \rightarrow 7F_1$ (590 nm) is independent of the symmetry of the local environment. The selection rules of the different transitions of Eu^{3+} ion are shown in table 1.

Table 1 Overview of the transitions observed in luminescence spectra of europium(III) compounds [2].

Transition ^a	Dipole character ^b	Wavelength range (nm)	Relative intensity ^c	Remarks
⁵ D ₀ → ⁷ F ₀	ED	570–585	vw to s	Only observed in C _n , C _{nv} and C _s symmetry
⁵ D ₀ → ⁷ F ₁	MD	585–600	s	Intensity largely independent of environment
⁵ D ₀ → ⁷ F ₂	ED	610–630	s to vs	Hypersensitive transition; intensity very strongly dependent on environment
⁵ D ₀ → ⁷ F ₃	ED	640–660	vw to w	Forbidden transition
⁵ D ₀ → ⁷ F ₄	ED	680–710	m to s	Intensity dependent on environment, but no hypersensitivity
⁵ D ₀ → ⁷ F ₅	ED	740–770	vw	Forbidden transition
⁵ D ₀ → ⁷ F ₆	ED	810–840	vw to m	Rarely measured and observed

^a Only transitions starting from the ⁵D₀ level are shown.

^b ED = induced magnetic dipole transition, MD = magnetic dipole transition.

^c vw = very weak, w = weak, m = medium, s = strong, vs = very strong.

1.2 Experimental set up of PL in LSI

Time-resolved photoluminescence spectroscopy (TRPL) is a variant to normal spectroscopy in which a pulse laser is used for the excitation, and a fast detector is used to measure the emission of a material as a function of time after the laser excitation (time delay).

The schematic diagram of the experimental setup for PL measurement is shown in figure 1 using a Shamrock SR-303i spectrometer (Lot Oriel) related to an ANDOR Intensified Charge Coupled Device (ICCD) camera. 355 and 532 nm laser excitations (third and second harmonic lines) provided by a pulse Nd:YAG INDI laser (spectra Physics) were used. The energy/pulse of the 532 nm laser on the sample was around 1.5 mJ. Thus, the power of the laser was optimized to detect the signal with the best signal/noise ratio without inducing any photobleaching or defect creation. The 90° luminescence collection is done via an optical fiber.

The 532 nm line has been used to investigate the emission of Eu³⁺ ions under electron irradiation. The emission of Eu²⁺ ions was measured under 355 nm laser excitation with a 200 ns delay and a short gate width of 30 μs were applied in order to enhance the emission of Eu²⁺ towards Eu³⁺ ions having a longer decay time.



Figure 2 Experimental setup for the photoluminescence measurements ($\lambda_{ext} = 266, 355$ and 532 nm (LSI)).

We also used another experimental set up displayed in Figure 3 for continuous micro-photoluminescence. This set up uses a 488 nm-Externally Doubled Diode Lasers (Spectra-Physics Excelsior-488 nm laser) and the detection is performed by a Shamrock LOT Oriol spectrometer coupled to an iDus CCD Andor Camera (figure 3). This set up was used to investigate the Eu^{3+} photoluminescence in the transverse side of the sample irradiated with 700 keV electron.

Note that same set up can be used to measure Raman spectra thanks to the Renishaw inVia Micro-Raman head. The 488 nm laser is injected into the optic fiber and connected to the remote Superhead placed on a very stable motorized stage with XYZ micrometric displacements. We used it to measure the Raman spectra of pristine phosphate samples just after the synthesis to check their amorphous character.

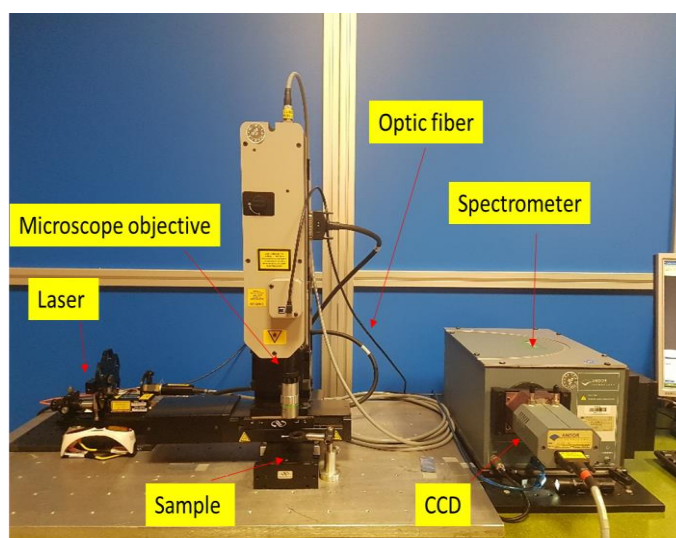


Figure 3 Micro-photoluminescence experiments with 488 nm laser excitation (LSI).

2 Raman spectroscopy

When light travels through any type of medium, there is a fraction of the incident light beam that gives rise to scattered light propagating along all other directions. This scattered light is the result of an induced dipole moment in the molecules by the oscillating electric field of the incident light. In this connection, the Raman effect is one type of light scattering like Rayleigh (elastic scattering), Compton and Brillouin effect. It corresponds to inelastic scattering of monochromatic light usually from a laser discovered by CV Raman and KS Krishnan et al. [3]. This effect had been predicted theoretically by Smekal in 1923 [4].

The inelastic Raman scattering effect can be explained by the quantum mechanical theory based on the consideration of energy level diagrams or by the classical theory where the light-matter interaction is viewed as a perturbation of the molecule's electric field.

2.1 Quantum theory

When light interacts with molecules, most of the photons are scattered without any change of their energy. This process occurs when the electrons in a molecule oscillate in resonance with the applied electric field of the incident light, and it is called Rayleigh or elastic scattering. However, a small number of photons (1 over 10^7) are inelastically scattered and undergoes a change in energy. The relationships between frequency, energy, wave number and the wavelength can be written as follows:

- ✓ $E = h\nu = hc\tilde{\nu}$ (h is Planck's constant, ν is frequency, c is the speed of light, and $\tilde{\nu}$ is wavenumber)
- ✓ $\tilde{\nu} = 1/\lambda$ (λ is wavelength)

The difference between the incident photons energy and inelastically scattered photons energy is called "Raman shift". A plot of the intensity of the inelastically scattered light as a function of the energy change is called Raman spectrum [5]. It is quite common to plot the Raman intensity as a function of the wavenumber (cm^{-1}) expressed as Raman shift.

Figure 3 shows a schematic of the Raman and Rayleigh scattering processes. First case, incident photons lose energy to the molecule, causing it to go to an excited, vibrational state ($m \rightarrow n$). Therefore, scattered photons will have less energy (Stokes) compared to the incident photon. In the second event, the molecules lose energy by going from a higher to lower vibrational state ($m \rightarrow n$). As a result, the incident photons gain energy from the molecule. In this situation, the Raman scattered photon will have higher than the incident photons (anti-Stokes). At room temperature, most molecules are in the vibrational ground state (m), so there is a greater probability that incident photons will lose energy to the molecules during the interaction. Therefore, Raman spectroscopy refers generally to Stokes Raman. Thus, Raman scattering is observed at lower energy or longer wavelength compared to that of the incident laser line [6].

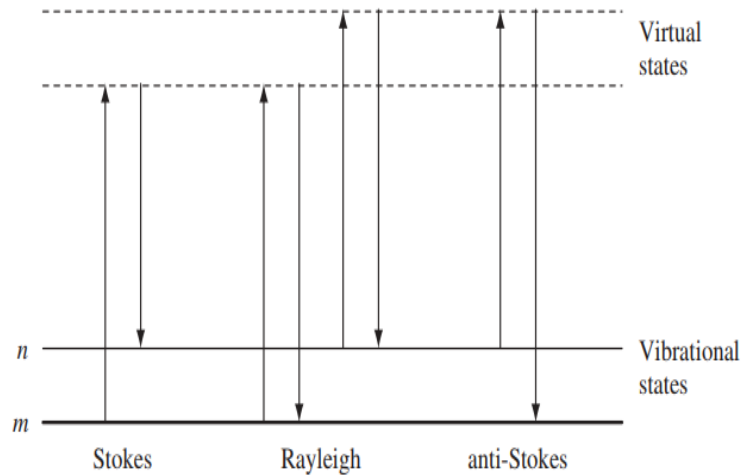


Figure 4 Diagram of Rayleigh and Raman scattering processes.

2.2 Classical theory

According to the classical theory of electromagnetic radiation, the Raman effect is based on molecule's polarizability α variation. The laser excitation can be considered as an oscillating electromagnetic wave with electrical vector E . When a sample is excited by the laser with frequency ν , it induces electric dipole moment P which deforms molecules [7].

Thus,

$$P = \alpha E$$

$$\text{With } E = E_0 \sin(2\pi \nu t)$$

E_0 is the strength of the applied field.

Because of periodical deformation, molecules start vibrating and such oscillating dipoles emit light at three different frequencies: the elastic Rayleigh scattering, the Stokes and the Anti-Stokes.

2.3 Experimental set up

We used two Raman spectrometers:

- Micro-Raman installed in our laboratory (LSI) using 488 nm-Externally Doubled Diode Lasers (Spectra-Physics Excelsior-488 nm laser). The system is described previously. We analyzed with it the structure of the different phosphate glasses irradiated by electron irradiation due to the large irradiated volume and homogeneous samples. However, the home made micro-Raman in LSI is not adapted to measure Raman diffusion when a good spatial resolution is required with a confocal mode (for instance the sample irradiated with the fs laser). Moreover, the 488 nm line was not adapted in some cases because of the emission of Er^{3+} for example. Therefore, we used a specific

micro-Raman (described below) in collaboration with Ludovic Bellot-Gurlet in MONARIS, Sorbonne university (described below) allowing a cartography mode.

- The Micro-Raman is a HR800 LabRam spectrometer (Horiba Jobin-Yvon) coupled to BX Olympus microscope with different long and short working distance objectives and equipped with Ar⁺ ion laser (458 nm laser excitation line used in our case) and Peltier Effect Cooled CCD detector (figure). In this work, a small laser spot obtained with ×100 objective (about 1x1x4 μm³) in a confocal mode and a 1800l/mm grating were used in order to obtain the best spatial resolution for the different modified region by femtosecond laser writing and the best Raman spectral resolution also. The power of illumination at the sample ranges between 5 and 6 mW.



Figure 5 Labram HR Raman spectrometer installed in MONARIS Laboratory

3 EPR spectroscopy

The electron paramagnetic resonance (EPR) is a powerful experimental technique for the analysis of paramagnetic centers (unpaired electron). Paramagnetic ions can be a free radical in liquid, solid and gaseous state, point defect in materials or transition and rare earth ions. In 1921, the experiment of Stern and Gerlach [8,9] displayed that a beam of silver atoms splits into lines when it is subjected to a magnetic field. Then, Uhlenbeck and Goudsmit et al. [10] introduced the spin as an intrinsic property of the electron. In 1944, Zavoisky realized the first experiment of EPR spectroscopy [11].

3.1 Zeeman effect

An electron is a negative charged particle that spins. It has a magnetic moment given by the following equation:

$$\mu = -g \beta S$$

Where g is the Landé factor, β is the Bohr magnetic moment, and S the spin angular momentum.

When a molecule containing a paramagnetic particle is placed in an external magnetic field, the magnetic moment of the unpaired electron interacts with it inducing the Zeeman effect:

$$H_{\text{zeeman}} = -\mu B = -g \beta S B$$

The energy levels with $2S+1$ degenerated levels are given by:

$$E_{m_s} = g m_s B b$$

We present a simple case of a two level system for a paramagnetic center with an electron spin $S = \frac{1}{2}$. (Figure 6).

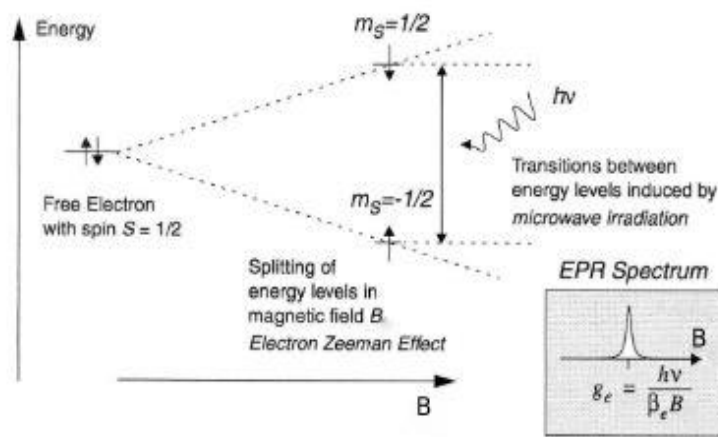


Figure 6 Energy level splitting of an unpaired electron exposed to a magnetic field with corresponding resonance frequencies. From [12].

The application of an external magnetic field B results in a splitting of the two energy level. The quantization of the energy level is due to the quantum mechanical nature of the electron spin. The splitting between the two energy states is called electron Zeeman interaction characterized by the spin quantum numbers $m_s = \pm \frac{1}{2}$ (Figure 6). The energy difference between the two Zeeman states is given by:

$$\Delta E = E(m_s = +\frac{1}{2}) - E(m_s = -\frac{1}{2}) = g \beta B$$

In a complex system as a glass, g must be replaced by a tensor \hat{g} in order to take into account its interaction with the surroundings. For an unpaired electron localized on a single atom, the spin-orbit must be considered and the Hamiltonian becomes:

$$H_{\text{zeeman}} = -\hat{g} \beta S B \quad \text{With} \quad \hat{g} = \begin{bmatrix} g_{xx} & g_{xy} & g_{xz} \\ g_{yx} & g_{yy} & g_{yz} \\ g_{zx} & g_{zy} & g_{zz} \end{bmatrix}$$

In certain cases, the unpaired electron is principally localized around a nucleus whose nuclear spin is different from zero. In this instance, the magnetic dipolar interaction between the nuclear and electron spin called hyperfine interaction should be taken into account.

If the hyperfine interaction is weaker than the Zeeman interaction, the following equation must be added to the Hamiltonian to evaluate the spin state energy:

$$H_{\text{hf}} = -S \cdot \hat{A} \cdot I$$

Where \hat{A} is the hyperfine tensor and I the nuclear spin operator. The hyperfine interaction gives a further splitting to the energy levels as given by the following equation (see figure 7):

$$E_{m_s m_l} = g m_s \beta B + A m_s m_l$$

Where m_s and m_l the projections of the electron spin and nuclear spin on the z-axis.

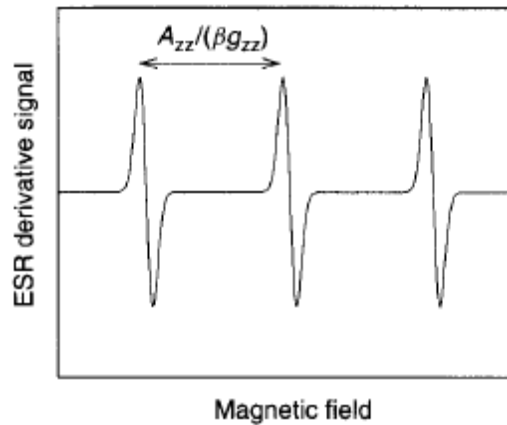


Figure 7 EPR derivative spectrum showing the three lines characteristic of the hyperfine [13]

3.2 Experimental set up

In this work, EPR measurements have been carried out at room temperature using a Bruker X-band EMX spectrometer in LSI (figure). The frequency was 9.8 GHz. The modulation frequency is normally set to 100 kHz. The recorded common EPR signal corresponds to the absorption's derivatives and was normalized by sample's mass and attenuator's gain. The glass samples used in this work are in solids form and not powders. The intensity of the signal obtained is proportional to the paramagnetic species concentrations. In our work, the EPR measurements are important to quantify the formation of divalent europium (paramagnetic ion $4f^7$) under irradiation as well as to identify the different paramagnetic point defects under electron and femtosecond laser irradiation relative to P atoms in phosphate glasses.



Figure 7 X-Band EPR spectrometer (LSI)

References

- [1] G.C. Righini, M. Ferrari, Photoluminescence of rare-earth-doped glasses, *La Rivista Del Nuovo Cimento*. 28 (2006) 1–53.
- [2] K. Binnemans, Interpretation of europium(III) spectra, *Coordination Chemistry Reviews*. 295 (2015) 1–45.
- [3] C.V. Raman, K.S. Krishnan, A new type of secondary radiation, *Nature*. 121 (1928) 501.
- [4] A. Smekal, Zur quantentheorie der dispersion, *Naturwissenschaften*. 11 (1923) 873–875.
- [5] E. Smith, G. Dent, *Modern Raman spectroscopy: a practical approach*, Wiley, 2019.
- [6] B.G. Liptak, *Instrument Engineers' Handbook, Volume One: Process Measurement and Analysis*, CRC press, 2003.
- [7] G. Keresztury, Raman Spectroscopy: Theory, *Handbook of Vibrational Spectroscopy*. (2006).
- [8] J. Kessler, *Polarized electrons*, Springer Science & Business Media, 2013.
- [9] W. Gerlach, O. Stern, Der experimentelle nachweis der richtungsquantelung im magnetfeld, *Zeitschrift Für Physik A Hadrons and Nuclei*. 9 (1922) 349–352.
- [10] G.E. Uhlenbeck, S. Goudsmit, Spinning electrons and the structure of spectra, *Nature*. 117 (1926) 264.
- [11] E. Zavoisky, The paramagnetic absorption of a solution in parallel fields, *J. Phys*. 8 (1944) 377.
- [12] D.T. Petasis, M.P. Hendrich, Quantitative interpretation of multifrequency multimode EPR spectra of metal containing proteins, enzymes, and biomimetic complexes, in: *Methods in Enzymology*, Elsevier, 2015: pp. 171–208.
- [13] M. Leone, S. Agnello, R. Boscaino, M. Cannas, F.M. Gelardi, *Silicon-Based Materials and Devices*, Academic San Diego, 2001.

List of Figures

FIGURE 1 PARTIAL ENERGY DIAGRAM OF Eu^{3+} ($4f^6$) SHOWING THE RELATIVE MAGNITUDE OF THE INTERELECTRONIC REPULSION (TERMS), SPIN-ORBIT COUPLING (LEVELS) AND CRYSTAL-FIELD EFFECTS (SUBLEVELS). THE DOWNWARD ARROWS INDICATE THE EXCITED STATES 5D_0 AND 5D_1 FROM WHICH LUMINESCENCE OCCURS [2].	18
FIGURE 2 EXPERIMENTAL SETUP FOR THE PHOTOLUMINESCENCE MEASUREMENTS ($\Delta\text{EXT} = 266, 355$ AND 532 NM (LSI)).	19
FIGURE 3 MICRO-PHOTOLUMINESCENCE EXPERIMENTS WITH 488 NM LASER EXCITATION (LSI).	20
FIGURE 4 DIAGRAM OF RAYLEIGH AND RAMAN SCATTERING PROCESSES .	22
FIGURE 5 LABRAM HR RAMAN SPECTROMETER INSTALLED IN MONARIS LABORATORY.	23
FIGURE 6 ENERGY LEVEL SPLITTING OF AN UNPAIRED ELECTRON EXPOSED TO A MAGNETIC FIELD WITH CORRESPONDING RESONANCE FREQUENCIES. FROM [12], [13].	24
FIGURE 7 EPR DERIVATIVE SPECTRUM SHOWING THE THREE LINES CHARACTERISTIC OF THE HYPERFINE	25

List of tables

TABLE 1 OVERVIEW OF THE TRANSITIONS OBSERVED IN LUMINESCENCE SPECTRA OF EUROPIUM(III) COMPOUNDS [2].	19
--	----

Chapter 2

Phosphate glasses: elaboration, properties and structure

Chapter 2 Phosphate glasses: elaboration, properties and structure

1	Glass samples	31
1.1	Glass composition	31
1.2	Glass synthesis.....	32
2	Glass structure bibliography.....	32
2.1	Mixed Alkali effect in phosphate glasses	33
2.2	Zinc containing glasses	34
3	Glass structure by NMR and Raman spectroscopy	36
3.1	Non-doped Metaphosphate glasses	36
3.1.1	Raman spectroscopy	36
3.1.2	NMR spectroscopy.....	38
3.2	Non-doped polyphosphate glasses	39
3.2.1	Raman spectroscopy	39
3.2.2	NMR spectroscopy.....	41
3.3	Eu-doped metaphosphate glasses	44
3.4	Eu-doped polyphosphate glasses.....	45
4	Glass transition temperature	48
4.1	Differential thermal analysis technique DTA.....	48
4.2	Results and discussion.....	49
4.2.1	Na- vs Mg-Na in metaphosphate glass.....	50
4.2.2	Rare earth effect.....	51
5	Density.....	51

1 Glass samples

1.1 Glass composition

Phosphate glasses studied in this work are metaphosphate and polyphosphate glasses. The glass compositions deal with mixing different alkaline and alkali-earth ions (Na, Li, K and Mg) and different polymerization degree. One metaphosphate glass contains zinc oxide whereas all polyphosphate are Zn polyphosphate. As well, three glasses contain two mixed alkali or alkali earth ions (Meta-Na-Li, Meta-Na-Mg and Poly-Zn-Na-K). Some glasses are undoped or doped with 1.2 mol% of Eu_2O_3 or Er_2O_3 . Nominal compositions of glasses are given in table 1.

Table 1 Nominal composition of metaphosphate and polyphosphate glasses

Sample label	Mol.%							
	P_2O_5	Na_2O	Li_2O	K_2O	ZnO	MgO	Eu_2O_3	Er_2O_3
Metaphosphate glasses								
Meta-Na	50.00	50.00						
Meta-Na-Eu	49.40	49.40					1.20	
Meta-Na-Er	49.40	49.40						1.20
Meta-Na-Li	50.00	25.00	25.00					
Meta-Na-Li-Eu	49.40	24.70	24.70				1.20	
Meta-Na-Li-Er	49.40	24.70	24.70					1.20
Meta-Na-Mg	50.00	33.30				16.70		
Meta-Na-Mg-Eu	49.40	32.90				16.50	1.20	
Meta-Na-Mg-Er	49.40	32.90				16.50		1.20
Meta-Zn	50.00				50.00			
Meta-Zn-Eu	49.40				49.40		1.20	
Polyphosphate glasses								
Poly-Zn-Na	33.40	20.00			46.60			
Poly-Zn-Na-Eu	33.00	19.80			46.00		1.20	
Poly-Zn-Na-Er	33.00	19.80			46.00			1.20
Poly-Zn-K	33.40			20.00	46.60			
Poly-Zn-K-Eu	33.00			19.80	46.00		1.20	
Poly-Zn-K-Er	33.00			19.80	46.00			1.20
Poly-Zn-K-Na	33.40	10.00		10.00	46.60			
Poly-Zn-K-Na-Eu	33.00	9.90		9.90	46.00		1.20	
Poly-Zn-K-Na-Er	33.00	9.90		9.90	46.00			1.20
Poly-Q¹/ Q²:50/50	40.00	40.00			20.00			
Poly-Q¹/ Q²:50/50-Eu	39.52	38.52			19.76		1.20	
Poly-Q¹/ Q²:50/50-Er	39.52	38.52			19.76			1.20

1.2 Glass synthesis

Phosphate glasses were prepared in our laboratory (Laboratoire des Solides Irradiés) by the standard melt-quenching method. Appropriate mixture of powders of Sodium carbonate Na_2CO_3 , Potassium carbonate K_2CO_3 , Lithium carbonate Na_2CO_3 , Zinc oxide ZnO , magnesium oxide MgO , Ammonium Dihydrogen Phosphate $\text{NH}_4\text{H}_2\text{PO}_4$ and Rare earth oxide Eu_2O_3 and Er_2O_3 have been thoroughly mixed according to the nominal glass composition of each glass (see Table 1). They were placed first in a silica crucible to avoid the interaction between P_2O_5 formation and Pt crucible at high temperature but quenched into a Pt-Au crucible.

For metaphosphate glasses, a 5 h step at 800°C (reached with a slow heating rate of $1^\circ\text{C}/\text{min}$) has been scheduled as a decarbonation step to remove CO_2 , H_2O and NH_3 . The temperature cycle for polyphosphate glasses is slightly different with a step at 850°C . The final melting phase has been executed during 30 mn to 1h at $900\text{-}1100^\circ\text{C}$ depending on the composition. After typically a total cycle of 10 to 12 hours, the melt was quenched into a Pt-Au crucible placed on a hot plate at 300°C . Then the glasses were annealed at 230 to 320°C depend on the glass composition in an air furnace three hours. Note that Meta-Li could not be stabilized under an amorphous phase because it crystallized. The most hygroscopic glass samples are conserved in desiccator.

2 Glass structure bibliography

The structure of phosphate glass is based on a cross-linked phosphorus tetrahedra. Knowing that the phosphorus atoms characterized by the electron configuration $[\text{Ne}] 3s^2 3p^3$ forming the sp^3 hybrid orbital outer electrons ($3s^2 3p^3$), each P-tetrahedron have three bonded oxygens and one doubly bonded oxygen because of the +5 valence of phosphorus. PO_4 tetrahedra are interconnected through "bridging oxygen" (P-O-P) and oxygen atoms that do not bond with other atoms are called "non-bridging oxygen" (NBO). Within this framework, the tetrahedra are classified using Q^n terminology where n presents the number of bridging oxygen per tetrahedra (figure 1).

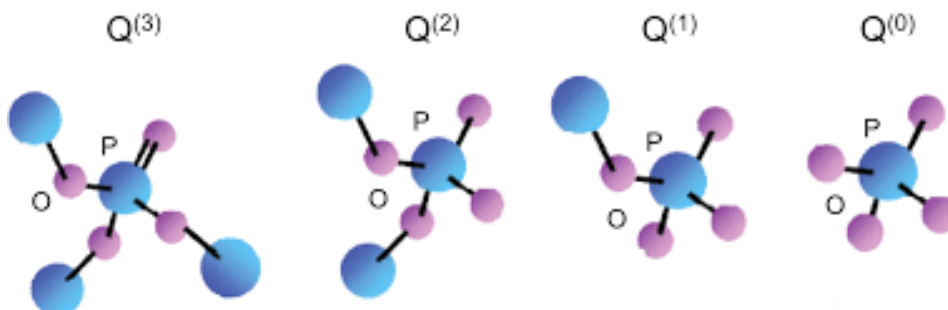


Figure 1 Q^n species that can be found in phosphate glasses

The vitreous P_2O_5 is composed of only Q^3 tetrahedra possessing three covalent bridging oxygen bonds to neighboring tetrahedra and one terminal oxygen (P-TO). The addition of a

modifier oxide like alkali, alkali earth or rare earth ion to v- P₂O₅ results in the creation of the non-bridging oxygen NBO. In particular, the addition of alkali oxide R₂O caused the depolymerization of phosphate network and can be described by the pseudo-reaction:



In this context, the concentration of Qⁿ tetrahedra in the xR₂O-(1-x)P₂O₅ glasses can be predicted based on the Van Wazer's reorganization theory [1] which describes the reaction of various Qⁿ tetrahedra with cations to form new structural units with decreasing bridging oxygen atoms.

In the case of ultraphosphate glasses (0 ≤ x ≤ 0.5), the fraction of Q² and Q³ is given by the relations:

$$f(Q^3) = \frac{(1-2x)}{(1-x)} ; f(Q^2) = \frac{x}{(1-x)}$$

Note that in metaphosphate glasses (x = 0.5), all the phosphate groups are Q² units.

Polyphosphate network (0.5 ≤ x ≤ 0.67) consists of chains of Q² tetrahedra terminated on both side by Q¹ tetrahedra. Their fractions are given by the relations:

$$f(Q^2) = \frac{(2-3x)}{(1-x)} ; f(Q^1) = \frac{(2x-1)}{(1-x)}$$

When the value of x is between 0.67 (pyrophosphate) and 0.75 (orthophosphate), the fractions of the Q¹ and Q⁰ units are given by the following relations:

$$f(Q^1) = \frac{(3-4x)}{(1-x)} ; f(Q^0) = \frac{(3x-2)}{(1-x)}$$

Many techniques have been used to study the phosphate glass structure including Raman spectroscopy, Infrared spectroscopy, Nuclear Magnetic Resonance (NMR), X-ray diffraction (XRD), Neutron diffraction (ND), X-ray photoelectron spectroscopy (XPS) and extended X-ray absorption fine structure (EXAFS).

2.1 Mixed Alkali effect in phosphate glasses

Mixed-alkali glass systems demonstrated non-linearity in electrical conductivity, thermal properties, viscosity and chemical durability [4]–[6]. This phenomenon is known as the “mixed-alkali effect” MAE and this effect seems more efficient when the difference in size between the two alkalis is pronounced. The two types of alkali ions are randomly mixed and have distinctly different conduction pathways of low dimensionality. This implies that A ions tend to block the pathways for the B ions and vice versa, and this is the main reason for the MAE [7]. Thereby, the MAE may be explained as a natural consequence of random ion mixing because ion transport is favored between well-matched energy sites and is impeded due to the structural mismatch between neighboring sites for dissimilar ions [8]. In this framework, many studies used structural method to understand the mixed alkali effect MAE in phosphate glasses like ³¹P and ²³Na MAS-NMR spectra in sodium lithium metaphosphate glasses by Sato

et al. [8]. The ^{31}P chemical shifts become less shielded with increasing $[\text{Na}]/[\text{Na} + \text{Li}]$ ratio. This issue is interpreted by the lower electronegativity of the sodium compared to lithium. The substitution of Na by Li results in more covalent P-O bonds and consequently a larger deshielding effect on the ^{31}P chemical shifts. The ^{31}P peak have greater full-width at half maximum (FWHM) for the intermediate mixed Na-Li glass compared with the single Li or Na metaphosphate glasses reflecting higher distribution of Na and P sites due to the presence of both Na and Li. Furthermore, the glass transition temperature reached a minimum at $[\text{Na}]/[\text{Na} + \text{Li}]$ Ratio = 0.6, thus showing a mixed alkali effect explained by the mixed alkali pairs Li-NBO-Na detected by NMR spectroscopy.

In addition, the infrared and Raman spectra of several series of mixed alkali metaphosphate glasses have been analyzed by Rouse et al.'s works [9]. The band frequencies due to the cation motion in the infrared spectra, which correlated to cation sites vibrations, do not shift with increasing the alkali substitution ratio, indicating that the significant geometry and oscillating forces associated with a particular cation are not affected by the introduction of a second alkali ion. In the other hand, Raman spectra present a different frequency attributed to vibration network band for each single alkali glasses in contrast to the mixed alkali glass that one band occurs and it varies linearly with increasing substitution ratio. This examination indicates that the cations are homogeneously distributed in mixed alkali glasses and the phosphate chains are associated with averaged cation environment whose effect on the chain modes. In summary, a simple vibrational model is presented which shows that the cation dependent shifts are due to small changes in network bond angles and variation of the cation sites forces and there is no MAE on the glass structure in those glasses.

In zinc alkali polyphosphate glasses ($46.6 \text{ ZnO} - 20\text{M}_2\text{O} - 33.4\text{P}_2\text{O}_5$ where M= Na, Li and K), the mixed alkali ion was tested in order to reduce the T_g and improve the stability [10]. It demonstrated that MAE can lead to a lower T_g however there is no improvement of the chemical stability in these samples.

2.2 Zinc containing glasses

The addition of zinc oxide in glasses affects the structure, physical, chemical, thermal as well as elastic properties. Zn^{2+} ions can enter the glass network, both as network modifier and network former [11]. As well, Zn atoms have a small coordination number about four differing to the modifier atoms in agreement with Zacharias's model [25]. The influence of the amount of zinc oxide on the structure was studied in many previous works. As an example, the lithium-iron-metaphosphate glasses were analyzed in [12]. Thus, the FTIR spectra showed significant spectral differences when the molar fraction of ZnO is increased. With the initial substitution of Li_2O with ZnO (about 2 mol. %), the P-O⁻ terminal group are connected due to the formation of P-O-Zn linkages. When the ZnO content is increased, the P=O bonds are broken down accompanied by the formation of (ZnO_4) tetrahedra. Thereby, ZnO acted as a glass network former, integrating the phosphate glass network. Moreover, the glass transition temperature decreased with increasing ZnO content whereas the density and the chemical stability increased.

Using X-ray and neutron diffraction techniques in zinc polyphosphate glasses, Hoppe et al. [13] reported that the change from ZnO_6 octahedra to ZnO_4 tetrahedra with raising the $[ZnO]/[P_2O_5]$ ratio from 0.5 to 1, causes decreasing packing density where most terminal oxygen atoms are in Zn-O-P linkages. In the range of higher ZnO content, an increasing fraction of terminal oxygen is coordinated by two or more Zn sites which results in a strong densification of the glass structure.

X-ray absorption spectroscopy (XAS) has been used by Moss et al.[14] to inspect the local environment of Zn within the calcium-sodium metaphosphate glasses. The X-ray absorption near edge spectroscopy (XANES) suggests that Zn atoms occupy mixed (4 and 6 fold) sites within the glass matrix. By EXAFS, they proved that the radial distance obtained for the Zn-O correlations are coherent with the Zn occupying a tetrahedral environment. The large error allows the Zn-O coordination number to be 4.9, which support the mixing sites.

Hoppe et al [24] displayed a structural model that is based on the coordination environment of the modifier cations in alkali, alkali earth, and zinc phosphate glasses and proposed that the structure of phosphate glasses would be dependent on the number of non-bridging oxygen available to coordinate the modifier ions (M^{a+} , where a is the valence). For glass with stoichiometry $x(M_{2/a}O)(1-x)P_2O_5$, the number of non-bridging oxygens per modifying ion is $N_{NBO} = a(1/x)$. Thus, the value $N_{NBO} < CN_M$ in the case of metaphosphate glasses and there is not enough individual non-bridging oxygen to satisfy the coordination environment of every M^{a+} ions and so these ions must share the available NBOs. As a result, M^{a+} coordination polyhedra share corners and edges and acts as bridges between neighboring Q^2 polyhedra. Consider first the single valent ions, MD simulations used in this thesis indicate that the coordination number of Na^+ is about 5. However, for the divalent ions Zn^{2+} , the CN turned to be about 4.

As we have mentioned before, we investigated here metaphosphate glasses ($x = 0.5$) constituted only by Q^2 units as well as polyphosphate glasses with a mixture of Q^1 and Q^2 species and we tried to illustrate the different glass schematically in figure 2.

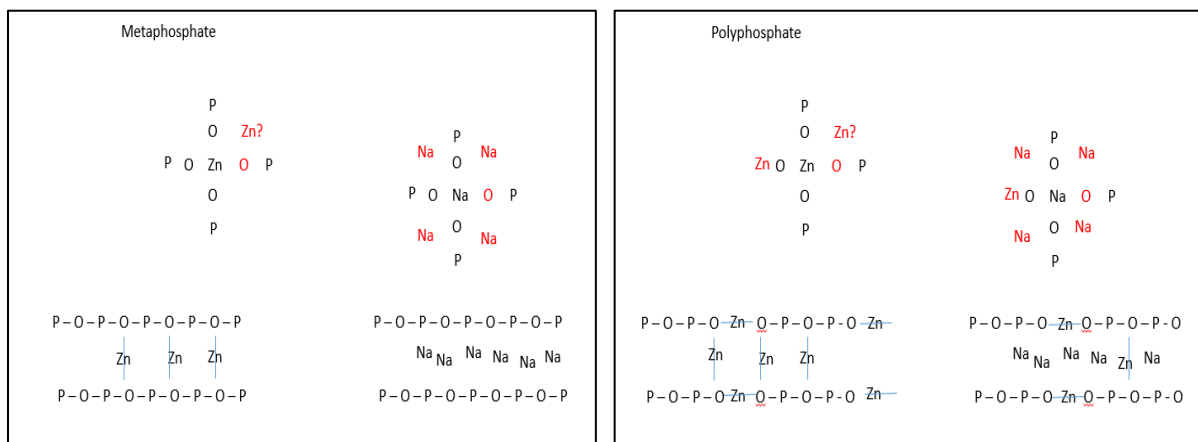


Figure 2 Schematic representation of zinc and sodium metaphosphate glasses (left) and zinc sodium polyphosphate glasses (right)

3 Glass structure by NMR and Raman spectroscopy

3.1 Non-doped metaphosphate glasses

3.1.1 Raman spectroscopy

Raman spectroscopy has been employed to study the short range structure of phosphate glasses. To begin, we are interested to study the structural properties of non-doped sodium metaphosphate glass (Figure 3).

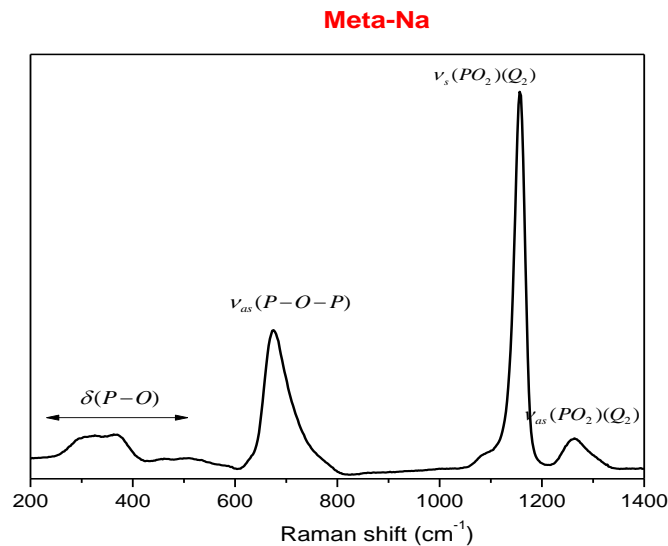


Figure 3 Raman spectra of non-doped sodium metaphosphate glass (Meta-Na)

Bands in the 600-850 cm^{-1} range are due to the symmetric and asymmetric stretching modes of bridging oxygen (BO) whereas the 900-1400 cm^{-1} range is due to symmetric and asymmetric stretching modes of P-non-bridging (NBO) or (terminal) O [15]. The detailed assignment of the Raman bands is given in table 2, based on literature.

Table 2 Vibrational frequencies (cm^{-1}) in metaphosphate glasses

Peak position (cm^{-1})	Assignment	Entity	Reference
290-450	$\delta(\text{P} - \text{O})$		[16], [17]
300-500	$\delta(\text{PO}_2)$		[18], [19]
630-690	$\nu_s(\text{P} - \text{O} - \text{P})$		[16]–[22]
777-807	$\nu_{as}(\text{P} - \text{O} - \text{P})$		[17]
1080-1120	P-O stretch	Terminal Q^1	[15], [17], [23]
1150-1160	$\nu_s(\text{PO}_2)$	Q^2	[16]–[18], [20]–[22]
1260-1270	$\nu_{as}(\text{PO}_2)$	Q^2	[18], [20]–[22]
1290-1330	$\nu(\text{P} = \text{O})$	Q^3	[16]

The broad bands in 250-500 cm^{-1} range are assigned to the bending vibrations $\delta(\text{P} - \text{O})$ [17], [23]. The band at 695 cm^{-1} corresponds to the symmetric stretching mode of bridging oxygen between two tetrahedra $(\text{P}-\text{O}-\text{P})_{\text{sym}}$ in metaphosphate chains $\nu_s(\text{P} - \text{O} - \text{P})$. The main band at $\sim 1162 \text{ cm}^{-1}$ corresponds to the symmetric stretching modes of the two non-bridging oxygen NBOs atoms bonded to phosphorus atoms $\nu_s(\text{PO}_2)$ in a Q^2 unit.

Furthermore, the shoulder at $\sim 1270 \text{ cm}^{-1}$ can be attributed to the asymmetric stretching modes $\nu_{\text{as}}(\text{PO}_2)$ of Q^2 units confirming with the two intense peak at ~ 1162 and 695 cm^{-1} that the Q^2 units are the main species as expected from the stoichiometry. The weak band at 1320 cm^{-1} due to the $\nu(\text{P}=\text{O})$ of Q^3 units. Even more, the remaining bands at $\sim 1120 \text{ cm}^{-1}$ can be assigned to the P-O stretch of Q^1 chain terminator [15].

Cation effect

Figure 4a and 4b exhibit respectively the real and normalized Raman spectra collected from the series of metaphosphate and compares the vibrational modes in Meta-Na, Meta-Na-Li, Meta-Na-Mg and Meta-Zn.

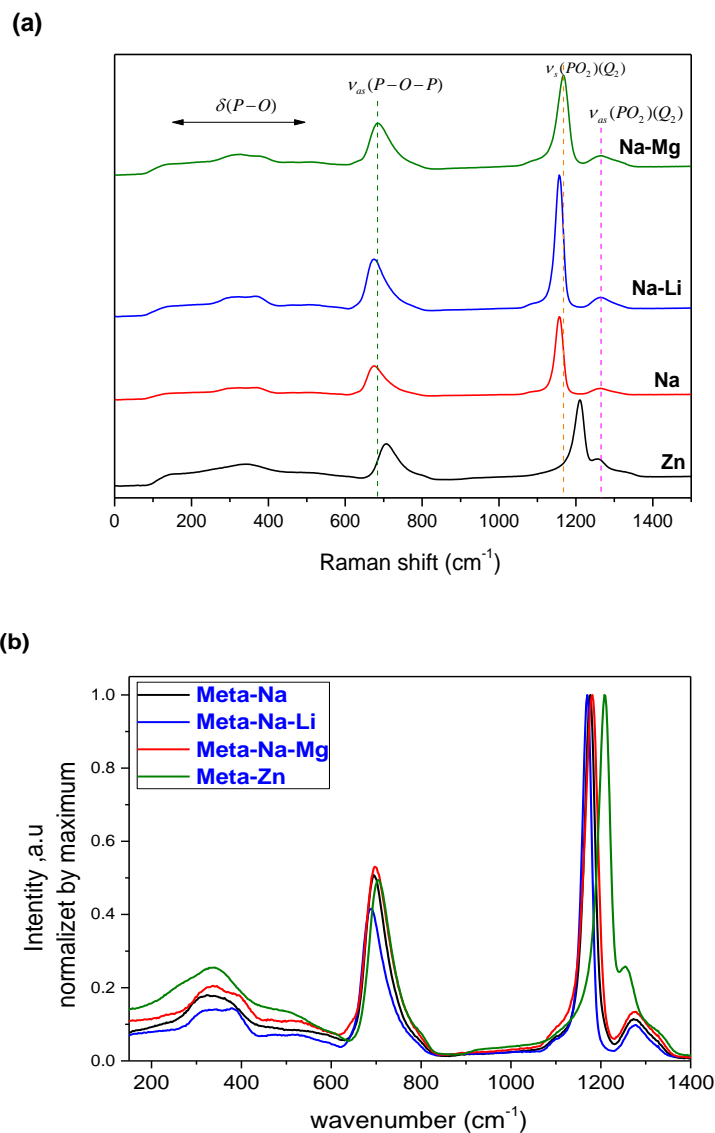


Figure 4 Comparison of Raman spectra of non-doped metaphosphate glasses: real (a) and normalized (b) spectra.

Certain bands at 350 cm^{-1} and 550 cm^{-1} were attributed to the bend mode of phosphate polyhedra with zinc modifier [25]. We see indeed that in presence of Zn they are more intense.

A significant shift is observed (Fig.4a and 4b) of the $\nu_s(\text{PO}_2)$ band from $\sim 1162 \text{ cm}^{-1}$ in Meta-Na to 1170 cm^{-1} in Meta-Na-Mg and $\sim 1205 \text{ cm}^{-1}$ in Meta-Zn. More precisely, the peak frequency of $\nu_s(\text{P} - \text{O} - \text{P})$ and $\nu_s(\text{PO}_2)$ bands are cation dependent and shifts to higher wavenumber in the order $\text{Na}^+ < \text{Na}^+ + \text{Li}^+ < \text{Na}^+ + \text{Mg}^{2+} < \text{Zn}^{2+}$ as the field strength of the modifying cations increases [15]. In this respect, Nelson et al. [26] reported the same effect in the series of alkali metaphosphate glasses. It is explained by the fact that O-P-O bond angle is larger for the larger cation and the increase of the bond angle causes a decrease in the frequency of PO_2 vibration.

In the same context, Rouse et al. [9] calculated the dependence of the shift of $\nu_s(\text{PO}_2)$ band on two parameters: the bond force constant for the M-O bond ($F_{\text{M-O}}$) determined from the cation motion bands in the far IR and the O-P-O bond angle (φ), both of which are governed primarily by metal cation size. As the $F_{\text{M-O}}$ increases in a series of metaphosphate (From 1 to $5.5 \times 10^4 \text{ dyn/cm}$ in Meta-Li to Meta-Cs respectively) and the bond angle φ decreases (From 118 to 112°), the PO_2 frequency increases by about 20 cm^{-1} . These key results are sufficient to accounts for the Raman features observed.

Of particular interest is the presence of separate band at ~ 1270 and 1350 cm^{-1} in zinc metaphosphate attributed to $\nu_{\text{as}}(\text{PO}_2)$ and $\nu_{\text{sym}}(\text{P} = \text{O})$ modes of respectively Q^2 and Q^3 units while these two bands are indistinguishable for single and mixed alkali and alkali earth metaphosphate glasses with the lowest intensity.

The FWHM of the $\nu_s(\text{PO}_2)$ as well as $\nu_s(\text{P} - \text{O} - \text{P})$ also increase with increasing cation field strength indicating an increase in the degree of disorder that may be due to changes in distributions of the Q^2 P-O bond length and bond angles [27].

3.1.2 NMR spectroscopy

In addition to vibrational spectra, solid state ^{31}P nuclear magnetic resonance (NMR) spectroscopy was performed in collaboration with S. Maron, LPCM Laboratory from Ecole polytechnique. This technique is particularly useful to determine quantitatively the Q^n units, so we mainly analyzed polyphosphate glasses, metaphosphate glasses supposed to be fully constituted of Q^2 units. Only one metaphosphate was analysed by NMR (meta Na). ^{31}P MAS-NMR (Magic Angle Spinning) spectrum of sodium metaphosphate glasses is presented in figure 5.

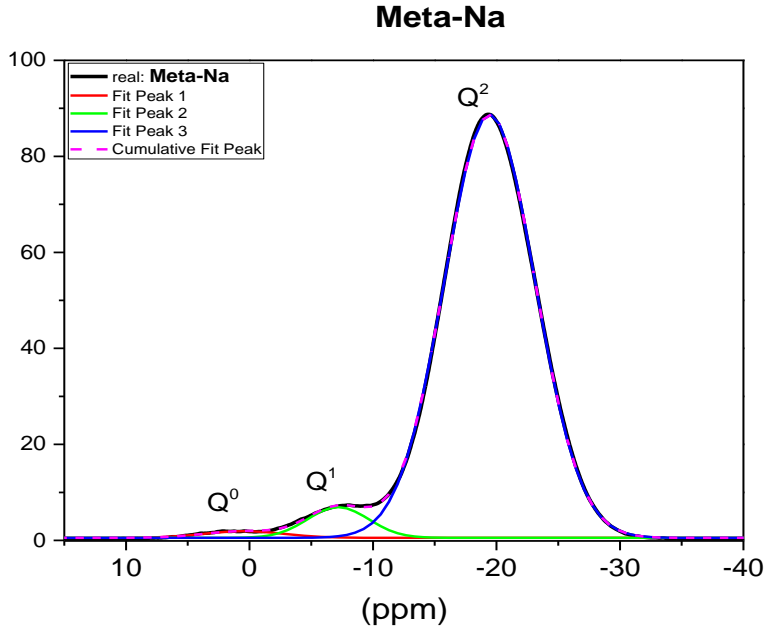


Figure 5 ^{31}P NMR spectrum deconvolution of sodium metaphosphate glasses

Peaks at 0.5 ppm and -7.2 ppm are attributed to Q^0 and Q^1 phosphate units respectively [28] indicating a slight amount of these two species with a relative proportion of 1.3% and 4.4% respectively as reported in table 3. The predominance of the peak at -19.4 ppm corresponds to the Q^2 units with relative proportion of about 94% in agreement with previous NMR studies of Montagne et al.[29] and Pickup et al.[30]. It confirms that the main Q^n unit present in metaphosphate glass is Q^2 in coherence with the prediction of Zachariassen 's model [2].

Table 3 Chemical shifts, Area and relative proportions (%) extracted from the simulation of the ^{31}P NMR spectra.

	Q^0 $\delta(\text{ppm})$ Area Rel.prop. %	Q^1 $\delta(\text{ppm})$ Area Rel.prop. %	Q^2 $\delta(\text{ppm})$ Area Rel.prop. %
Meta-Na	0.46 11.16 1.29	-7.17 39.69 4.6	-19.4 812 94.11

3.2 Non-doped polyphosphate glasses

3.2.1 Raman spectroscopy

Figure 6 compared the Raman spectra of sodium metaphosphate and sodium zinc polyphosphate glasses in the region of 250-1400 cm^{-1} . The drastic change in the structure with increasing cations contents is attested by an occurrence of new bands corresponding to Q^1 and Q^0 units. Their empirical assignment is listed in table 3.

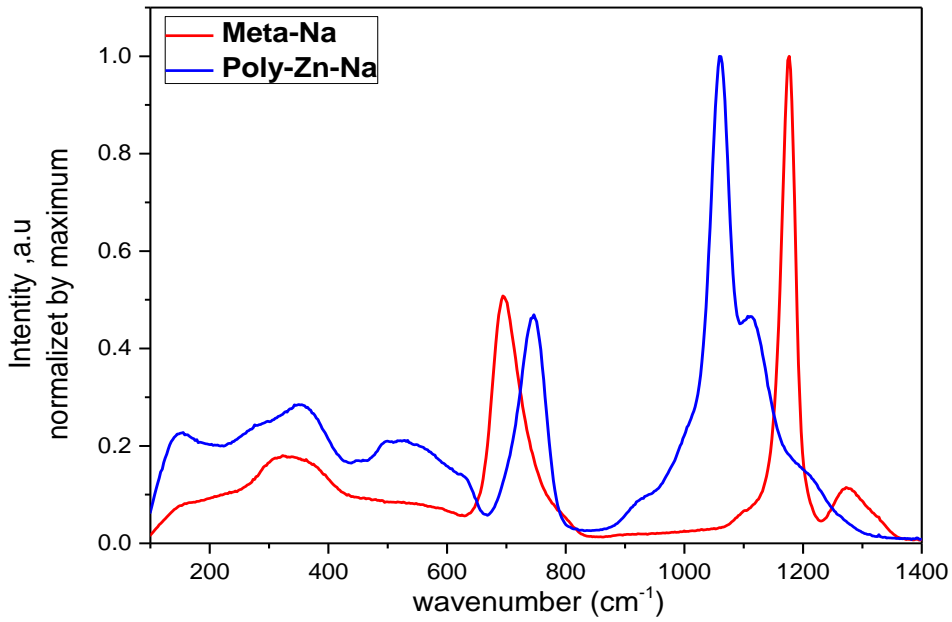


Figure 6 Raman spectra of sodium zinc polyphosphate glass compared to sodium metaphosphate glass, normalization by maximum.

Table 4 Vibrational frequencies (cm^{-1}) of the polyphosphate glasses

Peak position (cm^{-1})	Assignment	Entity	Reference
355	$\delta(\text{P} - \text{O} - \text{P})$		[31]
360-600	$\delta(\text{PO}_2)$		[32]
614-538-454	$\delta(\text{PO}_3)$		[31]
690-760	$\nu_s(\text{P} - \text{O} - \text{P})$		[25], [28], [31]–[34]
925-980	$\nu_{as}(\text{P} - \text{O} - \text{P})$	Q^1	[32], [34], [35]
940-970	$\nu_s(\text{PO}_4)^{3-}$	Q^0	[33],[34]
980-1020	$\nu_{as}(\text{PO}_4)^{3-}$	Q^0	[34]
999	$\nu_{as}(\text{P} - \text{O} - \text{P})$	Q^2	[35]
1010	P-O stretch	Terminal Q^1	[23], [33]
1037-1045	$\nu_{as}(\text{PO}_3)$		[32]
1020-1080	$\nu_s(\text{PO}_3^{2-})$	Q^1	[35],[33],[31],[34],[23]
1080-1120	P-O stretch	Terminal Q^1	[23], [28], [32]
1200-1210	$\nu_s(\text{PO}_2^-)$	Q^2	[33],[23],[35],[34]

Concerning the Poly-Zn-Na structure, three Raman bands at 732, 1056 and 1111 cm^{-1} dominate the spectra. The 732 cm^{-1} band is due to the symmetric stretching of bridging oxygen $\nu_s(\text{P} - \text{O} - \text{P})$ in Q^1 tetrahedra. The 1056 cm^{-1} band is attributed to $(\text{PO}_3)_{\text{sym}}$ modes of Q^1 species. The shoulder at $\sim 1200 \text{ cm}^{-1}$ is assigned to the $\nu_s(\text{PO}_2)$ of Q^2 . A shoulder with weak intensity at $\sim 950 \text{ cm}^{-1}$ corresponds to the symmetric stretching mode of non-bridging oxygen

atom (PO_4) in Q^0 tetrahedra ($\nu_s(\text{PO}_4)^{3-}$). Even more, bands at ~ 1022 and 1111 cm^{-1} correspond to the P-O stretch of Q^1 chain terminator [23].

3.2.2 NMR spectroscopy

The zinc alkali polyphosphate glasses Poly-Zn-Na and Poly-Zn-Na-K are also investigated using the 1D ^{31}P MAS-NMR experiments. In particular, we studied the effect of $\text{Zn}^{2+}/\text{M}^{1+}$ substitution (where $\text{M} = \text{Na}$ and $\text{Na}+\text{K}$) on the local and medium range order of the phosphate network. Figure 8 compared the 1D ^{31}P MAS-NMR spectra of the different polyphosphate glasses.

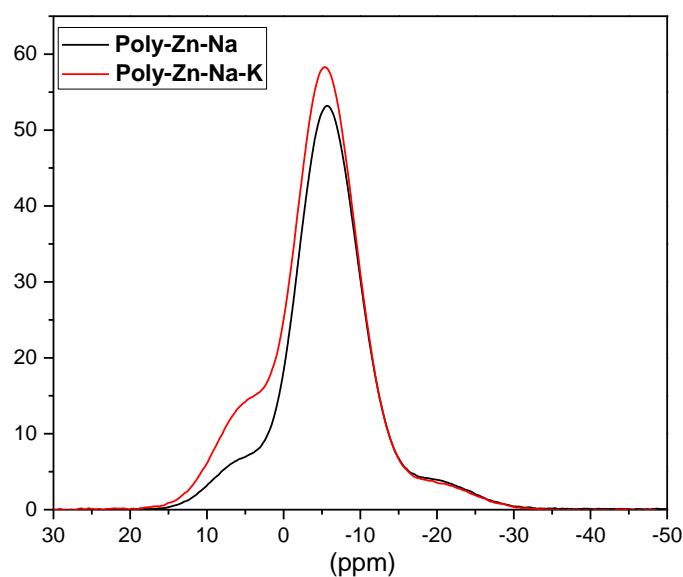


Figure 7 ^{31}P NMR spectra of single Na and Na-K mixed alkali polyphosphate glasses.

Thus, the spectra present one main band at -5.5 ppm accompanied by two additional resonance of lower intensity centered at around 5.8 and -20.4 ppm . These three peaks are characteristic of Q^1 , Q^0 and Q^2 species successively. These results are in accordance with Raman analysis that confirm the Q^1 tetrahedra domination for the polyphosphate composition.

To better determine the Q^n repartition and local environment of phosphorus atoms, the 1D ^{31}P MAS-NMR spectra are fitted with Gaussian as shown in figure 8 supported by parameters from 2D-NMR experiments in Rajbhandari's work [36]. It allows the distinction between 'dimeric' and 'chain-end' Q^1 leading to the assignment of Q^1 into $\text{Q}^{1,1}$ and $\text{Q}^{1,2}$ species. Thus, $\text{Q}^{1,1}$ sites are characteristic of Q^1 sites correlated to Q^1 sites forming $\text{P}_2\text{O}_7^{4-}$ dimmers.

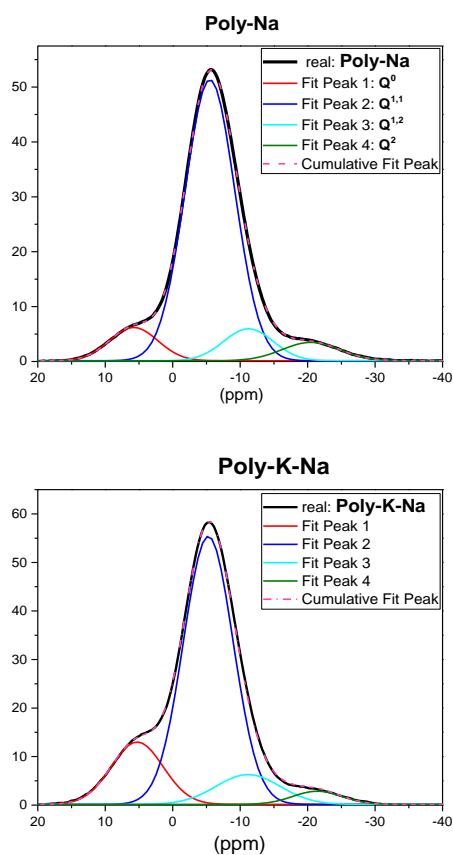


Figure 8 ^{31}P NMR spectrum deconvolution of Poly-Na and Poly-Na-K

The chemical shifts, full width at half maximum and relative proportions extracted from the 1D ^{31}P MAS-NMR spectra deconvolution for alkali zinc glasses are reported in table 5 in comparison with previous NMR studies of sodium and zinc polyphosphate composition.

Comparing the NMR results of this work with those extracted from Rajbhandari's work [36] for the similar zinc sodium polyphosphate samples, we observe a coherence in the chemical shift value whereas there is a disaccord in the relative proportion of the Q^2 units (5.8% in this work against 11.3% for Rajbhandari's glass).

A difference in the final chemical composition could explain such a difference with probably more Na content in our case.

Table 5 Chemical shifts, FWHM and relative proportions (%) extracted from the simulation of the ^{31}P NMR spectra.

	Q⁰ $\delta(\text{ppm})$ FWHM Rel.prop. %	Q^{1,1} $\delta(\text{ppm})$ FWHM Rel.prop. %	Q^{1,2} $\delta(\text{ppm})$ FWHM Rel.prop. %	Q² $\delta(\text{ppm})$ FWHM Rel.prop. %	
Poly-Zn-Na	5.8 8.4 8.7	-5.5 8.68 76.72	-11.2 8.63 8.69	-20.4 10 5.81	This work
Poly-Zn-Na-K	5.3 9.04 16.89	-5.3 8.69 69.77	-11.2 11.18 9.98	-21.4 8.52 3.37	This work
Poly-Zn-Na	7.6 8 6	-4.6 7.9 62.4	-8.5 8.3 20.3	-19.5 13 11.3	[36]
66.6-ZnO- 33.4P₂O₅	3.7 9.6 7	-10.6 11.4 52.9	-15.6 11.0 19.1	-28.4 13.5 21.0	[36]
	Q⁰ $\delta(\text{ppm})$ Rel.prop. %	Q¹ $\delta(\text{ppm})$ Rel.prop. %		Q² $\delta(\text{ppm})$ Rel.prop. %	
66.1ZnO- 33.9P₂O₅	3.6 12	-12 66		-29.1 22	[28]

The NMR spectrum of zinc polyphosphate (66.6 ZnO-33.4 P₂O₅) glass as reported in Table 5 presents a dominant peak at -10.6 ppm correspond to Q^{1,1} unit ensuing with peaks at near -15.6, -28.4 and 3.7 connected with Q^{1,2}, Q² and Q⁰ species respectively [35]. The relative proportions of these species are about 53, 19.3, 21 and 7% successively.

Substituting a quantity of ZnO by Na₂O₃ as in this work (~ 20% of Na₂O₃), we clearly observe a different chemical shift for example from around -10.6 ppm in zinc polyphosphate to near -5.5 ppm for the Q^{1,1} tetrahedra in presence of Na (in Poly-Zn-Na).

This evolution can be explained by the change induced by Zn²⁺/Na⁺ substitution in the chemical environment of the phosphate units. Rajbhandari et al. [36] explained this evolution by a higher electrostatic field strength for zinc atom ($Z/a^2(\text{Zn}) = 0.44 \times 10^{20} \text{ m}^{-2}$) compared to sodium ($Z/a^2(\text{Na}) = 0.1 \times 10^{20} \text{ m}^{-2}$).

As well, the proportion of the Q^{1,1} unit increases from 52.9 to 76.72% with the addition of Na₂O content indicating an increase in the dimeric entities and confirming a limited disorder in zinc sodium composition. The decrease of the Q² units is also visible when Zn²⁺ is replaced by 2Na⁺.

Let's now evaluating the mixed alkali ions in the glass network, NMR results (Table 5) show that Q⁰ units represent 16 % for Na/K against 8 % for Na glasses. Therefore, a mixed alkali effect may occur with a lower polymerization degree of the Na/K phosphate glass.

3.3 Eu-doped metaphosphate glasses

The addition of rare earth elements (1.2 mol. % of Eu_2O_3) slightly modify the structure of the host glass as seen in the Raman spectra of non-doped and Eu-doped metaphosphate glasses (figure 9).

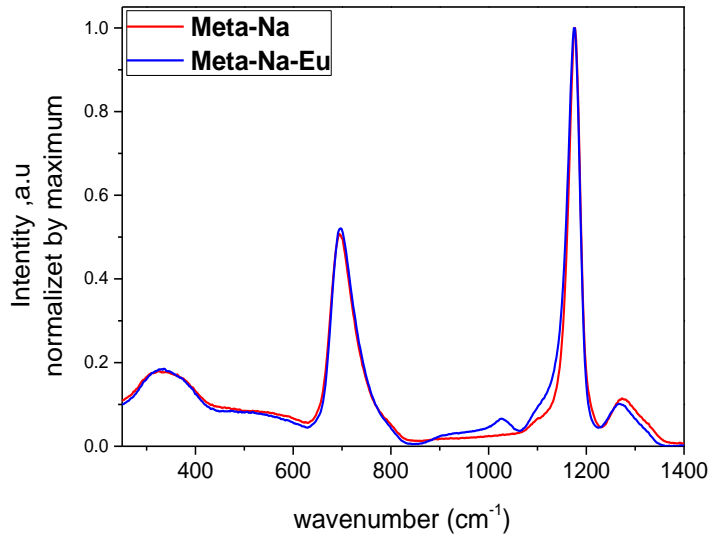


Figure 9 Raman spectra of non-doped and Eu doped sodium metaphosphate glasses, normalization by maximum

In the region of 250-1500 cm^{-1} , the most notable change is the occurrence of shoulder at about 1020 cm^{-1} and an additional contribution near 1110 cm^{-1} both attributed to the P-O stretch of the Q^1 chain terminator. It confirms the depolymerization of the glass network with europium doping, proving the role of RE ions as network modifier. Similarly, in the zinc metaphosphate glasses, the increase of the intensity of the bands in the range 900 to 1100 cm^{-1} (as seen in figure 10) approve that adding Eu^{3+} ions tend to depolymerize the glass network.

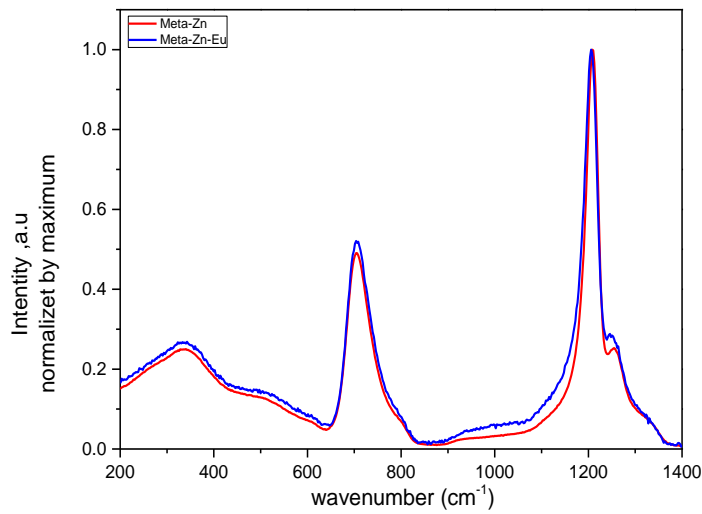


Figure 10 Raman spectra of non-doped and Eu doped zinc metaphosphate glasses, normalization by maximum.

3.4 Eu-doped polyphosphate glasses

The addition of europium ion to Na polyphosphate glass impacts the structure as expected. As seen in figure 11.a, Raman spectra of Eu doped sodium zinc polyphosphate glasses displayed stronger bands at 930 cm^{-1} and 1022 cm^{-1} attributed to the intermediate Q^1 and Q^0 units respectively compared to non-doped sample. As well, the band at near 1110 cm^{-1} due to the P-O stretch of Q^1 chain terminator undergoes an important increase in the intensity suggesting that RE ions contribute to the glass depolymerization [37]. On the other hand, Raman spectra of the mixed sodium-potassium zinc phosphate glass (figure 11.b) showed a stability of the network when introducing the lanthanide ions.

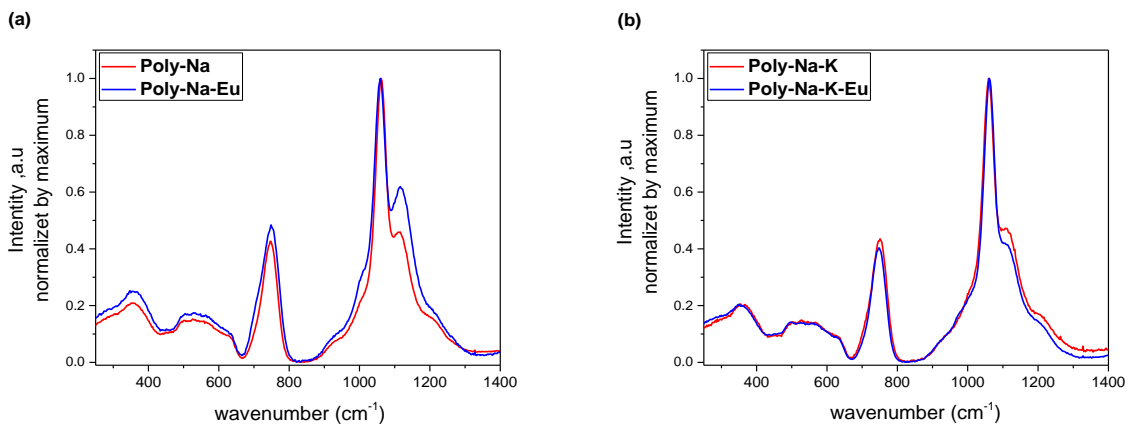


Figure 11 Comparison between Raman spectrum of non-doped and Europium doped polyphosphate glasses normalized by maximum

This is better illustrated by the figure 12 comparing the Raman spectra of the single Na, K and NaK mixed alkali polyphosphate glasses doped with europium ions. We observe a higher contribution of the bands at 1010 and 1110 cm^{-1} in the single alkali glasses. This can be explained by a mixed alkali effect observed on the Eu-doped glass polymerization with a lowest network polymerization for the Na/K composition in agreement with NMR results (for non-doped glasses).

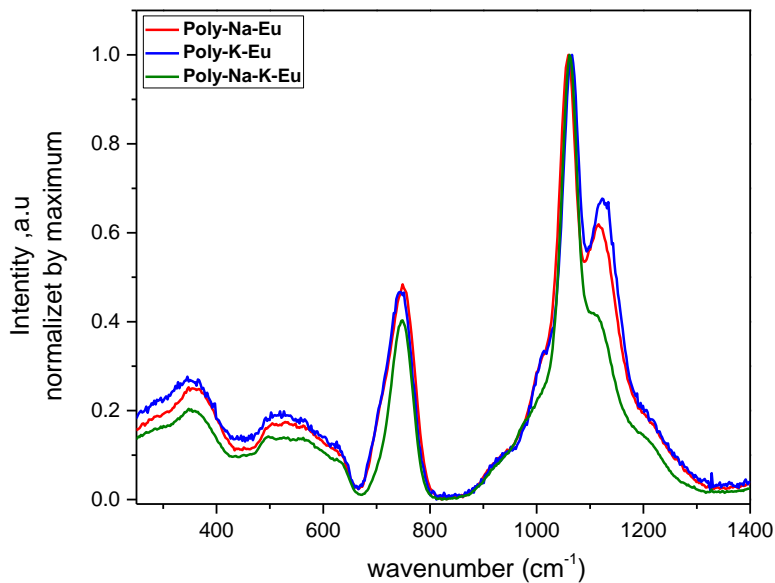


Figure 12 Raman spectrum of Europium doped polyphosphate glasses normalized maximum

Non-doped and Eu doped Poly-Zn-Na-(50/50:Q¹/Q²) glass with composition (20 ZnO-40 Na₂O-40 P₂O₅) is also prepared in order to obtain half Q¹ units and half Q² units. As well, it will be used to study the zinc effect in glasses under irradiation. ³¹P NMR (figure 13) as well as Raman spectra (not shown) confirm the 50/50 expected distribution of Q¹ and Q² species.

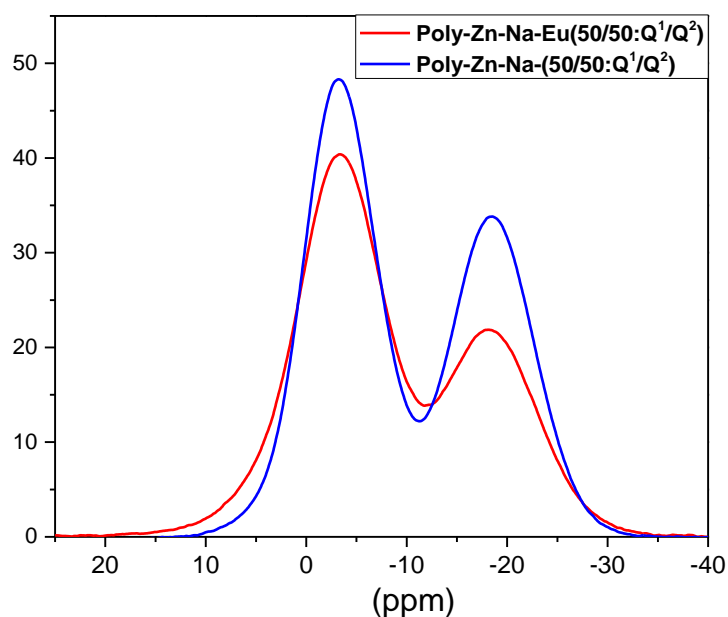


Figure 13 ^{31}P NMR spectra of non-doped and Eu doped Poly-Zn-Na-(50/50:Q¹/Q²) glass.

The chemical shifts, full width at half maximum and relative proportions extracted from the 1D ^{31}P MAS-NMR spectra deconvolution for non-doped and Eu doped Poly-(50/50:Q¹/Q²) are reported in table 6. For non-doped sample, the Q¹ species is slightly predominant with a relative proportion of 56% and 44% for Q². When doping with europium ion, the proportion of Q¹ increase up to 64% which confirms the network depolymerization.

Table 6 Chemical shifts, FWHM and relative proportions (%) extracted from the simulation of the ^{31}P NMR spectra of non-doped and Eu doped Poly-Zn-Na-(50/50:Q¹/Q²)

	Q ¹ δ(ppm) FWHM Rel.prop. %	Q ² δ(ppm) FWHM Rel.prop. %	
Poly-Zn-Na (50/50 :Q¹/Q²)	-3.3 8.57 55.58	-18.5 9.8 44.42	This work
Poly-Zn-Na-Eu (50/50 :Q¹/Q²)	-3.3 10.4 64.04	-18.4 10.7 35.96	This work

4 Glass transition temperature

Principally, a glass has two distinct reference temperatures. One is the melting point of the crystalline form T_m and the other is the glass transition temperature T_g corresponding to a viscosity η (or relaxation time τ) of 10^{13} poise.

Figure 14 shows the well-known graph of the volume-temperature relationship for a glass. If the crystalline form of the material is heated it expands with increasing temperature and at a certain temperature T_m it melts to a liquid. Here the crystalline form is in thermodynamic equilibrium with the liquid. The glassy form of the same material expands first as a solid. The constituent ions, atoms, or molecules begin to make translational motion, however, at T_g . In other words, glass becomes more or less fluid. Above T_g the material is in the state of supercooled liquid and expands at a higher rate [38].

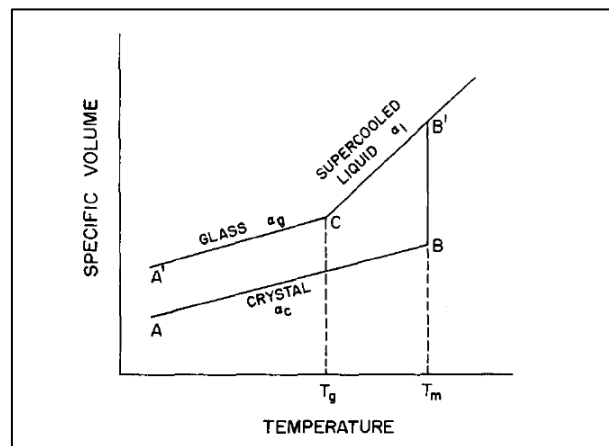


Figure 14 Volume-temperature relationship for a glass forming substance

As we said before, phosphate glasses are symbolized by their low glass transition temperature (T_g is in the range of 250-450°C) [10],[39],[40] compared to silicate glasses (about 900°C) [41]. Differential thermal analysis technique DTA was performed in PMC laboratory of Ecole Polytechnique to measure the glass transition temperature of our samples.

4.1 Differential thermal analysis technique DTA

DTA is a technique in which the difference in temperature between the powder sample and a reference is monitored against time or temperature while the temperature of the sample, in a specified atmosphere, is programmed.

The sample and the reference are placed symmetrically in the furnace controlled by a temperature program. During this process, a differential thermocouple allows to detect the temperature difference between the sample and the reference as well as the sample temperature (figure 15.a).

When the furnace heating begins, the reference and the sample begin heating with a slight delay depending on their respective capacity, and eventually heat up according to the furnace temperature. When the temperature increases and melting occurs in the samples, for

example, the temperature rise stops as shown in figure 15.b and the ΔT signal referred to DTA signal increases (endothermic phase). The temperature difference due to the sample endothermic change is shown as a negative direction. When the melting finishes, the temperature curve rapidly reverts to the baseline. Then, the ΔT signal reaches the peak, as shown in figure 15.b (exothermic phase) with a positive direction. From this, we can detect the glass transition temperature and the reaction temperature from the ΔT signal.

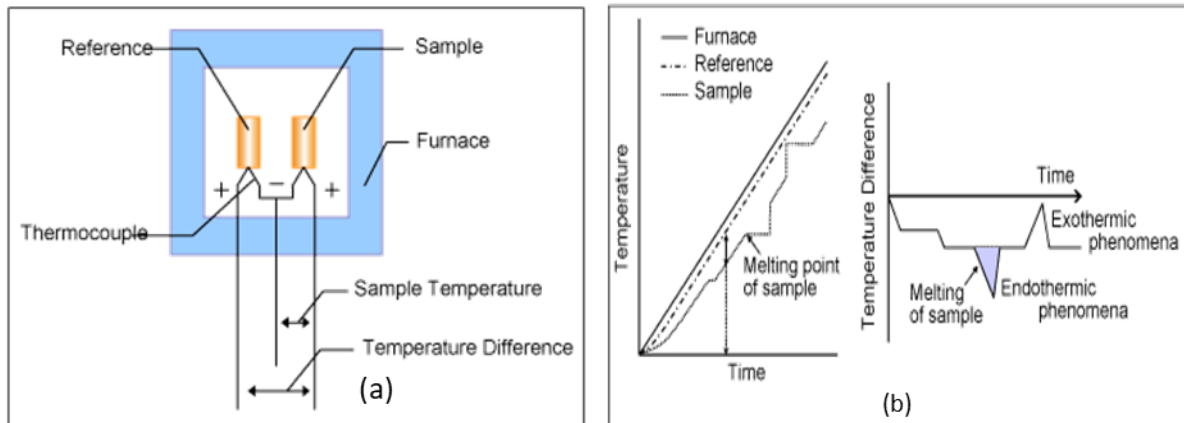


Figure 15 (a) Block diagram of DTA (right), Temperature change of the furnace, (b) the reference, the sample and the change in temperature difference (ΔT) against time detected with the differential thermocouple.

4.2 Results and discussion

Figure 16 shows the DTA curves of RE doped and non-doped polyphosphates glasses that exhibited clear exothermic phase. The T_g is measured by the intersection of two tangents around the peak. The glass transition temperature T_g of the different samples synthesized in this project are reported in table 7 and compared to literature.

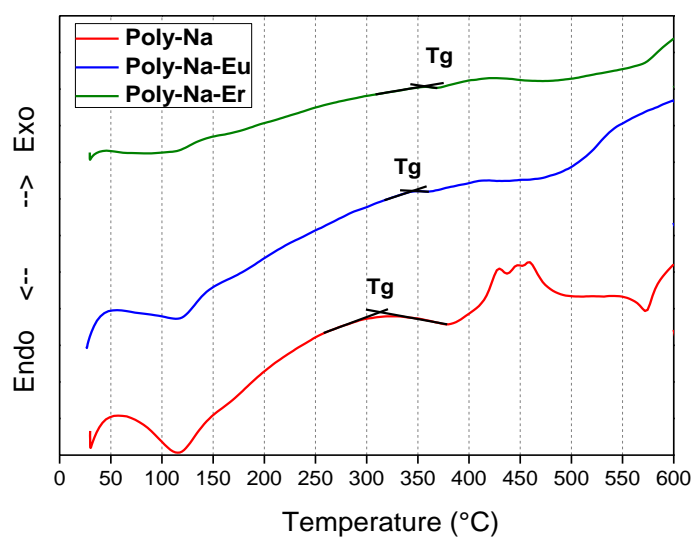


Figure 16 DTA curves of RE doped and non-doped sodium polyphosphate glasses

Table 7 Glass transition temperatures

Sample Name	Experimental T _g (°C) (DTA)	T _g (°C) From literature		
		T _g	Method	Ref
Metaphosphate glasses				
Meta-Na	251	280	DSC	[42],[43],[44]
		258/270	DTA	[45],[46]
Meta-Na-Eu	293			
Meta-Na-Er	301			
Meta-Na -Li	282			
Meta-Na-Li-Eu	289			
Meta-Na-Li-Er	311			
Meta-Na-Mg	367	380	DTA	[46]
Meta-Na-Mg-Eu	374			
Meta-Zn	446	460	DSC	[25]
		445	DTA	[33]
Meta-Zn-Eu	460			
Polyphosphate glasses				
Poly-Na	314	339	DSC	[10]
Poly-Na-Eu	345			
Poly-Na-Er	357			
Poly-K	361	376	DSC	[10]
Poly-K-Eu	400			
Poly-Na-K	331	312	DSC	[10]
Poly-Na-K-Eu	347			
Poly-50/50	274			
Poly-50/50-Eu	291			
Poly-50/50-Er	304			

4.2.1 Na vs Mg-Na in metaphosphate glass

For metaphosphate glasses, T_g increases from 251°C in Meta-Na to 367°C in Meta-Na-Mg in agreement with literature (table 7). This behavior corresponds to some changes in the nature of bonding in the structural network. T_g value is strictly related to the bond strength of the glass network which linked to the cation field strength (ratio of the charge to radius). Thus, if the monovalent cation Na⁺ is replaced by the divalent cation Mg²⁺, the cation cross-linking increased and the structure strengthened inducing a crucial increase of the glass transition temperature [43], [44], [47],[44],[47].

Likewise, the T_g rises substantially to 446°C in Meta-Zn. The P-O-Zn²⁺ bonds are formed replacing P-O-Na⁺ bonds while keeping the same fraction of P-O-P. The Meta-Na sample is entirely constituted by Q² tetrahedra that forms chains linked by more ionic bonds between sodium cations and the non-bridging oxygen NBO. By replacing Na₂O with ZnO, the higher electronegativity of the zinc (1.63) with respect to the sodium cation (0.93) one predicts the zinc-oxygen bond to be more covalent than the sodium-oxygen bond. This promoted a stronger cross-link between phosphate chains which increased drastically the T_g.

Moreover, the slower mobility of larger ionic radius Zn^{2+} compared to Na^+ increased the viscosity and therefore contribute to the increase of the T_g [46],[48].

In addition, the larger T_g value of the mixed sodium lithium metaphosphate glass compared to sodium glass could be explained by the larger ionic radius of Na^+ ($r_{Li^+} = 76 \text{ pm} < r_{Na^+} = 102 \text{ pm}$) that increases the ionic field strength of Li^+ relative to Na^+ [42].

Concerning the polyphosphate composition and comparing to results from literature, the DTA measurement showed an important decrease of the glass transition temperature from 433°C in $66.6ZnO + 33.4P_2O_5$ glass [10] to 314°C in Poly-Na with composition: $46.6ZnO + 20Na_2O + 33.4P_2O_5$ (show table 7). As explained before, these evolutions can be correlated by the replacement of Zn-O-P bond by more ionic and weaker Na^+ -O-P linkages. This weakening is strongly related to the decrease of T_g [10].

4.2.2 Rare earth effect

Inserting rare earth ions in the glass composition whatever the type of glass showed an increase in the glass transition temperature (Table 7). Taking the sodium polyphosphate glass as an example, the $T_g = 314^\circ\text{C}$ in Poly-Na and 345°C and 357°C in Poly-Na-Eu and Poly-Na-Er respectively. Therefore, in addition to its role of network modifier that depolymerize the glass network, the RE ions have another functionality that strengthen the network [49],[50].

5 Density

Density was measured for glass samples at room temperature using toluene as the immersion liquid. Density is measured by the fluid displacement method depending on Archimedes principle. According the Archimedes Law, the buoyancy equal the weight of displaced fluid. The density was obtained by employing the relation:

$$\rho = \frac{W_a \rho_t}{(W_a - W_t)}$$

Where W_a is the weight of the glass sample in air, W_t is the weight of the glass sample in toluene, $(W_a - W_t)$ is the buoyancy and ρ_t is the density of the buoyant liquid. All measurements were made using a digital balance adapted for this in IPGP in collaboration with D. Neuville and presented in table 8 and are in good agreement with literature.

Table 8 Density values of the different metaphosphate and polyphosphate glasses

Sample Name	Density (g/cm ³)	Density from literature	Ref
Metaphosphate			
Meta-Na	2.480	2.37 [51], 2.47 [30], 2.50 [52], 2.52 [15]	
Meta-Na-Eu	2.576		
Meta-Na-Er	2.565		
Meta-Na -Li			
Meta-Na-Li-Eu	2.572		
Meta-Na-Mg	2.553		
Meta-Na-Mg-Eu	2.589		
Meta-Zn	2.869	2.84 [53], 2.81 [54], 2.82 [55]	
Meta-Zn-Eu	2.892		
Polyphosphate			
Poly-Zn-Na	3.186	3.20 [10]	
Poly-Zn-Na-Eu	3.263		
Poly-Zn-Na-Er	3.319		
Poly-Zn-K	3.057		
Poly- Zn-K-Eu	3.137		
Poly- Zn-Na-K	3.200		
Poly- Zn-Na-K-Eu	3.221		
Poly-50/50	2.811		
Poly-50/50-Eu	2.853		
40P ₂ O ₅ -60ZnO		3.28 [56]	

- [1] J. R. Van Wazer, 'Phosphorus and its Compounds', 1958.
- [2] W. H. Zachariasen, 'The atomic arrangement in glass', *Journal of the American Chemical Society*, vol. 54, no. 10, pp. 3841–3851, 1932.
- [3] K. Suzuya, D. L. Price, C.-K. Loong, and S. W. Martin, 'Structure of vitreous P2O5 and alkali phosphate glasses', *Journal of Non-Crystalline Solids*, vol. 232–234, pp. 650–657, Jul. 1998.
- [4] R. M. Wenslow and K. T. Mueller, 'Cation sites in mixed-alkali phosphate glasses', *Journal of Non-Crystalline Solids*, vol. 231, no. 1–2, pp. 78–88, Jul. 1998.
- [5] J. E. Shelby, 'Properties of alkali–alkaline earth metaphosphate glasses', *Journal of Non-Crystalline Solids*, vol. 263–264, pp. 271–276, Mar. 2000.
- [6] J. E. Tsuchida *et al.*, 'Ionic conductivity and mixed-ion effect in mixed alkali metaphosphate glasses', *Physical Chemistry Chemical Physics*, vol. 19, no. 9, pp. 6594–6600, 2017.
- [7] J. Swenson, 'Experimental insight into the mixed mobile ion effect in glasses', *Solid State Ionics*, vol. 136–137, no. 1–2, pp. 1055–1060, Nov. 2000.
- [8] R. K. Sato, R. J. Kirkpatrick, and R. K. Brow, 'Structure of Li,Na metaphosphate glasses by 31P and 23Na MAS-NMR correlated with the mixed alkali effect', *Journal of Non-Crystalline Solids*, vol. 143, pp. 257–264, Jan. 1992.
- [9] G. B. Rouse Jr, P. J. Miller, and W. M. Risen Jr, 'Mixed alkali glass spectra and structure', *Journal of Non-Crystalline Solids*, vol. 28, no. 2, pp. 193–207, 1978.
- [10] P. Rajbhandari, L. Montagne, and G. Tricot, 'Investigation of zinc alkali pyrophosphate glasses. Part I: Development of low-Tg and high stability glasses', *Materials Chemistry and Physics*, vol. 155, pp. 17–22, Apr. 2015.
- [11] H. S. Liu and T. S. Chin, 'Low melting PbO-ZnO-P2O5 glasses. Part 2. A structural study by Raman spectroscopy and MAS-NMR', *Physics and chemistry of glasses*, vol. 38, no. 3, pp. 123–131, 1997.
- [12] R. Yang *et al.*, 'Structure and properties of ZnO-containing lithium–iron–phosphate glasses', *Journal of Alloys and Compounds*, vol. 513, pp. 97–100, Feb. 2012.
- [13] U. Hoppe, G. Walter, G. Carl, J. Neufeind, and A. C. Hannon, 'Structure of zinc phosphate glasses probed by neutron and X-ray diffraction of high resolving power and by reverse Monte Carlo simulations', *Journal of Non-Crystalline Solids*, vol. 351, no. 12–13, pp. 1020–1031, May 2005.
- [14] R. M. Moss *et al.*, 'The effect of zinc and titanium on the structure of calcium–sodium phosphate based glass', *Journal of Non-Crystalline Solids*, vol. 356, no. 25–27, pp. 1319–1324, Jun. 2010.
- [15] R. K. Brow, 'Review: the structure of simple phosphate glasses', *Journal of Non-Crystalline Solids*, vol. 263–264, pp. 1–28, Mar. 2000.
- [16] L. L. Velli, C. P. E. Varsamis, E. I. Kamitsos, D. Möncke, and D. Ehrhart, 'Structural investigation of metaphosphate glasses', vol. 46, no. 2, p. 5, 2005.
- [17] R. K. Brow, D. R. Tallant, J. J. Hudgens, S. W. Martin, and A. D. Irwin, 'The short-range structure of sodium ultraphosphate glasses', *Journal of Non-Crystalline Solids*, vol. 177, pp. 221–228, Nov. 1994.
- [18] C. Mugoni, H. Jain, M. Montorsi, M. Montecchi, A. Kovalskiy, and C. Siligardi, 'Structural origin of electrical conductivity of copper lithium metaphosphate glasses', *Journal of Non-Crystalline Solids*, vol. 447, pp. 91–97, Sep. 2016.
- [19] A. Chrissanthopoulos, C. Pouchan, and G. N. Papatheodorou, 'Structural Investigation of Vanadium-Sodium Metaphosphate Glasses', *Zeitschrift für Naturforschung A*, vol. 56, no. 11, Jan. 2001.
- [20] J. Koo, B.-S. Bae, and H.-K. Na, 'Raman spectroscopy of copper phosphate glasses', *Journal of non-crystalline solids*, vol. 212, no. 2–3, pp. 173–179, 1997.
- [21] J. J. Hudgens, R. K. Brow, D. R. Tallant, and S. W. Martin, 'Raman spectroscopy study of the structure of lithium and sodium ultraphosphate glasses', *Journal of Non-Crystalline Solids*, vol. 223, pp. 21–31, Jan. 1998.
- [22] J. J. Hudgens and S. W. Martin, 'Glass Transition and Infrared Spectra of Low-Alkali, Anhydrous Lithium Phosphate Glasses', *Journal of the American Ceramic Society*, vol. 76, no. 7, pp. 1691–1696, Jul. 1993.

- [23] R. K. Brow, D. R. Tallant, S. T. Myers, and C. C. Phifer, 'The short-range structure of zinc polyphosphate glass', *Journal of Non-Crystalline Solids*, vol. 191, no. 1–2, pp. 45–55, Nov. 1995.
- [24] U. Hoppe, G. Walter, R. Kranold, and D. Stachel, 'Structural specifics of phosphate glasses probed by diffraction methods: a review', *Journal of Non-Crystalline Solids*, vol. 263, pp. 29–47, 2000.
- [25] R. K. Brow, D. R. Tallant, S. T. Myers, and C. C. Phifer, 'The short-range structure of zinc polyphosphate glass', *Journal of Non-Crystalline Solids*, vol. 191, no. 1–2, pp. 45–55, Nov. 1995.
- [26] B. N. Nelson and G. J. Exarhos, 'Vibrational spectroscopy of cation-site interactions in phosphate glasses', *The Journal of Chemical Physics*, vol. 71, no. 7, p. 2739, 1979.
- [27] R. K. Brow, C. C. Phifer, G. L. Turner, and R. J. Kirkpatrick, 'Cation effects on ^{31}P MAS NMR chemical shifts of metaphosphate glasses', *Journal of the American Ceramic Society*, vol. 74, no. 6, pp. 1287–1290, 1991.
- [28] R. K. Brow, 'Review: the structure of simple phosphate glasses', *Journal of Non-Crystalline Solids*, vol. 263–264, pp. 1–28, Mar. 2000.
- [29] L. Montagne, G. Palavit, and R. Delaval, ' ^{31}P NMR in $(100-x)(\text{NaPO}_3)\text{-xZnO}$ glasses', *Journal of non-crystalline solids*, vol. 215, no. 1, pp. 1–10, 1997.
- [30] D. M. Pickup, I. Ahmed, P. Guerry, J. C. Knowles, M. E. Smith, and R. J. Newport, 'The structure of phosphate glass biomaterials from neutron diffraction and ^{31}P nuclear magnetic resonance data', *Journal of Physics: Condensed Matter*, vol. 19, no. 41, p. 415116, Oct. 2007.
- [31] S. Bruni *et al.*, 'Short Range Order of Sodium-Zinc, Sodium-Copper, and Sodium-Nickel Pyrophosphate Glasses by Diffractometric and Spectroscopic Techniques', *The Journal of Physical Chemistry*, vol. 99, no. 41, pp. 15229–15235, Oct. 1995.
- [32] G. T. Stranford, R. A. Condrate Sr, and B. C. Cornilsen, 'The Raman spectrum of α -zinc pyrophosphate', *Journal of Molecular Structure*, vol. 73, no. 1, pp. 231–234, 1981.
- [33] B. Tischendorf, J. U. Otaigbe, J. W. Wiench, M. Pruski, and B. C. Sales, 'A study of short and intermediate range order in zinc phosphate glasses', *Journal of Non-Crystalline Solids*, vol. 282, no. 2–3, pp. 147–158, Apr. 2001.
- [34] A. M. Efimov, 'IR fundamental spectra and structure of pyrophosphate glasses along the $2\text{ZnO P}_2\text{O}_5\text{-}2\text{Me}_2\text{O P}_2\text{O}_5$ join \checkmark Me being Na and Li', p. 18, 1997.
- [35] J.-C. Desmoulin, 'Synthèse et caractérisation de verres d'oxyde d'argent: évolution sous rayonnements ionisants et structuration multi-échelle par laser femtoseconde', PhD Thesis, Université de Bordeaux, 2016.
- [36] P. Rajbhandari, Y. Chen, B. Doumert, L. Montagne, and G. Tricot, 'Investigation of zinc alkali pyrophosphate glasses. Part II: Local and medium range orders analysed by 1D/2D NMR', *Materials Chemistry and Physics*, vol. 155, pp. 23–29, Apr. 2015.
- [37] L. Zhang, L. Wen, J. Zhang, and L. Hu, 'Spectroscopic and structural properties of YbF₃-doped fluorophosphate glasses', *Materials chemistry and physics*, vol. 91, no. 1, pp. 166–171, 2005.
- [38] S. Sakka, 'RELATION BETWEEN APPARENT GLASS TRANSITION TEMPERATURE AND LIQUIDUS TEMPERATURE FOR INORGANIC GLASSES', p. 18.
- [39] R. Metselaar, R. G. W. J. Nelissen, and D. L. Vogel, 'Dielectric losses of alkali metaphosphate glasses in the low temperature range 4–200 K, and their relation to the glass composition', *Journal of Non-Crystalline Solids*, vol. 44, no. 2–3, pp. 315–320, Jun. 1981.
- [40] S. Striepe and J. Deubener, 'Effect of lithium-to-magnesium ratio in metaphosphate glasses on crack-tip condensation and sub-critical crack growth', *Journal of Non-Crystalline Solids*, vol. 375, pp. 47–54, Sep. 2013.
- [41] I. Avramov, Ts. Vassilev, and I. Penkov, 'The glass transition temperature of silicate and borate glasses', *Journal of Non-Crystalline Solids*, vol. 351, no. 6–7, pp. 472–476, Mar. 2005.
- [42] G. L. Paraschiv, F. Muñoz, L. R. Jensen, Y. Yue, and M. M. Smedskjaer, 'Impact of nitridation of metaphosphate glasses on liquid fragility', *Journal of Non-Crystalline Solids*, vol. 441, pp. 22–28, Jun. 2016.
- [43] R. Oueslati Omrani *et al.*, 'Structural and thermochemical properties of sodium magnesium phosphate glasses', *Journal of Alloys and Compounds*, vol. 632, pp. 766–771, May 2015.

- [44] J. J. Hudgens and S. W. Martin, 'Glass Transition and Infrared Spectra of Low-Alkali, Anhydrous Lithium Phosphate Glasses', *Journal of the American Ceramic Society*, vol. 76, no. 7, pp. 1691–1696, Jul. 1993.
- [45] P. Y. Shih, S. W. Yung, and T. S. Chin, 'FTIR and XPS studies of P2O5–Na2O–CuO glasses', *Journal of Non-Crystalline Solids*, vol. 244, no. 2–3, pp. 211–222, Mar. 1999.
- [46] C. Mugoni, M. Montorsi, C. Siligardi, and H. Jain, 'Electrical conductivity of copper lithium phosphate glasses', *Journal of Non-Crystalline Solids*, vol. 383, pp. 137–140, Jan. 2014.
- [47] J. A. Wilder and J. E. Shelby, 'Property Variation in Alkali Alkaline-Earth Metaphosphate Glasses', *Journal of the American Ceramic Society*, vol. 67, no. 6, pp. 438–444, Jun. 1984.
- [48] R. Yang, Y. Wang, X. Hao, J. Zhan, and S. Liu, 'Influence of alkali and alkali-earth metal oxide substitutions on the properties of lithium–iron–phosphate glasses', *Journal of Non-Crystalline Solids*, vol. 357, no. 10, pp. 2192–2196, May 2011.
- [49] T. Charpentier, N. Ollier, and H. Li, 'RE 2 O 3 -alkaline earth-aluminosilicate fiber glasses: Melt properties, crystallization, and the network structures', *Journal of Non-Crystalline Solids*, vol. 492, pp. 115–125, Jul. 2018.
- [50] A. Jha, S. Shen, and M. Naftaly, 'Structural origin of spectral broadening of 1.5- μ m emission in Er³⁺-doped tellurite glasses', p. 13.
- [51] N. Zotov *et al.*, 'Effects of MnO-doping on the structure of sodium metaphosphate glasses', *Zeitschrift für Naturforschung A*, vol. 58, no. 7–8, pp. 419–428, 2003.
- [52] U. Hoppe, G. Walter, R. Kranold, D. Stachel, and A. Barz, 'The dependence of structural peculiarities in binary phosphate glasses on their network modifier content', *Journal of Non-Crystalline Solids*, vol. 192–193, pp. 28–31, Dec. 1995.
- [53] G. Walter, U. Hoppe, J. Vogel, G. Carl, and P. Hartmann, 'The structure of zinc polyphosphate glass studied by diffraction methods and ³¹P NMR', *Journal of Non-Crystalline Solids*, vol. 333, no. 3, pp. 252–262, Mar. 2004.
- [54] K. Meyer, 'Characterization of the structure of binary zinc ultraphosphate glasses by infrared and Raman spectroscopy', *Journal of Non-Crystalline Solids*, vol. 209, no. 3, pp. 227–239, Feb. 1997.
- [55] S. Toyoda, S. Fujino, and K. Morinaga, 'Density, viscosity and surface tension of 50RO–50P2O5 (R: Mg, Ca, Sr, Ba, and Zn) glass melts', *Journal of Non-Crystalline Solids*, vol. 321, no. 3, pp. 169–174, Jul. 2003.
- [56] K. A. Matori, M. I. Sayyed, H. A. A. Sidek, M. H. M. Zaid, and V. P. Singh, 'Comprehensive study on physical, elastic and shielding properties of lead zinc phosphate glasses', *Journal of Non-Crystalline Solids*, vol. 457, pp. 97–103, Feb. 2017.

List of Figures

FIGURE 1 Q ^N SPECIES THAT CAN BE FOUND IN PHOSPHATE GLASSES.....	32
FIGURE 2 SCHEMATIC REPRESENTATION OF ZINC AND SODIUM METAPHOSPHATE GLASSES (LEFT) AND ZINC SODIUM POLYPHOSPHATE GLASSES (RIGHT).....	35
FIGURE 3 RAMAN SPECTRA OF NON-DOPED SODIUM METAPHOSPHATE GLASS (META-NA)	36
FIGURE 4 COMPARISON OF RAMAN SPECTRA OF NON-DOPED METAPHOSPHATE GLASSES: (A) REAL AND (B) NORMALIZED SPECTRA.....	37
FIGURE 5 ³¹ P NMR SPECTRUM DECONVOLUTION OF SODIUM METAPHOSPHATE GLASSES	39
FIGURE 6 RAMAN SPECTRA OF SODIUM ZINC POLYPHOSPHATE GLASS COMPARED TO SODIUM METAPHOSPHATE GLASS, NORMALIZATION BY MAXIMUM.....	40
FIGURE 7 ³¹ P NMR SPECTRA OF SINGLE NA AND NA-K MIXED ALKALI POLYPHOSPHATE GLASSES.....	41
FIGURE 8 ³¹ P NMR SPECTRUM DECONVOLUTION OF POLY-NA AND POLY-NA-K.....	42
FIGURE 9 RAMAN SPECTRA OF NON-DOPED AND EU DOPED SODIUM METAPHOSPHATE GLASSES, NORMALIZATION BY MAXIMUM.....	44
FIGURE 10 RAMAN SPECTRA OF NON-DOPED AND EU DOPED ZINC METAPHOSPHATE GLASSES, NORMALIZATION BY MAXIMUM.....	45
FIGURE 11 COMPARISON BETWEEN RAMAN SPECTRUM OF NON-DOPED AND EUROPIUM DOPED POLYPHOSPHATE GLASSES NORMALIZED BY MAXIMUM	45
FIGURE 12 RAMAN SPECTRUM OF EUROPIUM DOPED POLYPHOSPHATE GLASSES NORMALIZED MAXIMUM... ..	46
FIGURE 13 ³¹ P NMR SPECTRA OF NON-DOPED AND EU DOPED POLY-ZN-NA-(50/50:Q ¹ /Q ²) GLASS.	47
FIGURE 14 VOLUME-TEMPERATURE RELATIONSHIP FOR A GLASS FORMING SUBSTANCE.....	48
FIGURE 15 (A) BLOCK DIAGRAM OF DTA (RIGHT), TEMPERATURE CHANGE OF THE FURNACE, (B) THE REFERENCE, THE SAMPLE AND THE CHANGE IN TEMPERATURE DIFFERENCE (ΔT) AGAINST TIME DETECTED WITH THE DIFFERENTIAL THERMOCOUPLE.....	49
FIGURE 16 DTA CURVES OF RE DOPED AND NON-DOPED SODIUM POLYPHOSPHATE GLASSES.....	49

List of Tables

TABLE 1 NOMINAL COMPOSITION OF METAPHOSPHATE AND POLYPHOSPHATE GLASSES.....	31
TABLE 2 VIBRATIONAL FREQUENCIES (CM ⁻¹) IN METAPHOSPHATE GLASSES	36
TABLE 3 CHEMICAL SHIFTS, AREA AND RELATIVE PROPORTIONS (%) EXTRACTED FROM THE SIMULATION OF THE ³¹ P NMR SPECTRA.	39
TABLE 4 VIBRATIONAL FREQUENCIES (CM ⁻¹) OF THE POLYPHOSPHATE GLASSES	40
TABLE 5 CHEMICAL SHIFTS, FWHM AND RELATIVE PROPORTIONS (%) EXTRACTED FROM THE SIMULATION OF THE ³¹ P NMR SPECTRA.....	43
TABLE 6 CHEMICAL SHIFTS, FWHM AND RELATIVE PROPORTIONS (%) EXTRACTED FROM THE SIMULATION OF THE ³¹ P NMR SPECTRA OF NON-DOPED AND EU DOPED POLY-ZN-NA-(50/50:Q ¹ /Q ²)	47
TABLE 7 GLASS TRANSITION TEMPERATURES.....	50
TABLE 8 DENSITY VALUES OF THE DIFFERENT METAPHOSPHATE AND POLYPHOSPHATE GLASSES.....	52

Chapter 3

Molecular dynamics modelling of europium doped and non-doped metaphosphate and polyphosphate glasses

Chapter 3 Molecular dynamics modelling of europium doped and non-doped metaphosphate and polyphosphate glasses

1	Rare earth environment in phosphate glasses.....	59
2	Molecular Dynamics method	60
2.1	Molecular Dynamics simulation details	60
2.2	Analysis techniques	62
2.2.1	Partial Pair Distribution Functions.....	62
2.2.2	Accumulated coordination numbers.....	63
2.2.3	Partial and total structure factors	64
3	Molecular dynamic modeling of metaphosphate glasses with medium model (~ 2500 atoms) .	64
3.1	Molecular dynamic modeling of non-doped metaphosphate glasses	64
3.1.1	Image of models: Meta-Na vs Meta-Zn.....	65
3.1.2	Diffraction structure factor	65
3.1.3	Pair distribution function and coordination number	67
3.1.4	M-O correlations	71
3.2	Europium doped metaphosphate glasses.....	73
3.2.1	Image of models: Non-doped and Eu doped glass.....	74
3.2.2	Structure factors.....	75
3.2.3	Pair Distribution Functions and coordination number.....	76
4	Polyphosphate glasses with medium model (~ 2500 atoms).....	80
4.1	Images of models	80
4.2	Diffraction structure factors.....	81
4.3	Pair Distribution Functions and coordination number.....	81
5	Phosphate glasses with big model (~ 25000 atoms)	88
5.1	Images of models	89
5.2	Structure factors.....	91
5.3	Pair distribution function and coordination number	92

1 Rare earth environment in phosphate glasses

Many techniques are used to study the rare earth (RE) environment in RE doped phosphate glasses. Previous work in the literature used Extended X-Ray Absorption Fine Structure (EXAFS), Neutron Diffraction (ND) and Molecular Dynamic simulation (MD) to obtain information about the interatomic distances, types of surrounding atoms, coordination numbers and short range structural disorder.

The europium doped phosphate glasses have been presented in many papers and reviews and in this part I will focus on the results obtained under methods cited before.

Let's start with EXAFS and XRD techniques. The origin of EXAFS started with Kronig (1930) [1]. As a technique, it has advantages over x-ray diffraction in that it provides pair distribution functions containing only atomic correlations involving the atom whose absorption spectra is being probed. X-ray diffraction (XRD) leads to a composite radial distribution function in which all atom pairs in the material are represented, weighted by the product of their respective atomic numbers. The x-ray-diffraction results provide information on the general phosphate glass network, while the EXAFS is a direct probe of the local atomic environment of the RE atoms [2].

Meda et al. [3] studied the local environment of Eu^{3+} ions in zinc metaphosphate glasses ($0.9 \text{Zn}(\text{PO}_3)_2 - 0.1 \text{Eu}(\text{PO}_3)_3$) using XRD and the results indicate that the rare earth ions are surrounded on average by a polyhedron of about 7.4(2) oxygens at 2.36 Å and about 1.6(2) oxygens at 2.68 Å. Contrary to P-O distance and coordination number that do not change, there was a difference of coordination of the zinc ion in the doped and non-doped glasses (4.6 against 4.2 respectively) that could be explained by the substitution of an appreciable amount of Zn^{2+} by Eu^{3+} ions [3].

Bowron et al. [2] used a combination of XRD and EXAFS methods to determine the local environment of different rare earth ions in metaphosphate glasses $\text{R}(\text{PO}_3)_3$ (Pr, Nd, Eu, Gd, Tb and Ho) containing high concentrations of rare earth R^{3+} ions. The x-ray-diffraction results provide information on the general phosphate glass network thus it was established that the network is constructed from PO_4 tetrahedra. The P-O correlation was observed at 1.57 Å in agreement with Musinu's work [4]. The O-O distance has been determined to be 2.5 Å in non-doped glass [4] but the similarity of the distance of O-O and R-O cannot let to determine this distance [2].

On the other hand, the EXAFS is a direct probe of the local atomic environment of the RE atoms. The coordination number of the RE ions with oxygen is between 6 and 8 and the distances R-O decrease from 2.38 to 2.20 Å with increasing atomic number establishing a contraction of the RE ionic radii. However, the second R-O correlation proved to be more consistent between samples with an associated distance of between 3.8 and 4.1 Å, although the variation in coordination number is still large between 1 and 5 oxygens. In the case of europium doped glass, the coordination number $N_{\text{Eu-O}} = 7.6$ and the $R_{\text{Eu-O}} = 2.28$ Å [5],[6],[2],[7]. In the work of Anderson et al.[8], EXAFS technique has been used to study the lanthanide environment in RE doped metaphosphate glasses $\text{R}(\text{PO}_3)_3$ (R = La, Ce, Pr, Nd, Sm, Eu, Gd, Tb,

Dy, Ho, and Er) under variable temperature. The results indicate a decrease of the R-O distance implying a contraction of lanthanide ion in the glass matrix with increasing atomic number. This results are in accord with Bowron's work [5],[6]. The coordination number N_{RO} is intermediate between 6 and 7 and there is no significant change in R-O distance or N_{RO} with varying temperature between 79 and 293 K. There is no evidence of R-R correlation up to 4 Å whereas the R-P and the second R-O correlation are observed respectively at 3.3-3.6 Å and approximately 4 Å [8].

Moreover, Shikerkar et al.[9] examined the structure of RE doped glasses in presence of aluminium ((La₂O₃)₁₀(R₂O₃)₁₀(Al₂O₃)₅(P₂O₅)₇₅) with R representing the different lanthanide) using XRD and neutron diffraction and indicating that the basic PO₄ tetrahedral unit remains stable with an average P-O distance of 1.54 Å and a coordination number $N_{PO} = 4$. He also obtained a similar result with previous papers [5],[6],[8] concerning the lanthanide contraction and an average of N_{RO} between 6 and 8 [9].

Furthermore, Wada et al. (2004) used EXAFS to study the local environment and the polarization of Eu³⁺ ions in borate, silicate and phosphate glasses. The Eu-O distance decrease with increasing the alkali and alkali earth content in silicate and borate glasses contrary to phosphate glasses that the distance tended to be constant but the second Eu-O distance decreased [10].

2 Molecular Dynamics method

2.1 Molecular Dynamics simulation details

We studied in this chapter the molecular dynamic simulation of europium doped and non-doped metaphosphate glasses with comparison to zinc polyphosphate glasses (table 1).

Table 1 Glass composition

	P ₂ O ₅	K ₂ O	Na ₂ O	ZnO	Eu ₂ O ₃
Meta-Na	50		50		
Meta-Na-Eu	49.4		49.4		1.2
Meta-Zn	50			50	
Meta-Zn-Eu	49.4			49.4	1.2
Poly-Zn-Na	33.4		20	46.6	
Poly-Zn-Na-Eu	32.99		19.76	46.04	1.2
Poly-Zn-K	33.4	20		46.6	
Poly-Zn-K-Eu	32.99	19.76		46.04	1.2

In the literature, there are several interatomic potentials to simulate the structure of rare earth doped phosphate glasses and to choose the best potential, we tested three known potentials: Buckingham with three body potential (TBP) [11], Born Mayer Huggins with TBP [12] and Morse potential (no TBP) [13]. The choice of a good potential depends on several criteria:

- The coordination number defects of P-O and O-O correlations.
- The static X-ray and neutron diffraction structure factor $S(Q)$ with comparison to the experimental structure factor if it is available in the literature.
- The simulated pressure (from output file after room temperature simulation)
- The atomic distribution in the box (using MS Modeling or Oleox2)

After many tests of molecular dynamic simulation of europium doped and non-doped metaphosphate glasses with small (500 atoms) and medium size model (2500 atoms), it was found that the Buckingham potential (with TBP) is the best interatomic potential for our glasses. The functional form of the Buckingham potential used in this work is:

$$U(r) = A \exp(r/\rho) - C/r^6 \quad \text{Equation 1}$$

With A , ρ and C are the potential parameters.

We have used 60% of the formal charge: -1.2e for oxygen O, 3e for phosphorus P, 0.6e for sodium Na, 1.2e for zinc Zn and 1.8e for europium.

The potential parameters for the different atomic pairs were taken from previous work in the literature cited in the table 2:

Table 2 Buckingham interatomic potential parameters for different pair correlations.

Pair	A	ρ	C	Ref
P-O	27722.00	0.1819	86.860	[11]
Na-O	4383.76	0.2438	30.700	[1]
Eu-O	5950.52	0.2536	27.818	[14]
Zn-O	34131.1	0.1717	9.77	[15]
O-O	1844.00	0.3436	192.58	[11]

In the other hand, the three body potential of O-P-O and P-O-P bonds have the form:

$$V_{iji}(\theta) = \frac{1}{2} k_{iji} (\theta - \theta_{iji}) \quad \text{Equation 2}$$

With j is the element type of the center atoms and k_{iji} and θ_{iji} the potentials parameters of the TBP presented in the table 3 and was used for non-doped and Eu doped metaphosphate and polyphosphate glasses.

Table 3 Interatomic potential parameters of three body potentials TBP

	k_{iji} (ev)	θ_{iji} (°C)	Ref
P-O-P	3.0	135.58	[11]
O-P-O	3.5	109.47	[11]

To start the molecular dynamic simulation using DLPOLY software, we need to prepare three file:

- FIELD file: We should enter the number of atoms, the atomic mass and the charge of every species as well as the potential parameters.
- CONFIG file: In the MD simulation, the total number of atoms should be placed in a cubic box and we need to put the number of atoms, the cubic box size and the density of the glass. The densities of glasses were measured (in Institut de Physique de Globe de Paris IPGP) and compared with literature and all the information about the box size and the numbers of atoms was calculated and presented in table 4. The initial configuration has random positions for atoms which are moved apart to avoid overlap.

Table 4 Density, Box size and number of atoms used in MD simulation models for Eu doped and non-doped metaphosphate glasses.

	Density (g/cm ³)	Box size (Å)	Number of atoms						Tot Number
			O	P	Na	K	Zn	Eu	
Meta-Na	2.48	32.43	1500	500	500				2500
Meta-Na-Eu	2.58	32.34	1500	494	494			12	2500
Meta-Zn	2.87	31.85	1500	500			250		2250
Meta-Zn-Eu	2.89	32.79	1500	494			247	12	2253
Poly-Zn-Na	3.18	31.63	1454	416	249		290		2409
Poly-Zn-Na-Eu	3.26	31.75	1464	412	247		288	15	2426
Poly-Zn-K	3.06	32.76	1454	416		249	288		2409
Poly-Zn-K-Eu	3.16	32.75	1464	412		247	288	15	2426

- CONTROL file: In this part, we are interested in the temperature and duration of the MD modelling. In the first step of the MD simulation known as stage 0, the MD calculations were run at a low temperature of 1 K. For the duration we used 40000 time steps of 1 fs. In the second part and using the previous results from stage 0 "REVCON file" as a CONFIG file for stage 1, the system was cooled gradually from 3300 K to 300 K during 190000 time steps equilibration and then we collected the system statistics during 40000 time steps at 300 K from 190000 to 230000 time steps (See table 1 in annex).

2.2 Analysis techniques

2.2.1 Partial Pair Distribution Functions

The radial distribution function $g(r)$ is used for the material atomic distribution. It illustrates the probability to find an atom in a spherical shell of thickness dr at a distance r from a reference atom (fig 1). It is used to identify the average separation distance between two atoms in a pair correlation.

From $dn(r)$ that present the number of atoms at a distances between r and dr around a reference atom, we can evaluate the radial distribution function $g(r)$:

$$dn(r) = \frac{N}{V} g(r) \times 4 \pi r^2 dr \quad \text{Equation 3}$$

$$g(r) = \frac{dn(r)}{\rho^4 \pi r^2 dr} \quad \text{Equation 4}$$

Where V and N present the volume and the total number of atoms respectively, and ρ is number density.

In a multicomponent system containing more than one element type such as binary system which contains atoms of species i and j , the radial distribution function $g_{ij}(r)$ is defined given the probability to find nearest neighbor atom of type j at a distance r from atom of type i in the spherical shell dr . This function is presented as the following equation:

$$g_{ij}(r) = \frac{dn_{ij}(r)}{\rho_j 4 \pi r^2 dr} \quad \text{with } \rho_j = \frac{N_j}{V} = \frac{NC_j}{V} \quad \text{Equation 5}$$

Where ρ_j the number density of atoms j and c_j is the concentration of atoms species j .

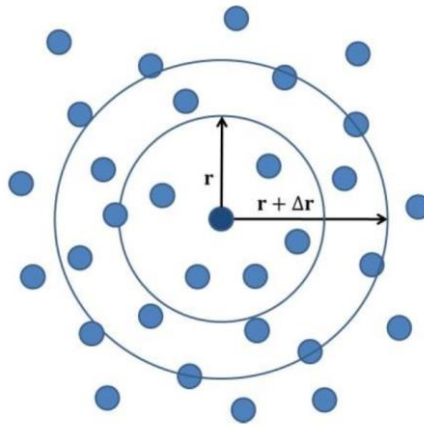


Figure 1 A shell of radius r and thickness Δr around a reference atom

The radial distribution function gives information about the local structure around different atoms species present in the system of interest. In that respect, the interatomic distance between two atoms is defined as the position of the first peak of the radial correlation distribution function.

Even more, the coordination number (CN) is calculated from the cut-off distance that is determined by the first minimum of the radial distribution function and is defined as the distance beyond which two atoms are not bonded.

2.2.2 Accumulated coordination numbers

The coordination number CN is defined as the average number of atoms j surrounding an atom of type i at up to distance $r_0 = \text{cut-off}$ and can be obtained from the integration of the pair distribution function.

We calculate the cumulative radial distribution function $n_{ij}(r)$ which is the integration from 0 to r of the number dn_{ij} in a thickness dr' and volume $4\pi r'^2 dr'$ as presented in the following equation:

$$n_{ij}(r) = \int_0^r 4\pi\rho_j g_{ij}(r')r'^2 dr' \quad \text{Equation 6}$$

Thereafter, we can compute the coordination number of j around i also known as CN (N_{ij}) from the integrating at a distance r_0 correspond to the cut-off distance:

$$CN = n_{ij}(r_0) = 4\pi \int_0^{r_0} \rho_j g_{ij}(r')r'^2 dr' \quad \text{Equation 7}$$

2.2.3 Partial and total structure factors

Structure factor can be obtained from scattering experiments using x-ray and neutron diffraction techniques to provide a direct measure of bond lengths and coordination numbers. These two methods are adopted as a probe to investigate the structure of glasses, thus X-rays scatter from electrons and neutrons scatter from the nucleus. On the other hand, the X-rays and neutron diffraction structure factors can be computed from the theory as used in MD simulation and compared to those from experimental techniques.

2.2.3.1 Neutron structure factors:

The neutron partial structure factor $S_{ij}(Q)$ are calculated by Fourier transformation of the pair distribution function $g_{ij}(r)$ using the following equation:

$$S_{ij}(Q) = 1 + \int_0^{R_{\max}} 4\pi r^2 (g_{ij}(r) - 1) \frac{\sin(Qr)}{Qr} dr \quad \text{Equation 8}$$

Where Q is the scattering vector and ρ_0 is the number density and R_{\max} is range over which $g_{ij}(r)$ is integrated. The total neutron structure factor $S_N(Q)$ can then evaluated from the partial structure factor:

$$S_N(Q) = (\sum_{i,j=1}^n c_i c_j b_i b_j)^{-1} \sum_{i,j=1}^n c_i c_j b_i b_j S_{ij}(Q) \quad \text{Equation 9}$$

Where c_i , c_j are the fraction of atoms type i and j respectively and b_i and b_j are the neutron scattering length for species i and j

2.2.3.2 X-ray structure factors

Similar to neutron diffraction, the x-ray structure factor can be computed as a sum partial structure factors using the same equation as neutron diffraction with replacing the b_i values with the atomic scattering factor $f_i(Q)$.

3 Molecular dynamic modeling of metaphosphate glasses with medium model (~ 2500 atoms)

3.1 Molecular dynamic modeling of non-doped metaphosphate glasses

The main emphasis of this part of work was to describe the short range order of sodium and zinc metaphosphate glasses using molecular dynamic simulation method.

3.1.1 Image of models: Meta-Na vs Meta-Zn

To start, we used the MS MODELING software to make the image representing the atoms distribution in sodium and zinc metaphosphate glasses after the MD simulations (Figure 2). As expected, the polyhedra are PO_4 tetrahedra network formers and the red spheres are oxygen atoms. The orange spheres (Left, fig.2) are sodium atoms that are modifiers and the grey spheres (Right, fig.2) are zinc that are modifiers and formers. Thus, the network modifier as Na forms weak bonds to oxygen (< 60 kcal) in contrast to the intermediate oxide as ZnO that have a higher bond strength in the range of 60-80 kcal that can intervene as network formers [16].

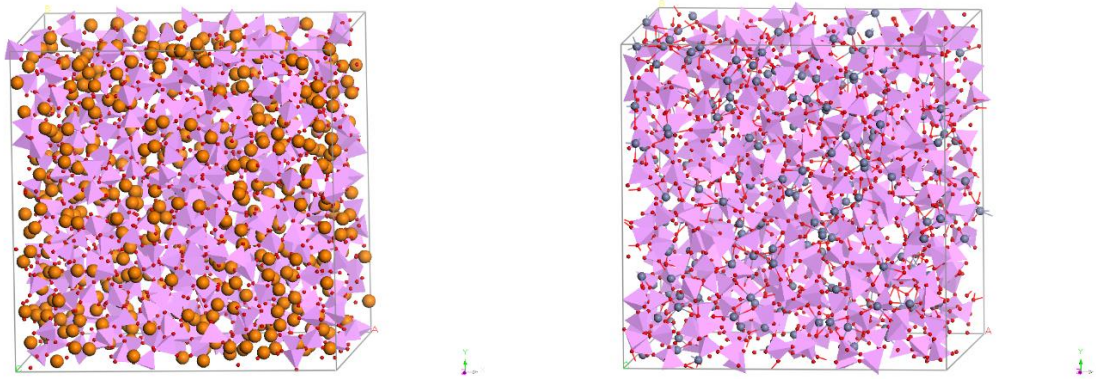


Figure 2 Image of MD models of Meta-Na (left) and Meta-Zn (right): red spheres are oxygen O, tetrahedra are PO_4 , orange spheres are sodium Na, grey spheres are zinc Zn.

3.1.2 Diffraction structure factor

In addition, we have determined the X-ray and neutron diffraction structure factors $S(Q)$ from the MD models using the Interactive Structure Analysis of Amorphous and Crystalline Systems (I.S.A.A.C.S) program. Comparing between the glass models in this work and neutron and X-rays diffraction experiments from literature [17]–[19], the structure factors $S_N(Q)$ and $S_X(Q)$ for sodium metaphosphate Meta-Na and zinc metaphosphate Meta-Zn are shown in figure 3 and 4 respectively. The $S(Q)$ for models are in fair agreement with experiments even if there is a dissimilarity in peak signals and positions. There is less good agreement with $S(Q)$ from X-ray diffraction (fig 3.b and 4.b) because the $S_X(Q)$ is more impacted by the medium range order correlated with the distribution of cations [11]. On the other hand, $S_N(Q)$ is more impacted by short range order associated with the distribution of oxygen. Another reason for the difference between the simulation models and experiments that the simulated glass structure has not annealed as well as the experimental structure maybe due to the very rapid quench that is imposed by the simulation model [20].

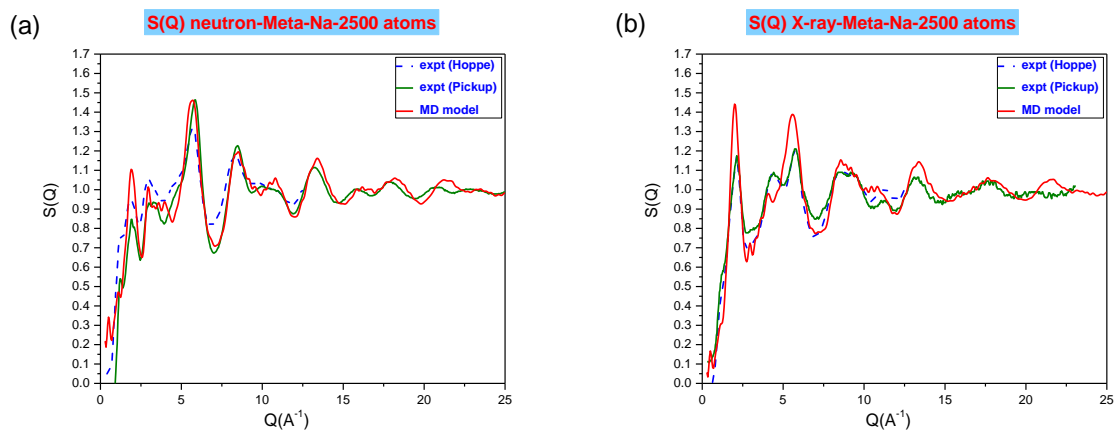


Figure 3 Neutron (a) and X-ray (b) diffraction structure factors $S(Q)$ from MD simulation (red lines) and experiments (green [7] and broken lines [8]) for non-doped sodium metaphosphate glass.

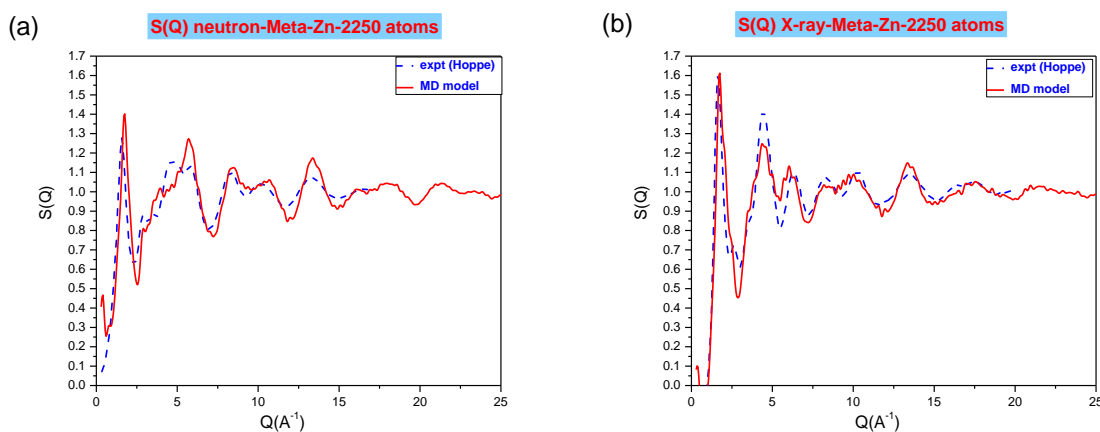


Figure 4 Neutron (a) and X-ray (b) diffraction structure factors $S(Q)$ from MD simulation (red lines) and experiments (broken lines [6]) for non-doped zinc metaphosphate glass.

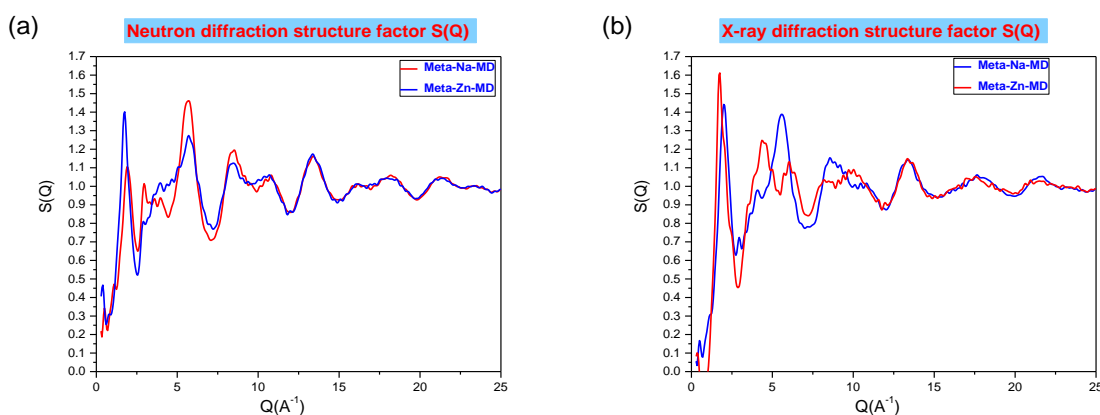


Figure 5 Neutron (a) and X-ray (b) diffraction structure factors $S(Q)$ from MD simulation for non-doped zinc and sodium metaphosphate glasses

3.1.3 Pair distribution function and coordination number

Generally, for amorphous material, $g(r)$ displays short-range order of major peak close to the average interatomic distance of neighbour atoms and less pronounced oscillating peaks at larger distances. Above all, to determine the partial pair distribution function $g_{ij}(r)$ between different correlations where i and j present the elements types of atoms, we used the XANAL program (fig. 6 and 7). The cumulative distribution functions $CN_{ij}(r)$ are displayed in figure 8. Moreover, the nearest neighbour distances R_{ij} and coordination numbers N_{ij} are reported in tables 5,6 and 7 for P-O, P-P, O-O, M-O, M-P and M-P pairs (where M = Zn, Na).

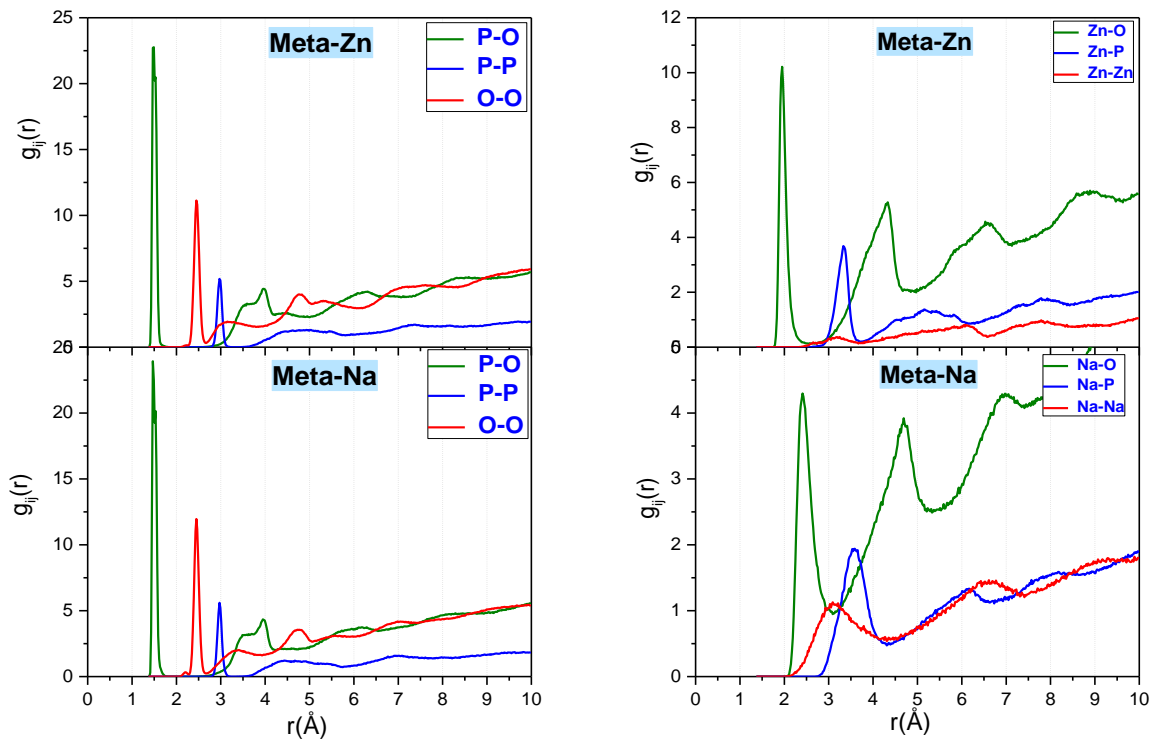


Figure 6 Partial pair distribution function $g_{ij}(r)$ for MD simulation of zinc metaphosphate glass (Top) and sodium metaphosphate glass (Bottom). (P-O, P-P and O-O pair distribution functions (left); M-O, M-P and M-M distribution functions (right)) (Medium model MM)

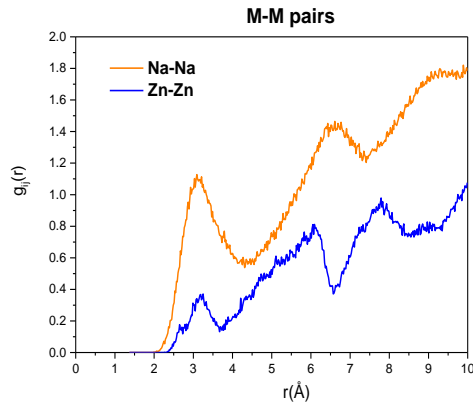


Figure 7 Comparison of M-M pair distribution function $g_{MM}(r)$ for MD simulation of zinc and sodium metaphosphate glass

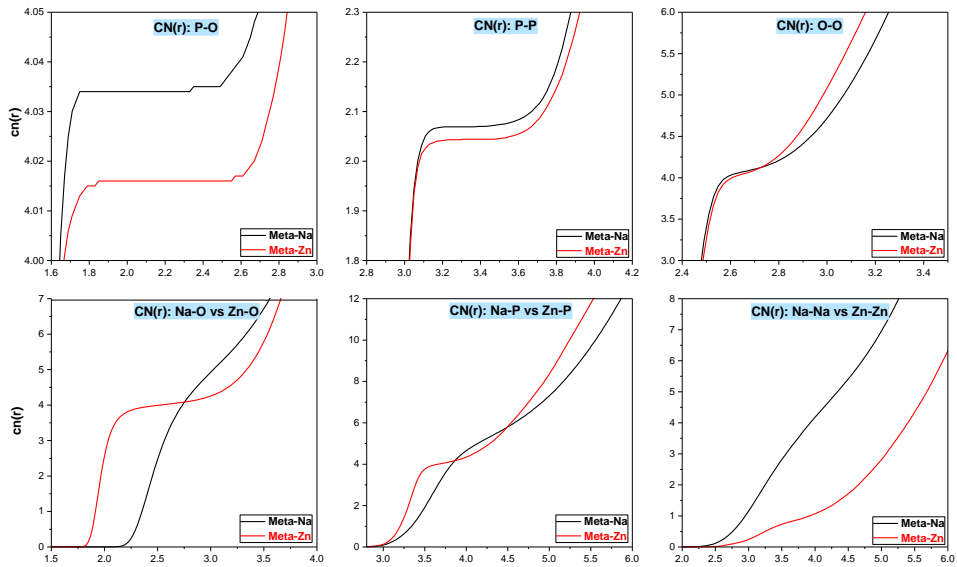


Figure 8 Cumulative distribution functions $CN_{ij}(r)$ for different atomic correlations present in Meta-Zn and Meta-Na (medium models MM)

Table 5 Nearest neighbor distances R_{ij} , and coordination number N_{ij} of P-O, P-P and O-O correlations from MD simulations compared to experiments and previous MD models in metaphosphate glasses Meta-Na and Meta-Zn. (Medium Model MM)

Glass	P-O		P-P		O-O		Method	Ref
	$R_{PO}(\text{Å})$	N_{PO}	$R_{PP}(\text{Å})$	N_{PP}	$R_{OO}(\text{Å})$	N_{OO}		
					Cutoff = 2.65 Å			
Meta-Na	1.50	4.03	2.97	2.06	2.45	4.07	MD	This work
	1.54	3.95	2.93	2.08	2.52	3.96	XRD-ND	[17],[18]
	1.5	4.00	2.99	2	2.53	4.00	MD	[11]
Meta-Zn	1.51	4.01	2.97	2.04	2.45	4.04	MD	This work
	1.53	4.19	2.98	1.87	2.48	4.53	XRD	[21]
	1.49				2.47		MD	[22]

Table 6 Nearest neighbor distances R_{ij} , and coordination number N_{ij} of Na-O, Na-P and Na-Na correlations from MD simulations compared to experiments and previous MD models in sodium metaphosphate glasses (Meta-Na). (Medium Model MM).

Glass	Na-O		Na-P		Na-Na		Method	Ref
	$R_{NaO}(\text{Å})$	N_{NaO}	$R_{NaP}(\text{Å})$	N_{NaP}	$R_{NaNa}(\text{Å})$	N_{NaNa}		
	Cut-off 3.05		Cut-off 4.20		Cut-off 4.80			
Meta-Na	2.42	5.07	3.59	5.13	3.09	6.27	MD	This work
	2.39	5.08					XRD-ND	[17]
	2.38	4.96	3.56	4.7		7.00	MD	[11]
		5.10		5.9		4.80	RMC	[23]

Table 7 Nearest neighbor distances R_{ij} , and coordination number N_{ij} of Zn-O, Zn-P and Zn-Zn correlations from MD simulations compared to experiments and previous MD models in sodium metaphosphate glasses (Meta-Zn). (Medium Model MM).

Glass	Zn-O		Zn-P		Zn-Zn		Method	Ref
	$R_{ZnO}(\text{Å})$	N_{ZnO}	$R_{ZnP}(\text{Å})$	N_{ZnP}	$R_{ZnZn}(\text{Å})$	N_{ZnZn}		
	Cut-off 2.50		Cut-off 3.70		Cut-off 4.00			
Meta-Zn	1.95	3.98	3.33	4.03	3.25	1.07	MD	This work
	1.96	4.87	3.25	4.09	3.25	1.36	XRD	[21]
	1.95	4.00					XRD	[23]
	1.95	6 (50%)					XRD	[4]
	1.99	3.7					MD	[22]

3.1.3.1 The phosphorus-oxygen correlation

The P-O pair distribution function are shown in the bottom and the top of figure 6 for sodium and zinc metaphosphate glass respectively. The two partial pair distribution functions (PDFs) exhibit a sharp and well defined first peak followed by a decrease to null value demonstrating a clear separation between the first and second coordination shells.

The P-O nearest neighbours distance determined from the first peak, was found to be 1.50 and 1.51 Å (Table 5) for Meta-Na and Meta-Zn with cutoff at 2Å.

The P-O distance for this model are in good agreement with experimental results found in literature. Thus, Hoppe et al.[17] has reported a P-O nearest neighbor distance as 1.54 Å for sodium metaphosphate glass using X-ray (XRD) and Neutron diffraction (ND). The P-O distance for zinc metaphosphate glass was found to be 1.53 Å as determined by Maturaba et al. [21] using XRD experiment (Table 5). Similar results were obtained by Al Hasni [11] et al. and Tischendorf et al. [22] using MD method.

Moreover, the split first peak of $g_{PO}(r)$ shows a two well separated peaks located at approximately 1.47 and 1.53 Å which are attributed to bonds of phosphorus atoms to non-bridging oxygen P-NBO and bridging oxygen P-BO successively and similarly to as expected from neutron diffraction [17]. In this way, the percentage of bridging and non-bridging oxygen in metaphosphate glasses are reported in Table 9 and are in agreement with theory.

Even more, the full width at half maximum FWHM of the first peak are also extracted to be 0.1 Å for both glasses. This distribution combined with the clear separation between the first and second peak coordination shells indicate a presence of high degree of short range order in the phosphate network.

The average coordination number N_{PO} for both sodium and zinc glasses were calculated from the cumulative coordination number $N_{PO}(r)$ using the cutoff radius of 2 Å which correspond to the first minimum of the distribution function of the first peak and were found to be 4.03 and 4.01 as expected by ND and X-rays studies [17], [21]. In this way and as shown in table 9, over 96.5% of phosphorus ions are four coordinated which consists of PO_4 tetrahedra units linked together in chains to form the basic phosphate network units in phosphate glasses. In theory, a metaphosphate has 100% PO_4 tetrahedra. So the average N_{PO} of about 4.03 instead of 4 indicate a slight defect in the molecular dynamic model.

3.1.3.2 The phosphorus-phosphorus and oxygen-oxygen correlations

P-P correlations

The first peak in $g_{PP}(r)$ at ~ 2.97 Å (cutoff = 3.3 Å) for sodium and zinc glasses represents the P-P nearest neighbors in phosphate network.

The average P-P coordination of 2 for Meta-Na and Meta-Zn indicates that there are two phosphorus atoms surrounding each phosphorus atoms within a cutoff radius of 3.3 Å. This value of 2 is expected due to metaphosphate having Q^2 units and has been confirmed by diffraction method [17], [21]. The similarity of the P-P distances and coordination number for the Na and Zn metaphosphate glasses indicates that the basic phosphate network is unaffected by the type of cation present in glasses.

O-O correlations

The O-O interionic bond distance were found to be 2.45 Å (cutoff = 2.65 Å) due to O-P-O configurations and the partial pair distribution function for both glasses exhibited in figure 6

show that the first peak does not return to a null values indicating some overlap between the first and the second coordination shells. The model values of R_{OO} are in the range of [0.03 - 0.1 Å] shorter than the diffraction results of 2.55 and 2.48 Å for Meta-Na and Meta-Zn successively (see table 5) and this can be due to the potential parameters used in this models. The cumulative distribution functions $n_{OO}(r)$ for O-O pair (fig. 8) show a different behavior in large radius that can indicate the small effect of the type of cation modifier in the second nearest environment of the basic phosphate network whereas the average coordination number is found to be about four for the two glasses. These results are in excellent agreement with experimental results for Meta-Na [17] however the number $n_{OO}(r)$ of 4.5 for Zn metaphosphate glass using XRD method was reported by Maturaba et al. [21] and is clearly different compared to this work. This value of 4.5 is probably unreliable.

3.1.3.3 Coordination environment of the network modifier (Zn and Na)

This part will discuss the short range of the modifier ions and the effect of the network modifying cations on the structure of the two metaphosphate glasses.

The different modifiers atoms present in the two glasses will result in different local environment around the modifier ions such as the nearest neighbours distance and coordination number.

In typical cases, the cutoff for the first coordination shell is indicated by the null value in the partial pair distribution function between the first and second coordination peaks. Whereas in the case of modifiers cations, peaks of M-O, M-P and M-M PDFs don't return to the null values indicating some overlap between the first and second coordination shells. Thus the cutoff distances were chosen at the minimums in the PDF between the first and second peaks, and will change for each cation.

3.1.4 M-O correlations

The metal-oxygen (M-O) pair and cumulative distribution functions were investigated and presented in figure 6 and 8 establishing the effect of the cation modifiers on the metaphosphate glass structure. The nearest neighbours distance were determined to be 2.42 Å for Na-O and 1.95 Å for Zn-O. This shift to shorter distance for Meta-Zn is due to the smaller ionic radius of zinc ions ($r_{Zn} \sim 0.88$ Å) compared to sodium ions ($r_{Na} \sim 1.16$ Å) as well as to higher electronegativity and bond strengths of zinc [11],[20].

Stanworth et al [24] reported that the electronegativity of the cations which are intermediates (network forming and modifying in the same time) as zinc is in the range of 2 compared to glass network modifier (near 1). Sun et al. [16] reported in his model that network modifier as Na forms weak bonds to oxygen (< 60 kcal) in contrast to the intermediate oxide as ZnO that have a higher bond strength in the range of 60-80kcal. Moreover, the divalent cations make stronger cross-links between the phosphate chains compared to monovalent cation that tends to bonds more to one chains.

The M-O average coordination number from the MD simulation as shown in table 6 and 7 was found to be 5.1 using cutoff of 3.07 Å for Meta-Na. The N_{ZnO} was determined to be 3.9 for Meta-Zn using cutoff of 2.7 Å.

The M-O coordination number N_{MO} play a critical role. However, this number is not well defined in the literature. Thus, Masturaba et al [21] found this number at about 4.8 for zinc metaphosphate glass using XRD experiment. Hoppe et al. [23] found this number at 4.0 for the same glass. For sodium metaphosphate glass, there is a good accord between this model and experimental results of Hoppe et al. [17] who reported this number N_{NaO} as 5 using XRD and ND methods. This larger coordination number satisfied the Zachariasen's criteria [25]. Thus Na atoms used as network modifier to break the linkages between PO_4 tetrahedra and increase the number of non-bridging oxygen NBO.

According to Sun's criteria (1947), Zn acts as an intermediate cation that can intervene as a network former. Hoppe et al.[23] explains this contribution in his model by the formation of ZnO_4 tetrahedra corner-linked with PO_4 tetrahedra in zinc metaphosphate glass. According to requirement of charge compensation, the NBO are favored for M-O coordination. The NBO atoms can occupy sites in Zn-NBO-P bridges leading to the fill of the space less efficiently, even less than in sodium metaphosphate glass. Thus, **Zn atoms tends to have small coordination number about four differing to the modifier atoms in agreement with Zacharias's model** [25].

M-P correlations

The nearest neighbor distance R_{MP} and the coordination number N_{MP} are presented in tables 6 and 7 and confirms previous conclusion for M-P stated in this work.

M-M correlations

The metal-metal (M-M) distribution function in these models are displayed in figure 6. There is a maxima of the first peak in $g_{MM}(r)$ around 3.09 Å for Meta-Na and 3.25 Å for Meta-Zn. Furthermore, the MD simulation shows that the environment of the Zn-Zn correlation differs significantly from that of Na-Na correlation (fig. 7).

In order to study the M-M coordination number the $n_{MM}(r)$ are further analyzed in figure 8 and tables 6 and 7. There is a clearly difference in the cumulative distribution function and the N_{MM} was found to be 6.27 (cutoff = 4.8 Å) for Na-Na correlations. This is in coherence with the value of 7 determined by Al Hasni [11] using MD simulations. In the other hand, the N_{ZnZn} have a value of 1.07 conform to results from XRD experiment [21].

As reported et al. [23] in his model, the first peak of $g_{NaNa}(r)$ is due to the MO_n polyhedral sharing common bridging oxygen neighbours. In case of sodium metaphosphate glass the N_{NaNa} coordination number strongly increased due to the growing deficiencies of bridging oxygens BOs.

As discussed before, the zinc metaphosphate structure is formed of corner linked PO_4 and ZnO_4 tetrahedra and this can explains the low coordination number of Zn-Zn correlations.

Even more, we note that Meta-Na has $2 \times \text{Na}$ compared to Zn in Meta-Zn so naively we would expect N_{NaNa} to be $2 \times$ value of N_{ZnZn} . For Na with ionic charge +1, each Na-O-P neighbours is involving another Na to balance ionic charge of -2 on oxygen. So we expect N_{NaNa} to be similar to N_{NaO} .

Instead for Zn with ionic charge +2, each Zn-O-P neighbor usually does not involve another Zn. So we expect N_{NaNa} to be closer to zero.

Table 8 Q^n distributions from MD simulations models and ^{31}P NMR experiment.

MD Method						
Sample/ Rel.prop./%	Q^0	Q^1	Q^2	Q^3	Q^4	Q^5
Meta-Na	1.80	22.76	48.64	22.76	1.64	2.40
Meta-Zn	1.80	22.76	48.64	22.76	1.64	2.40
NMR Method						
Meta-Na	1.29	4.60	94.11	0.00	0.00	

Table 9 Coordination-number distribution for phosphorus and oxygen atoms in metaphosphate glasses (Medium Model MM)

	Coordination-Number (%)		
Phosphorus			
	CN = 4	CN = 5	Average CN
Meta-Na	96.560	3.440	4.03
Meta-Zn	98.422	1.578	4.01
Oxygen			
	CN = 1	CN = 2	
Meta-Na	65.520	34.480	
Meta-Zn	65.741	34.059	

3.2 Europium doped metaphosphate glasses

In this part of chapter, we are interested to interpret the results obtained from molecular dynamics simulations for europium doped zinc and sodium metaphosphate glasses. In particular, we compared the nearest neighbours distance and coordination number of different atomic correlations P-O, P-P, O-O, M-O, M-P and M-M between non-doped and europium doped glasses and more precisely the RE doping effect in the structure and the local environment around modifier ions.

The molecular dynamic simulation used in this section used a medium model with 2500 atoms. This model is unreliable to determine precisely the local environment around lanthanide ions by reason of the few number of europium atoms (15 atoms) (Table 4). In this regard, we delayed the interpretation of the local environment around the europium ions until the last section of this chapter using big models with about 25000 atoms.

Figure 9 and 10 exhibit the images of the MD models of non-doped and europium doped sodium and zinc metaphosphate glasses successively. The images were created using MS MODELING software and present the distribution of the different atoms presented in glasses.

Figure 11 and 12 compared the neutron and X-ray diffraction factors $S(Q)$ respectively extracted from the MD simulation for non-doped and Eu doped glasses that we observe a small effect due to small amount of Eu_2O_3 .

The radial pair distribution function $g_{ij}(r)$ for the different atomic correlations P-O, P-P, O-O, M-O, M-P and M-M are presented in figure 13.

Afterward, the cumulative distribution functions $n_{ij}(r)$ are shown in figure 14. In that regard the nearest neighbours distance R_{ij} and the coordination number N_{ij} are outlined in table 10,11 and 12.

3.2.1 Image of models: Non-doped and Eu doped glass

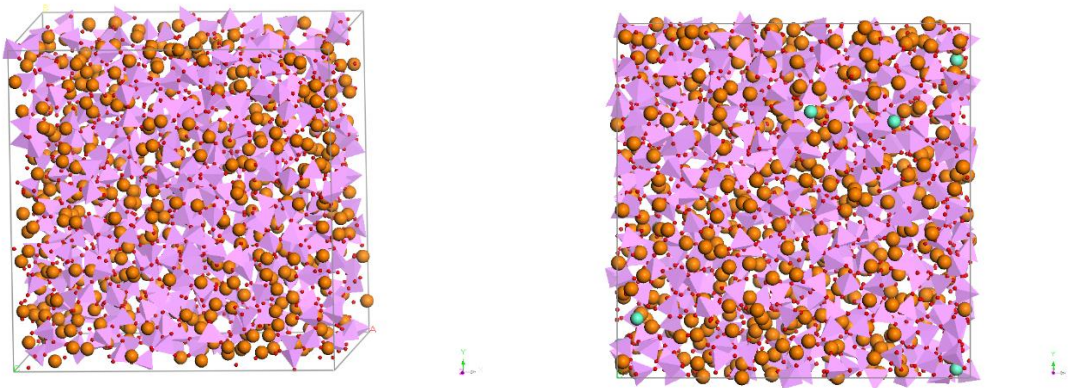


Figure 9 Image of MD models of Meta-Na (left) and Meta-Na-Eu (right): red spheres are oxygen O, tetrahedra are PO_4 , orange spheres are sodium Na and sky blue spheres are europium Eu.

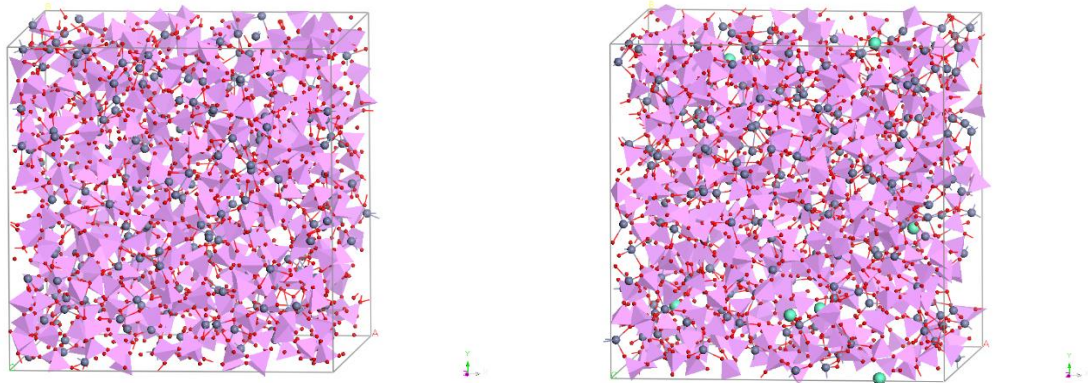


Figure 10 Image of MD models of Meta-Zn (left) and Meta-Zn-Eu (right): red spheres are oxygen O, tetrahedra are PO_4 , grey spheres are zinc Zn and sky blue spheres are europium Eu.

3.2.2 Structure factors

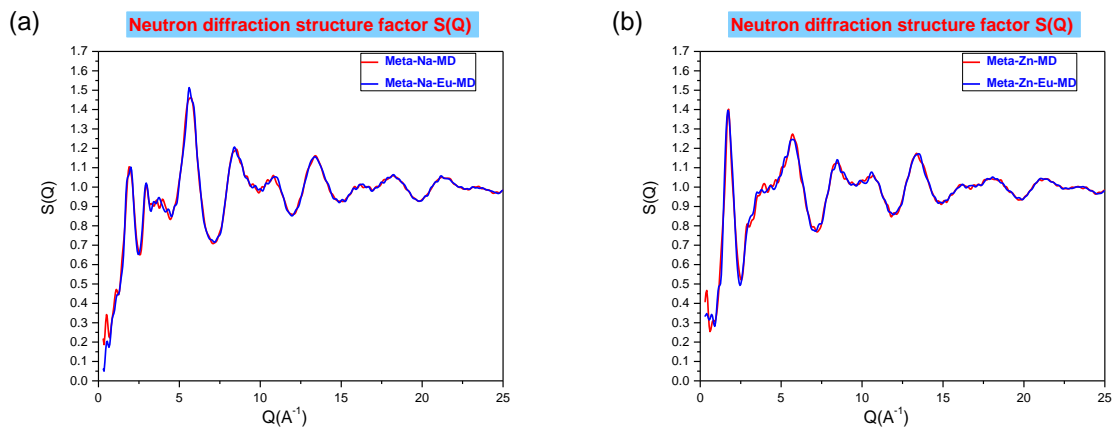


Figure 11 Neutron diffraction structure factors $S(Q)$ from MD simulation for non-doped and europium doped sodium (a) and zinc (b) metaphosphate glasses.

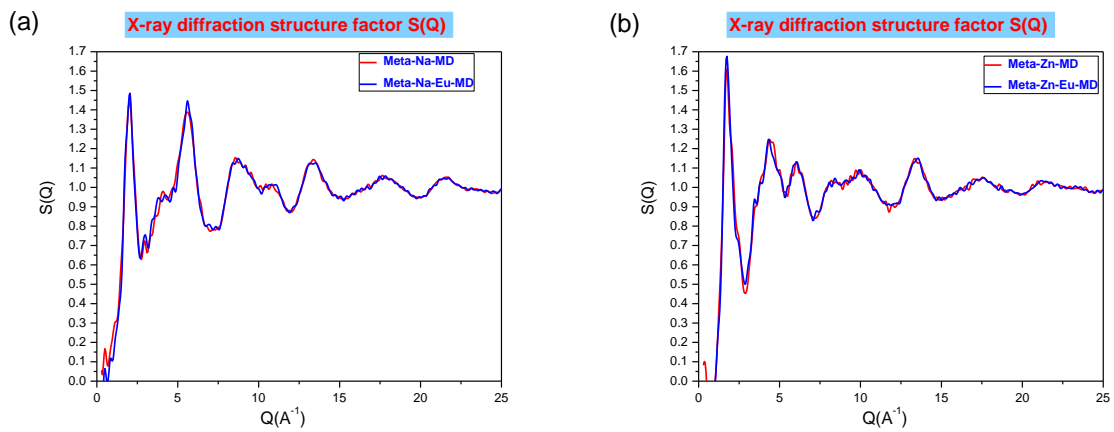


Figure 12 X-ray diffraction structure factors $S(Q)$ from MD simulation for non-doped and europium doped sodium (a) and zinc (b) metaphosphate glasses.

3.2.3 Pair Distribution Functions and coordination number

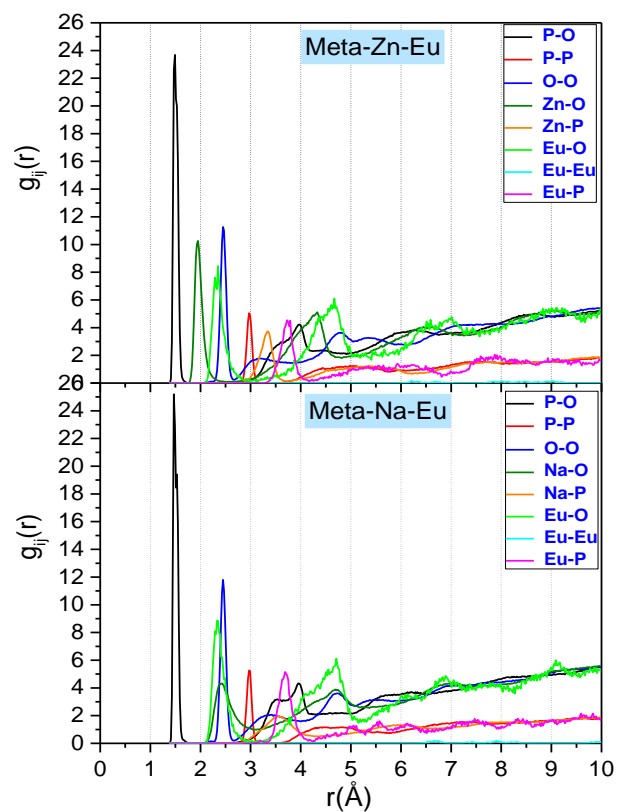


Figure 13 Partial pair distribution function $g_{ij}(r)$ for MD simulation of Meta-Zn-Eu (above) and Meta-Na-Eu (below).

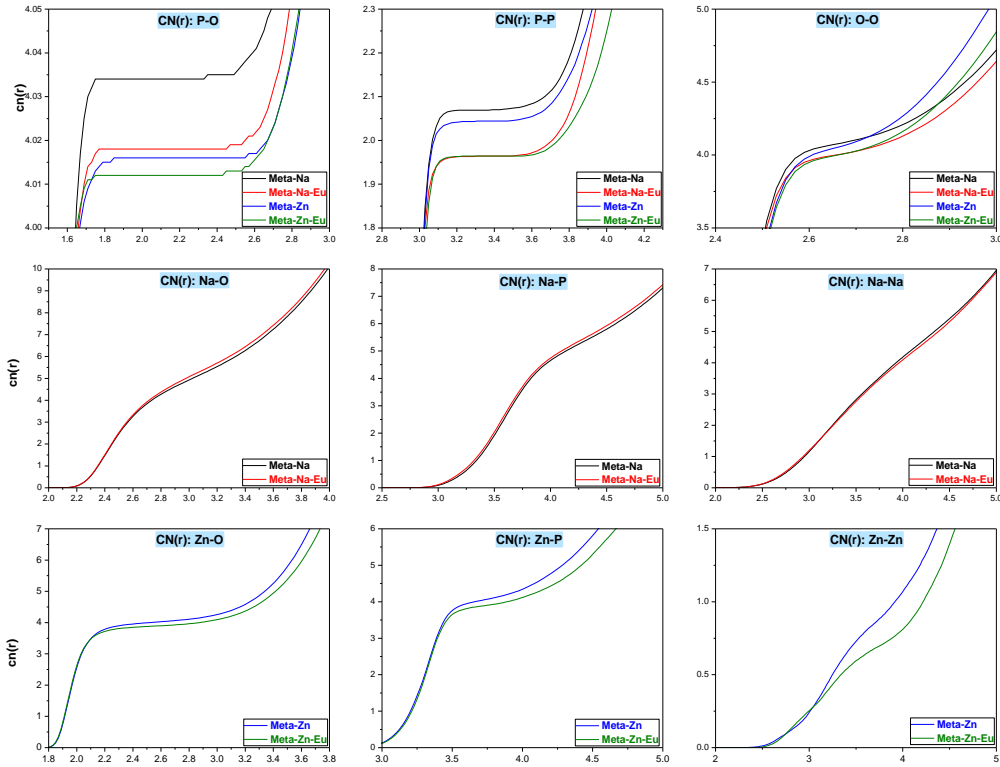


Figure 14 Cumulative coordination number $CN_{ij}(r)$ for MD simulation of Meta-Zn-Eu, Meta-Na-Eu, Meta-Zn and Meta-Na (Medium Model MM)

P-O, P-P and O-O correlations

As reported in figure 13 the P-O, P-P and O-O pair distribution functions showed no significant change in the nearest neighbor distance when doping with europium. However the cumulative distribution function $CN_{ij}(r)$ display a smaller decrease of N_{PP} and N_{OO} in the range of ~ 0.1 for Eu doped glasses (fig. 14 and table 10). This is because adding a small amount of Eu_2O_3 is increasing modifier and non-bridging oxygens.

M-O, M-P and M-M correlations

We studied in this part the doping europium effect in the local environment around cations modifier (Zn, Na) in zinc and sodium metaphosphate glasses.

Starting with the sodium environment, the PDFs (fig. 13) showed no change in the nearest neighbours distance for Na-O, Na-P and Na-Na pairs and the R_{ij} value are reported in table 11 and 12. In contrast, there is a small increase of coordination number N_{NaO} and N_{NaP} following by a decrease of N_{NaNa} as clearly obvious in the cumulative coordination function $n_{ij}(r)$ seen in figure 14.

For europium doped zinc metaphosphate glass, the results extracted from the MD model indicates no significant change in the distance of Zn-O and Zn-P pairs compared to non-doped glass. The nearest distance for Zn-Zn correlation slightly decreases from 3.25 \AA in non-doped glass to about 3.16 \AA when doping europium.

Instead the cumulative coordination number functions $n_{ij}(r)$ showed a change in coordination environment when doping europium. Thus, the n_{ZnO} value undergoes a slight decrease from 3.98 to 3.87 in non-doped and RE doped glass respectively. The same behavior is proved for Zn-P and Zn-Zn pairs. This results is contradictory with Medda et al.'s work [3] that studied the local environment of Eu^{3+} ions in zinc metaphosphate glasses ($0.9 Zn(PO_3)_2 \cdot 0.1 Eu(PO_3)_3$) using X-ray diffraction XRD. The results indicate that the rare earth ions surrounded an average by a polyhedron of about 7.4(2) oxygens at 2.36 Å and about 1.6(2) oxygens at 2.68 Å. Contrary to P-O distance and coordination number that come out very close, there was a difference of coordination of the zinc ion in the non-doped and Eu glasses (4.2 against 4.6) that could be explained by the substitution of an appreciable amount of Zn^{2+} by Eu^{3+} ions.

Table 10 Nearest neighbor distances R_{ij} , and coordination number N_{ij} of P-O, P-P and O-O correlations from MD simulations in non-doped and Eu doped metaphosphate glasses: Meta-Na, Meta-Zn, Meta-Na-Eu and Meta-Zn-Eu (Medium Model MM)

Glass	P-O		P-P		O-O	
	$R_{PO}(\text{Å})$	N_{PO}	$R_{PP}(\text{Å})$	N_{PP}	$R_{OO}(\text{Å})$	N_{OO}
					Cut-off = 2.65 Å	
Meta-Na	1.50	4.034	2.97	2.06	2.45	4.07
Meta-Zn	1.51	4.017	2.97	2.04	2.45	4.04
Meta-Na-Eu	1.50	4.015	2.97	1.96	2.45	3.99
Meta-Zn-Eu	1.51	4.012	2.97	1.96	2.45	3.99

Table 11 Nearest neighbor distances R_{ij} , and coordination number N_{ij} of Na-O, Na-P and Na-Na correlations from MD simulations in non-doped and Eu doped sodium metaphosphate glasses: Meta-Na and Meta-Na-Eu (Medium Model MM).

Glass	Na-O		Na-P		Na-Na	
	$R_{NaO}(\text{Å})$	N_{NaO}	$R_{NaP}(\text{Å})$	N_{NaP}	$R_{NaNa}(\text{Å})$	N_{NaNa}
	Cut-off 3.05 Å		Cut-off 4.20 Å		Cut-off 4.80 Å	
Meta-Na	2.42	5.07	3.59	5.13	3.09	6.27
Meta-Na-Eu	2.43	5.22	3.57	5.23	3.11	6.21

Table 12 Nearest neighbor distances R_{ij} , and coordination number N_{ij} of Zn-O, Zn-P and Zn-Zn correlations from MD simulations in non-doped and Eu doped zinc metaphosphate glasses: Meta-Na and Meta-Na-Eu (Medium Model MM).

Glass	Zn-O		Zn-P		Zn-Zn	
	$R_{ZnO}(\text{Å})$	N_{ZnO}	$R_{ZnP}(\text{Å})$	N_{ZnP}	$R_{ZnZn}(\text{Å})$	N_{ZnZn}
	Cut-off 2.50 Å		Cut-off 3.70 Å		Cut-off 4 Å	
Meta-Zn	1.95	3.98	3.33	4.03	3.25	1.07
Meta-Zn-Eu	1.95	3.87	3.35	3.87	3.16	0.82

Table 13 Q^n distribution for phosphorus atoms in non-doped and Eu doped metaphosphate glass from MD simulations models (MM)

MD simulation (MM)						
Sample/Rel.	Q^0	Q^1	Q^2	Q^3	Q^4	Q^5
Meta-Na	1.80	22.76	48.64	22.76	1.64	2.40
Meta-Na-Eu	0.81	25.10	54.65	16.40	2.42	0.60
Meta-Zn	1.80	22.76	48.64	22.76	1.64	2.40
Meta-Zn-Eu	1.21	25.91	51.41	19.17	1.87	0.40

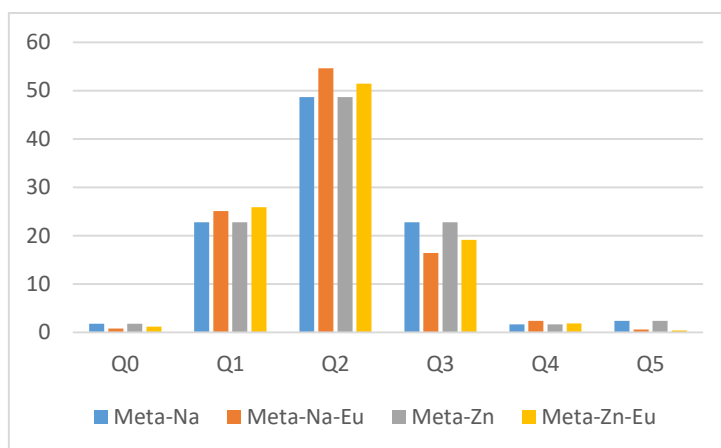


Figure 15 Q^n distributions from MD simulations models

Table 14 Coordination-number distribution for Phosphorus atoms in metaphosphate glasses (Medium Model MM)

	Coordination-Number (%)		Average CN
	4	5	
Meta-Na	96.560	3.440	4.03
Meta-Na-Eu	98.180	1.820	4.01
Meta-Zn	98.422	1.578	4.01
Meta-Zn-Eu	98.860	1.140	4.01

- There is a small increase of coordination number N_{NaO} and N_{NaP} following by a decrease of N_{NaNa} in sodium metaphosphate glass when it doped with europium.
- The n_{ZnO} , n_{ZnP} , n_{ZnZn} value undergoes a slight decrease in RE doped zinc metaphosphate glass.

4 Polyphosphate glasses with medium model (~ 2500 atoms)

Short and medium range order has been investigated in non-doped and europium doped polyphosphate glasses with composition $20M_2O-46.6ZnO-33.4P_2O_5$ and $19.7M_2O-46ZnO-33P_2O_5-1.2Eu_2O_3$ respectively ($M=Zn,Na$). MD models with medium number of atoms (~2500 atoms) have been used to study the cation environment and the effect of doping europium in the glass network as well as the local environment around zinc and alkali ions present in these glasses. The nearest neighbour distances and coordination number of different atomic correlations are compared with results obtained for zinc and sodium metaphosphate glasses to better understand the role of modifier and intermediate ions in the structure and local environment around cations.

4.1 Images of models

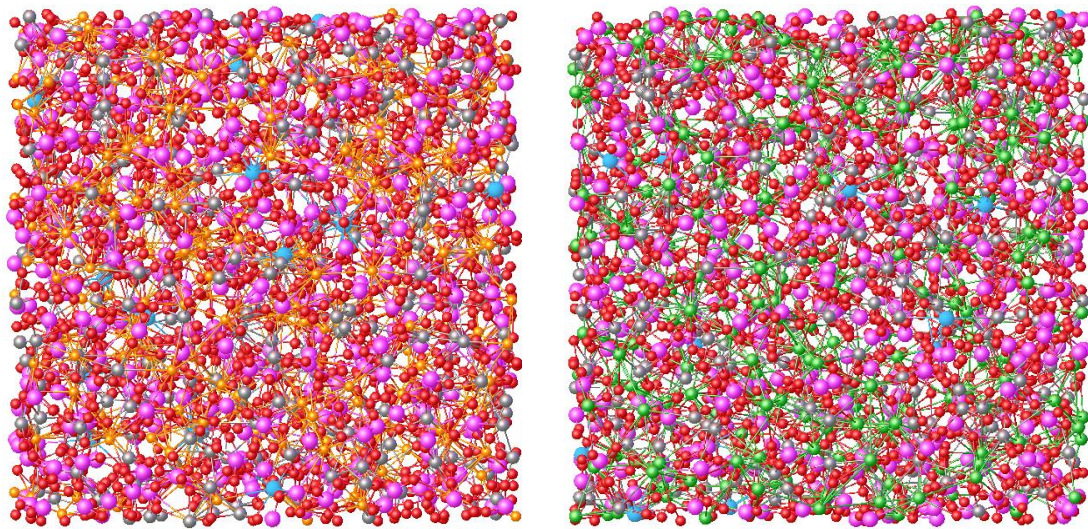


Figure 16 Image of MD models of Poly-Na-Eu (left) and Poly-K-Eu (right): red spheres are oxygen O, violet spheres are phosphorus P, grey spheres are zinc Zn, orange spheres are sodium Na, green sphere are K and blue sky spheres are europium Eu.

4.2 Diffraction structure factors

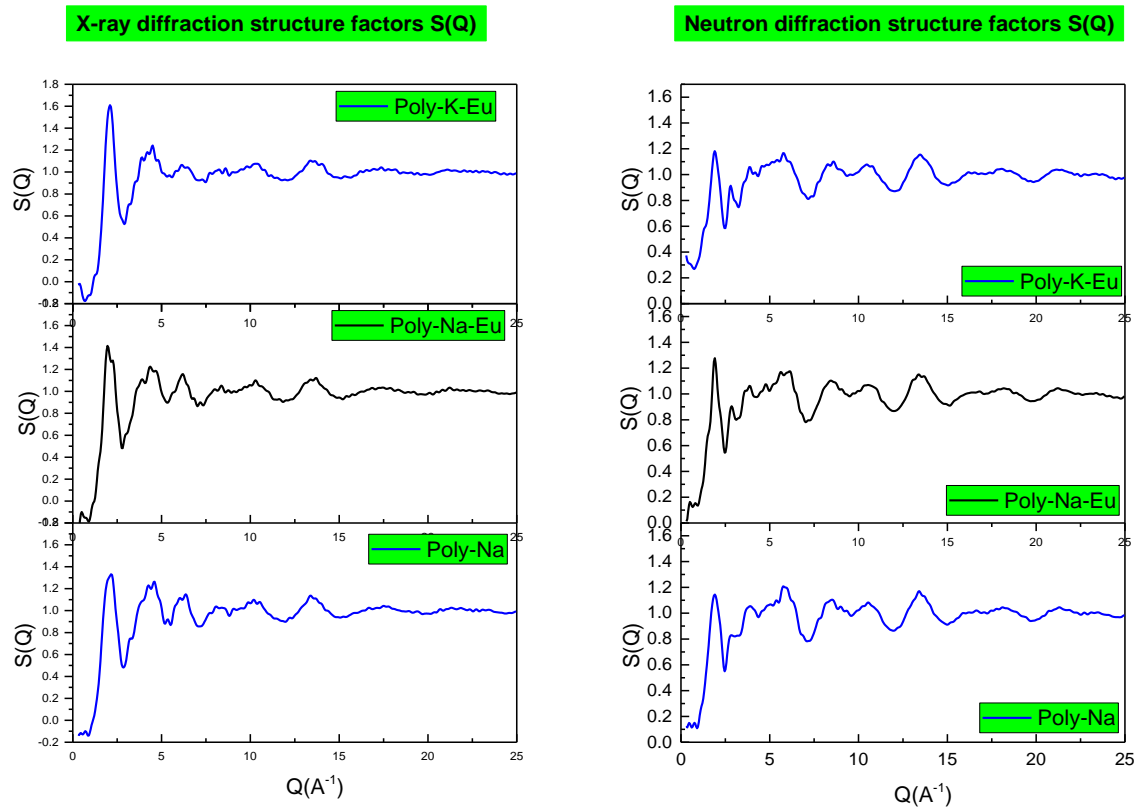


Figure 17 X-ray (Left) and Neutron (Right) diffraction structure factors $S(Q)$ from MD simulation for non-doped and Eu doped sodium and potassium polyphosphate glass.

4.3 Pair Distribution Functions and coordination number

Figure 18 displayed the partial pair distribution function $g_{ij}(r)$ for the different correlation present in Poly-Zn-Na and Poly-Zn-Na-Eu (in the top) Poly-K and Poly-K-Eu (in the bottom). The cumulative distribution functions $n_{ij}(r)$ are displayed in figure 19.

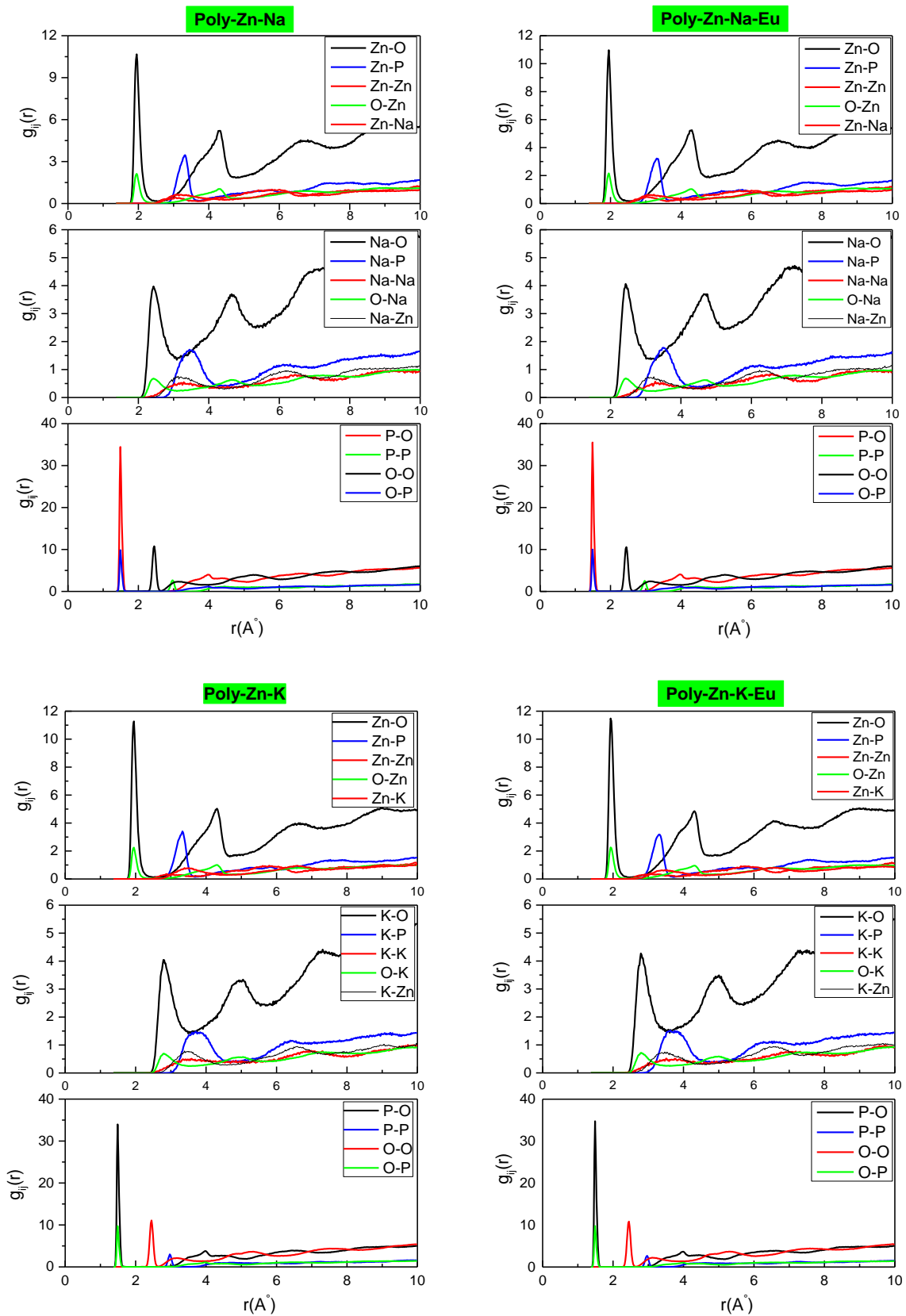


Figure 18 Partial pair distribution function $g_{ij}(r)$ of non-doped and Eu doped sodium zinc polyphosphate glasses (Top) and potassium zinc polyphosphate glasses (Bottom). (Medium model MM)

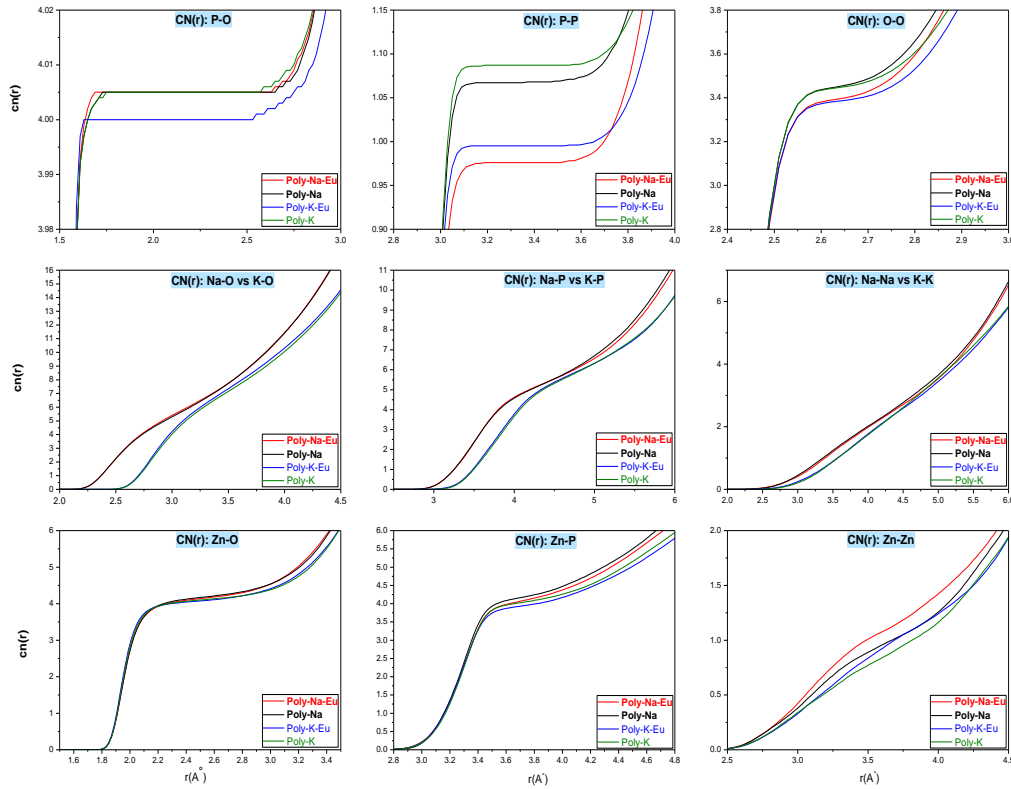


Figure 19 Cumulative coordination number $CN_{ij}(r)$ of Poly-Na-Zn, Poly-Na-Zn-Eu, Poly-K-Zn-Eu and Poly-K-Zn-Eu (Medium Model MM)

P-O, P-P and O-O correlations

The P-O, P-P and O-O nearest neighbours distances determined by the maxima of the first peak are reported in table 15. In this framework and comparing to metaphosphate glasses, these results showed no variation in the bond length in PO_4 tetrahedra which are the basic building block of phosphate glasses.

The P-O coordination number turned out to be ~ 4 for both sodium zinc and potassium zinc polyphosphate glasses confirming the PO_4 tetrahedra units present to form the basic phosphate network. However, the coordination number N_{PP} changes from ~ 2 in metaphosphate glasses to around 1 in polyphosphate composition. Even more, the N_{OO} change from ~ 4 to 3.4 (table 15). This change is due to the depolymerized polyphosphate glass (Density increase from 2.48 g/cm^3 in meta to 3.18 g/cm^3 in Poly).

Thus, the addition of metal oxides up to polyphosphate composition give rise to the depolymerization of the network and the formation of small units. Poly-Na and Poly-K have O:P ratio of 7:2 which correspond to average Q^1 . For the average Q^1 , we expect $N_{OO} = 3.42$. This evidence are proved by NMR and Raman spectroscopy used in this work that exhibited a majority of Q^1 units with presence of Q^2 groups for the present polyphosphate glasses and confirmed the Van Wazer's model [26]. This explain the value of 3.4 attributed to N_{OO} .

Europium effect

As for metaphosphate glass, there is a small change in the coordination number of P-P and O-O pairs in europium doped glasses. In this way, the cumulative distribution function $n_{ij}(r)$ show a small decrease ~ 0.2 for P-P pairs and ~ 0.05 for O-O correlations as reported in table 15. Therefore, europium atoms play a role of modifier network in glass.

Coordination environment of the network modifier Na, K and Zn:

As reported in Tables 16 and 17, the nearest neighbour distances were found to be 2.43 Å for Na-O and 2.79 Å for K-O pairs in Poly-Na and Poly-K. This difference is due to the larger ionic radius for potassium (~ 1.52 Å) compared to sodium (~ 1.16 Å). Even more, the Zn-O correlations have a shorter distance with a value of 1.95 Å in both polyphosphate glasses (Table 18) and there is no discrepancy compared to metaphosphate sample. This increase in the nearest neighbours distances in the order $Zn^{2+} < Na^+ < K^+$ could be explained by the field strength cations thus defined by the ion valence divided by square of ion-oxygen bond distance (z/a^2) and increase in the order $K^+ < Na^+ < Zn^{2+}$ [27]. Remarkably, the increase of modifier field strength causes the formation of strongest P-O-P bonds with shorter distances as explained Hoppe et al.[23].

In this respect, the M-P and M-M pair distribution function extracted from the MD simulations revealed a decrease in the nearest neighbours distances as the average strength field increase with a reduction of the basicity of glasses.

In contrast, the results extracted from the MD models of sodium and zinc metaphosphate glasses show a noticeable variation in the nearest neighbours distance around cation atoms.

Na vs K

Even more, the nature of the modifier network appears to have an effect on the cation coordination environment. Thus N_{KO} has a higher value of 6.63 (cutoff = 3.4) compared to N_{NaO} with a value of 5.5 (cutoff = 3.05) (Table 3) resulting in a mixture of 5,6 and 7 coordinated cation sites [28]. This is due to the asymmetric M-O peak of the radial distribution function in K and Na polyphosphate glasses. Hoppe et al. [29] explained the increase of coordination number in metaphosphate glasses by the increasing M-O distance that changes the mutual order of the M atoms with the tendency of clustering of M sites due to MO_n polyhedra sharing oxygen atoms. It was also found that the M-O coordination number does not significantly change across the polyphosphate composition. Thus around metaphosphate composition, all non-bridging oxygen atoms can form bridges which leads to lowest coordination number with presence of isolated MO_n polyhedra. However, for polyphosphate composition an increase of NBO lead to a small variation of coordination number. Instead, the high fraction of oxygen is coordinated by two or more cations sites which results in a strong densification of the glass structure [30].

The Zn-O coordination number N_{ZnO} is around 4 [4.06-4.16] and is invariant across the entire ZnO concentration. Musini et al [31] investigated the cationic environment in 0.3ZnO-

0.35Na₂O₃-0.35P₂O₅ glass composition using X-Ray diffraction experiment and he reported the average N_{ZnO} of 4.5 suggesting the prevalence of tetrahedral geometry.

Walter et al. [30] and Tischendorf et al. [22] have studied the binary zinc phosphate glasses from ultraphosphate to polyphosphate composition using diffraction and MD methods and they found no change in zinc-oxygen coordination number with increasing ZnO molar fraction. In addition, Suzaya et al. [32] does not show a significant variation in N_{MgO} and the total coordination number is approximately 6 in the range from 40% to 64% mol MgO.

Furthemore, many studies found the coordination number at near five for zinc phosphate glass [33],[34]. For example, Suzuya et al.[33] used X-rays and ND to study zinc polyphosphate glasses (50-70% ZnO) and he revealed that the Zn-O average number is around five [4.5-4.9]. In this regards, it should be noted that coordination number N_{ZnO} have a mixture of 3,4 and 5 coordinated Zn sites.

These results could be explained that Zn cation play a typical role as a network modifier when the fraction of non-bridging-oxygen (NBO) increase as predicted by the Van Wazer's model [26]. On the other hand, the Zn ions in ZnO₄ tetrahedra acts as network former by creating creating the more open structure of zinc phosphate glass and forming the linkage of ZnO₄ and PO₄ tetrahedra which explains the small coordination number around zinc compared to the modifier atoms [33].

Table 15 Nearest neighbor distances R_{ij} and coordination number N_{ij} of P-O, P-P and O-O correlations from MD simulations in non-doped and Eu doped polyphosphate compared to metaphosphate glasses (Medium Model MM).

Glass	P-O		P-P		O-O	
	R _{PO} (Å)	N _{PO}	R _{PP} (Å)	N _{PP}	Cut-off = 2.65 Å	
					R _{OO} (Å)	N _{PO}
Meta-Na	1.50	4.034	2.97	2.06	2.45	4.07
Meta-Zn	1.51	4.017	2.97	2.04	2.45	4.04
Meta-Na-Eu	1.50	4.015	2.97	1.96	2.45	3.99
Meta-Zn-Eu	1.51	4.012	2.97	1.96	2.45	3.99
Poly-Na	1.49	4.005	2.97	1.07	2.45	3.46
Poly-Na-Eu	1.49	4.005	2.97	0.98	2.45	3.39
Poly-K	1.49	4.005	2.97	1.08	2.45	3.45
Poly-K-Eu	1.49	4.000	2.97	0.99	2.45	3.39

Table 16 Nearest neighbor distances R_{ij} and coordination number N_{ij} of Na-O, Na-P, Na-Na and Na-Zn correlations from MD simulations in non-doped and Eu doped polyphosphate compared to metaphosphate glasses (Medium Model MM)

	Na-O		Na-P		Na-Na		Na-Zn	
	Cut-off = 3.05 Å		Cut-off = 4.20 Å		Cut-off = 4.80 Å		Cut-off = 4.20 Å	
	R_{NaO} (Å)	N_{NaO}	R_{NaP} (Å)	N_{NaP}	R_{NaNa}	N_{NaNa}	R_{NaZn}	N_{NaZn}
Meta-Na	2.42	5.07	3.59	5.13	3.09	6.27		
Meta-Na-Eu	2.43	5.22	3.57	5.23	3.11	6.21		
Poly-Na	2.43	5.51	3.45	5.01	3.29	3.28	3.13	2.87
Poly-Na-Eu	2.43	5.60	3.49	5.01	3.34	3.17	3.23	2.80

Table 17 Nearest neighbor distances R_{ij} and coordination number N_{ij} of K-O, K-P, K-K and K-Zn correlations from MD simulations in non-doped and Eu doped potassium polyphosphate (Medium Model MM)

	K-O		K-P		K-K		K-Zn	
	Cut-off = 3.40 Å		Cut-offs = 4.75 Å		Cut-off = 5.20 Å		Cut-off = 4.50 Å	
	R_{KO} (Å)	N_{KO}	R_{KP} (Å)	N_{KP}	R_{KK} (Å)	N_{KK}	R_{KZn} (Å)	N_{KZn}
Poly-K	2.79	6.63	3.71	5.80	3.59	3.95	3.39	3.00
Poly-K-Eu	2.79	6.75	3.63	5.82	3.53	3.79	3.47	3.07

Table 18 Nearest neighbor distances R_{ij} and coordination number N_{ij} of Zn-O, Zn-P and Zn-Zn correlations from MD simulations in non-doped and Eu doped polyphosphate compared to metaphosphate glasses (Medium Model MM)

	Zn-O		Zn-P		Zn-Zn	
	Cut-off = 2.50 Å		Cut-off = 3.70 Å		Cut-off = 4 Å	
	R_{ZnO} (Å)	N_{ZnO}	R_{ZnP} (Å)	N_{ZnP}	R_{ZnZn} (Å)	N_{ZnZn}
Meta-Zn	1.95	3.98	3.33	4.03	3.25	1.07
Meta-Zn-Eu	1.95	3.87	3.35	3.87	2.81	0.82
Poly-Na	1.95	4.16	3.33	4.17	3.05	1.23
Poly-Na-Eu	1.95	4.13	3.31	4.06	3.01	1.42
Poly-K	1.95	4.07	3.33	4.01	2.87	1.15
Poly-K-Eu	1.93	4.06	3.31	3.92	3.05	1.23

Table 19 Q^n distributions from MD simulations models and ^{31}P NMR experiment.

MD Method						
Sample/ Rel.prop./%	Q^0	Q^1	Q^2	Q^3	Q^4	Q^5
Poly-Zn-Na	24.76	46.63	26.20	1.92	0.48	0.00
Poly-Zn-Na-Eu	26.46	52.91	18.20	1.94	-	0.49
Poly-Zn-K	22.11	51.20	23.07	3.12	0.48	0.00
Poly-Zn-K-Eu	27.67	47.33	22.81	2.18	0.00	0.00
NMR Method						
Sample/ Rel.prop./%	Q^0	$Q^{1,1}$	$Q^{1,2}$	Q^2	Q^3	Q^4
Poly-Zn-Na	8.72	76.72	8.69	5.81	0.00	0.00

Table 20 Coordination number distribution for phosphorus and oxygen atoms in polyphosphate glasses

	Coordination-Number (%)	
	Phosphorus	
	CN = 4	CN = 5
Poly-Zn-Na	99.52	0.48
Poly-Zn-Na-Eu	99.51	0.48
Poly-Zn-K	99.52	0.48
Poly-Zn-K-Eu	100.00	0.00
	Oxygen	
	CN = 1	CN = 2
Poly-Zn-Na	84.04	15.27
Poly-Zn-Na-Eu	85.25	13.73
Poly-Zn-K	83.49	15.54
Poly-Zn-K-Eu	84.56	14.00

- The coordination number N_{PP} changes from ~ 2 in metaphosphate glasses to around 1 in polyphosphate composition. Even more, the N_{OO} change from ~ 4 to 3.4. This change is due to the depolymerized polyphosphate glass.
- As for metaphosphate glass, there is a small change in the coordination number of P-P and O-O pairs in europium doped polyphosphate glasses. This increase in the nearest neighbours distances in the order $\text{Zn}^{2+} < \text{Na}^+ < \text{K}^+$ could be explained by the field strength cations thus increase in the order $\text{K}^+ < \text{Na}^+ < \text{Zn}^{2+}$.
- The nature of the modifier network appears to have an effect on the cation coordination environment. Thus, N_{KO} has a higher value of 6.63 compared to N_{NaO} with a value of 5.5. The N_{ZnO} is around 4 and is invariant across the entire ZnO concentration.

5 Phosphate glasses with big model (~ 25000 atoms)

The medium models using about 2500 atoms is limited to predict the local environment around lanthanide ions due to the few number of ions present in this model (~ 15 and 12 in metaphosphate and polyphosphate respectively). That's why we multiplied the number of atoms by 10 (~ 25000 atoms) to compensate the low concentration of europium and reduce the edge effect of simulation box [11].

Figure 20 and 21 exhibit the images of the MD models (big models) of europium doped sodium metaphosphate and zinc sodium polyphosphate glasses respectively.

Figure 11 and 12 compared the big and medium models of respectively neutron and X-ray diffraction factors $S(Q)$ for Eu doped glasses that we observe no effect between the two model.

The radial pair distribution function $g_{ij}(r)$ for the different atomic correlations P-O, P-P, O-O, M-O, M-P, M-M, Eu-O, Eu-P, Eu-Eu and Eu-M are exhibited in figures 23, 24, 25, 26, 27 and 28. Moreover, the cumulative distribution functions $n_{ij}(r)$ are shown in figure 29, 30 and 31.

As well, the nearest neighbours distance R_{ij} and the coordination number N_{ij} are outlined in table 21-28.

In this part, we interested to study the local environment of europium ions using the big models.

5.1 Images of models

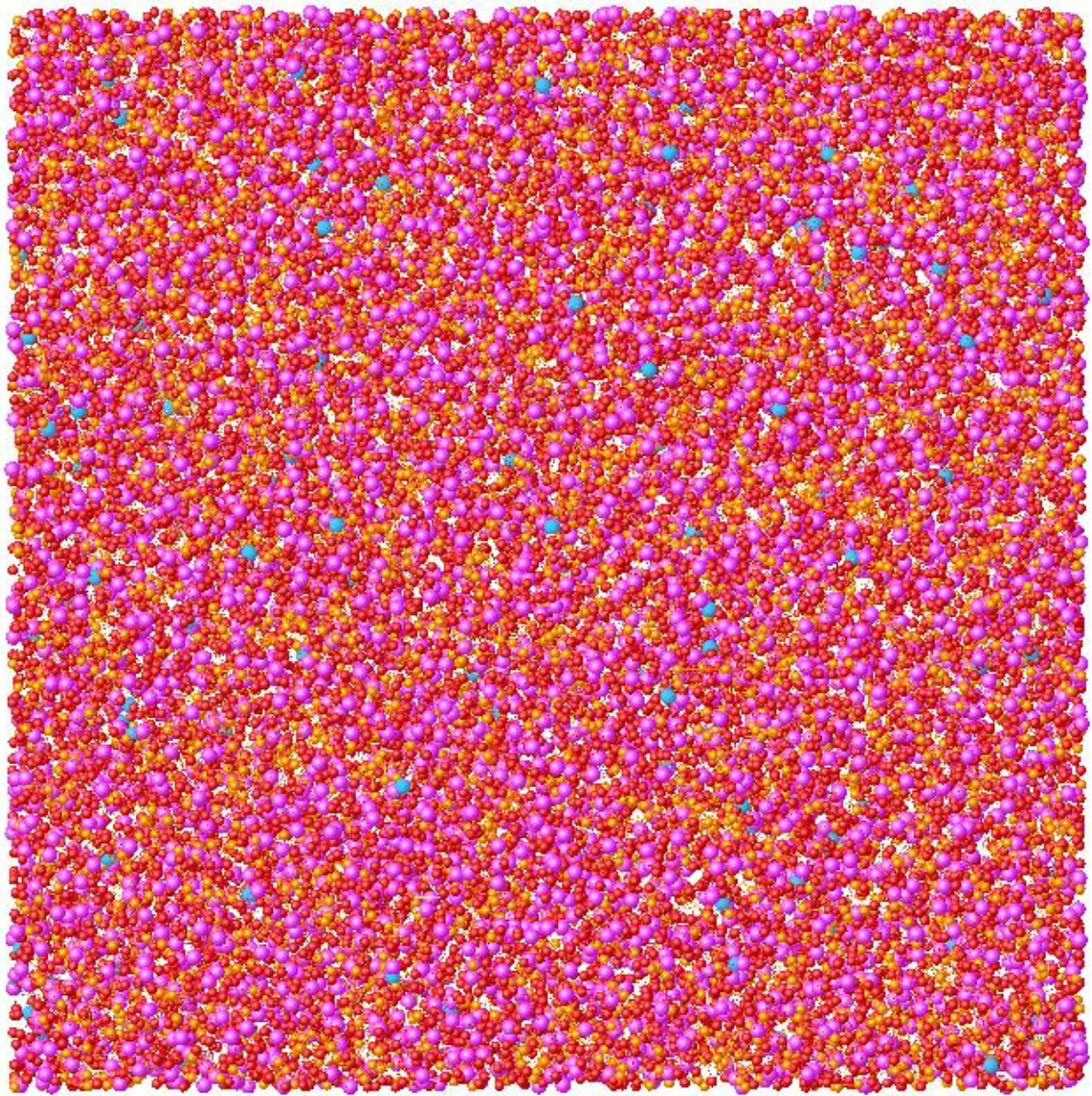


Figure 20 Image of MD models of Meta-Na-Eu: red spheres are oxygen O, violet spheres are phosphorus P, Orange spheres are sodium Na and Blue sky spheres are europium Eu (with big model: About 25000 atoms)

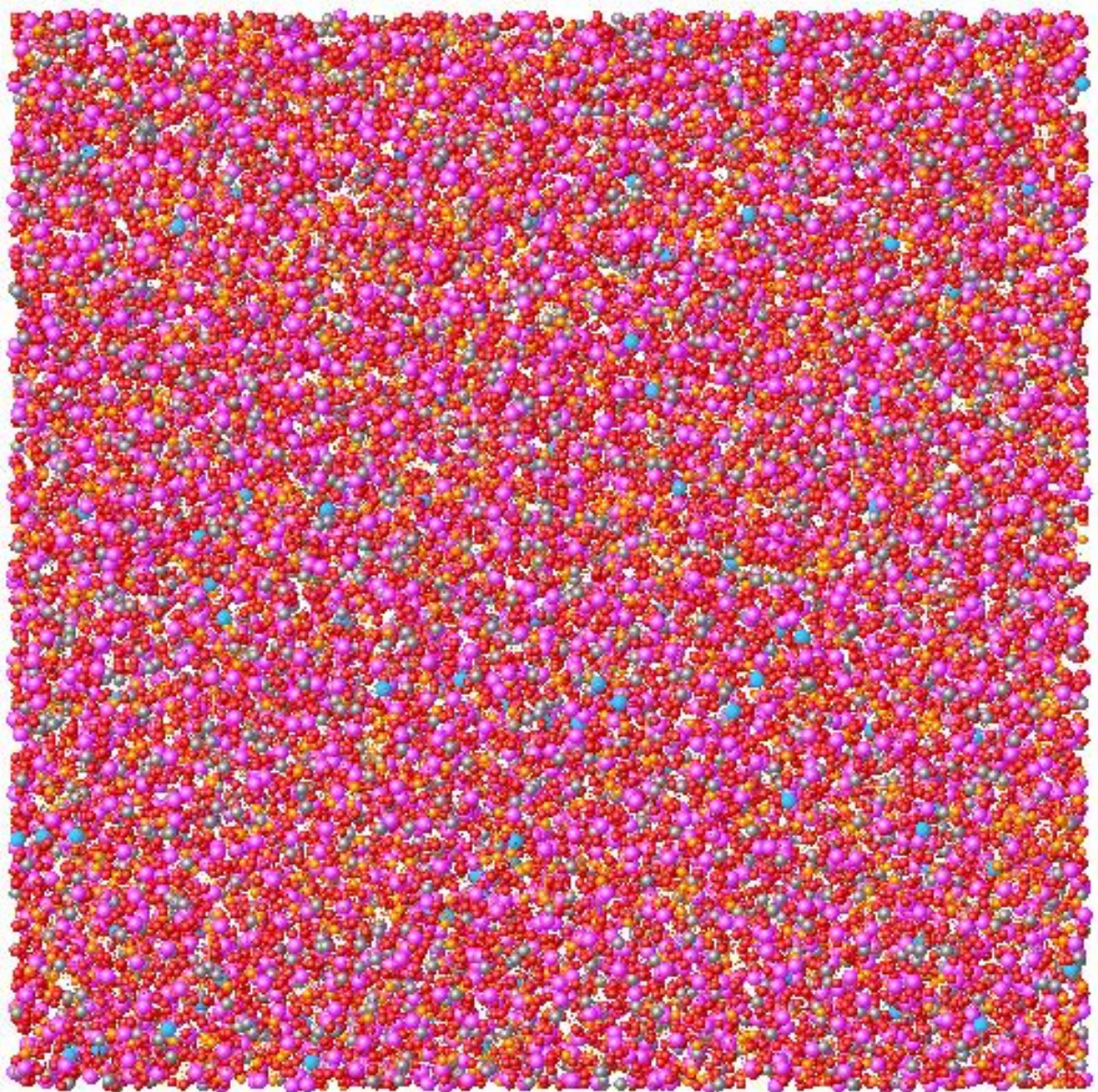


Figure 21 Image of MD models of Poly-Zn-Na-Eu: red spheres are oxygen O, violet spheres are phosphorus P, Grey spheres are zinc Zn, Orange spheres are sodium Na and Blue sky spheres are europium Eu (with big model: About 25000 atoms)

5.2 Structure factors

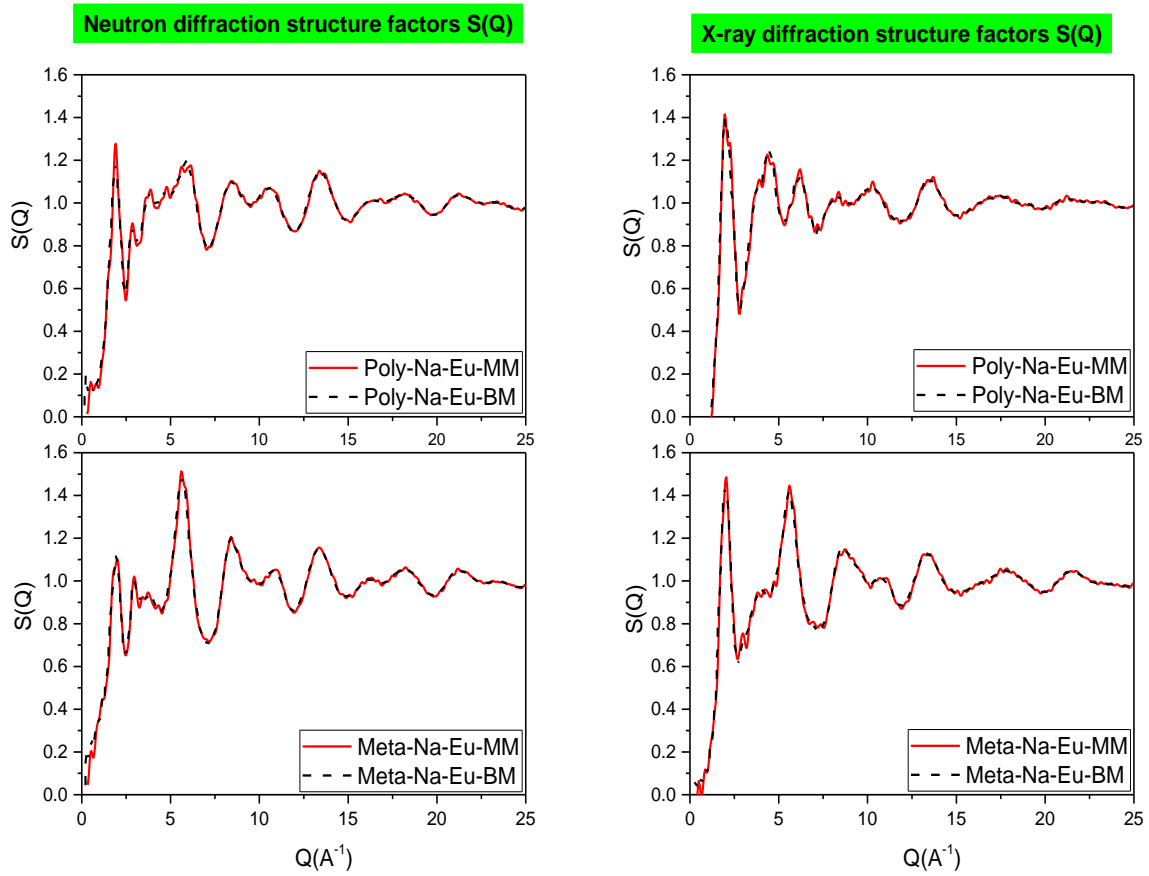
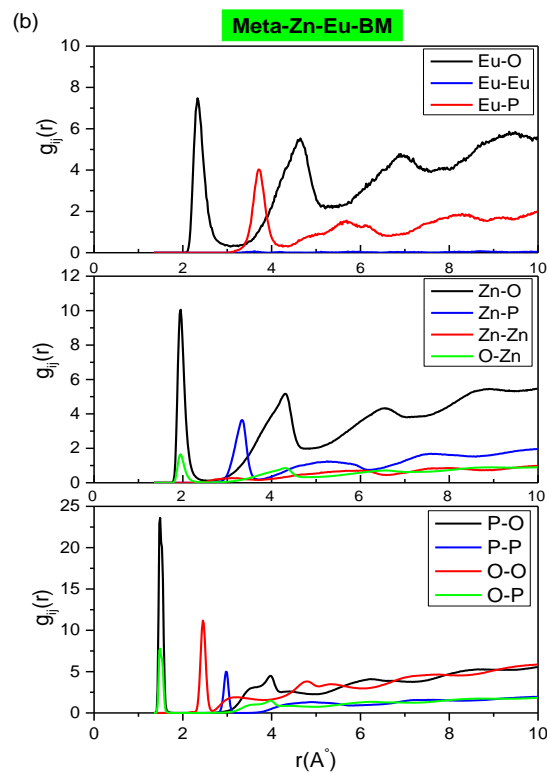
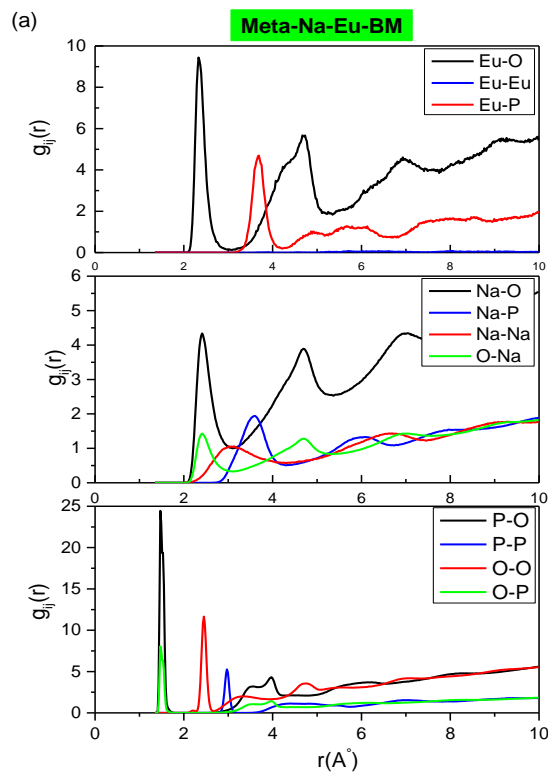


Figure 22 Neutron(Left) and X-ray (Right) diffraction structure factors $S(Q)$ comparison between big BM and medium model MM for Eu doped sodium metaphosphate and sodium zinc polyphosphate glasses

5.3 Pair distribution function and coordination number



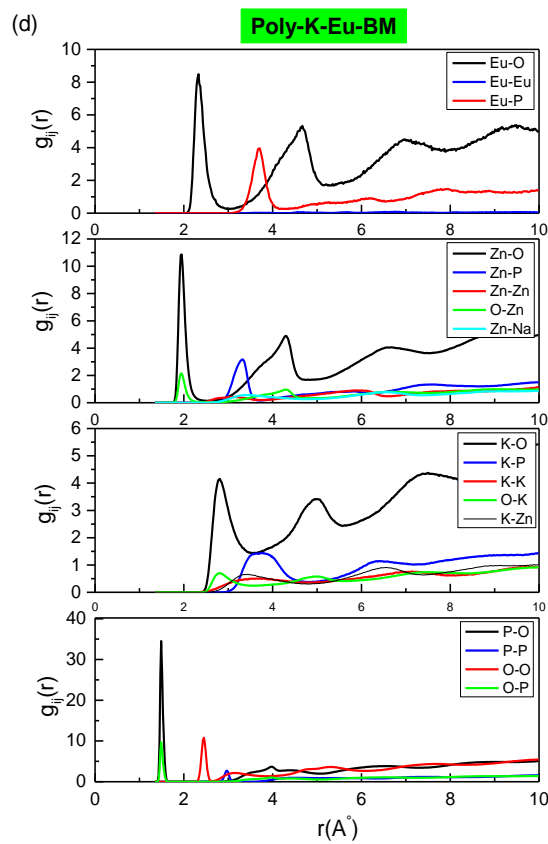
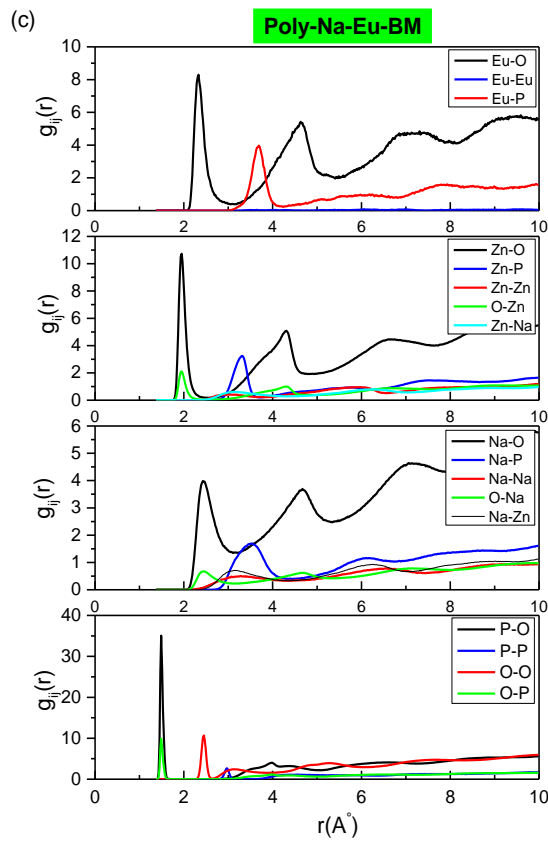


Figure 23 Partial pair distribution function $g_{ij}(r)$ of Meta-Na-Eu (a), Meta-Zn-Eu (b), Poly-Zn-Na-Eu (c) Poly-Zn-K-Eu (d), (Big model BM)

Europium environment

Eu-O correlation

The europium-oxygen pair distribution functions for europium doped metaphosphate and polyphosphate glasses extracted from the big models (BM) are shown in figures 23 and 24. The first peak in $g_{\text{EuO}}(r)$ at 2.33 Å as reported in table 25 represent the Eu-O nearest neighbours distances for both metaphosphate and polyphosphate glasses.

Few studies investigated the coordination environment around lanthanides ions in RE doped metal and metal alkali phosphate glasses. For Eu doped aluminum lithium ultraphosphate glass, EXAFS studies found Eu-O bond length of around 2.35 Å [10]. Martin et al [11] reported the Dy-O bond length as 2.3 Å in aluminophosphate glass with $\text{DyAl}_{0.3}\text{P}_{3.05}\text{O}_{9.62}$ composition using MD simulations. Du et al. [35] also showed a first peak of $g_{\text{Ce-O}}$ at 2.28 Å for $76\text{P}_2\text{O}_5-19\text{Al}_2\text{O}_3-5\text{CeO}_2$ glass composition. In the case of Eu doped metaphosphate glasses $\text{Eu}(\text{PO}_3)_3$, R_{EuO} turned out to be ~ 2.3 Å [6], [36]–[38].

In all four glass investigated in this work, the Eu-O pair distribution have much higher intensity in the first peak than Eu-P or Eu-Eu because cation (+) must be coordinated to oxygen (-) and therefore a coordination of europium by oxygen [35]. Furthermore, the first peak in $g_{\text{EuO}}(r)$ showed a slight asymmetric indicating a slightly distorted coordination environment.

For Meta-Na-Eu glass, the majority of Eu has six-fold (82.47%) with the remaining europium (20.89%) having five-fold and (14.37%) having seven-fold coordination giving an average $N_{\text{EuO}}=6.15$ (Table 28) and the coordination number was calculated using cutoff distance of 3 Å. There is no previous work that studied the RE ions coordination environment for RE doped sodium metaphosphate glass. However, many results for $\text{Eu}(\text{PO}_3)_3$ glass reported the Eu-O coordination number in the range from 6 to 7 using EXAFS and XRD experiments [6],[36]–[39]. In the case of Meta-Zn-Eu, the total Eu-O coordination of 5.52 (Table 25) obtained from the BM model is significantly smaller than the coordination of Meta-Na-Eu. Even more and contradictory to sodium metaphosphate glass, the majority of Eu has five-fold (42.17%) and six-fold (47.74%) with a few number of three, four, seven and eight-fold.

The cumulative distribution function $n_{\text{EuO}}(r)$ as displayed in figure 25 and 26 showed that the europium coordination environment for polyphosphate composition is in the intermediate range between the one for sodium and zinc metaphosphate glass. Thus, the N_{EuO} value increase in the order Meta-Zn-Eu < Poly-K-Zn-Eu < Poly-Na-Zn-Eu < Meta-Na-Eu as reported in table 25. The same order is shown using medium model MM with a lower value of N_{EuO} of 5.18 for Meta-Zn-Eu compared to results 5.52 extracted from BM .

For Poly-Zn-Na-Eu using BM simulation, the Eu-O coordination has a value of 5.94 and the coordination number distribution for europium ions has 65.4% of six-fold, 21.9% five-fold and 11.8% of seven-fold coordination. Moreover, there is a limited number of four and eight-fold with 0.2% and 0.7% respectively (Table 28). The same behaviors is also seen in potassium polyphosphate glass with higher coordination number of six-fold (64.7%).

This is similar to Martin's work that detailed an average coordination of 5.8 for Dy-O correlation in Dy alumino-polyphosphate glass using MD simulation. The majority of Dy has

five-fold and six-fold with all Dy is bonded to non-bridging oxygen [40]. However, the total Dy-O values of $N_{DyO} = 6.7$ using neutron diffraction for the same glass is significantly larger than results obtained for MD simulation [40]. For cerium alumino-polyphosphate glass, the N_{CeO} is determined to be 6.8 using MD method [35]. For aluminum lithium ultraphosphate glass, it was noted the value of 6 for the Eu-O coordination number [10]. In this context, Martin et al related the O-O distribution function that has a broad peak from 2.8 and 3.5 Å with the Dy-O and Al-O coordination environment [40].

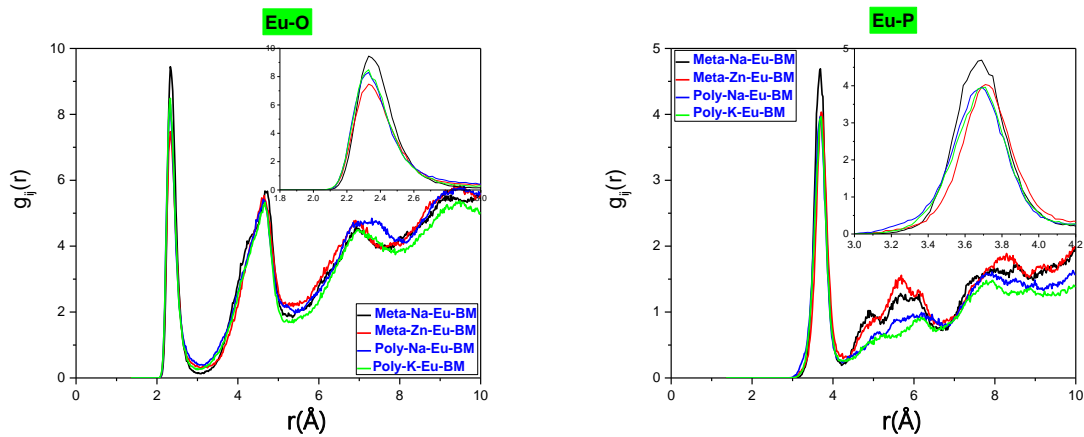


Figure 24 Eu-O (Left) and Eu-P (Right) pair distribution function $g_{ij}(r)$ of europium doped metaphosphate and polyphosphate glasses (Big Model BM).

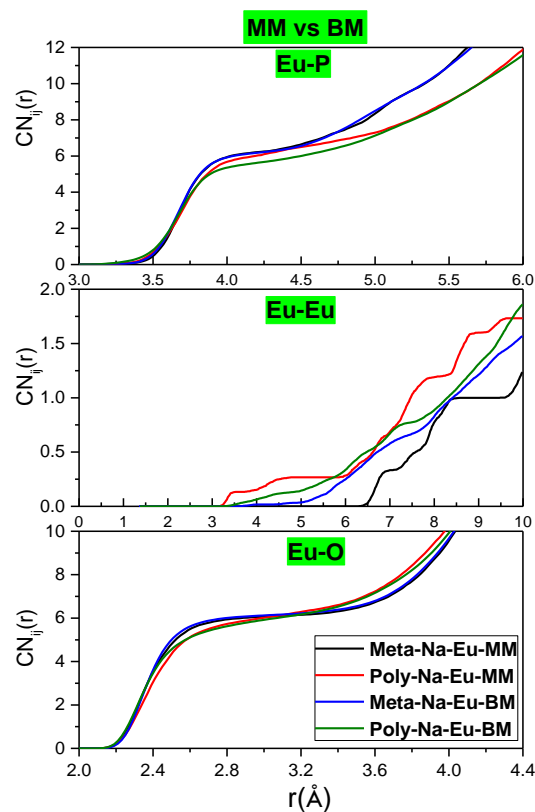


Figure 25 Cumulative coordination number $n_{ij}(r)$ comparison between BM and MM

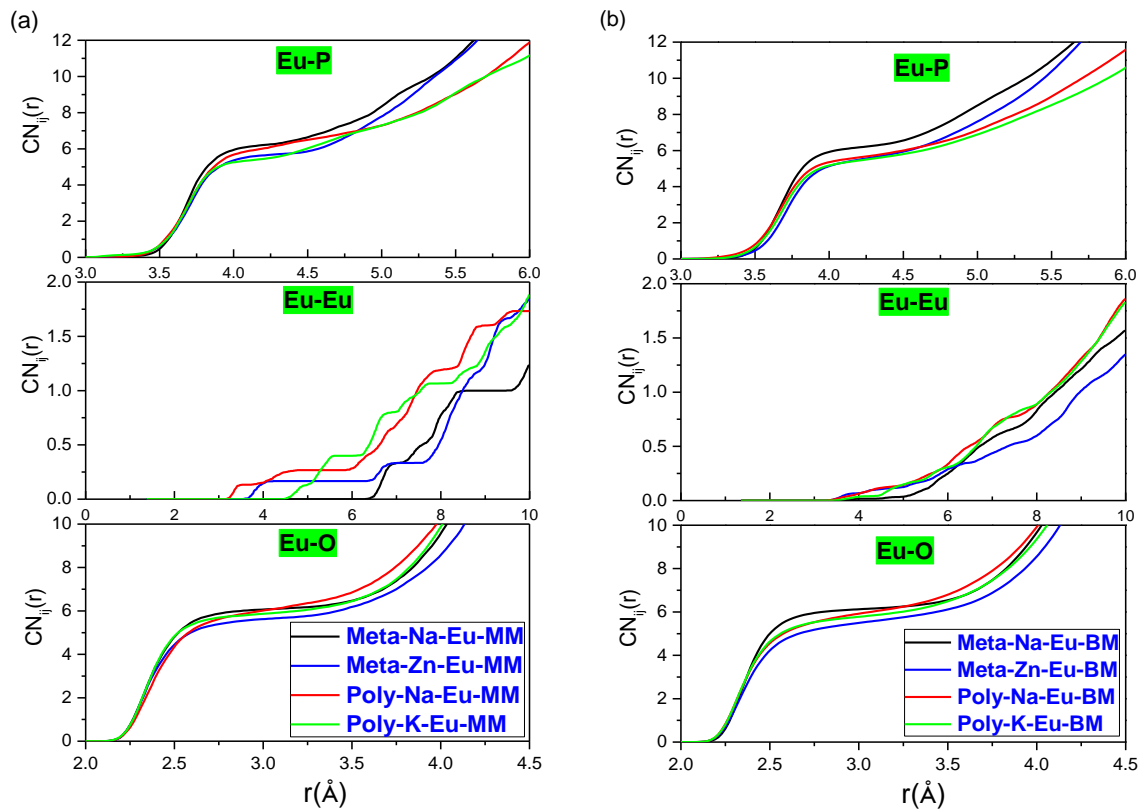


Figure 26 Eu-O, Eu-Eu and Eu-P coordination number $CN_{ij}(r)$ for medium MM (Left) and big model BM (Right).

Eu-P correlations

In order to investigate the distribution of network-forming cations around europium ions, the Eu-P pair distribution function were calculated using BM. The first peak in $g_{EuP}(r)$ at $\sim 3.7 \text{ \AA}$ represent the Eu-P present in this work and there is no significant variation between BM and MM. These results are coherent with experimental results for RE doped phosphate glasses. In this way, the R_{EuP} has a value in the range from 3.6 to 3.8 \AA using EXAFS experiments for Eu doped metaphosphate glass ($\text{Eu}(\text{PO}_3)_3$) [38],[6]. Martin et al.[40] reported the Dy-P bond length value of 3.7 \AA in aluminium phosphate glass using MD models.

The Eu-P distribution function as exhibited in figure 24 showed a broad second peak from 4.3 to 6.8 \AA with different peak position and with different feature between metaphosphate and polyphosphate glasses indicating a variation in the second coordination shell. Further, the FWHM of the first peak (Inset fig. 24) increases in the order $\text{Zn}^{2+} < \text{K}^+/\text{Zn}^{2+} < \text{Na}^+/\text{Zn}^{2+} < \text{Na}^+$ suggesting a wide distribution of europium ions in sodium metaphosphate glass compared to other glasses.

The coordination number N_{EuP} turned out to be 6.11, 5.44, 5.60 and 5.40 for Meta-Na-Eu, Meta-Zn-Eu, Poly-Zn-Na-Eu and Poly-Zn-K-Eu respectively. The same behavior of Eu-P and Eu-O coordination number is detected for metaphosphate glasses that we observe a significant decrease in the coordination number when replacing Na^+ by Zn^{2+} ions. On the other hand, the N_{EuP} significantly decreased from 6.11 in Meta-Na-Eu to 5.60 and 5.40 in Poly-Zn-Na-Eu and

Poly-Zn-K-Eu respectively while the N_{EuO} undergoes a slight change from 6.15 to around 5.94 and 5.80.

There is a discrepancy of the coordination number value with medium model MM due to the fewer number of europium ion present in this models. For this reason, we take into account the results extracted from the big model BM.

Eu-Eu correlation

Figure 27 compared the Eu-Eu pair distribution function between the two models and confirm the limited medium model to investigate the local environment around europium ions. Figure 28 exhibited a lower intensity of the first peak in $g_{EuEu}(r)$ for sodium metaphosphate glass compared to zinc glasses. This means a more Eu-Eu pairs in presence of zinc oxide. A slight increase of the coordination number of Eu-Eu pairs in polyphosphate glasses compared to metaphosphate glasses is showed in figure 26. This could be explained by the higher number of europium Atom/ \AA^3 in polyphosphate samples compared to metaphosphate.

Moreover, we observe a lower N_{EuEu} in sodium metaphosphate glass compared to zinc glasses at shorter distance until 6.2 \AA (Figure 26) that the sodium ions stopped the shorter distance between europium compared to zinc ions.

At longer distance, the amplitude in the cumulative coordination number $n_{EuEu}(r)$ of Meta-Zn-Eu is lower. It can be explained by the lower number of Eu Atom/ \AA^3 in Meta-Zn-Eu (3.40×10^{-4} Eu Atom/ \AA^3) compared to Meta-Na-Eu (3.55×10^{-4} Eu Atom/ \AA^3).

For polyphosphate composition, the coordination environment at longer distance is similar in both Poly-Zn-Na-Eu and Poly-Zn-K-Eu.

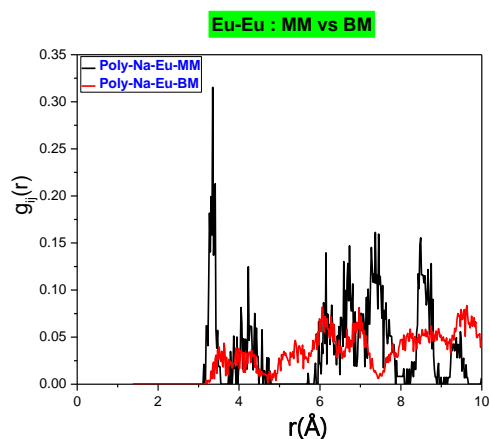
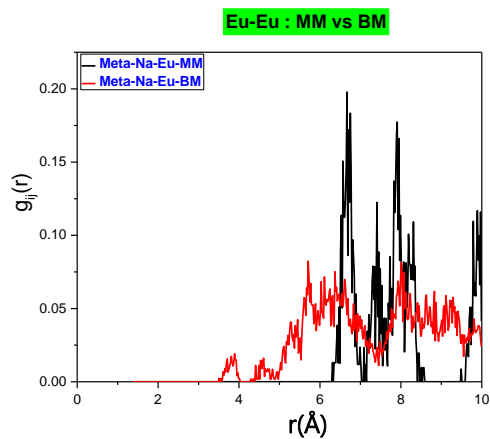


Figure 27 Eu-Eu pair distribution function $g_{ij}(r)$: comparison between BM and MM of Meta-Na-Eu (Left) and Poly-Zn-Na-Eu (Right)

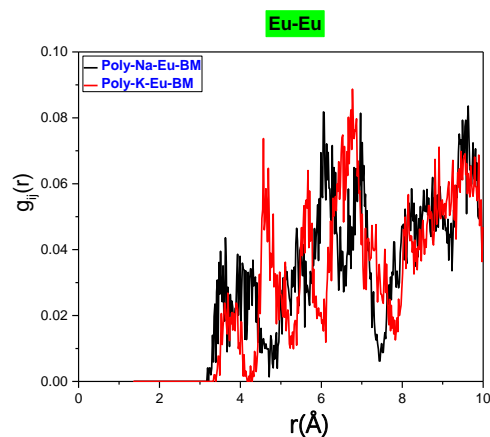
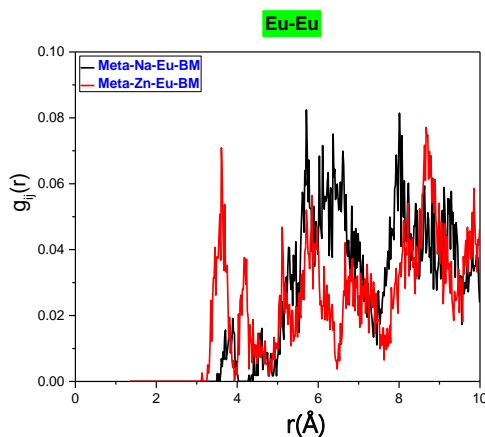


Figure 28 Eu-Eu pair distribution function $g_{ij}(r)$ of metaphosphate and polyphosphate glasses (Big Model BM)

Eu-M (Zn/Na/K) correlations

Figure 29 and 30 displayed the Eu-M pair distribution function $g_{ij}(r)$ (M=Na, K and Zn) in the different metaphosphate and polyphosphate compositions. The cumulative distribution functions $n_{ij}(r)$ are displayed in figure 31.

The ratio of Na in Meta-Na-Eu to Zn in Meta-Zn-Eu is 2:1. However, looking at number of Eu-Na pairs in Meta-Na-Eu compared to Eu-Zn in Meta-Zn-Eu, the ratio is 2.61: 0.72 (see figure 31 and table 26). From this results, we can suggest that sodium is more likely to coordinate to europium compared to zinc ions.

In polyphosphate composition, the number of zinc atoms (= 288 atoms) is higher than the number of sodium (=247 atoms). In this way, the N_{EuZn} is expected to be higher because of higher number of zinc atoms. Whereas, the N_{EuZn} is lower than the N_{EuNa} (1.38 vs 1.89 respectively) in Poly-Zn-Na-Eu (see figure 31 and table 26). Again, the sodium coordination to sodium is higher then due to composition alone.

For Poly-Zn-K-Eu, the coordination number of Eu-K and Eu-Zn pairs are similar (~ 1.40 vs 1.39).

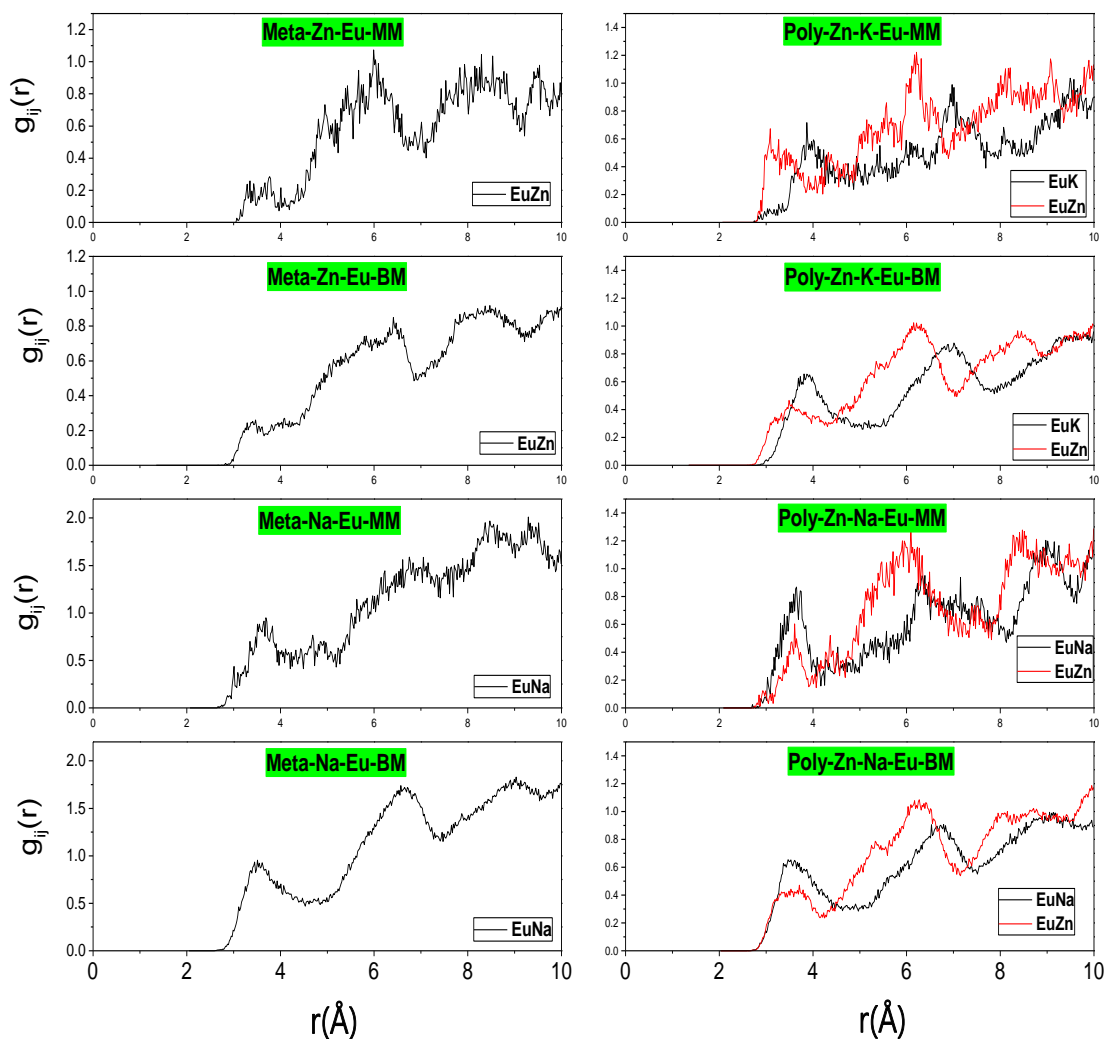


Figure 29 Eu-M pair distribution function $g_{ij}(r)$ ($M=Na, K$ and Zn): comparison between BM and MM of metaphosphate (Left) and polyphosphate glasses (Right).

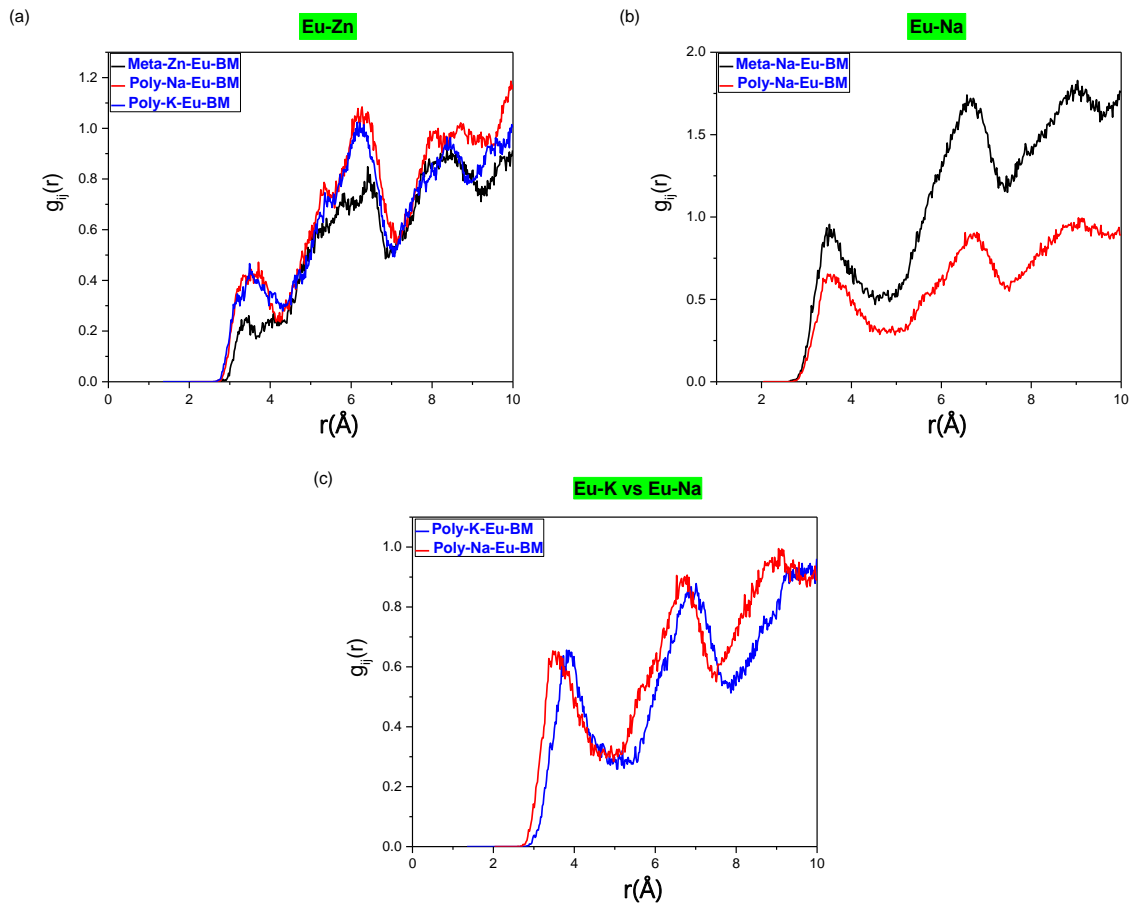


Figure 30 Eu-Zn (a), Eu-Na (b) and Eu-Na and Eu-K (c) pair distribution function $g_{ij}(r)$ of metaphosphate and polyphosphate glasses. (Big models)

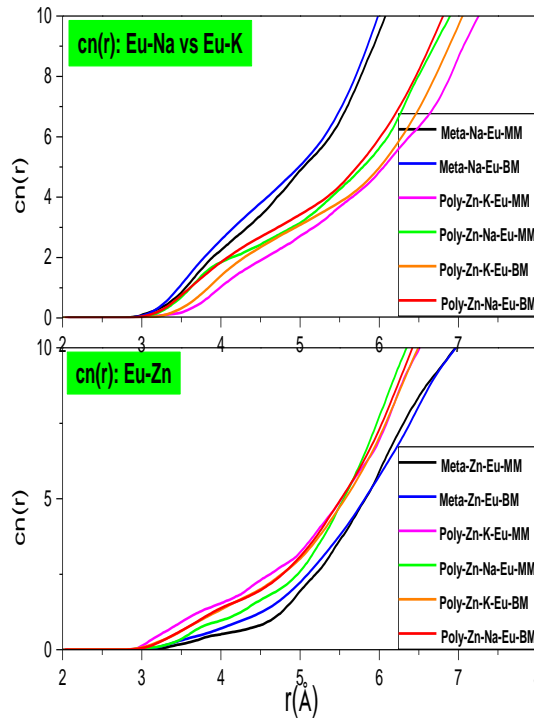


Figure 31 Eu-M coordination number $CN_{ij}(r)$ ($M=Zn, Na$ and K): comparison between MM and BM of metaphosphate and polyphosphate glasses.

Eu-O-Eu

Table 27 displayed the results of Xhst analysis of europium clustering in metaphosphate and polyphosphate composition presenting the distribution of europium ions in clusters based on the direct Eu-O-Eu bonding criterion. In Meta-Na glass, the majority of europium ions (~98.3%) are isolated, 1.65% form pairs and 0.02% are in clusters of three.

However, glasses containing zinc oxide have a smaller percentage of isolated europium ions. Thus, in Meta-Zn-Eu around 89.7% of RE ions are isolated while 4.5%, 5.6% and 0.13% are in pairs, clusters of three and four successively. For Poly-Na-Eu, 87.9% of europium are isolated, around 8% are clustered in pair, 2.7% are clusters of three and the rest are in clusters of four. The obvious difference in isolated europium ions for zinc glasses compared to sodium metaphosphate glass suggest that the presence of zinc oxide in glass increases the clustering tendency of europium ions.

Table 21 Nearest neighbor distances R_{ij} and coordination number N_{ij} of P-O, P-P and O-O correlations from MD simulations in Eu doped glasses: Comparison between Medium MM and Big Model BM

Glass	P-O		P-P		O-O	
	$R_{PO}(\text{Å})$	N_{PO}	$R_{PP}(\text{Å})$	N_{PP}	Cut-offs 2.65 Å	
	$R_{OO}(\text{Å})$	N_{PO}				
Meta-Na-Eu-MM	1.50	4.01	2.97	1.96	2.45	3.99
Meta-Zn-Eu-MM	1.51	4.01	2.97	1.96	2.45	3.99
Poly-Zn-Na-Eu-MM	1.49	4.01	2.97	0.97	2.45	3.39
Poly-Zn-K-Eu-MM	1.49	4.00	2.97	0.99	2.45	3.39
Meta-Na-Eu-BM	1.50	4.03	2.97	1.98	2.45	4.00
Meta-Zn-Eu-BM	1.51	4.01	2.97	1.96	2.45	3.99
Poly-Zn-Na-Eu-BM	1.49	4.00	2.97	0.99	2.45	3.40
Poly-Zn-K-Eu-BM	1.49	4.00	2.97	1.02	2.45	3.40

Table 22 Nearest neighbor distances R_{ij} and coordination number N_{ij} of Na-O, Na-P, Na-Na and Na-Zn correlations from MD simulations in Eu doped glasses: Comparison between Medium MM and Big Model BM

Glass	Na-O		Na-P		Na-Na		Na-Zn	
	Cut-off = 3.05 Å		Cut-off = 4.20 Å		Cut-off = 4.80 Å		Cut-off = 4.20 Å	
	$R_{NaO}(\text{Å})$	N_{NaO}	$R_{NaP}(\text{Å})$	N_{NaP}	R_{NaNa}	N_{NaNa}	R_{NaZn}	N_{NaZn}
Meta-Na-Eu-MM	2.43	5.22	3.57	5.23	3.11	6.21		
Poly-Zn-Na-Eu-MM	2.43	5.60	3.49	5.01	3.34	3.17	3.23	2.80
Meta-Na-Eu-BM	2.33	5.17	3.61	5.23	3.01	6.35		
Poly-Zn-Na-Eu-BM	2.35	5.54	3.53	4.94	3.29	3.30	3.15	2.76

Table 23 Nearest neighbor distances R_{ij} and coordination number N_{ij} of K-O, K-P, K-K and K-Zn correlations from MD simulations in Eu doped glasses: Comparison between Medium MM and Big Model BM

Glass	K-O		K-P		K-K		K-Zn	
	Cut-off 3.4 Å		Cut-off 4.75 Å		Cut-off 5.20 Å		Cut-off 4.50 Å	
	$R_{KO}(\text{Å})$	N_{KO}	$R_{KP}(\text{Å})$	N_{KP}	$R_{KK}(\text{Å})$	N_{KK}	$R_{KZn}(\text{Å})$	N_{KZn}
Poly-Zn-K-Eu-MM	2.79	6.75	3.63	5.82	3.53	3.79	3.47	3.07
Poly-Zn-K-Eu-BM	2.81	6.75	3.79	5.77	3.71	3.98	3.45	2.94

Table 24 Nearest neighbor distances R_{ij} and coordination number N_{ij} of Zn-O, Zn-P and Zn-Zn correlations from MD simulations in Eu doped glasses: Comparison between Medium MM and Big Model BM

	Zn-O		Zn-P		Zn-Zn	
	Cut-off 3.5 Å		Cut-off 3.7 Å		Cut-off 4 Å	
	$R_{ZnO}(\text{Å})$	N_{ZnO}	$R_{ZnP}(\text{Å})$	N_{ZnP}	$R_{ZnZn}(\text{Å})$	N_{ZnZn}
Meta-Zn-Eu-MM	1.95	3.86	3.35	3.86	3.16	0.82
Meta-Zn-Eu-BM	1.95	3.94	3.33	3.98	3.21	0.99
Poly-Zn-Na-Eu-MM	1.95	4.13	3.31	4.06	3.01	1.42
Poly-Zn-K-Eu-MM	1.93	4.06	3.31	3.92	3.05	1.23
Poly-Zn-Na-Eu-BM	1.95	4.16	3.31	4.06	3.03	1.45
Poly-Zn-K-Eu-BM	1.95	4.09	3.33	3.93	3.15	1.44

Table 25 Nearest neighbor distances R_{ij} and coordination number N_{ij} of Eu-O, Eu-P and Eu-Eu correlations from MD simulations in Eu doped glasses: Comparison between Medium MM and Big Model BM

Glass	Eu-O		Eu-P		Eu-Eu	
	Cut-off 3.00 Å		Cut-off 4.15 Å			
	$R_{EuO}(\text{Å})$	N_{EuO}	$R_{EuP}(\text{Å})$	N_{EuP}	$R_{EuEu}(\text{Å})$	N_{EuEu}
Meta-Na-Eu-MM	2.33	6.06	3.69	6.16	6.67	
Poly-Zn-Na-Eu-MM	2.39	6.02	3.71	5.93	3.35	
Poly-Zn-K-Eu-MM	2.31	5.87	3.69	5.40	4.77	
Meta-Zn-Eu-MM	2.35	5.18	3.73	5.14	6.21	
Meta-Na-Eu-BM	2.33	6.15	3.69	6.11	3.89	
Poly-Zn-Na-Eu-BM	2.33	5.94	3.69	5.60	3.63	
Poly-Zn-K-Eu-BM	2.33	5.80	3.71	5.40	3.69	
Meta-Zn-Eu-BM	2.33	5.52	3.71	5.44	3.61	

Table 26 Nearest neighbor distances R_{ij} and coordination number N_{ij} of Eu-O, Eu-P and Eu-Eu correlations from MD simulations in Eu doped glasses: Comparison between Medium MM and Big Model BM.

Glass	Eu-Na		Eu-K		Eu-Zn	
	Cut-off 5.00 Å		Cut-off 5.4 Å		Cut-off 4.2 Å	
	$R_{EuNa}(\text{Å})$	N_{EuNa}	$R_{EuK}(\text{Å})$	N_{EuK}	$R_{EuZn}(\text{Å})$	N_{EuZn}
Meta-Na-Eu-MM	3.65	2.22				
Meta-Zn-Eu-MM					3.35	0.49
Poly-Na-Eu-MM	3.65	1.89			3.61	0.97
Poly-K-Eu-MM			3.87	1.02	3.09	1.55
Meta-Na-Eu-BM	3.51	2.61				
Meta-Zn-Eu-BM					3.47	0.72
Poly-Na-Eu-BM	3.51	1.89			3.55	1.38
Poly-K-Eu-BM			3.81	1.40	3.49	1.39

Table 27 Q^n distributions of Eu from MD simulations models: Comparison between Medium MM and Big Model BM

Sample/ Rel.prop./%	Eu ³⁺			
	Isolated	1	2	3
Meta-Na-Eu-MM	100.00	0.00	0.00	0.00
Poly-Zn-K-Eu-MM	99.34	0.66	0.00	0.00
Meta-Zn-Eu-MM	83.99	4.46	11.55	0.00
Poly-Zn-Na-Eu-MM	75.97	10.56	0.13	13.33
Meta-Na-Eu-BM	98.33	1.65	0.02	0.00
Poly-Zn-K-Eu-BM	92.07	5.06	2.87	0.00
Meta-Zn-Eu-BM	89.74	4.52	5.61	0.13
Poly-Zn-Na-Eu-BM	87.96	8.08	2.72	1.24

Table 28 Coordination-number distribution for europium atoms in metaphosphate glasses (Big Model BM)

	Coordination-Number (%)						Average CN
	3	4	5	6	7	8	
Meta-Na-Eu-BM	0.00	0.02	2.89	82.47	14.37	0.26	6.15
Poly-Zn-Na-Eu-BM	0.00	0.21	21.91	65.40	11.78	0.71	5.94
Poly-Zn-K-Eu-BM	0.00	0.20	29.03	64.75	5.62	0.40	5.80
Meta-Zn-Eu-BM	0.08	6.40	42.17	47.74	3.29	0.31	5.52

- The N_{EuO} showed that the europium coordination environment for polyphosphate composition is in the intermediate range between the one for sodium and zinc metaphosphate glass. Thus, the N_{EuO} value increase in the order Meta-Zn-Eu (5.52) < Poly-K-Zn-Eu (5.82) < Poly-Na-Zn-Eu (5.94) < Meta-Na-Eu (6.15).
- The same behavior of Eu-P and Eu-O coordination number is detected for metaphosphate glasses that we observe a significant decrease in the coordination number when replacing Na⁺ by Zn²⁺ ions. As well, the N_{EuP} significantly decreased from 6.11 in Meta-Na-Eu to 5.60 and 5.40 in Poly-Zn-Na-Eu and Poly-Zn-K-Eu respectively.
- A more Eu-Eu pairs in presence of zinc oxide and a slight increase of the coordination number of Eu-Eu pairs in polyphosphate glasses compared to metaphosphate glasses.
- The obvious difference in isolated europium ions for zinc glasses compared to sodium metaphosphate glass suggest that the presence of zinc oxide in glass increases the clustering tendency of europium ions.

- [1] S. J. Gurman, N. Binsted, et I. Ross, « A rapid, exact curved-wave theory for EXAFS calculations », *Journal of Physics C: Solid State Physics*, vol. 17, n° 1, p. 143-151, janv. 1984.
- [2] D. T. Bowron, R. J. Newport, B. D. Rainford, G. A. Saunders, et H. B. Senin, « EXAFS and x-ray structural studies of (Tb 2 O 3) 0.26 (P 2 O 5) 0.74 metaphosphate glass », *Physical Review B*, vol. 51, n° 9, p. 5739-5745, mars 1995.
- [3] M. P. Medda, G. Piccaluga, G. Pinna, M. Bettinelli, et G. Cormier, « Coordination of Eu³⁺ Ions in a Phosphate Glass by X-ray Diffraction », *Zeitschrift für Naturforschung A*, vol. 49, n° 10, janv. 1994.
- [4] A. Musinu, G. Piccaluga, G. Pinna, D. Narducci, et S. Pizzini, « Short-range order of Zn and Cu in metaphosphate glasses by X-ray diffraction », *Journal of Non-Crystalline Solids*, vol. 111, n° 2-3, p. 221-227, nov. 1989.
- [5] D. T. Bowron, G. Bushnell-Wye, R. J. Newport, B. D. Rainford, et G. A. Saunders, « X-ray diffraction studies of rare-earth metaphosphate glasses », *Journal of Physics: Condensed Matter*, vol. 8, n° 19, p. 3337-3346, mai 1996.
- [6] D. T. Bowron, G. A. Saunders, R. J. Newport, B. D. Rainford, et H. B. Senin, « EXAFS studies of rare-earth metaphosphate glasses », *Physical Review B*, vol. 53, n° 9, p. 5268-5275, mars 1996.
- [7] D. T. Bowron, « A study of rare earth doped silicate and phosphate glasses », PhD Thesis, University of Kent, 1994.
- [8] R. Anderson *et al.*, « An extended x-ray absorption fine structure study of rare-earth phosphate glasses near the metaphosphate composition », *Journal of Materials Research*, vol. 14, n° 12, p. 4706-4714, déc. 1999.
- [9] A. G. Shikerkar, J. A. E. Desa, P. S. R. Krishna, et R. Chitra, « Diffraction studies of rare-earth phosphate glasses », *Journal of non-crystalline solids*, vol. 270, n° 1-3, p. 234-246, 2000.
- [10] N. Wada, K. Kojima, et K. Ozutsumi, « Glass composition dependence of Eu³⁺ polarization in oxide glasses », *Journal of Luminescence*, vol. 126, p. 53-62, 2007.
- [11] University of Kent *et al.*, « Molecular dynamics modelling of sodium and calcium metaphosphate glasses for biomaterial applications », *Physics and Chemistry of Glasses: European Journal of Glass Science and Technology Part B*, vol. 57, n° 6, p. 245-253, déc. 2016.
- [12] G. G. Boiko, N. S. Andreev, et A. V. Parkachev, « Structure of pyrophosphate 2ZnO· P₂O₅–2Na₂O· P₂O₅ glasses according to molecular dynamics simulation », *Journal of non-crystalline solids*, vol. 238, n° 3, p. 175-185, 1998.
- [13] A. Pedone, G. Malavasi, M. C. Menziani, A. N. Cormack, et U. Segre, « A New Self-Consistent Empirical Interatomic Potential Model for Oxides, Silicates, and Silica-Based Glasses », *The Journal of Physical Chemistry B*, vol. 110, n° 24, p. 11780-11795, juin 2006.
- [14] « [teter_potentials-buckingham potentiel of europium.pdf](#) ». .
- [15] W. Sun, V. Ageh, H. Mohseni, T. W. Scharf, et J. Du, « Experimental and computational studies on stacking faults in zinc titanate », *Applied Physics Letters*, vol. 104, n° 24, p. 241903, juin 2014.
- [16] K.-H. Sun, « Fundamental condition of glass formation », *Journal of the American Ceramic Society*, vol. 30, n° 9, p. 277-281, 1947.
- [17] U. Hoppe, G. Walter, G. Carl, J. Neufeind, et A. C. Hannon, « Structure of zinc phosphate glasses probed by neutron and X-ray diffraction of high resolving power and by reverse Monte Carlo simulations », *Journal of Non-Crystalline Solids*, vol. 351, n° 12-13, p. 1020-1031, mai 2005.
- [18] U. Hoppe, G. Walter, D. Stachel, A. Barz, et A. C. Hannon, « Neutron and X-ray Diffraction Study on the Structure of Ultraphosphate Glasses », *Zeitschrift für Naturforschung A*, vol. 52, n° 3, janv. 1997.
- [19] D. M. Pickup, I. Ahmed, P. Guerry, J. C. Knowles, M. E. Smith, et R. J. Newport, « The structure of phosphate glass biomaterials from neutron diffraction and ³¹P nuclear magnetic resonance data », *Journal of Physics: Condensed Matter*, vol. 19, n° 41, p. 415116, oct. 2007.
- [20] A. J. Parsons *et al.*, « Neutron scattering and ab initio molecular dynamics study of cross-linking in biomedical phosphate glasses », *Journal of Physics: Condensed Matter*, vol. 22, n° 48, p. 485403, 2010.
- [21] E. Matsubara, K. Sugiyama, Y. Waseda, M. Ashizuka, et E. Ishida, « Structural analysis of zinc metaphosphate glass by anomalous X-ray scattering », *Journal of Materials Science Letters*, vol. 9, n° 1, p. 14-16, janv. 1990.

- [22] B. C. Tischendorf, T. M. Alam, R. T. Cygan, et J. U. Otaigbe, « The structure and properties of binary zinc phosphate glasses studied by molecular dynamics simulations », *Journal of Non-Crystalline Solids*, vol. 316, n° 2-3, p. 261-272, févr. 2003.
- [23] U. Hoppe, G. Walter, R. Kranold, et D. Stachel, « Structural specifics of phosphate glasses probed by diffraction methods: a review », *Journal of Non-Crystalline Solids*, vol. 263, p. 29-47, 2000.
- [24] J. E. Stanworth, « Tellurite glasses », *Nature*, vol. 169, n° 4301, p. 581, 1952.
- [25] W. H. Zachariasen, « The atomic arrangement in glass », *Journal of the American Chemical Society*, vol. 54, n° 10, p. 3841-3851, 1932.
- [26] J. R. Van Wazer, « Phosphorus and its Compounds », 1958.
- [27] R. K. Brow, « Review: the structure of simple phosphate glasses », *Journal of Non-Crystalline Solids*, vol. 263-264, p. 1-28, mars 2000.
- [28] E. Metwalli et R. K. Brow, « Modifier effects on the properties and structures of aluminophosphate glasses », *Journal of non-crystalline solids*, vol. 289, n° 1-3, p. 113-122, 2001.
- [29] U. Hoppe, R. Kranold, A. Barz, D. Stachel, J. Neufeind, et D. A. Keen, « Combined neutron and X-ray scattering study of phosphate glasses », *Journal of non-crystalline solids*, vol. 293, p. 158-168, 2001.
- [30] G. Walter, U. Hoppe, J. Vogel, G. Carl, et P. Hartmann, « The structure of zinc polyphosphate glass studied by diffraction methods and ^{31}P NMR », *Journal of Non-Crystalline Solids*, vol. 333, n° 3, p. 252-262, mars 2004.
- [31] S. Bruni *et al.*, « Short Range Order of Sodium-Zinc, Sodium-Copper, and Sodium-Nickel Pyrophosphate Glasses by Diffractometric and Spectroscopic Techniques », *The Journal of Physical Chemistry*, vol. 99, n° 41, p. 15229-15235, oct. 1995.
- [32] K. Suzuya, D. L. Price, C.-K. Loong, et S. Kohara, « The structure of magnesium phosphate glasses », *Journal of Physics and Chemistry of Solids*, vol. 60, n° 8-9, p. 1457-1460, 1999.
- [33] K. Suzuya, K. Itoh, A. Kajinami, et C.-K. Loong, « The structure of binary zinc phosphate glasses », *Journal of non-crystalline solids*, vol. 345, p. 80-87, 2004.
- [34] E. Sourial, T. Peres, J. A. Capobianco, A. Speghini, et M. Bettinelli, « A structural investigation of $\text{Mg}(\text{PO}_3)_2$, $\text{Zn}(\text{PO}_3)_2$ and $\text{Pb}(\text{PO}_3)_2$ glasses using molecular dynamics simulation », *Physical Chemistry Chemical Physics*, vol. 1, n° 8, p. 2013-2018, 1999.
- [35] J. Du *et al.*, « Structure of Cerium Phosphate Glasses: Molecular Dynamics Simulation: Structure of Cerium Phosphate Glasses », *Journal of the American Ceramic Society*, vol. 94, n° 8, p. 2393-2401, août 2011.
- [36] R. Anderson, T. Brennan, G. Mountjoy, R. J. Newport, et G. A. Saunders, « An EXAFS study of rare-earth phosphate glasses in the vicinity of the metaphosphate composition », *Journal of Non-Crystalline Solids*, vol. 232-234, p. 286-292, juill. 1998.
- [37] J. M. Cole *et al.*, « An x-ray diffraction and ^{31}P MAS NMR study of rare-earth phosphate glasses, $(\text{R}_2\text{O}_3)_x(\text{P}_2\text{O}_5)_{1-x}$, $x = 0.175-0.263$, $\text{R} = \text{La, Ce, Pr, Nd, Sm, Eu, Gd, Tb, Dy, Ho, Er}$ », *Journal of Physics: Condensed Matter*, vol. 13, n° 18, p. 4105-4122, mai 2001.
- [38] G. Mountjoy, J. M. Cole, T. Brennan, R. J. Newport, G. A. Saunders, et G. W. Wallidge, « A rare earth L3-edge EXAFS and L1-edge XANES study of Ce, Nd and Eu phosphate glasses and crystals in the composition range from metaphosphate to ultraphosphate », *Journal of Non-Crystalline Solids*, vol. 279, n° 1, p. 20-27, janv. 2001.
- [39] J. M. Cole *et al.*, « A rare-earth K-edge EXAFS study of rare-earth phosphate glasses, $(\text{R}_2\text{O}_3)_x(\text{P}_2\text{O}_5)_{1-x}$, $x = 0.187-0.239$, $\text{R} = \text{La, Nd, Sm, Eu, Gd, Dy, Er}$ », *Journal of Physics: Condensed Matter*, vol. 13, n° 31, p. 6659-6674, août 2001.
- [40] R. A. Martin, G. Mountjoy, et R. J. Newport, « A molecular dynamics model of the atomic structure of dysprosium aluminophosphate glass », *Journal of Physics: Condensed Matter*, vol. 21, n° 7, p. 075102, févr. 2009.

List of Figures

FIGURE 1 A SHELL OF RADIUS R AND THICKNESS ΔR AROUND A REFERENCE ATOM	63
FIGURE 2 IMAGE OF MD MODELS OF META-NA (LEFT) AND META-ZN (RIGHT): RED SPHERES ARE OXYGEN O, TETRAHEDRA ARE PO_4 , ORANGE SPHERES ARE SODIUM NA, GREY SPHERES ARE ZINC ZN.	65
FIGURE 3 NEUTRON (A) AND X-RAY (B) DIFFRACTION STRUCTURE FACTORS $S(Q)$ FROM MD SIMULATION (RED LINES) AND EXPERIMENTS (GREEN [7] AND BROKEN LINES [8]) FOR NON-DOPED SODIUM METAPHOSPHATE GLASS.	66
FIGURE 4 NEUTRON (A) AND X-RAY (B) DIFFRACTION STRUCTURE FACTORS $S(Q)$ FROM MD SIMULATION (RED LINES) AND EXPERIMENTS (BROKEN LINES [6]) FOR NON-DOPED ZINC METAPHOSPHATE GLASS.	66
FIGURE 5 NEUTRON (A) AND X-RAY (B) DIFFRACTION STRUCTURE FACTORS $S(Q)$ FROM MD SIMULATION FOR NON-DOPED ZINC AND SODIUM METAPHOSPHATE GLASSES	66
FIGURE 6 PARTIAL PAIR DISTRIBUTION FUNCTION $G_{ij}(R)$ FOR MD SIMULATION OF ZINC METAPHOSPHATE GLASS (TOP) AND SODIUM METAPHOSPHATE GLASS (BOTTOM). (P-O, P-P AND O-O PAIR DISTRIBUTION FUNCTIONS (LEFT); M-O, M-P AND M-M DISTRIBUTION FUNCTIONS (RIGHT)) (MEDIUM MODEL MM)	67
FIGURE 7 COMPARISON OF M-M PAIR DISTRIBUTION FUNCTION $G_{MM}(R)$ FOR MD SIMULATION OF ZINC AND SODIUM METAPHOSPHATE GLASS	68
FIGURE 8 CUMULATIVE DISTRIBUTION FUNCTIONS $CN_{ij}(R)$ FOR DIFFERENT ATOMIC CORRELATIONS PRESENT IN META-ZN AND META-NA (MEDIUM MODELS MM)	68
FIGURE 9 IMAGE OF MD MODELS OF META-NA (LEFT) AND META-NA-EU (RIGHT): RED SPHERES ARE OXYGEN O, TETRAHEDRA ARE PO_4 , ORANGE SPHERES ARE SODIUM NA AND SKY BLUE SPHERES ARE EUROPIUM EU.	74
FIGURE 10 IMAGE OF MD MODELS OF META-ZN (LEFT) AND META-ZN-EU (RIGHT): RED SPHERES ARE OXYGEN O, TETRAHEDRA ARE PO_4 , GREY SPHERES ARE ZINC ZN AND SKY BLUE SPHERES ARE EUROPIUM EU.	74
FIGURE 11 NEUTRON DIFFRACTION STRUCTURE FACTORS $S(Q)$ FROM MD SIMULATION FOR NON-DOPED AND EUROPIUM DOPED SODIUM (A) AND ZINC (B) METAPHOSPHATE GLASSES.	75
FIGURE 12 X-RAY DIFFRACTION STRUCTURE FACTORS $S(Q)$ FROM MD SIMULATION FOR NON-DOPED AND EUROPIUM DOPED SODIUM (A) AND ZINC (B) METAPHOSPHATE GLASSES.	75
FIGURE 13 PARTIAL PAIR DISTRIBUTION FUNCTION $G_{ij}(R)$ FOR MD SIMULATION OF META-ZN-EU (ABOVE) AND META-NA-EU (BELOW).	76
FIGURE 14 CUMULATIVE COORDINATION NUMBER $CN_{ij}(R)$ FOR MD SIMULATION OF META-ZN-EU, META-NA-EU, META-ZN AND META-NA (MEDIUM MODEL MM)	77
FIGURE 15 Q^N DISTRIBUTIONS FROM MD SIMULATIONS MODELS	79
FIGURE 16 IMAGE OF MD MODELS OF POLY-NA-EU (LEFT) AND POLY-K-EU (RIGHT): RED SPHERES ARE OXYGEN O, VIOLET SPHERES ARE PHOSPHORUS P, GREY SPHERES ARE ZINC ZN, ORANGE SPHERES ARE SODIUM NA, GREEN SPHERE ARE K AND BLUE SKY SPHERES ARE EUROPIUM EU.	80
FIGURE 17 X-RAY (LEFT) AND NEUTRON (RIGHT) DIFFRACTION STRUCTURE FACTORS $S(Q)$ FROM MD SIMULATION FOR NON-DOPED AND EU DOPED SODIUM AND POTASSIUM POLYPHOSPHATE GLASS.	81
FIGURE 18 PARTIAL PAIR DISTRIBUTION FUNCTION $G_{ij}(R)$ OF NON-DOPED AND EU DOPED SODIUM ZINC POLYPHOSPHATE GLASSES (TOP) AND POTASSIUM ZINC POLYPHOSPHATE GLASSES (BOTTOM).(MEDIUM MODEL MM)	82
FIGURE 19 CUMULATIVE COORDINATION NUMBER $CN_{ij}(R)$ OF POLY-NA-ZN, POLY-NA-ZN-EU, POLY-K-ZN-EU AND POLY-K-ZN-EU (MEDIUM MODEL MM)	83
FIGURE 20 IMAGE OF MD MODELS OF META-NA-EU: RED SPHERES ARE OXYGEN O, VIOLET SPHERES ARE PHOSPHORUS P, ORANGE SPHERES ARE SODIUM NA AND BLUE SKY SPHERES ARE EUROPIUM EU (WITH BIG MODEL: ABOUT 25000 ATOMS)	89
FIGURE 21 IMAGE OF MD MODELS OF POLY-ZN-NA-EU: RED SPHERES ARE OXYGEN O, VIOLET SPHERES ARE PHOSPHORUS P, GREY SPHERES ARE ZINC ZN, ORANGE SPHERES ARE SODIUM NA AND BLUE SKY SPHERES ARE EUROPIUM EU (WITH BIG MODEL: ABOUT 25000 ATOMS)	90
FIGURE 22 NEUTRON(LEFT) AND X-RAY (RIGHT) DIFFRACTION STRUCTURE FACTORS $S(Q)$ COMPARISON BETWEEN BIG BM AND MEDIUM MODEL MM FOR EU DOPED SODIUM METAPHOSPHATE AND SODIUM ZINC POLYPHOSPHATE GLASSES	91
FIGURE 23 PARTIAL PAIR DISTRIBUTION FUNCTION $G_{ij}(R)$ OF META-NA-EU (A), META-ZN-EU (B), POLY-ZN-NA-EU (C) POLY-ZN-K-EU (D), (BIG MODEL BM)	93

FIGURE 24 EU-O (LEFT) AND EU-P (RIGHT) PAIR DISTRIBUTION FUNCTION $G_{ij}(R)$ OF EUROPIUM DOPED METAPHOSPHATE AND POLYPHOSPHATE GLASSES (BIG MODEL BM).-----	95
FIGURE 25 CUMULATIVE COORDINATION NUMBER $N_{ij}(R)$ COMPARISON BETWEEN BM AND MM -----	95
FIGURE 26 EU-O, EU-EU AND EU-P COORDINATION NUMBER $CN_{ij}(R)$ FOR MEDIUM MM (LEFT) AND BIG MODEL BM (RIGHT).-----	96
FIGURE 27 EU-EU PAIR DISTRIBUTION FUNCTION $G_{ij}(R)$: COMPARISON BETWEEN BM AND MM OF META-NA-EU (LEFT) AND POLY-ZN-NA-EU (RIGHT)-----	98
FIGURE 28 EU-EU PAIR DISTRIBUTION FUNCTION $G_{ij}(R)$ OF METAPHOSPHATE AND POLYPHOSPHATE GLASSES (BIG MODEL BM)-----	98
FIGURE 29 EU-M PAIR DISTRIBUTION FUNCTION $G_{ij}(R)$ (M=NA, K AND ZN): COMPARISON BETWEEN BM AND MM OF METAPHOSPHATE (LEFT) AND POLYPHOSPHATE GLASSES (RIGHT).-----	99
FIGURE 30 EU-ZN (A), EU-NA (B) AND EU-NA AND EU-K (C) PAIR DISTRIBUTION FUNCTION $G_{ij}(R)$ OF METAPHOSPHATE AND POLYPHOSPHATE GLASSES. (BIG MODELS)-----	100
FIGURE 31 EU-M COORDINATION NUMBER $CN_{ij}(R)$ (M=ZN, NA AND K): COMPARISON BETWEEN MM AND BM OF METAPHOSPHATE AND POLYPHOSPHATE GLASSES.-----	101

List of Tables

TABLE 1 GLASS COMPOSITION -----	60
TABLE 2 BUCKINGHAM INTERATOMIC POTENTIAL PARAMETERS FOR DIFFERENT PAIR CORRELATIONS. -----	61
TABLE 3 INTERATOMIC POTENTIAL PARAMETERS OF THREE BODY POTENTIALS TBP -----	61
TABLE 4 DENSITY, BOX SIZE AND NUMBER OF ATOMS USED IN MD SIMULATION MODELS FOR EU DOPED AND NON-DOPED METAPHOSPHATE GLASSES.-----	62
TABLE 5 NEAREST NEIGHBOR DISTANCES R_{ij} , AND COORDINATION NUMBER N_{ij} OF P-O, P-P AND O-O CORRELATIONS FROM MD SIMULATIONS COMPARED TO EXPERIMENTS AND PREVIOUS MD MODELS IN METAPHOSPHATE GLASSES META-NA AND META-ZN. (MEDIUM MODEL MM)-----	69
TABLE 6 NEAREST NEIGHBOR DISTANCES R_{ij} , AND COORDINATION NUMBER N_{ij} OF NA-O, NA-P AND NA-NA CORRELATIONS FROM MD SIMULATIONS COMPARED TO EXPERIMENTS AND PREVIOUS MD MODELS IN SODIUM METAPHOSPHATE GLASSES (META-NA).(MEDIUM MODEL MM).-----	69
TABLE 7 NEAREST NEIGHBOR DISTANCES R_{ij} , AND COORDINATION NUMBER N_{ij} OF ZN-O, ZN-P AND ZN-ZN CORRELATIONS FROM MD SIMULATIONS COMPARED TO EXPERIMENTS AND PREVIOUS MD MODELS IN SODIUM METAPHOSPHATE GLASSES (META-ZN).(MEDIUM MODEL MM).-----	69
TABLE 8 Q^N DISTRIBUTIONS FROM MD SIMULATIONS MODELS AND ^{31}P NMR EXPERIMENT.-----	73
TABLE 9 COORDINATION-NUMBER DISTRIBUTION FOR PHOSPHORUS AND OXYGEN ATOMS IN METAPHOSPHATE GLASSES (MEDIUM MODEL MM) -----	73
TABLE 11 NEAREST NEIGHBOR DISTANCES R_{ij} , AND COORDINATION NUMBER N_{ij} OF P-O, P-P AND O-O CORRELATIONS FROM MD SIMULATIONS IN NON-DOPED AND EU DOPED METAPHOSPHATE GLASSES: META-NA, META-ZN, META-NA-EU AND META-ZN-EU (MEDIUM MODEL MM)-----	78
TABLE 12 NEAREST NEIGHBOR DISTANCES R_{ij} , AND COORDINATION NUMBER N_{ij} OF NA-O, NA-P AND NA-NA CORRELATIONS FROM MD SIMULATIONS IN NON-DOPED AND EU DOPED SODIUM METAPHOSPHATE GLASSES: META-NA AND META-NA-EU (MEDIUM MODEL MM).-----	78
TABLE 13 NEAREST NEIGHBOR DISTANCES R_{ij} , AND COORDINATION NUMBER N_{ij} OF ZN-O, ZN-P AND ZN-ZN CORRELATIONS FROM MD SIMULATIONS IN NON-DOPED AND EU DOPED ZINC METAPHOSPHATE GLASSES: META-NA AND META-NA-EU (MEDIUM MODEL MM).-----	78
TABLE 14 Q^N DISTRIBUTION FOR PHOSPHORUS ATOMS IN NON-DOPED AND EU DOPED METAPHOSPHATE GLASS FROM MD SIMULATIONS MODELS (MM)-----	79
TABLE 15 COORDINATION-NUMBER DISTRIBUTION FOR PHOSPHORUS ATOMS IN METAPHOSPHATE GLASSES (MEDIUM MODEL MM)-----	79
TABLE 16 NEAREST NEIGHBOR DISTANCES R_{ij} AND COORDINATION NUMBER N_{ij} OF P-O, P-P AND O-O CORRELATIONS FROM MD SIMULATIONS IN NON-DOPED AND EU DOPED POLYPHOSPHATE COMPARED TO METAPHOSPHATE GLASSES (MEDIUM MODEL MM).-----	85

TABLE 17 NEAREST NEIGHBOR DISTANCES R_{ij} AND COORDINATION NUMBER N_{ij} OF NA-O, NA-P, NA-NA AND NA-ZN CORRELATIONS FROM MD SIMULATIONS IN NON-DOPED AND EU DOPED POLYPHOSPHATE COMPARED TO METAPHOSPHATE GLASSES (MEDIUM MODEL MM)-----	86
TABLE 18 NEAREST NEIGHBOR DISTANCES R_{ij} AND COORDINATION NUMBER N_{ij} OF K-O, K-P, K-K AND K-ZN CORRELATIONS FROM MD SIMULATIONS IN NON-DOPED AND EU DOPED POTASSIUM POLYPHOSPHATE (MEDIUM MODEL MM)-----	86
TABLE 19 NEAREST NEIGHBOR DISTANCES R_{ij} AND COORDINATION NUMBER N_{ij} OF ZN-O, ZN-P AND ZN-ZN CORRELATIONS FROM MD SIMULATIONS IN NON-DOPED AND EU DOPED POLYPHOSPHATE COMPARED TO METAPHOSPHATE GLASSES (MEDIUM MODEL MM)-----	86
TABLE 20 Q^N DISTRIBUTIONS FROM MD SIMULATIONS MODELS AND ^{31}P NMR EXPERIMENT.-----	87
TABLE 21 COORDINATION NUMBER DISTRIBUTION FOR PHOSPHORUS AND OXYGEN ATOMS IN POLYPHOSPHATE GLASSES-----	87
TABLE 21 NEAREST NEIGHBOR DISTANCES R_{ij} AND COORDINATION NUMBER N_{ij} OF P-O, P-P AND O-O CORRELATIONS FROM MD SIMULATIONS IN EU DOPED GLASSES: COMPARISON BETWEEN MEDIUM MM AND BIG MODEL BM-----	102
TABLE 22 NEAREST NEIGHBOR DISTANCES R_{ij} AND COORDINATION NUMBER N_{ij} OF NA-O, NA-P, NA-NA AND NA-ZN CORRELATIONS FROM MD SIMULATIONS IN EU DOPED GLASSES: COMPARISON BETWEEN MEDIUM MM AND BIG MODEL BM-----	102
TABLE 23 NEAREST NEIGHBOR DISTANCES R_{ij} AND COORDINATION NUMBER N_{ij} OF K-O, K-P,K-K AND K-ZN CORRELATIONS FROM MD SIMULATIONS IN EU DOPED GLASSES: COMPARISON BETWEEN MEDIUM MM AND BIG MODEL BM-----	102
TABLE 24 NEAREST NEIGHBOR DISTANCES R_{ij} AND COORDINATION NUMBER N_{ij} OF ZN-O, ZN-P AND ZN-ZN CORRELATIONS FROM MD SIMULATIONS IN EU DOPED GLASSES: COMPARISON BETWEEN MEDIUM MM AND BIG MODEL BM-----	103
TABLE 25 NEAREST NEIGHBOR DISTANCES R_{ij} AND COORDINATION NUMBER N_{ij} OF EU-O, EU-P AND EU-EU CORRELATIONS FROM MD SIMULATIONS IN EU DOPED GLASSES: COMPARISON BETWEEN MEDIUM MM AND BIG MODEL BM-----	103
TABLE 26 NEAREST NEIGHBOR DISTANCES R_{ij} AND COORDINATION NUMBER N_{ij} OF EU-O, EU-P AND EU-EU CORRELATIONS FROM MD SIMULATIONS IN EU DOPED GLASSES: COMPARISON BETWEEN MEDIUM MM AND BIG MODEL BM.-----	103
TABLE 27 Q^N DISTRIBUTIONS OF EU FROM MD SIMULATIONS MODELS: COMPARISON BETWEEN MEDIUM MM AND BIG MODEL BM-----	104
TABLE 28 COORDINATION-NUMBER DISTRIBUTION FOR EUROPIUM ATOMS IN METAPHOSPHATE GLASSES (BIG MODEL BM)-----	104

Chapter 4

Study of phosphate glasses under electron irradiation

Chapter 4 Study of phosphate glasses under electron irradiation

1	Electron irradiation conditions (SIRIUS Accelerator).....	112
2	Phosphate glass structure under electron irradiation	114
2.1	Bibliography part (Glass network evolution under irradiation)	114
2.1.1	Generality on glass evolution under irradiation.....	114
2.1.2	Phosphate glasses	115
2.2	Metaphosphate glass structure under 2.5 MeV irradiation.....	116
2.2.1	Alkali and mixed-alkali metaphosphate glasses	116
2.2.2	Zinc metaphosphate glasses under irradiation	117
2.3	Polyphosphate glass structure under 2.5 MeV irradiation	119
2.4	Glass structure evolution under 700 keV electron irradiation.....	121
3	Eu ³⁺ ion environment evolution under electron irradiation	125
3.1	Asymmetry Ratio in pristine glasses.....	125
3.2	Asymmetry ratio evolution under 2.5 MeV irradiation.....	126
3.2.1	Energy and dose effect (700 keV vs 2.5 MeV).....	130
3.2.2	Influence of the alkaline ion type.....	132
3.3	⁵ D ₀ → ⁷ F ₀ transition under 2.5 MeV irradiation:	134
3.3.1	Energy shift.....	135
3.3.2	Broadening of the ⁵ D ₀ → ⁷ F ₀ emission band	135
3.3.3	Electron energy Effect (700 keV vs 2.5 MeV)	136
3.4	⁵ D ₀ Energy level lifetime	139
4	Eu ³⁺ ion reduction into Eu ²⁺ under electron irradiation	141
4.1	PL spectroscopy analysis	141
4.2	EPR spectroscopy analysis.....	144
4.3	Energy effect: 2.5 MeV vs 700 keV.....	149

1 Electron irradiation conditions (SIRIUS Accelerator)

The glass samples were irradiated by using SIRIUS electron accelerator fabricated by National Electronics Corporation (NEC) and installed in our laboratory “Laboratoire des Solides Irradiés (LSI), Palaiseau, France” (Figure 1). This Pelletron type electron accelerator is characterized by high electron energy that can be modified in the range of 150 keV-2.5 MeV with a current in a 150 nA-50 μ A range. The accelerator is composed of 4 main parts.

- Electron production
- Two stage acceleration of electrons
- Steering of electrons
- Scattering chambers

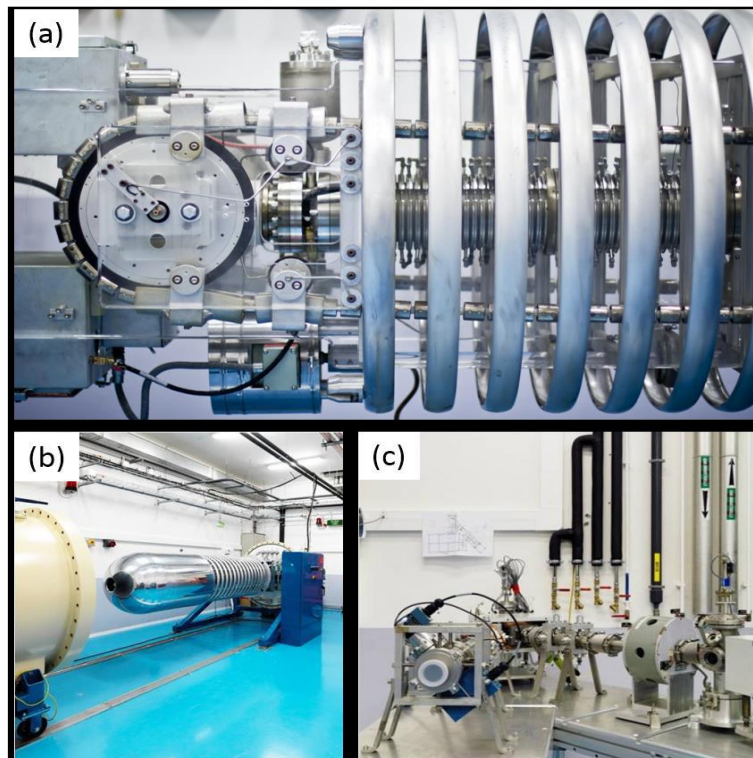


Figure 1 SIRIUS accelerator in LSI (a) close view of inside – Pelletron charging system, (b) accelerator chamber, and (c) irradiation beam lines.

The concept of this accelerator is the generation of electrostatic charge by mechanical transportation system made of a chain of pellets (short conductive tubes connected by links made of insulating material) used to build up high voltage terminals. The system is confined by a pressure vessel filled with insulating sulfur hexafluoride gas SF_6 . It is equipped with an evacuated beamline and the acceleration of electrons is done between the high voltage terminals and the ground. The accelerated electrons come out from the scattering chambers (figure 1b) and their trajectories are controlled by a magnetic field (steering of ions) up to the end of beamline.

As well, the accelerator is equipped with in-situ analysis methods such as photoluminescence and cathodoluminescence, helpful in our case to control the rare earth environment evolution in a real time under irradiation.

Irradiation conditions

In this work, we used two different energies for electrons: 2.5 MeV electron beam with integrated doses from 10^5 Gray (Gy) to 4.15×10^9 Gy and 700 keV electrons at 10^8 and 10^9 Gy (see table 1). The non-doped glasses are irradiated with dose from 10^5 to 10^8 Gy.

Table 1 Electron irradiation conditions

Beam energy	Dose, Gy
2.5 MeV	10^5
	10^6
	10^7
	10^8
	5×10^8
	1.5×10^9
	4.15×10^9
700 keV	10^8
	10^9

In case of 2.5 MeV, all the sample volume (4x4x0.8mm) was homogeneously irradiated contrary to 700 keV energy where electron beam is stopped in the glass at a depth of 900 and 765 μm in respectively metaphosphate and polyphosphate glasses depending on the density (sample thickness ~ 1.4 mm). The sample holder in copper was maintained around 30°C with a water cooling system. The current was measured 5-7 μA at the sample. After irradiation, the samples undergo a change of color towards the transparent brown as displayed in figure 2. The irradiated sample were conserved in desiccator.

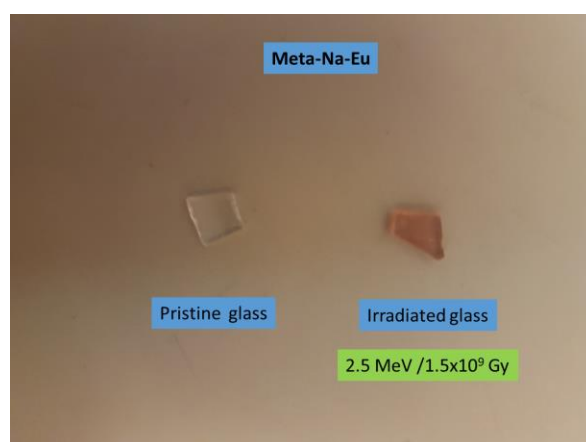


Figure 2 Color change of Meta-Na-Eu glass after 2.5 MeV electron irradiation

2 Phosphate glass structure under electron irradiation

2.1 Bibliography part (Glass network evolution under irradiation)

2.1.1 Generality on glass evolution under irradiation

The radiation effect on the glass properties and structure were investigated in a large number of works in literature including silica, silicate, borate, aluminoborosilicate, borotellurite and phosphate glasses etc.

Among the properties affected one can cite the optical (light transmission, refractive index, polarizability...) and mechanical properties (density, hardness, Young Modulus and fracture toughness). Most of them are correlated with point defects creation leading to the Radiation Induced Attenuation or Radiation Induced Emission in optical fibers for instance.

From a structural point of view, silica glass under irradiation (gamma, X rays, electron and neutron) has been largely studied.

Devine et al.[1] reported a decrease of the Si-O-Si angle and an increase of Si-O-Si angle distribution in silica glasses under neutron irradiation. The rings statics is also modified with a larger distribution in the irradiated glass with an increase of 3 and 4 membered rings. As well, the compaction of the glass was reported with a maximum of densification of about 3%. This saturation value is observed to be the same under all types of irradiations (ions, electron, neutron or UV photon). Howitt et al. [2] investigated the Na silicate glasses under gamma irradiation at energies of 1.17, 1.33 and 0.66 MeV and at dose of the order of MGy. Using TEM technique, they observed the formation of bubbles attributed to oxygen. However no bubbles were detected in the same glass irradiated by gamma rays at higher doses [3]. Ollier et al. [4] also mentioned that oxygen bubbles could be observed in Li borosilicate glasses depending on the electron irradiation conditions: fluxes and temperature.

Moreover, the most studied glass is nevertheless probably the aluminoborosilicate glass being the storage matrix for French High Level nuclear waste.

The effect of alpha, 1/3.5/7 MeV multi-energy gold ions and 74 MeV Krypton ions irradiations on the structure of aluminoborosilicate glasses were studied by Mendoza et al. [5] using Raman spectroscopy. The results suggest similar effects on the glass properties induced by the different kinds of irradiation that are used to study both the effect of electronic and nuclear (ballistic) interaction on the borosilicate glass, revealing a depolymerization of silicate network and a decrease of the boron coordination number from 4 to 3 (ballistic origin).

Boizot et al.[6] studied the structural evolution of aluminoborosilicate glasses under 2.5 MeV β -irradiation up to doses of 10^9 Gy order. Raman spectroscopy showed at dose higher than 10^9 Gy: (i) production of dissolved molecular oxygen, (ii) An increase of glass polymerization and (iii) a decrease of the network formers rings average sizes correlated to glass densification process. As well, these structural evolutions are correlated to the migration of alkaline ions during irradiations. In this connection, Ollier et al. studied the structure and boron environment in a series of mixed Na/K and Na/Li aluminoborosilicate glasses under 1.8 MeV electrons irradiations at dose close to 10^9 Gy. They showed an increase of BO_3 species, implying a conversion of BO_4 into BO_3 species under irradiation. This increase is a little more

efficient for Li then Na then K. Another interesting point to be underlined is that the mixed alkali ions affects the structural modification under irradiation. Thus, in mixed Na/Li aluminoborosilicate glass, polymerization is stable whereas BO_4 is converted into BO_3 species. An opposite trend is observed in mixed Na/K glass where polymerization increase and boron conversion is absent.

This result was used and justified the present part of this PhD studying a potential mixed alkali effect (Na/Li and Na/K) on the meta and polyphosphate glass structure evolution and to check its impact on the Eu environment evolution under irradiation.

2.1.2 Phosphate glasses

It is important to study the interaction of irradiation with a phosphate glass system as it may lead to various changes in the structural, optical and electrical properties of the glasses. For these reasons, the structure of an irradiated glass is a key parameter that determines its properties and performance.

Information on the structure and properties in these types of glasses under irradiation is rather limited in literature. In this subject, it has been shown that phosphate glasses suffer a structural variation under gamma or alpha irradiation [7]–[9] but the integrated dose does not exceed 10^8 Gy. The structural changes can be related to bond breaking as well as rearrangement of bonds taking place during irradiation which appears to be dependent on the dose irradiation and glass composition. Moreover, the relaxation process release some of the excess energy stored in the structure resulting in change in the bond angle [9]. In this respect, Exahros et al. [7] reported a shift of the symmetric stretching mode $\nu_s(\text{PO}_2)$ towards lower wavenumber in binary metaphosphate glasses $\text{Y}(\text{PO})_3$ and NaPO_3 when irradiated by 5.5 MeV gamma at dose = 1.3×10^8 Gy indicating an increase of the bond angle and therefore, suggesting an expansion of the chain and contraction of the terminal ionic sites.

Further, the growth of the intensity ratio $I(\text{POP})/I(\text{PO}_2)$ under irradiation is explained by the electronic excitation at ionic sites in the glass [7]. Thus, excitation from bonding phosphorus, NBO orbitals would decrease the covalence of this interaction by decreasing the bond polarizability. The decrease in the Raman intensity for the out of chain PO_2 will result.

A slight change in the vitreous network of lithium ultraphosphate glasses after gamma irradiation at low dose of 6×10^4 Gy was detected where there was a possible change in bond angles and/or band length between the structural buildings units or the depolymerization of the phosphate network [8].

As well, it has been established that phosphate glasses produce many kinds of defect and colors centers formed as a result of capturing of electrons and holes pairs when irradiated by high energy particles or radiation such as UV, gamma rays and neutrons [8], [10]–[13]. The induced defect effectively break the connectivity of the network while accumulation of such broken linkages results in local structural collapse or randomly rebinding [14]. Ebeling et al. [12] reported the presence of phosphorus and oxygen related X-ray radiation induced defects in phosphate glass such as phosphorus oxygen hole center (POHC) absorbing in visible spectral region at 540, 430 and 325 nm. Pukhkaya et al. [10] announced a strong impact of the glass

network type on the defect nature in Yb doped phosphate glasses after 2.5 MeV electron irradiation at various doses that the formation of POHC defect is found to be strongly correlated to Q^2 tetrahedra. A competitive formation between POHC and P-related peroxy radicals (two banded oxygen are linked to phosphorus) has been detected at high dose from 10^7 Gy. Ultraphosphate glasses contain the larger defect type: Peroxy-radicals, PO_3^{2-} (P_1), PO_4^{4-} (P_2) and PO_4^{2-} (P_4) whose formation are related to the presence of Q^3 tetrahedra. In metaphosphate glasses, a combination of P_1 and P_3 defect was detected (The structure of P_3 has been not understood yet) and in polyphosphate sample, only P_3 defect were found. The aim of this part of work is to better understand the structural evolution in metaphosphate and polyphosphate glasses under electron irradiation in a dose regime (105-109) Gy not fully explored in literature and by using Raman spectroscopy that is a sensitive technique to study the radiation induced structural change.

2.2 Metaphosphate glass structure under 2.5 MeV irradiation

2.2.1 Alkali and mixed-alkali metaphosphate glasses

We studied in this part the glass structural change occurring under irradiation using Raman spectroscopy. Figure 3 compares the Raman spectrum of Eu-doped sodium metaphosphate glass in the 250-1400 cm^{-1} region before and after 2.5 MeV irradiation at various doses from 10^5 to 4.15×10^9 Gy. On this matter, the figure displays no obvious variation of the Raman curves implying no significant network evolution whatever the dose in Meta-Na-Eu.

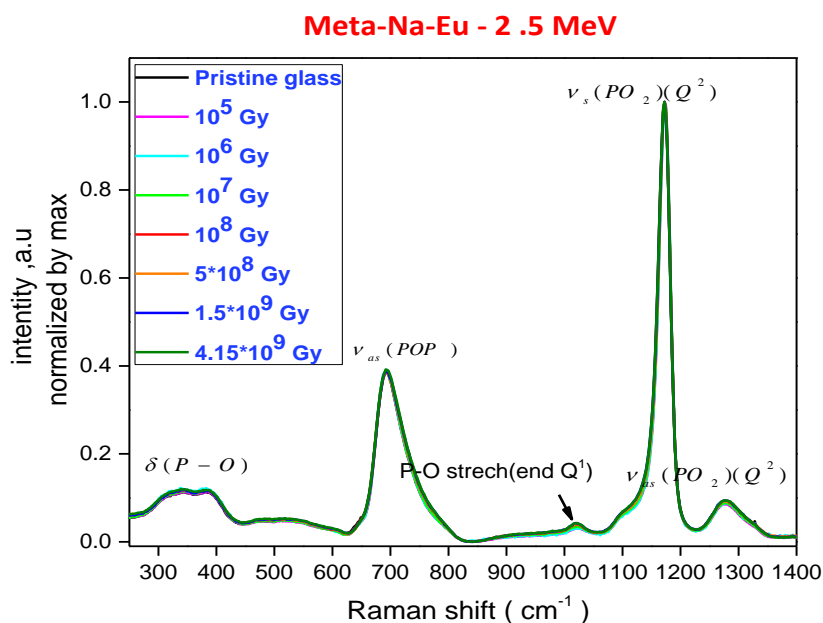


Figure 3 Raman spectra of Meta-Na-Eu irradiated by electron of 2.5 MeV at various dose compared to pristine glass, normalization by maximum

For irradiated Meta-Na-Mg-Eu (Figure 4), we observe a small increase of the band at 1020 cm^{-1} attributed to P-O stretch of Q^1 chain terminator. It indicates at doses from 10^8 Gy a slight decrease in the network polymerization of the sodium magnesium metaphosphate glass. But the main modification concerns the band at 1168 cm^{-1} due to the $\nu_s(PO_2)$ stretching motion

of NBO in Q^2 species that is shifted towards lower wavenumber (1161 cm^{-1}) at highest dose of $4.15 \times 10^9\text{ Gy}$. It suggests an increase of the O-P-O bond angle. This variation is in agreement with the literature that Exahros et al. [7] reported the same shift towards lower wavenumber in binary metaphosphate glasses $Y(\text{PO})_3$ and NaPO_3 under 5.5 MeV gamma irradiation at dose = $1.3 \times 10^8\text{ Gy}$. Moreover, the bands at ~ 1168 and 680 cm^{-1} suffers a slight broadening under irradiation suggesting a decrease of disorder that may be due to change in the distribution of the Q^2 P-O bond length and bond angles [15]. Similarly, the vitreous network of mixed Na/Li metaphosphate glasses (not shown) exhibits same modifications than Na/Mg glass.

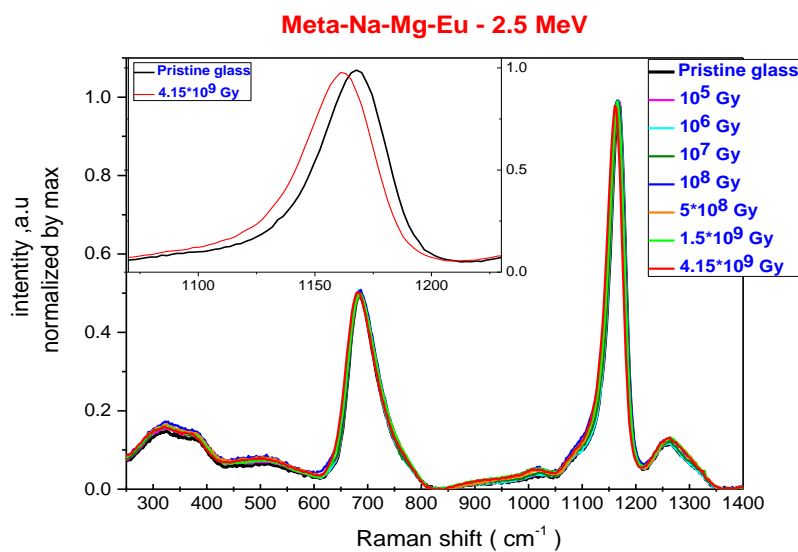


Figure 8 Raman spectra of Meta-Na-Mg-Eu irradiated by electron of 2.5 MeV, normalization by maximum.

2.2.2 Zinc metaphosphate glasses under irradiation

Replacing Na oxide by zinc oxide in the metaphosphate composition, we note that the glass becomes less stable under irradiation (Figure 5).

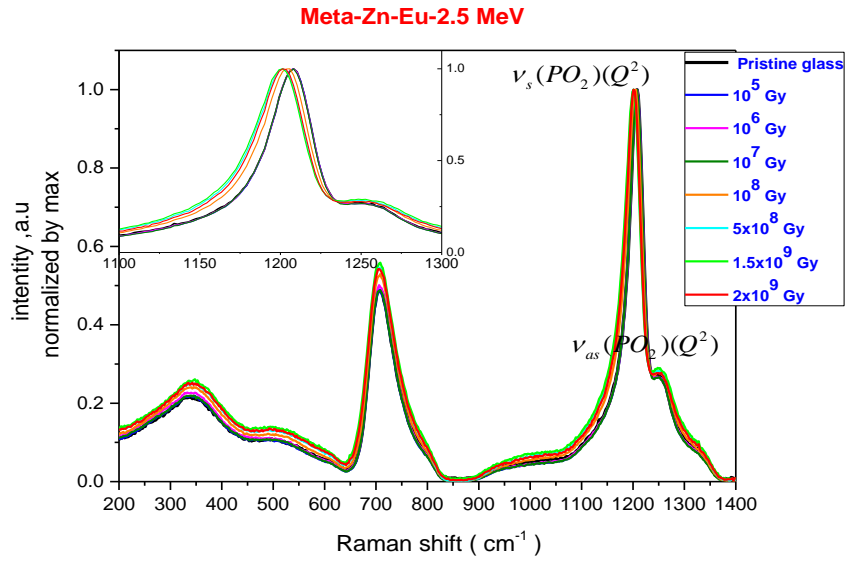


Figure 5 Raman spectra of Meta-Zn-Eu irradiated by electron of 2.5 MeV at various dose compared to pristine glass, normalization by maximum.

We observe an increase of the band intensity in the region 200-650 cm^{-1} corresponding to the bending mode of phosphate tetrahedra with Zn modifier. Even more, the band at 706 cm^{-1} due to symmetric stretching mode of bridging oxygen $\nu_s(\text{POP})$ in Q^2 species and 758 cm^{-1} in Q^1 species undergoes a broadening as well as an increase of the peak intensity under irradiation that are reported as a function of dose logarithm in Figure 6. We can distinguish from figure 6 that there is no broadening of the 706 cm^{-1} band until 10^7 Gy, after the FWHM starts to increase from 61 cm^{-1} in non-irradiated sample to 69 cm^{-1} . We interpret this broadening as an increase of inhomogeneity in the P-O-P environment under electron irradiation at high dose from 10^8 Gy. On the other hand, the variation of the area of this band (Fig. 6) is a result from both the broadening and the increase of the peak intensities representing a relative stronger contribution of the symmetric stretching mode of bridging oxygen in $(\text{P-O-P})_{\text{sym}}$ after irradiation compared to (PO_2) due probably to a modification of ionic site porizability in agreement with [7].

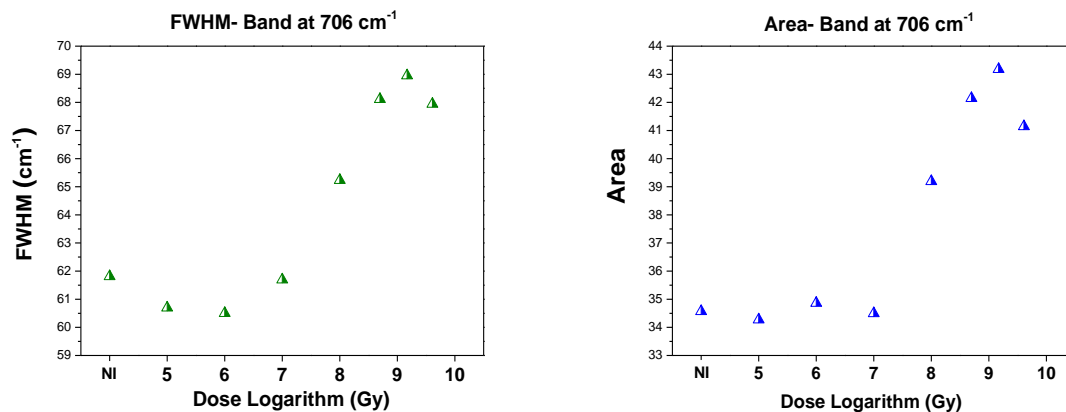


Figure 6 The full width at half maximum FWHM (left) and the Area (right) of the band at 706 cm^{-1} due to $\nu_s(\text{POP})$ as a function of dose logarithm in Meta-Zn-Eu under electron irradiation.

Regarding to the 900-1400 cm^{-1} region, radiation induces an increase of the different contributions in the 900-1100 cm^{-1} region attributed to P-O stretch of Q^1 chain terminator around 1000 cm^{-1} and the symmetric stretching mode of NBO $\nu_s(\text{PO}_3^{2-})$ of Q^1 units around 1050 cm^{-1} meaning more Q^1 species with the potential reduction of chain length by bond breaking under irradiation.

In addition, the band at $\sim 1203 \text{ cm}^{-1}$ corresponding to $\nu_s(\text{PO}_2)$ in Q^2 tetrahedra suffers a broadening under irradiation. In this respect, the FWHM increases from 37 cm^{-1} in pristine glass to 45 cm^{-1} at sample irradiated at $1.5 \times 10^9 \text{ Gy}$ (Figure 7). This broadening with those at 706 cm^{-1} denote a larger distribution of bond angles and chain lengths of Q^2 groups under irradiation [16]. Brow et al. [15] explain the increase of the FWHM of the $\nu_s(\text{PO}_2)$ and $\nu_s(\text{POP})$ with increasing cation field strength by the increase of disorder that may be due to change in the distribution of the Q^2 P-O bond length and bond angles. This broadening of the band due to $\nu_s(\text{PO}_2)$ is accompanied by a shift towards lower wavenumbers as exhibited in the inset of figure 5. The peak maximum shifts from 1208 cm^{-1} in pristine glass to $\sim 1200 \text{ cm}^{-1}$ in irradiated sample at high dose suggesting the increase in the O-P-O bond angle or to variation in the local cationic environment. Thus, Rouse et al. [17] noted that the $\nu_s(\text{PO}_2)$ band decreases in the frequency as the phosphate chain length is longer, indicative of the increase in the average PO_2 angle.

On the other hand, Swenson et al. [18] reported a shift of this band to lower frequencies when replacing Li by Rb in metaphosphate glasses and concluded a variation in the local cationic environment of each PO_2 unit. The $\nu_s(\text{PO}_2)$ band can be regarded as a sensitive local probe of its cationic environment [18]. From these results, we note that Mg^{2+} and Zn^{2+} environments are less stable than Na^+ in metaphosphate glasses under irradiation.

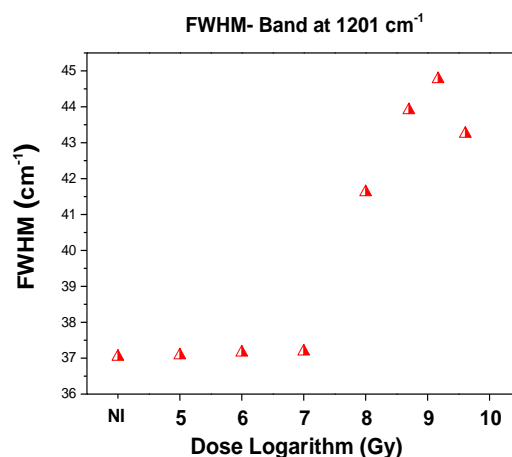


Figure 7 The full width at half maximum FWHM of the band at 1201 cm^{-1} due to $\nu_s(\text{PO}_2)$ as a function of dose logarithm in Meta-Zn-Eu under electron irradiation.

2.3 Polyphosphate glass structure under 2.5 MeV irradiation

In this part, we analyzed the structure evolution of the polyphosphate composition under irradiation. Figure 8 displays the Raman spectra of Na zinc polyphosphate glass irradiated by

2.5 MeV electron irradiation at various dose and compared to pristine glass. Figure 9 is relative to K and Na/K glasses.

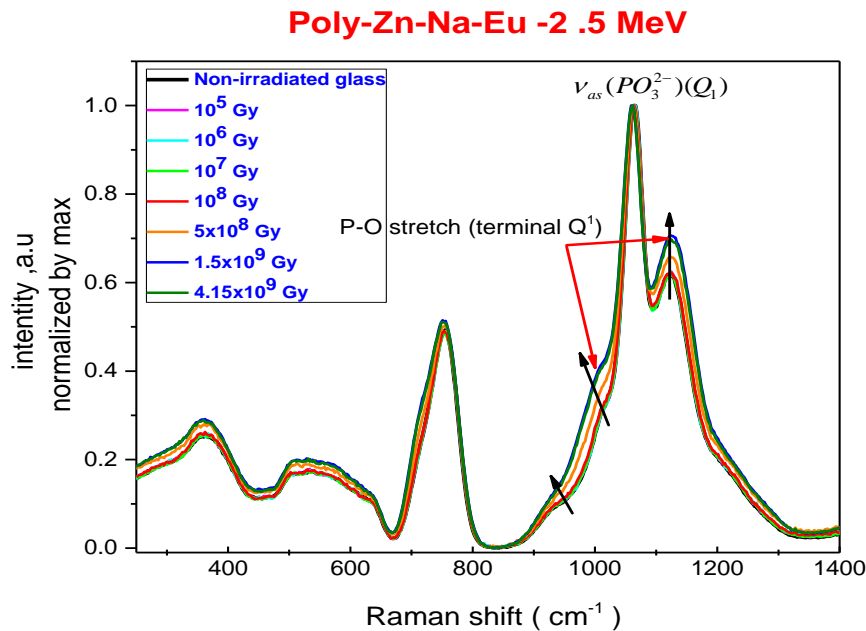


Figure 8 Raman spectra of Poly-Zn-Na-Eu irradiated by electron of 2.5 MeV at various dose compared to pristine glass, normalization by maximum

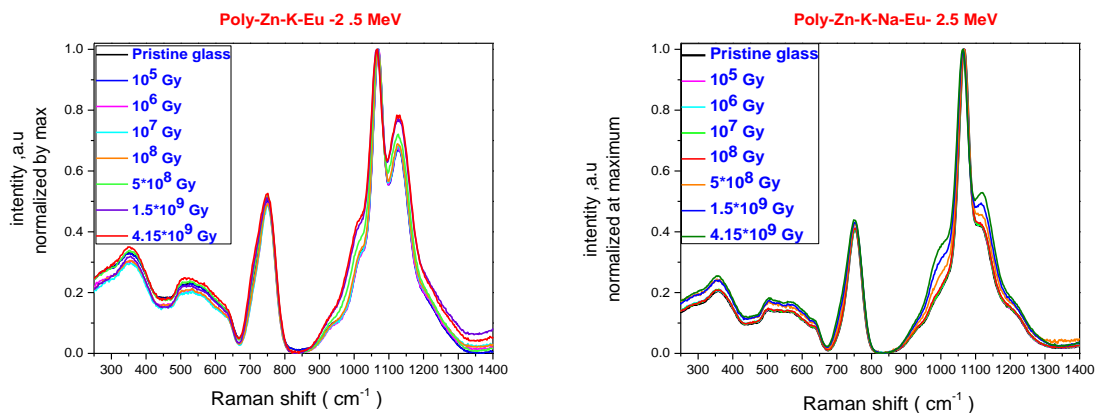


Figure 9 Raman spectra of Poly-Zn-K-Eu (left) and Poly-Zn-Na-K-Eu (right) irradiated by electron of 2.5 MeV at various dose compared to pristine glass, normalization by maximum

Like zinc metaphosphate glass, the zinc polyphosphate glasses undergo significant variations of their vitreous network from integrated doses of 5×10^8 Gy (Fig. 8 and 9).

We note a development of the shoulder at 700 cm^{-1} due to the symmetric stretching of bridging oxygen $\nu_s(\text{P-O-P})$ in Q^2 units and a strong modification of the $900\text{-}1300 \text{ cm}^{-1}$ region. In this connection, we observe a significant increase in the intensity of the bands at near 1020 and 1120 cm^{-1} from 10^8 Gy dose. Both bands corresponds to the P-O stretch of Q^1 chain terminators [19]. These results demonstrate that irradiation shortens the chains by creating

more Q¹ terminators. Even more, a small shoulder develops at 980 cm⁻¹ corresponding to NBO stretch in Q⁰ species and confirm the formation of broken bonds under irradiation.

The intensity of the Raman bands at 1020 and 1120 cm⁻¹ due to the P-O stretch of Q¹ terminal, are plotted as a function of dose logarithm (figure 10). We observed first the normal correlation between both band variations.

This figure precise that the bond breaking occurs from 10⁸ Gy dose with the massive creation of terminal bond in polyphosphate glasses.

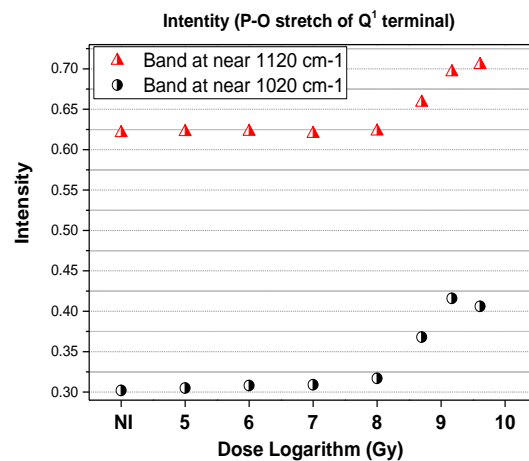


Figure 10 intensity of the bands at 1020 and 1120 cm⁻¹ due to P-O stretch of Q¹ terminal as a function of dose logarithm in Poly-Zn-Na-Eu under 2.5 MeV electron irradiation.

2.4 Glass structure evolution under 700 keV electron irradiation

Figure 11 and 12 present the Raman spectra respectively of sodium zinc polyphosphate irradiated by 700 keV electron irradiation at dose of 10⁹Gy and zinc metaphosphate glasses irradiated at dose 2.5×10⁸ Gy. The Raman spectra were acquired along the glass edge with a step of 200 μm beginning from the irradiated surface up to 1.4 μm depth (The sample thickness about 1.5 mm). The evolution of the Raman spectra described above for 2.5 MeV irradiation are very close to the modifications exhibited in Figures 11 and 12 for a same dose. However, it is interesting to notice that in polyphosphate glasses mostly the change of the glass structure appears in a larger zone than the penetration depth of electrons.

Poly-Na-Eu-700keV-10⁹ Gy

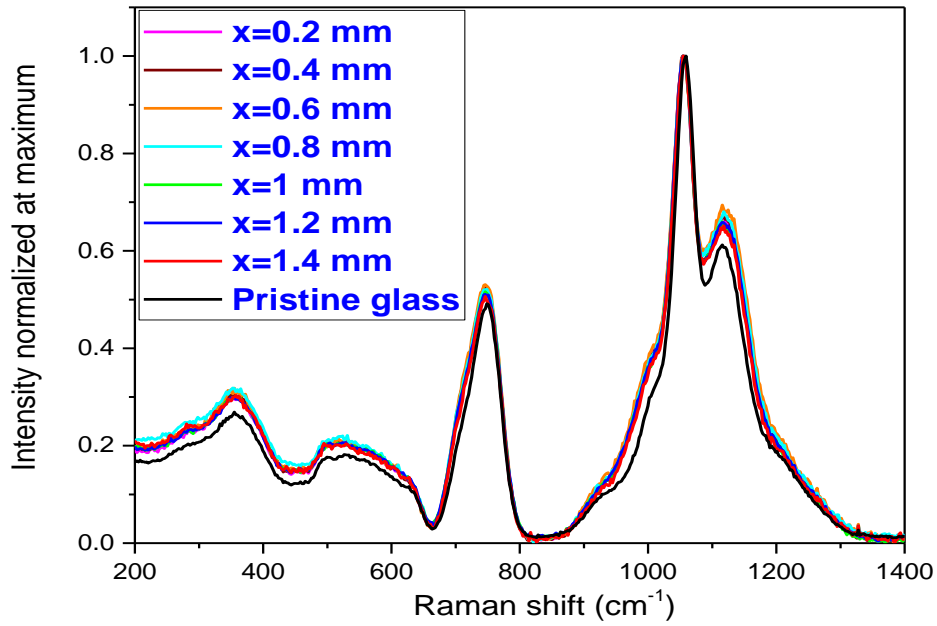


Figure 11 Raman spectrum of Poly-Zn-Na-Eu under 700 keV electron irradiation at dose 10⁹Gy in the larger volume of the sample

Meta-Zn-Eu-700keV-2.5*10⁸ Gy

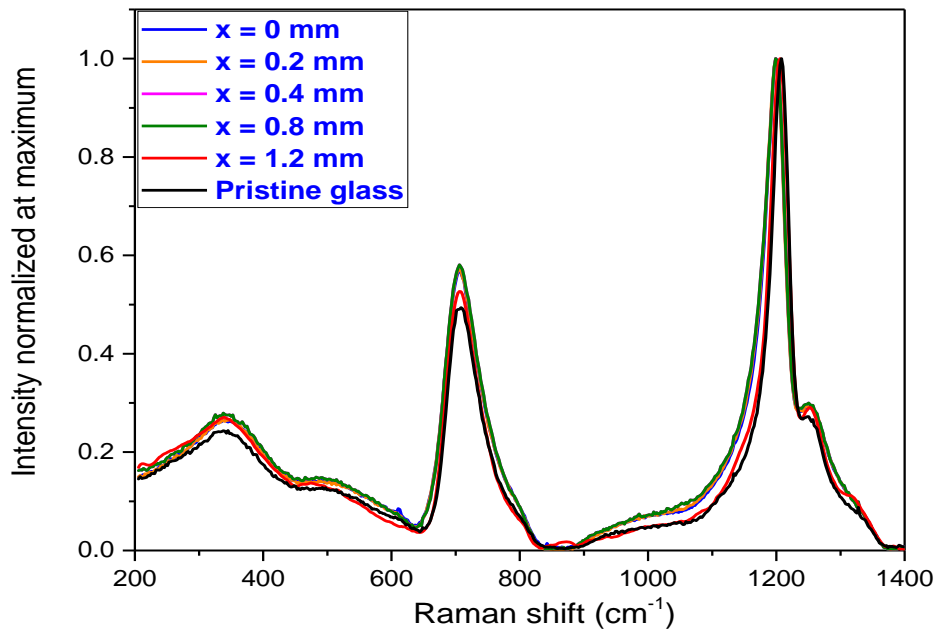


Figure 12 Raman spectrum of Meta-Zn-Eu under 700 keV electron irradiation at dose 2.5x10⁸Gy in the larger volume of the sample

- No significant network evolution in Na metaphosphate glass whatever the dose under 2.5 MeV electron and the glass remain stable.
- An increase of the O-P-O bond angle and/or variation in the local cationic environment were detected in mixed Na/Li, Na/Mg and Zn metaphosphate glasses at high dose from 10^8 Gy. As well, a growth of the disorder that may be due to change in the distribution of the Q² P-O bond length and bond angles. We note that these changes are more efficient in zinc metaphosphate glass.
- In polyphosphate glasses, there is a significant variation of the structure under 2.5 MeV irradiation and the bond breaking occurs at high dose from 10^8 Gy dose with the massive creation of Q¹ terminators.
- The same behavior of the structure evolution is revealed under 700 keV for Zn metaphosphate and polyphosphate. As well, the structure appears to be changed in a larger volume than the penetration depth of electron.

4 Bibliographic part (RE environment evolution under irradiation)

Rare earth ions doped in glasses are widely found in many domains that can be concerned by radiative environment such as optics (laser, phosphor...) and nuclear industry (RE being most of Fission products in nuclear glass). RE ions spectroscopic properties are strongly dependent on the local environment (It is defined by the nature and arrangement of the ligands around the rare earth ions) determined by the crystal field strength and symmetry around the rare earth sites [1]. Therefore, irradiation can affect the environment of RE and thus the glass structure and properties including chemical, electrical, mechanical, magnetic and optical properties. This is why radiation can also be used to produce specific properties in glass.

A larger number of studies using various types of irradiation (gamma [20], [21], [22], electron [20][23], ions [24], X-ray [25] or femtosecond laser [26], [27], [28], [29]) search to evaluate the radiation impact on the local environment of several RE ions (Eu, Yb, Dy, Tb, Ce, Er, Sm...) in glasses. As well, different glass family in silicate [30] such aluminoborosilicate [20], [29], borosilicate [22], aluminosilicate [26], or phosphate [21], fluorozirconate, fluoroaluminate [27] and oxyfluoride glasses [31] were studied. The main irradiation effect is the valence state change of the rare earth that will be discussed in 3.1.1 part. Another effect is the modification of the local environment of the rare earth ions. Thus, Ollier et al. [20] reported in aluminoborosilicate glasses a change in the Yb³⁺ EPR spectrum at dose higher than 10⁸ Gy which are attributed to a variation into Yb³⁺ proportion between different sites as well as a Yb³⁺ site symmetry change. In this regard, other works reported a decrease of the site symmetry of Eu³⁺ in glasses after gamma [1], and electron irradiation [2].

RE ions valence state modification

The reduction of RE³⁺ to RE²⁺ was observed for Sm³⁺, Eu³⁺, Dy³⁺, Yb³⁺ in several glass matrix under X-ray, gamma, electron and fs laser irradiation.

For example, Malchukova et al. [32] exhibited the formation of at least two Eu²⁺ sites in aluminoborosilicate glass upon beta irradiation using (EPR and Luminescence).

Under 2.5 MeV electron irradiation, Ollier et al. [23] used the in-situ cathodoluminescence and time-resolved photoluminescence to study the reduction of Sm³⁺ to Sm²⁺ ions during irradiation into aluminoborosilicate glasses. They showed that the Sm²⁺ emission lines appear in the first step of irradiation and that reduction of Sm³⁺ ions is a complex phenomenon with transient species.

The photo-reduction of RE³⁺ to RE²⁺ under femtosecond laser pulses was evidenced by Qiu et al. [28] in Eu doped fluorozirconate glass or by Nogami in [29] in aluminoborosilicate glasses.

More surprisingly, some trivalent RE like Nd and Er which are not known as stable under a divalent state were also reduced under irradiation. Rai et al. [11] reported an increase in absorption peak at 530 nm in Nd doped phosphate glasses which was attributed to Nd²⁺ trapping an electron under gamma irradiation at low doses (5-500 kGy). In the same way, Rai et al. [33] reported possible conversion of Er³⁺ to Er²⁺ under neutron diffraction. Babu et al. [34] also noted a possible reduction of erbium valence from Er³⁺ to Er²⁺ in silica

glass under gamma irradiation when the samples are co-doped with Al. They associated this reduction with the formation of the aluminum oxygen hole centers.

On the other hand, the oxidation of RE^{3+} to RE^{4+} for particular RE ions like terbium (Tb) and cerium (Ce) was also reported. In this framework, Baccaro et al. [35] reported the gamma radiation effect in the Ce doped silicate glasses and observed that the presence of Ce^{3+} suppressed the dominant peak around 540 nm in the absorption spectra after irradiation presumably due to the change state between Ce^{3+} and Ce^{4+} . Even more, Ebendorff et al. [36] examined the effect of Tb^{3+} ion on X-ray induced defect formation in phosphate sample.. Therefore, $(Tb^{3+})^+$ represents a hole centers due to the missing electron compared to Tb^{4+} leading to the suppression of the formation of intrinsic phosphate related hole centers, absorbing in the visible region.

3 Eu^{3+} ion environment evolution under electron irradiation

We are studying here the possibility to control the Eu^{3+} local environment in different phosphate glasses via the used of two electron beam energy (2.5 MeV and 700 keV). We will analyse with EPR and PL (emission spectra and 5D_0 lifetime).

Eu^{3+} can be used as a structural probe, especially in glasses where the fluorescence line narrowing (FLN) technique can bring information on the local structure around rare earth ions [10]. It is moreover possible to obtain information on the site symmetry via the asymmetry ratio (As) defined as the integrated emission intensity of $^5D_0 \rightarrow ^7F_2$ to $^5D_0 \rightarrow ^7F_1$. It is a sensitive parameter to characterize the deviation or distortion from centrosymmetric geometry of Eu^{3+} ions [11-13]. Concerning Eu^{3+} , an increase of As under electron, gamma and gold ion irradiation was shown in Eu-doped glasses indicating a decrease of the site symmetry [24], [31], [37]. This is generally associated to a broadening of the $^5D_0 \rightarrow ^7F_0$ band under gamma [37] and ion irradiation [24] indicating a larger site distribution of the Eu^{3+} ions.

3.1 Asymmetry Ratio in pristine glasses

$^5D_0 \rightarrow ^7F_2$ transition is a forced electric dipole transition and it is hypersensitive in nature, i.e. sensitive to the Eu^{3+} second neighbors. The emission intensity of this transition is strongly affected by the crystal field. More precisely, this transition intensity increase with the ligands valence or with decreasing site symmetry. However, the magnetic dipole transition $^5D_0 \rightarrow ^7F_1$ is less sensitive to Eu^{3+} crystal field and is chosen as a reference.

For the present work, the asymmetry ratio has been measured under 532 nm laser excitation in non-irradiated glasses and compared to previous works as announced in table 2. As values in literature varied between 2.3 and 4.4 in glasses. A higher value of As indicates a higher Eu-O covalency or a lower symmetry of Eu^{3+} ions [38].

In non-irradiated phosphate glasses, the As measured value is homogeneous in the whole glass volume. It is slightly higher in Meta-Zn-Eu (As = 3.6) compared to Meta-Na-Mg-Eu (As=3.2) and Na or Na-Li metaphosphate glasses where As = 3.1. This is due to the lower CN of Eu in Meta-Zn-Eu ($N_{EuO} = 5.52$) compared to Meta-Na-Eu ($N_{EuO} = 6.15$) as reported in Chapter 3 using MD calculations. Moreover, MD simulation show that Meta-Zn-Eu glass gets a

significant proportion of 5 coordinated Eu^{3+} (42 %) compared to Meta-Na-Eu glasses where Eu^{3+} ions are mainly 6-coordinated; this confirms the increase of As in Meta-Zn glasses (average lower site symmetry). In literature, Oomen et al. [39] reported values ranging between 3.4 and 4.1 in metaphosphate glasses doped with 2% of Eu_2O_3 ($49\text{P}_2\text{O}_5-49\text{MO}-2\text{Eu}_2\text{O}_3$ where M= Mg, Ca, Sr and Ba). Further, they noted that the asymmetry ratio has a tendency to decrease for larger modifier ions as well it depends on the thermal history of the glasses. As in polyphosphate glasses are between 3.2 and 3.5 in agreement with Rao et al. [40] (As = 3.7) or Saad et al. [41] (As = 2.9).

Table 2 Asymmetry ratio of Eu^{3+} ions in unirradiated phosphate glasses.

Glass composition	As	Ref
Meta-Na-Eu	3.1	Present work
Meta-Na-Li-Eu	3.1	Present work
Meta-Na-Mg-Eu	3.3	Present work
Meta-Zn-Eu	3.6	Present work
Poly-Zn-Na-Eu	3.2	Present work
Poly-Zn-K-Eu	3.5	Present work
Poly-Zn-Na-K-Eu	3.4	Present work
Poly-Q¹/Q²:50/50-Eu	3.2	Present work
66P2O5-32MgO-2Eu2O3	4.3	[39]
66P2O5-32CaO-2Eu2O3	4.1	[39]
66P2O5-32BaO-2Eu2O3	3.2	[39]
49P2O5-49MgO-2Eu2O3	4.1	[39]
49P2O5-49CaO-2Eu2O3	3.8	[39]
49P2O5-49BaO-2Eu2O3	3.4	[39]
44.5P2O5-44.5Na2O-10ZnO-1Eu2O3	2.9	[41]
44P2O5-17K2O-9Al2O3-29CaF2-1Eu2O3	2.5	[42]
44P2O5-17K2O-9Al2O3-23PbF2-6Na2O-1Eu2O3	2.3	[43]
39ZnO-35P2O5-20MgO-5TiO2-1Eu2O3	2.4	[38]
55.5P2O5-14K2O-6KF-14.5MgO-9Al2O3-1Eu2O3	3.0	[44]
55.5P2O5-14K2O-6KF-14.5SrO-9Al2O3-1Eu2O3	2.8	[44]
41P2O5-21K2O-20MgO-7Na2O-10CaO-1Eu2O3	3.7	[40]
31P2O5-11K2O-20MgO-7Na2O-30CaO-1Eu2O3	2.9	[40]
60.5P2O5-14K2O-13.5SrO-11Al2O3-1Eu2O3	4.4	[45]

3.2 Asymmetry ratio evolution under 2.5 MeV irradiation

Figure 13 compares the luminescence spectra of Eu^{3+} in irradiated and non-irradiated metaphosphate glasses. The emission spectra of Eu^{3+} have been normalized to the ${}^5\text{D}_0 \rightarrow {}^7\text{F}_2$ and recorded under 532 nm excitation. The emission lines corresponding to ${}^5\text{D}_0 \rightarrow {}^7\text{F}_J$ (J = 0,1,2...) transitions are assigned to ${}^5\text{D}_0 \rightarrow {}^7\text{F}_0$ at 575 nm, ${}^5\text{D}_0 \rightarrow {}^7\text{F}_1$ at 591 nm, ${}^5\text{D}_0 \rightarrow {}^7\text{F}_2$ at 613

nm, ${}^5D_0 \rightarrow {}^7F_3$ at 652 nm and ${}^5D_0 \rightarrow {}^7F_4$ at 701 nm. Comparing the pristine and irradiated glasses by 2.5 MeV electron at dose 1.5×10^9 Gy, we clearly see the increase of the emission intensity ratio between ${}^5D_0 \rightarrow {}^7F_2$ and ${}^5D_0 \rightarrow {}^7F_1$ after irradiation (fig.13). As well, figure 14 displayed a strong decrease of the emission band of Eu^{3+} following by an occurrence of broad band in the 400-500 nm region due to the reduction of Eu^{3+} to Eu^{2+} ions. The formation of divalent europium will be discussed in the part 4 of this chapter.

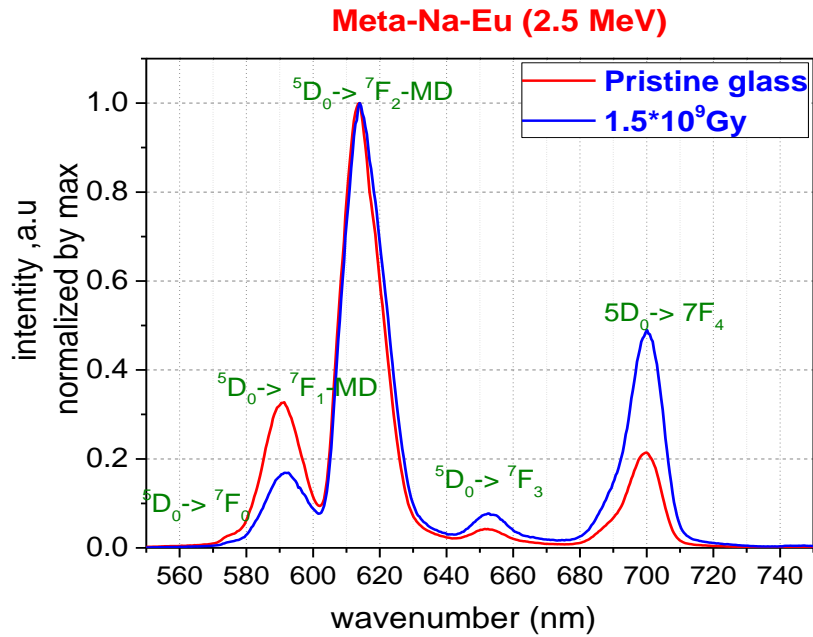


Figure 13 Luminescence spectra of Eu^{3+} doped metaphosphate glass Meta-Na-Eu before and after electron irradiation ($\lambda_{ext} = 532$)

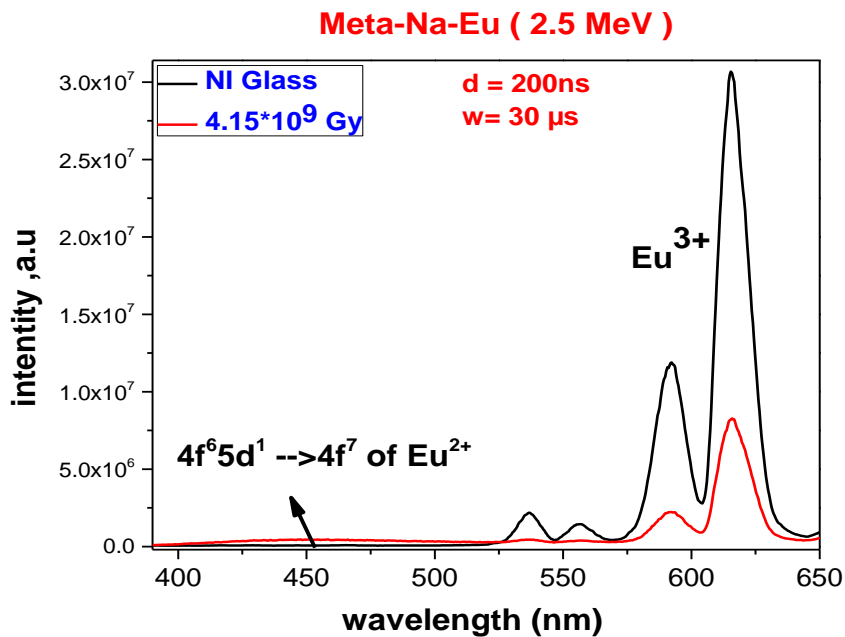


Figure 14 The PL emission spectra of Eu-doped metaphosphate glass Meta-Na-Eu

Fig. 15 presents the variation of the asymmetry ratio (A_s) of different Eu-doped metaphosphate glass compositions: Meta-Na-Eu, Meta-Na-Li-Eu, Meta-Na-Mg-Eu and Meta-Zn-Eu as a function of the dose logarithm for 2.5 MeV electrons.

Obviously, A_s is seriously increased under irradiation even for low doses. The values exceed 5 at 10^5 Gy dose ($A_s = 5.3$) up to 6.0 at high dose (1.5×10^9 Gy) in Meta-Na-Eu. This increase is less important in presence of zinc: $A_s = 4.2$ at 1.5×10^9 Gy. In the 10^5 - 10^8 Gy dose range, A_s reaches a constant value whatever the glass composition. It must be underlined that for dose = 1.5×10^9 Gy, a maximum value can be obtained for all compositions except Meta-Zn-Eu, followed by a slight decrease of A_s at 4.15×10^9 Gy.

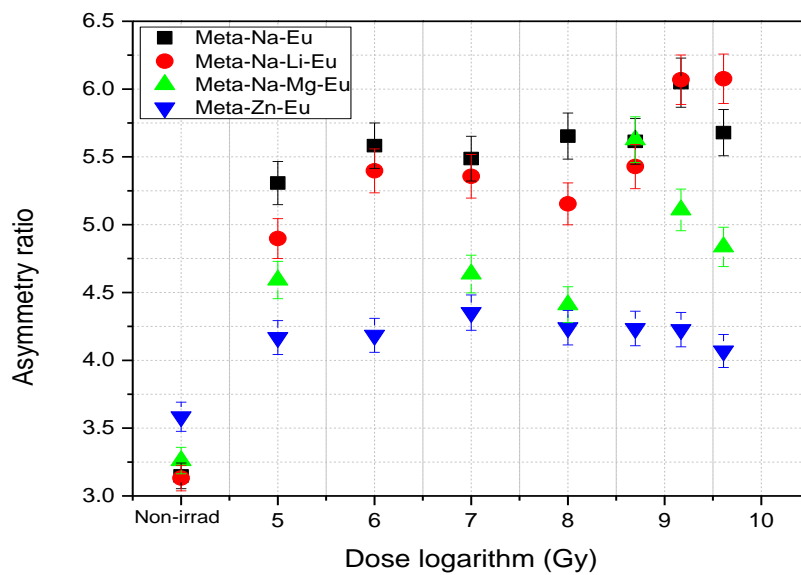


Figure 15 Variation of the asymmetry ratio A_s of Eu^{3+} ions after 2.5 MeV electron irradiation as a function of the logarithmic dose in (a) metaphosphate glasses: Meta-Na-Eu, Meta-Na-Li-Eu, Meta-Na-Mg-Eu and Meta-Zn-Eu. ($\lambda_{ext}=532$)

The comparison between the A_s variation of europium doped metaphosphate (Meta-Na-Eu) and polyphosphate glasses (Poly-Zn-Na-Eu) for 2.5 MeV electron irradiation is displayed in Figure 16. It emphasizes a less important increase in polyphosphate glasses compared to Na metaphosphate glass: A_s variation operates between 3.2 in non-irradiated glass and 3.9 in Poly-Zn-Na-Eu irradiated at dose = 4.15×10^9 Gy. For all polyphosphate compositions, the A_s evolution undergoes two trends: a constant increase in the 10^5 - 10^8 Gy dose regime and a progressive enhancement with increasing dose from high dose of 1.5×10^9 Gy.

In agreement, a general A_s increase was noticed and reported in literature for different glass matrix and different radiation types. Rahimian et al. [31] show an increase of this ratio from 2.5 to 4.4 in oxyfluoride glass with composition $64.5 \text{ P}_2\text{O}_5$ - 35 CaF_2 - $0.1 \text{ Eu}_2\text{O}_3$ after 10 MeV electron irradiation at dose 10 kGy. Bonfils et al. [24] demonstrated that the asymmetry ratio raised from 5.72 in pristine glass to 6.92 in irradiated borosilicate glass with gold ions at ion fluence of $3.2 \times 10^{14} \text{ cm}^{-2}$. A slight growth of A_s was observed from 2.95 to 3.05 in Eu doped

borosilicate glass under Gamma irradiation with dose of 900 kGy [37]. Under femtosecond laser irradiation, Nogami et al. [30] provided an increase from 3.45 to 4.15 of the As ratio in zinc silicate glasses before and after irradiation respectively.

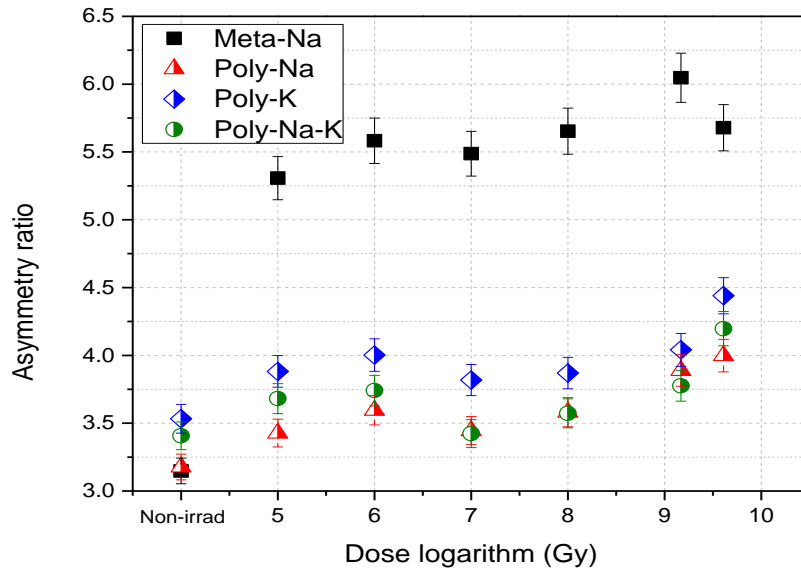


Figure 16 Variation of the asymmetry ratio A_s of Eu^{3+} ions after 2.5 MeV electron irradiation as a function of the logarithmic dose in polyphosphate glasses (Poly-Zn-Na-Eu, Poly-Zn-K-Eu and Poly-Zn-Na-K-Eu) compared to metaphosphate glass Meta-Na-Eu. ($\lambda_{\text{ext}}=532$)

We demonstrated here different trends in the A_s variation under irradiation according to the glass composition and the dose deposited by the electrons. Thus, we note a strong increase of this ratio in Eu doped single and mixed alkali metaphosphate glasses. We also remark that the A_s values are constant until 10^8 Gy, reach a maximum at dose 1.5×10^9 Gy, then undergoes a slight decrease at high dose 4.15×10^9 Gy.

This increase almost twice from about 3.1-3.3 to 5.6-6 indicate a significant decrease of the site symmetry of the Eu^{3+} as well as/or a higher Eu-O covalency in alkali phosphate glasses after electron irradiation.

However, in zinc phosphate glasses like Meta-Zn-Eu and Poly-Zn-M-Eu (where M= Na, K and Na+K), this effect is attenuated. From these results, we note that the presence of zinc oxide limits the A_s variation and induce therefore a lower reduction of the site symmetry of the RE^{3+} in glasses after electron irradiation. We note also that Mg has a similar effect to Zn, as in the Meta-Na-Mg. Instead Li and K have a similar effect to Na.

As well, the evolution of A_s at 4 GGy is different in polyphosphate compared to metaphosphate where we observe an increase of A_s for the 2 highest doses from 1.5×10^9 Gy. Consequently, the Eu^{3+} ions irradiated at high dose tends to localize in lower symmetry sites. This may be due to an increase of the NBO number as shown by Raman spectra (depolymerization increase at doses > 1 GGy) that could modify the coordination number of Eu^{3+} ions decreasing the site symmetry.

To better understand the role of zinc in the RE environment, we have used the dynamic molecular simulations to determine the local environment of Eu^{3+} ions according to the

phosphate glass composition in terms of nearest neighbour distances and coordination number as reported in the chapter 3.

We note a higher average N_{NaO} coordination number (5.2) in Meta-Na-Eu while the N_{ZnO} was determined to be around four [4.03-4.16] for Eu doped zinc phosphate glasses. This can be interpreted by the fact that Na atoms used as network modifier whereas ZnO acts as an intermediated oxide that can behave as network former. Hoppe et al. [46] explains that Zn^{2+} ions act as network former by forming a linkage between ZnO_4 and PO_4 tetrahedra in zinc phosphate glasses which explains the small coordination numbers around zinc compared to the modifier atoms.

3.2.1 Energy and dose effect (700 keV vs 2.5 MeV)

The Eu^{3+} emission spectra were obtained under 488 nm excitation and we calculated As along the glass edge with a step of 200 μm beginning from the irradiated surface up to 2 mm depth. As values under 700 keV electrons at doses 10^8 and 10^9 Gy are plotted respectively in figure. 17.a and 17.b for metaphosphate glasses and in Fig. 18.a and 18.b for polyphosphate glasses. For comparison, As values obtained with 2.5 MeV electron under 488 nm are also reported in the figure as well as the value of pristine glass. We note that the value of As ratio obtained under 532 or 488 nm are different. For example, the As in Meta-Na-Eu is found to be 3.8 under 488 nm exc. (2.5 MeV at dose of 1.5×10^9 Gy), against 6 under 532 nm excitation. This difference can be due to a difference in the absorption at 488 nm and 532 nm due to irradiation induced - point defect absorption bands. In particular, POHC point defect display 2 absorption bands at 410 and 540 nm [47].

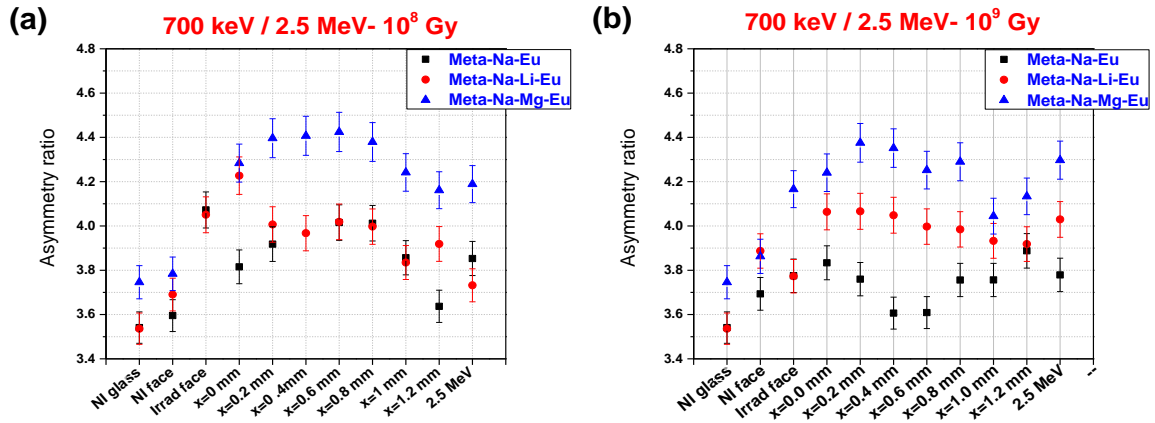


Figure 17 Variation of the asymmetry ratio A_s of the Eu^{3+} ions as a function of the thickness in Eu-doped metaphosphate glasses irradiated by electron of 700 keV and compared to 2.5 MeV irradiation (a) at dose = 10^8 Gy and (b) at dose = 10^9 Gy. The emission spectra were measured under 488 nm excitation and saved at every 200 μm in all the thickness of the sample.

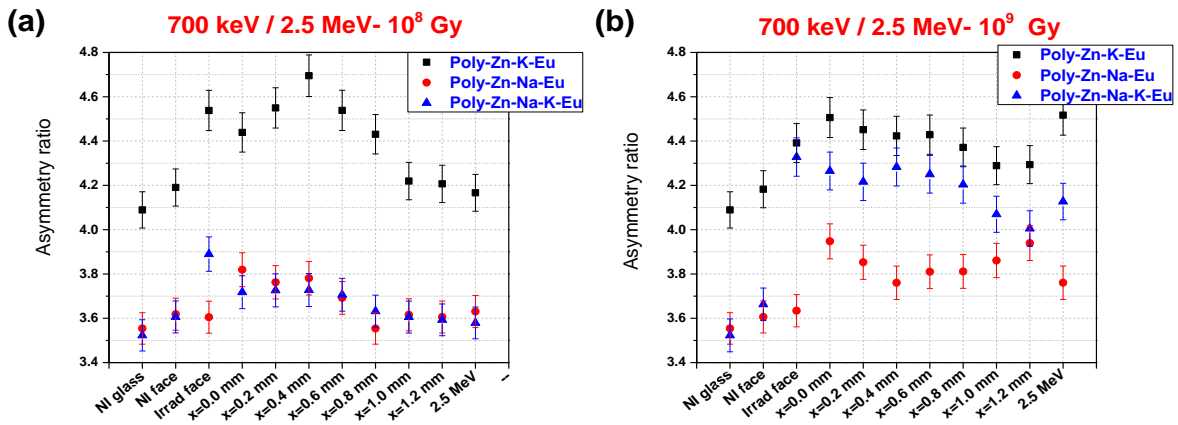


Figure 18 Variation of the asymmetry ratio A_s of the Eu^{3+} ions as a function of the thickness in Eu-doped polyphosphate glasses irradiated by electron of 700 keV and compared to 2.5 MeV irradiation (a) at dose = 10^8 Gy and (b) at dose = 10^9 Gy. The emission spectra were measured under 488 nm excitation and saved at every 200 μm in all the thickness of the sample

Figures 17 and 18 show a gradual increase of the A_s in the irradiated zone for both metaphosphate and polyphosphate glasses suggesting a reduction of the Eu^{3+} site symmetry and/or a higher Eu-O covalency. Moreover, it is interesting to underline that the modification of Eu^{3+} site symmetry occurs in a larger zone than the penetration depth of the 700 keV electron especially in polyphosphate glasses (765 μm) with some fluctuations of A_s values in the 0-1 mm interval.

Thus, this is obvious for polyphosphate samples that the A_s ratio at 10^8 Gy dose undergoes a significant evolution up to the thickness of 800 μm whereas for 10^9 Gy dose, the A_s evolution occurs in a largest zone up to 1.2 mm. This is probably linked to a more efficient migration of alkaline ions in this case in the whole glass volume. This assumption is corroborated by the Raman results showing a glass structure evolution up to 1.2 mm.

Furthermore, we observe (as seen in figures 17 and 18) an impact of the energy (2.5 MeV vs 700 keV) in the asymmetry ratio evolutions. At 10^8 Gy dose, the A_s undergoes a lower variation under 2.5 MeV electron compared to 700 keV irradiation in both metaphosphate and

polyphosphate. For a dose of 10^9 Gy, the site symmetry modification is similar under both energies irradiation in all kinds of phosphate glasses.

3.2.2 Influence of the alkaline ion type

Under 700 keV and 2.5 MeV irradiation at 10^8 Gy dose, the As variation is similar in both Meta-Na-Eu and Meta-Na-Li-Eu (Fig. 17.a). Whereas at 10^9 Gy dose, the As undergoes a larger increase in Na/Li metaphosphate glass compared to sodium and NaMg metaphosphate glass (Fig. 17.b). The same behavior is also seen for zinc polyphosphate compositions. Thus, at dose 10^8 Gy, we observe a similar change of the asymmetry ratio in Poly-Zn-Na-Eu and Poly-Zn-Na-K-Eu. However, at higher dose of 10^9 Gy, the As suffers a higher increase in the mixed Na/K polyphosphate sample (fig 17a and 18a). This could mean that the mixed alkali ions in glasses ((Na+Li) in metaphosphate and (Na+K) in polyphosphate) supports a larger reduction of the Eu^{3+} site symmetry under 700 keV irradiation at higher dose of 10^9 Gy.

On the other hand, the nature of the modifier cation seems to play a crucial role in the distortion of the local environment of the RE ions under irradiation implying a potential alkaline ion migration in the process of Eu^{3+} site distortion. Thus, we note a higher increase of the As ratio in presence of potassium compared to sodium and the Na/K glass behaves like Na or K polyphosphate glass depending on the dose.

- As variation from 3.1-3.3 in pristine glasses to 5.6-6 at high dose (1.5×10^9 Gy) indicates a significant decrease of the site symmetry of the Eu^{3+} as well as/or a higher Eu-O covalency in alkali metaphosphate glasses after irradiation.
- In phosphate glasses containing ZnO, the variation of the asymmetry ratio is less pronounced.
- Under 700 keV, the As increased in a larger volume than the penetration depth of electrons especially in polyphosphate glasses (penetration depth of 765 μm) with some fluctuation of As values in the 0-1 mm interval.
- At 10^8 Gy dose, the As undergoes a lower variation under 2.5 MeV electron compared to 700 keV irradiation in both metaphosphate and polyphosphate. For a dose of 10^9 Gy, the site symmetry modification is similar under both energies irradiation in all kinds of phosphate glasses.
- At higher dose of 10^9 Gy under 700 keV irradiation, the mixed alkali ions in glasses ((Na+Li) in metaphosphate and (Na+K) in polyphosphate) supports a larger reduction of the Eu^{3+} site symmetry suggesting the role migration of alkaline ion in lowering the site symmetry of Eu^{3+} ions.

3.3 ${}^5D_0 \rightarrow {}^7F_0$ transition under 2.5 MeV irradiation:

Figures 19.a and 19.b display the ${}^5D_0 \rightarrow {}^7F_0$ emission spectrum respectively in Meta-Na-Eu and Poly-Zn-Na-Eu irradiated at different doses with 2.5 MeV electrons under 488 nm excitation.

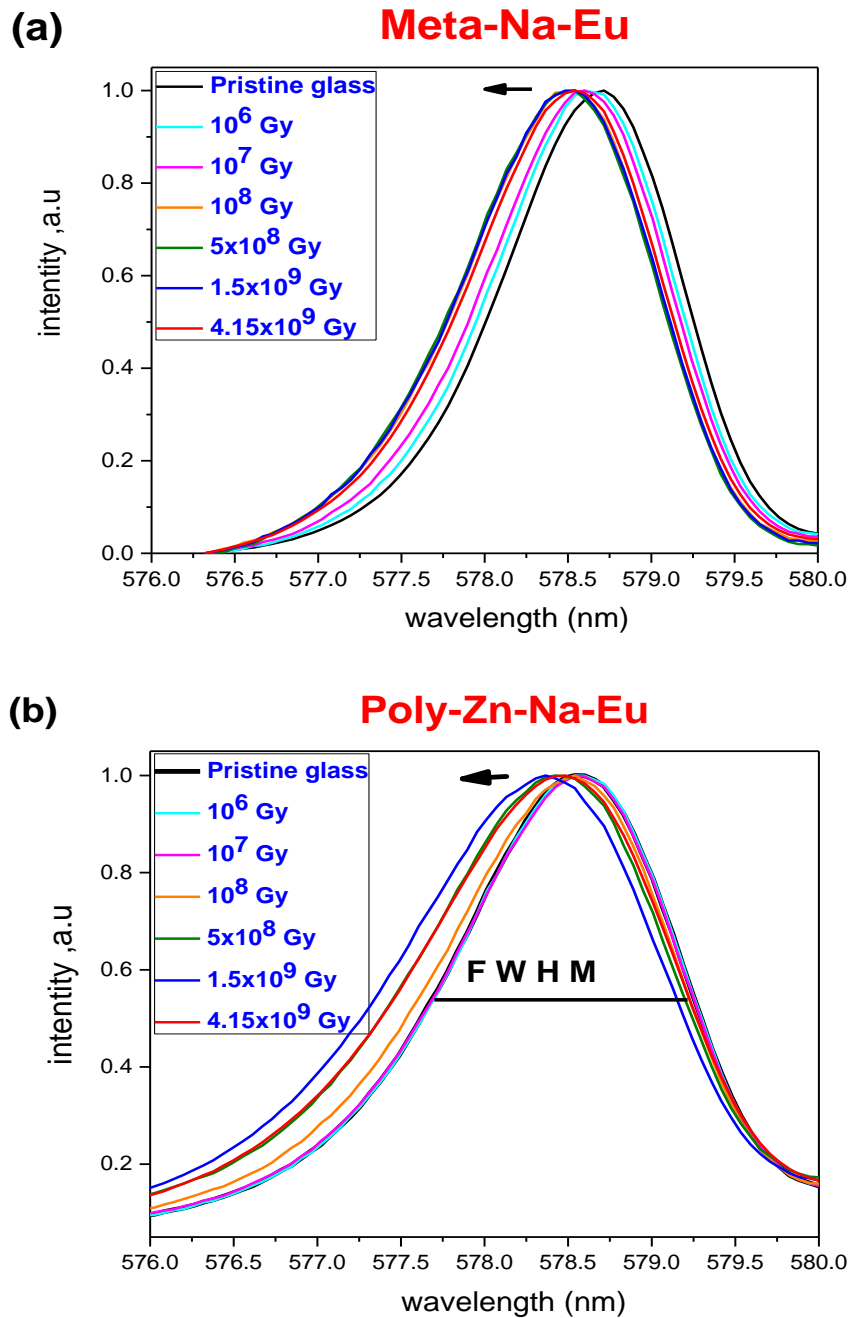


Figure 19 Zoom of the normalized emission band attributed to the ${}^5D_0 \rightarrow {}^7F_0$ transition of the Eu^{3+} ions in (a) metaphosphate glass Meta-Na-Eu and (b) polyphosphate glass Poly-Zn-Na-Eu irradiated by electron of 2.5 MeV at various doses.

3.3.1 Energy shift

We notice a shift of the maximum of the emission band of the ${}^5D_0 \rightarrow {}^7F_0$ transition towards lower wavelength (blue-shift) in all phosphate glasses. The maximum shift value is of 0.23 nm order but considering the use of a grating of 1200 l/mm, the spectral resolution is 0.28 nm so it means that we will not consider such a shift even if it seems to depend on the dose. .

3.3.2 Broadening of the ${}^5D_0 \rightarrow {}^7F_0$ emission band

Before irradiation, we observe that 2 groups according to the FWHM (figure 20): one concerning the polyphosphate glasses with a FWHM around 50 cm^{-1} and another around 37 cm^{-1} for metaphosphate compositions. One exception concerns the Meta-Zn-Eu belonging to the group of polyphosphate. Once again the presence of ZnO impacts the Eu^{3+} environment and the site dispersion is higher when Zn is in the glass structure.

From MD simulations, these values can be understood considering the fact that two different average coordination numbers for Eu^{3+} ions seem to occur in Meta-Na (6.15) whereas Meta-Zn and Zn polyphosphate glasses with value of respectively 5.52 and 5.94 leading logically to a larger ${}^5D_0 \rightarrow {}^7F_0$ emission.

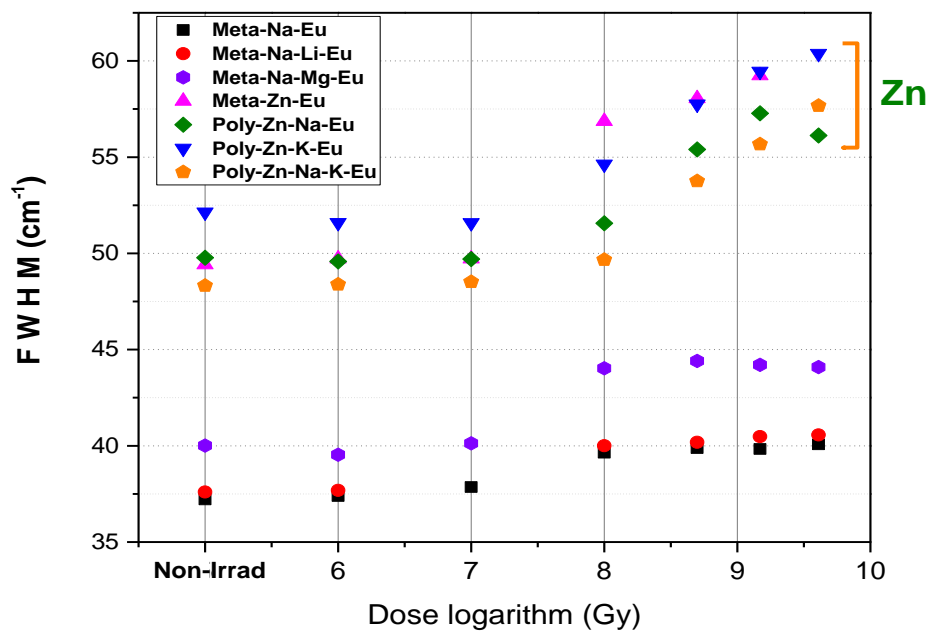


Figure 20 Variation of the full width at half maximum FWHM after 2.5 MeV electron irradiation as a function of the logarithmic dose in (a) metaphosphate glasses: Meta-Na-Eu, Meta-Na-Li-Eu and Meta-Na-Mg-Eu and (b) in polyphosphate glass Poly-Zn-Na-Eu, Poly-Zn-K-Eu and Poly-Zn-Na-K-Eu ($\lambda_{ext}=488 \text{ nm}$)

Under irradiation, we evidenced a broadening of the ${}^5D_0 \rightarrow {}^7F_0$ emission band with increasing dose (see Figure 19). Both energy levels 5D_0 and 7F_0 being not splitted by the crystal field and

${}^5D_0 \rightarrow {}^7F_0$ being a spin forbidden transition, the shape evolution is directly informative of the Eu^{3+} site number. For example, a pronounced shoulder or a clear splitting of the band, as well as a strong broadening of the band can indicate the presence of a second Eu^{3+} site in the glass. Here the broadening is not huge (10 cm^{-1}) and rather indicates a larger dispersion of Eu^{3+} sites in the irradiated glasses than a creation of a second Eu^{3+} site under irradiation. From figure 20, we see that the FWHM increase concerns mainly Zn glasses and Meta-Na-Mg-Eu while for alkali metaphosphate glasses, the FWHM increases with around 3 cm^{-1} after 2.5 MeV irradiation at high dose

This broadening of the band depends on the glass composition but also on the radiation dose. For glasses without any ZnO, until 10^7 Gy , there is no broadening in the ${}^5D_0 \rightarrow {}^7F_0$ emission band. Then, from 10^8 Gy , the Eu^{3+} sites dispersion overcomes whatever the dose.

In the other hand and in presence of zinc oxide in phosphate glasses, we remark a similar behavior between 10^5 and 10^7 Gy . Whereas at higher doses, the FWHM follows a quasi linear growth with increasing dose.

Compared to earlier research, our measured FWHM variations are lower than in other glass compositions. Bonflis et al. [24] showed an increase of the FWHM of the ${}^5D_0 \rightarrow {}^7F_0$ emission band from 93 to 133 cm^{-1} under gold ion irradiation in Eu-doped borosilicate glasses. Even more, Mohapatra et al. [37] reported an increase of FWHM from 120 to 168 cm^{-1} in Eu-doped barium borosilicate glasses after gamma irradiation at dose 900 kGy . We can underline that both glasses were borosilicate glasses with the attested presence of two types of Eu^{3+} sites (one is related to silicate environment and the other is related to borate environment) in the glass explaining a higher initial FWHM and maybe a much more important increase than in phosphate glasses.

3.3.3 Electron energy Effect (700 keV vs 2.5 MeV)

Figures 21.a and 21.b show the ${}^5D_0 \rightarrow {}^7F_0$ emission band respectively in Meta-Na-Eu and Poly-Zn-Na-Eu respectively, under 700 keV electron irradiation at dose 10^8 Gy .

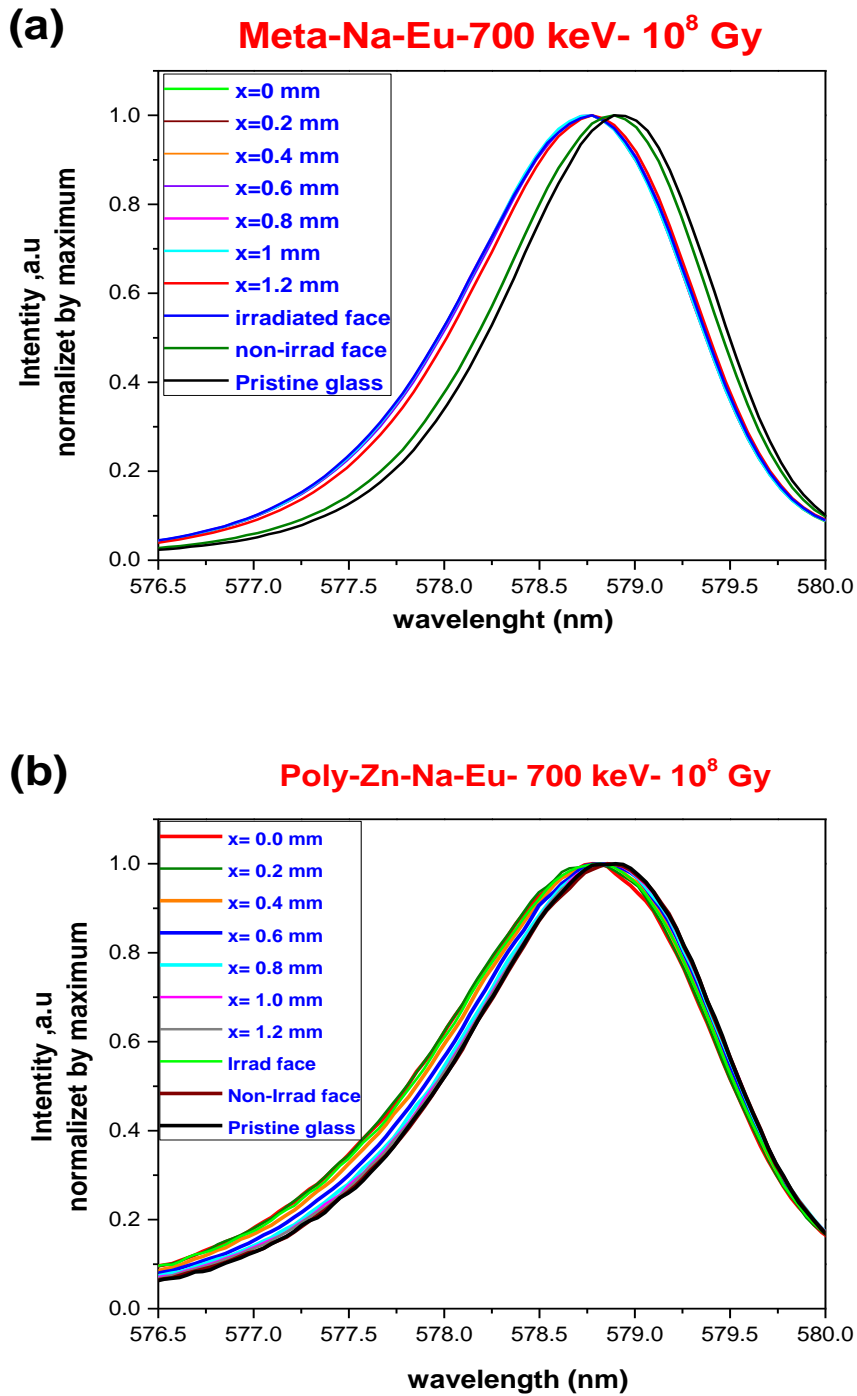


Figure 21 Zoom of the normalized emission band attributed to the ${}^5D_0 \rightarrow {}^7F_0$ transition of the Eu^{3+} ions in (a) Meta-Na-Eu and (b) Poly-Zn-Na-Eu after 700 keV electron irradiation at dose = 10^8Gy . The emission spectra were measured under 488 nm excitation and saved at every 200 μm in all the thickness of the sample.

We observe a different behavior in presence of zinc. Thus, the energy shift and the broadening band are homogeneous in the volume sample of Meta-Na-Eu (Fig. 21.a) contrary to zinc phosphate glasses where they change gradually along the thickness from depth = 600/700 μm

to non-irradiated surface (Fig. 21.b). However, the maximum shift value is 0.12 nm it is lower compared to the spectral resolution.

Figure 22 compares the variation of the FWHM as a function of the position under irradiation by electron of 700 keV at dose = 10^8 Gy in Meta-Na-Eu, Meta-Zn-Eu, Poly-Zn-Na-Eu and Poly-Eu-($Q^1/Q^2=50/50$).

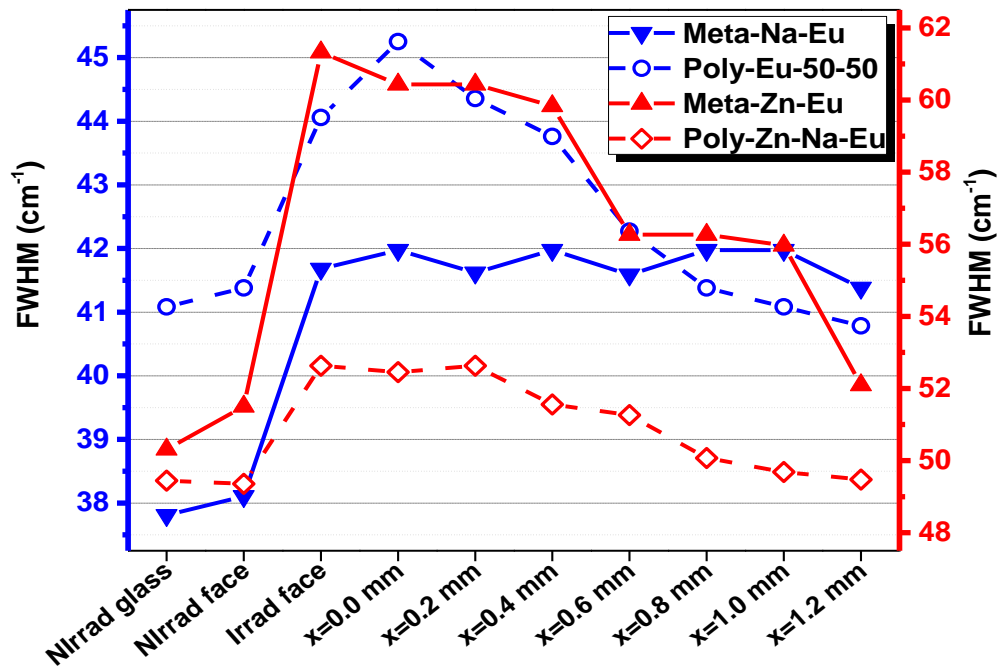


Figure 22 Variation of the full width at half maximum FWHM as a function of the thickness under irradiation by electron of 700 keV at dose = 10^8 Gy in Meta-Na-Eu, Meta-Zn-Eu, Poly-Zn-Na-Eu and Poly-Eu-50-50. (The emission spectrum were measured under 488 nm excitation and saved at every 200 μ m in all the thickness of the sample)

These results confirm the different compartments in the $^5D_0 \rightarrow ^7F_0$ emission band evolution after irradiation between glasses containing and excluding zinc. The FWHM decreases gradually in the slice until reaching the initial value of pristine glass in zinc phosphate glasses contrary to glass without zinc (Meta-Na-Eu) where the change operates in the same whole volume. Even more, the maximum FWHM change Δ_{FWHM} is strictly more important in Meta-Zn-Eu ($\Delta_{FWHM} = 11 \text{ cm}^{-1}$) compared to other glasses: Meta-Na-Eu ($\Delta_{FWHM} = 3.2 \text{ cm}^{-1}$) and Poly-Zn-Na-Eu ($\Delta_{FWHM} = 3.0 \text{ cm}^{-1}$).

There is no energy effect on these broadenings in metaphosphate compositions whereas it decrease from 10 cm^{-1} under 2.5 MeV to 3 cm^{-1} under 700 keV in polyphosphate glass (Poly-Zn-Na-Eu).

- The broadening of the ${}^5D_0 \rightarrow {}^7F_0$ emission band after 2.5 MeV electron irradiation indicating a larger dispersion of the Eu^{3+} sites.
- This broadening depends on the glass composition and the radiation dose. For glasses without any ZnO, until 10^7 Gy, there is no expansion in the ${}^5D_0 \rightarrow {}^7F_0$ emission band. Then, from 10^8 Gy, the Eu^{3+} sites dispersion suffer the same slight increase whatever the dose.

On the other hand and in presence of zinc oxide in glasses, a similar comportment between 10^5 and 10^8 Gy as in alkali glasses. Whereas higher doses, the FWHM follows a linear growth with increasing dose.

- Under 700 keV, the FWHM decrease gradually in the slice until reaching the initial value of pristine glass in zinc phosphate glasses contrary to glass without zinc (Meta-Na-Eu) where the change operates in the same whole volume.

3.4 5D_0 Energy level lifetime

The $\text{Eu}^{3+} {}^5D_0$ energy level lifetime evolution τ under 2.5 MeV electron irradiation for various doses in metaphosphate and polyphosphate glasses are presented in table 3. They were measured under 266 nm excitation and extracted from a single exponential decay curve.

Table 3 The $\text{Eu}^{3+} {}^5D_0$ energy level lifetime evolution τ under 2.5 MeV electron irradiation for various dose in metaphosphate and polyphosphate glasses.

Glass / Dose	5D_0 Lifetime (ms)				
	NI	10^5 Gy	5×10^8 Gy	1.5×10^9 Gy	4.15×10^9 Gy
Meta-Na-Eu	2.68	2.38	2.38	-	2.34
Meta-Zn-Eu	2.23	2.20	1.99	1.94	1.86
Poly-Zn-Na-Eu	2.41	2.38	2.11	2.18	2.02
Poly-Eu-50-50	2.66	2.52	2.25	2.34	2.18

For non-irradiated glasses, the 5D_0 energy level lifetime ranges between 2.23 and 2.68 ms. It is of the same order than in literature [48]–[51]. As an example, Meza-Rocha et al. [51] reported a value of 2.26 ms in Eu doped zinc polyphosphate glass.

Moreover, we clearly observed a decrease of the lifetime under electron irradiation for all glasses and doses (table 3). However, the lifetime decrease seems to be independent of the dose for metaphosphate glasses contrary to polyphosphate. In terms of variation, in Meta-Na-

Eu, the decrease is about 13% from pristine glass to 4.15×10^9 Gy irradiated one. Zinc phosphate glasses undergoes a higher decrease of 17, 16 and 18 % in respectively Meta-Zn-Eu, Poly-Zn-Na-Eu and Poly-Eu-50-50 samples.

Compared to literature, we found that $^2F_{5/2}$ lifetime of Yb^{3+} ions is decreased from 1.4 ms in pristine glass to 0.9 ms at dose 10^9 Gy (decrease of 36%) in polyphosphate glass [52] and Ladaci et al. [53] showed a decrease of $Er^{3+} \ ^4I_{13/2}$ lifetime from 9 to 6 ms (33% decrease) at dose 10^7 Gy in phosphosilicate optical fibers. It seems that that the $5D_0$ energy lifetime of Eu^{3+} is less affected by irradiation compared to Er^{3+} and Yb^{3+} . It must be underlined that both ions Yb^{3+} and Er^{3+} emit in the IR part of the spectrum.

This difference could be related to the creation of P_1 defect in phosphate glasses under irradiation that absorb in the infrared region [54].

- **A slight decrease (max 18 %) of the $Eu^{3+} \ ^5D_0$ energy level lifetime occurs after irradiation compared to other RE in literature such as Er^{3+} and Yb^{3+} . It depends on the dose for polyphosphate glasses but not for metaphosphate.**

4 Eu³⁺ ion reduction into Eu²⁺ under electron irradiation

In this part, we studied the formation of divalent europium under irradiation. The results were published in Mahfoudhi and Ollier [55] (see appendix). More precisely, we discussed how it is possible to impact both the site symmetry and the amount of produced Eu²⁺ by optimizing the electron energy (700 keV vs 2.5 MeV) and the integrated dose from 10⁵ to 4x10⁹ Gy. The site dependence versus the nature of the glass (metaphosphate and polyphosphate) additionally will be also analyzed.

4.1 PL spectroscopy analysis

A zoom of the time-resolved photoluminescence emission spectra under 355 nm excitation in the 400-525 nm range is exhibited in Figures 23a and 23b. They correspond respectively to metaphosphate glass (Meta-Na-Eu) and polyphosphate glass (Poly-Zn-Na-Eu) irradiated by electrons of 2.5 MeV at various doses from 10⁵ Gy to 4.15x10⁹ Gy (delay = 200 ns and gate width = 30 μs). It seems that the large emission band at 460 nm increases with dose in metaphosphate glasses (Fig 23a) while the emission spectra in polyphosphate glasses show a new narrow band between 400 and 450 nm. The intensity of this band tends to decrease with dose as shown in Fig. 23b. Nevertheless, a large band centered at 490 nm is visible on those spectra.

The broad emission band around 460 nm occurring under irradiation can be attributed to the 4f⁶5d¹ → 4f⁷ transition of Eu²⁺ ions. Indeed, the lifetime of the blue emission band centered at 450 nm in different glasses displays a short lifetime from 150 ns (metaphosphate) to 2.76 μs (polyphosphate). These values are in agreement with literature examples reporting lifetimes of Eu²⁺ ions in glasses between 0.2 and 1.3 μs in fluoride phosphate glasses Ehrt et al. [16,17].

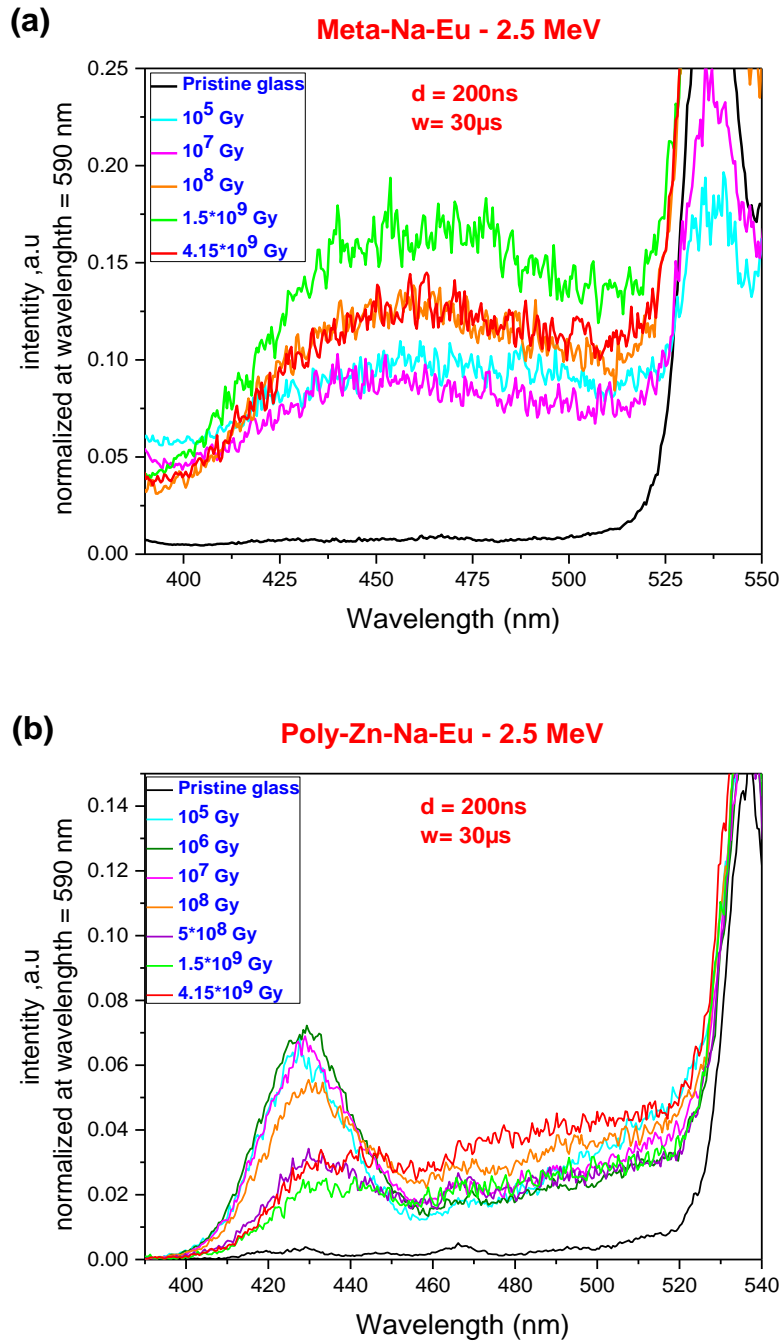


Figure 23 The PL emission spectra of (a) Eu-doped metaphosphate glass Meta-Na-Eu and (b) Eu-doped polyphosphate glass Poly-Zn-Na-Eu after 2.5 MeV electron irradiation at various doses from 10^5 to over 10^9 Gy. ($\lambda_{ext}=355$ nm)

Fig 24a and 24b compare the emission spectra of Meta-Na-Eu and Poly-Zn-Na-Eu irradiated by electrons of 700 keV and 2.5 MeV respectively at similar doses 10^8 and 10^9 Gy.

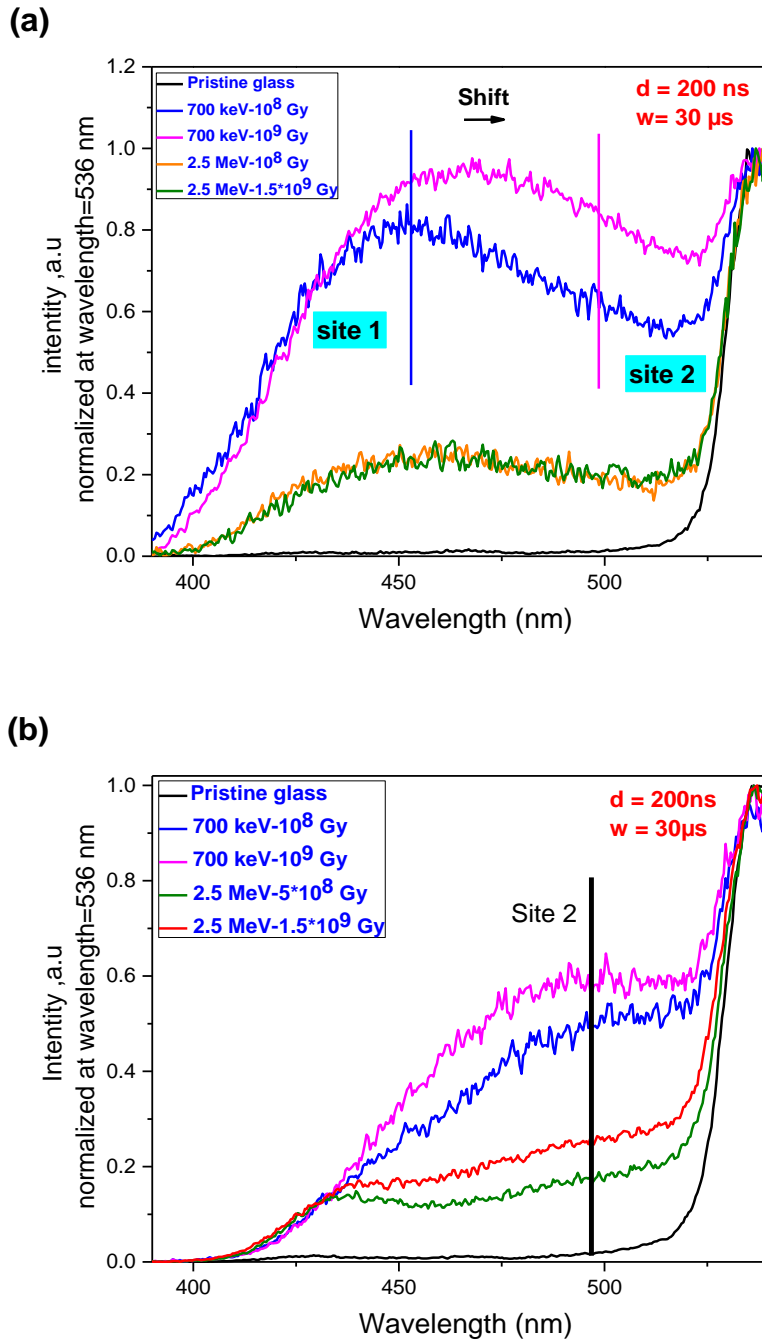


Figure 24 The PL emission spectra of (a) Eu-doped metaphosphate glass (Meta-Na-Eu) and (b) Eu-doped polyphosphate glass (Poly-Zn-Na-Eu) after 700 keV and 2.5 MeV electron irradiation at 10⁸ and 10⁹ Gy doses. ($\lambda_{ext}=355$ nm)

Fig 24a shows that the intensity of the emission band centered at 450 nm and attributed to Eu²⁺ ion is strongly increased after 700 keV electron irradiation compared to 2.5 MeV energy. Moreover, a red shift of the broad emission band occurs when the dose increases from 10⁸ to 10⁹ Gy for 700 keV electrons in Na metaphosphate glass. This emission shape variation could be explained by the existence of two different Eu²⁺ sites and the ratio between both sites depending on the dose. A careful fit of each emission spectra was performed, the results obtained for metaphosphate and polyphosphate at 700 keV and 10⁹ Gy are shown in Figure

25. We observed 2 components at 450 and 500 nm in both glasses attesting the presence of 2 sites for Eu^{2+} ions.

The shift of the $5d \rightarrow 4f$ emission band of Eu^{2+} to higher wavelengths in literature was attributed to an increase of crystal field or to a higher covalency [57]. Nevertheless, there is no clear evidence from our spectroscopic measurements that (Eu^{3+}) ions occurred from a direct trapping on two original Eu^{3+} sites already existing in the pristine glasses.

Fig 24b displays as well a strong increase of the 500 nm band intensity after 700 keV electron irradiation compared to 2.5 MeV in polyphosphate glass.

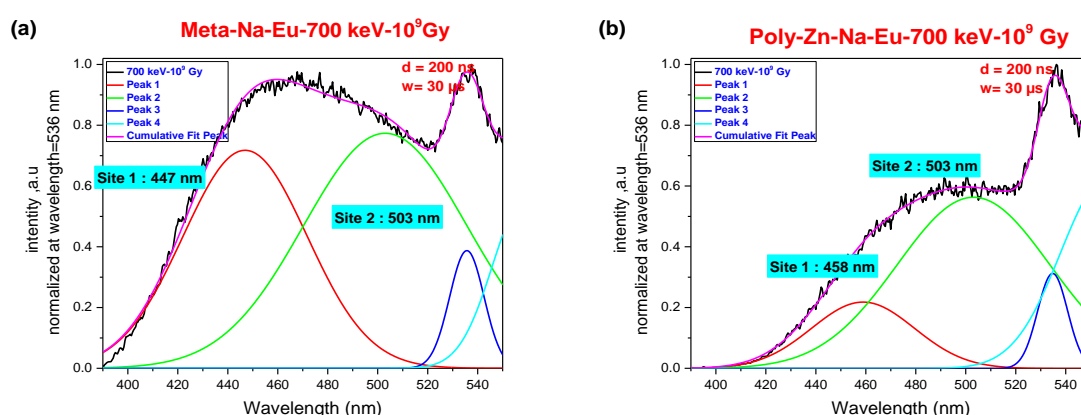


Figure 25 A fit of the emission spectra of the Eu^{2+} ions in (a) Eu -doped metaphosphate glass (Meta-Na-Eu) and (b) Eu -doped polyphosphate glass (Poly-Zn-Na-Eu) after 700 keV electron irradiation at 10^9 Gy dose. Two components at near 450 and 500 nm in both glasses attesting the presence of 2 sites for Eu^{2+} ions.

4.2 EPR spectroscopy analysis

Electronic paramagnetic resonance (EPR) spectroscopy is a powerful tool to obtain complementary quantitative data on Eu^{2+} formation under irradiation (indeed Eu^{2+} is a $4f^7$ paramagnetic ion). Fig. 26 displays the EPR spectra of Poly-Zn-Na-Eu glasses before and after 2.5 MeV irradiation for various doses. After irradiation, new signals at 1095 G ($g = 6.3$), 2466 G ($g=2.8$) and 3500 G ($g=2.0$) can be observed. These components are known as the “U” EPR signal and can be attributed to Eu^{2+} ions associated to a low-symmetry site whereas the signal at 1492 Gauss ($g = 4.7$) corresponds to a high-symmetry site of divalent europium [12]. Actually, Eu^{2+} ions were detected in all irradiated phosphate glasses whatever the dose. The presence of two types of sites for divalent Eu^{2+} ions has already been mentioned in aluminoborosilicate [9,10], aluminosilicate [59], phosphate and fluoride-phosphate glasses [11,12]. These studies associate generally the high symmetry site ($g=4.7$) to a strong crystal field that could correspond to 6-coordinated Eu^{3+} ions. We therefore assign the high symmetry site to the emission at 500 nm and the low-symmetry one to the emission at 450 nm.

The low-symmetry site ($g=6.3$) with a lower crystal field would rather deal with Eu^{2+} ions with a higher coordination number into a modifier position. As well, we can observe at $g = 2$ a sharp saturated line that corresponds to the P-related point defects such as POHC (Phosphorus

Oxygen Hole Centers). The detailed nature of point defects associated to P will not be described here. Furthermore, we can notice that all the signals associated to Eu^{2+} directly correlated to the Eu^{2+} amount increases with the irradiation dose.

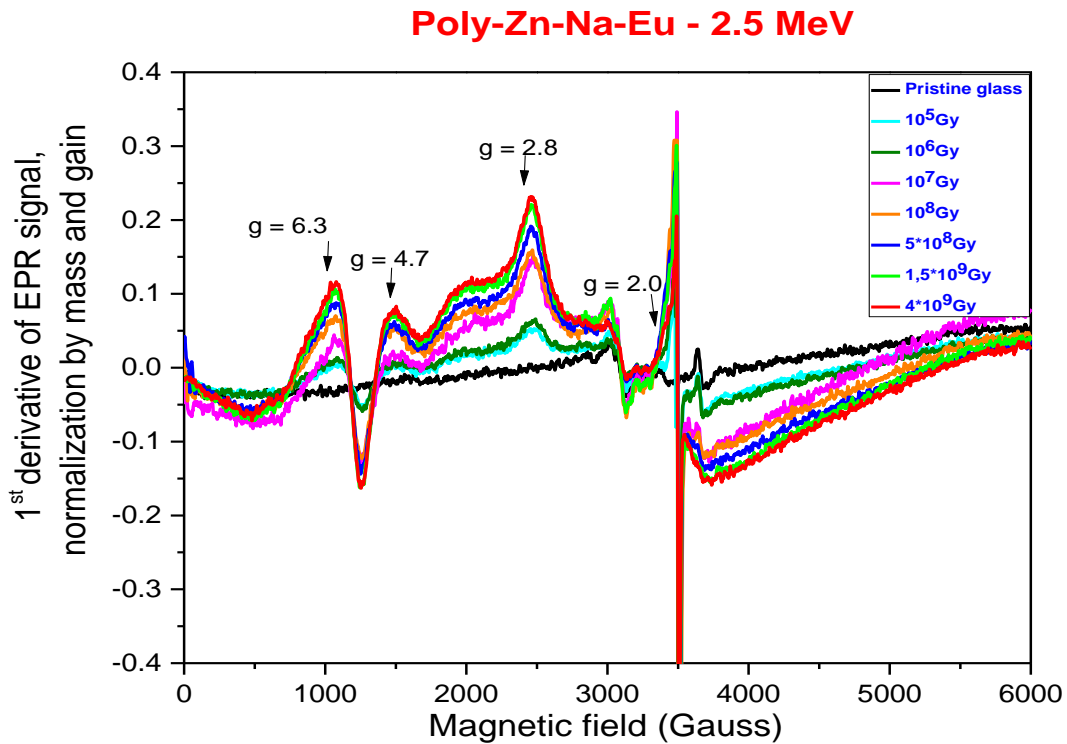


Figure 26 EPR spectra normalized by mass and gain of Poly-Zn-Na-Eu glass irradiated by electron of 2.5 MeV at various doses.

At first, it can be seen that the glass composition and the glass polymerization impact the nature of the Eu^{2+} sites. The ratio between both sites from one composition to another one can be extracted from EPR measurements. Table 4 reports the ratio between low-symmetry site ($g=6.3$) and high-symmetry site ($g=4.7$) for 4 glass compositions (700 keV, 10^9 Gy). It seems that the presence of Zn favors the formation of the high-symmetry site.

Table 4 Ratio between low-symmetry site ($g=6.3$) and high-symmetry site ($g=4.7$) for different phosphate glasses irradiated by 700 keV at 10^9 Gy dose.

700 keV- 10^9 Gy				
	Low-symmetry site	High-symmetry site	Symmetry Ratio	ZnO (mol. %)
Meta-Na-Eu	0.16 ± 0.02	0.04 ± 0.01	3.92	-
Meta-Na-Mg-Eu	0.14 ± 0.02	0.05 ± 0.01	2.88	-
Poly-Zn-Na-Eu	0.51 ± 0.08	0.23 ± 0.03	2.20	46.00
Meta-Zn-Eu	0.08 ± 0.01	0.08 ± 0.01	1.06	49.40

Figure 27 exhibit the PL emission spectra of Eu-doped meta and polyphosphate glasses after 700 keV irradiation at dose 10^9 Gy and confirms the predominance of site 2 (500 nm) in

polyphosphate by the red shift of the emission band. This result is supported by the table 4 where we can notice the huge intensity of the high symmetry site in polyphosphate compared to metaphosphate glasses (factor 7). This result is moreover in agreement with [57] based on the fact that polyphosphate contain more NBO than metaphosphate glasses.

However, a direct comparison of the ratio between high and low symmetry sites obtained from EPR and PL is delicate. Indeed, PL method cannot deliver absolute quantitative ratio due to two main effects: first, the photobleaching occurring under the 355 nm laser excitation inducing a decrease of the Eu^{2+} emission intensity and secondly, a mismatching between PL and EPR measurements could be due to the interaction between Eu^{2+} and other luminescent species occurring under irradiation. Additional emission bands in the 400-600 nm region were detected like the emission of diamagnetic P-defects at 410 nm [61]. This band was observed in NaMg metaphosphate glasses [54] and Na metaphosphate. The P-defect emission band in presence of Zn is not visible anymore but a new band at 435 nm (see Fig 24b) appears after irradiation. To the best of our knowledge, such an emission band was never reported yet in irradiated phosphate glasses but we deduced that it is directly correlated to the presence of Zn. Therefore, it could be attributed to unusual Zn oxidation state like Zn^+ or to $(\text{Zn}^{2+})\text{-EC}$. A $g = 1.99$ EPR component in Zn metaphosphate glass was tentatively attributed to $(\text{Zn}^{2+})\text{-EC}$ in [62].

Zn doping gets a strong positive effect on the reduction efficiency of Eu^{3+} as it can be seen in Figure 26.

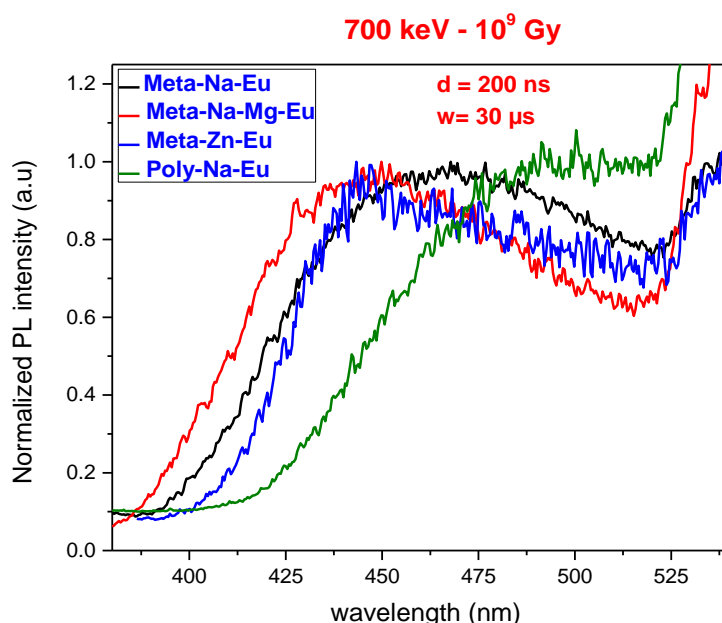


Figure 27 The PL emission spectra of Eu-doped meta and polyphosphate glasses (Meta-Na-Eu, Meta-Na-Mg-Eu, Meta-Zn-Eu and Poly-Zn-Na-Eu) after 700 keV at dose 10^9 Gy. ($\lambda_{ext}=355$)

Fig 28a and 28b report the intensity of the EPR signals at $g = 6.3$ and $g = 4.7$ of Meta-Na-Eu, Meta-Zn-Eu, Poly-Zn-Na-Eu and Poly-Zn-Na-Eu($\text{Q}^1/\text{Q}^2:50/50$) corresponding to low and high

symmetry sites of Eu^{2+} respectively as a function of the dose logarithm under 2.5 MeV irradiation.

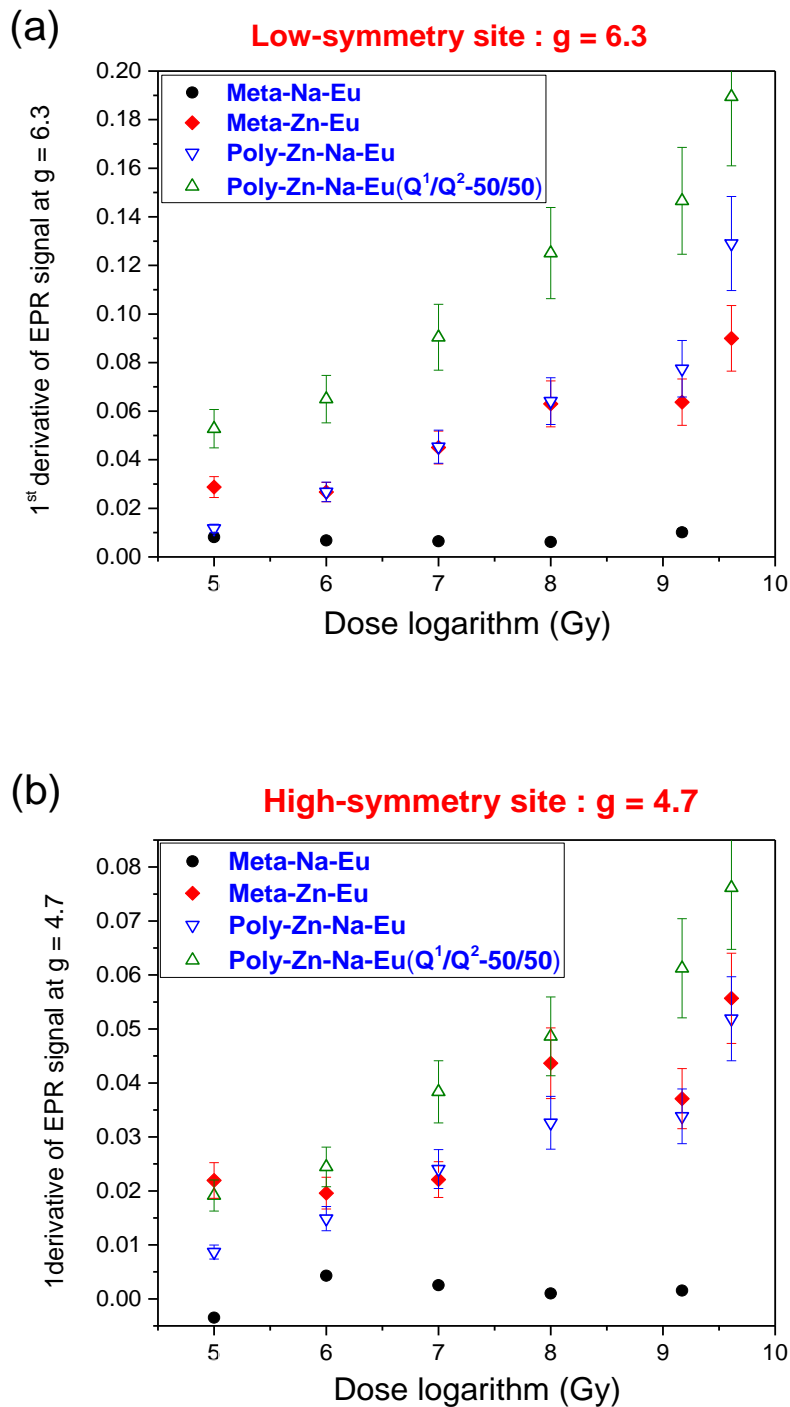


Figure 28 Variation of the EPR signal intensity (a) $I_{g=6.3}$ and (b) $I_{g=4.7}$ attributed respectively to low and high site symmetry of Eu^{2+} ion in Meta-Na-Eu, Meta-Zn-Eu, Poly-Zn-Na-Eu and Poly-Zn-Na-Eu- $(Q^1/Q^2:50/50)$ glasses irradiated by 2.5 MeV at various doses: from 10^5 Gy to over 10^9 Gy.

We observe in fig 28a and 28b that both signals are weak and constant regardless of the dose in Meta-Na-Eu glass. In contrast, in presence of zinc oxide in the glasses, a quasi-linear increase

of both lines at $g = 6.3$ and $g = 4.7$ occurs with the dose logarithm. The formation of Eu^{2+} is more efficient in Poly-Zn-Na-Eu ($Q^1/Q^2:50/50$) than in Poly-Zn-Na-Eu, while meta-Zn-Eu and Poly-Zn-Na-Eu exhibits quite similar efficiency of Eu^{3+} reduction under irradiation. Moreover, it can be notice that a lowest amount of Eu^{2+} is formed under the high-symmetry site. The comparison between the Eu^{2+} amount produced in metaZn and metaNa (up to a factor 9) supports the results that Zn doping gets a strong positive effect on the reduction efficiency of Eu^{3+} . Indeed, the proportion of high symmetry site is increased by increasing the amount of Zn as attested by the table 4.

At 2.5 MeV, it seems that there is no dose effect on the ratio between site 1 and site 2. The existence of a “plateau” displayed in Figure 29 supports this result as well as the stable shape of the photoluminescence spectra in 10^6 - 10^8 Gy range shown in figure 23. When dose becomes higher than 10^9 Gy, we can observe an increase of the ratio between both sites indicating a clear predominance of modifier sites on network modifier sites. We know from [6] that some alkali motion are involved in 2.5 MeV electron irradiated glasses when dose is higher $>10^9$ Gy. In phosphate glasses, Raman spectra of polyphosphate glasses showed some depolymerization effects for doses $>10^9$ Gy [54]. This network modification could induce a higher production of low-symmetry sites for Eu^{2+} ions. This hypothesis is supported by the nature of the low-symmetry site expected as “a modifier” site. The increase of the number of NBO under irradiation is in agreement with this scenario. The deviation from a linear behavior visible in Fig 26 was furthermore already observed for similar doses ($>10^9$ Gy) in aluminoborosilicate glass [58].

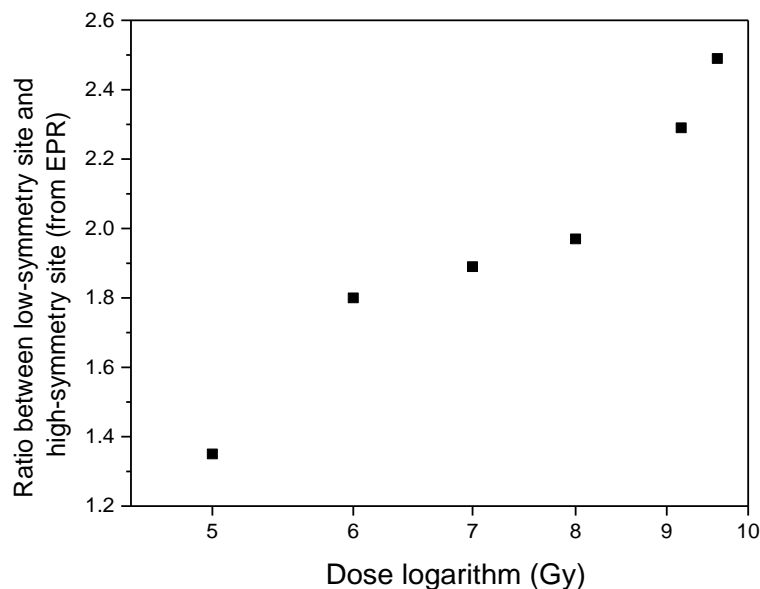


Figure 29 The ratio between Eu^{2+} low-symmetry site and high-symmetry site for Poly-Zn-Na-Eu glass under 2.5 MeV irradiations as a function of dose logarithm.

4.3 Energy effect: 2.5 MeV vs 700 keV

In Figure 30, the intensity of $I_{g=6.3}$ signal corresponding to the low-symmetry Eu^{2+} site (Fig. 32a) and $I_{g=4.7}$ to the high-symmetry site (Fig. 30b) are reported for all glasses. It allows to compare the Eu^{3+} reduction efficiency between 2.5 MeV (empty symbols) and 700 keV (full symbols) at 10^8 Gy and 10^9 Gy doses.

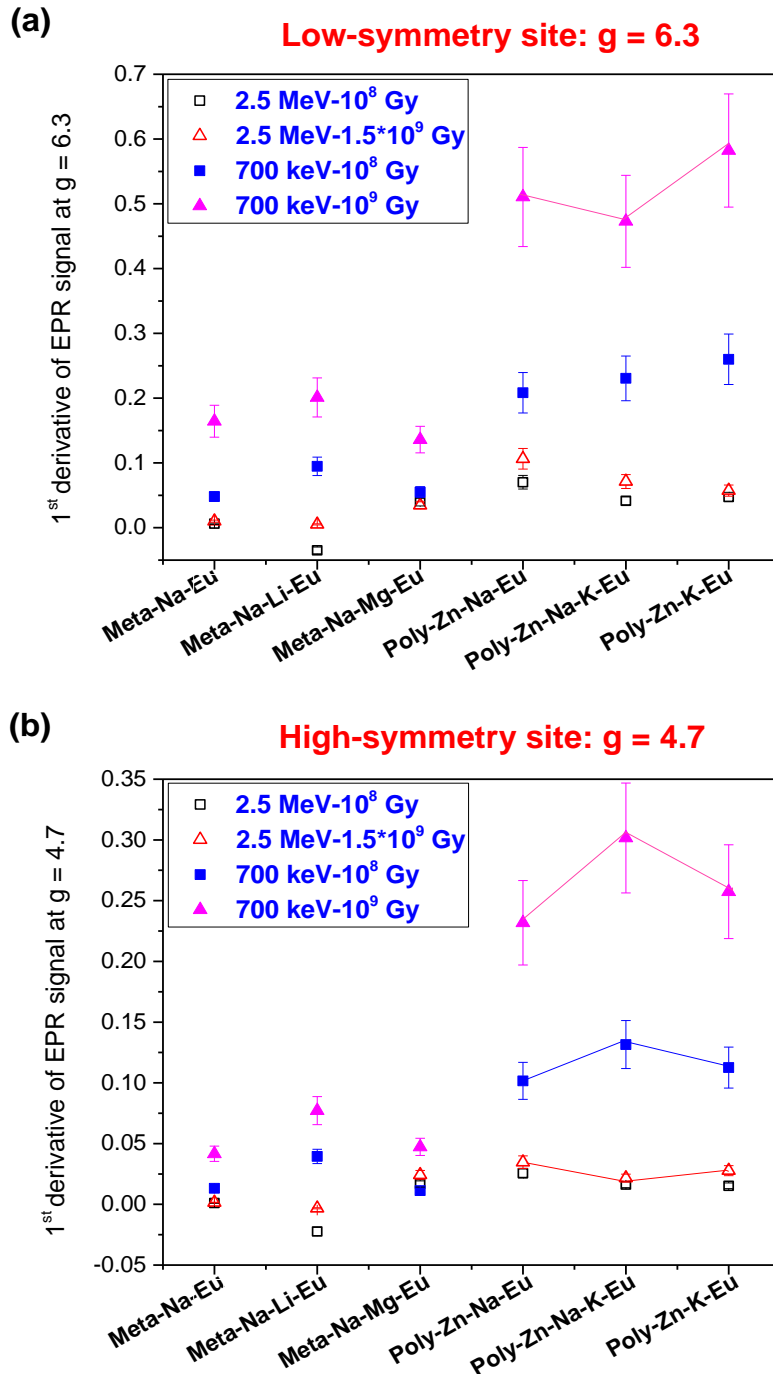


Figure 30 Comparison between 2.5 MeV and 700 keV electron irradiation of the EPR signal intensity (a) $I_{g=6.3}$ and (b) $I_{g=4.7}$ attributed respectively to low and high symmetry site of Eu^{2+} ion in meta and polyphosphate glasses for 10^8 and 10^9 Gy doses.

We observe a huge increase of the signal intensity under 700 keV irradiation compared to 2.5 MeV and the generation of Eu^{2+} ions is more important in polyphosphate than in metaphosphate compositions. More accurately and by comparing same integrated dose, it is obvious to notice that 700 keV energy is much more efficient to reduce Eu^{3+} ions than 2.5 MeV. Thus, $I_{g=6.3}$ (corresponding to the low symmetry site) is increased from 1 (2.5 MeV at 10^9 Gy) to 16 (700 keV, 10^9 Gy) in Meta-Na-Eu while the intensity of high symmetry sites in the same conditions is multiplied by 20. In polyphosphate glasses, a larger amount of Eu^{2+} ions is produced under 700 keV compared to metaphosphate but the increase of Eu^{2+} reduced ions (expressed in percent) under both site symmetry shifting from 2.5 MeV to 700 keV energy is lower in Polyphosphate compared to Metaphosphate glasses. Thus, $I_{g=6.3}$ is multiplied by 8 from 700 keV to 2.5 MeV (at 10^9 Gy) (against 16 in Meta) and 11 for the signal at $g = 4.7$ (against 20 in Meta).

In addition, it is worth to notice that a mixed alkali effect occurs in Na/K polyphosphate glass for both energies 2.5 MeV and 700 keV, especially for the high symmetry site but also for the low symmetry site within 700 keV/ 10^9 Gy conditions.

Actually, a non-linear variation (with either a maximum or a minimum) of Eu^{2+} amount can be observed in Figures 30a and 30b.

Therefore, the mixed NaK zinc polyphosphate glass for the high-symmetry site exhibits the highest increase of Eu^{2+} amount from 2.5 MeV to 700 keV. It means that the reduction of Eu^{3+} ions (especially for the high symmetry site) is probably associated to a rearrangement of the Eu^{3+} initial site including the alkaline ions and O migration in the glass network. This result let us suspect that a direct reduction process for 2 Eu^{3+} preexisting sites is probably not the right scenario but one type of Eu^{2+} ions could be generated after modification of the Eu^{3+} environment.

We know that transport of alkaline ions is the dominant mechanism in low energy electron (typ. 50 keV) irradiated glasses with the creation of channels [63]. At 700 keV due to the thickness of the sample (larger than the penetration depth of the electrons), we expect also that migration of alkaline ions under the electrical field generated is effective. This difference with 2.5 MeV could explain the larger efficiency to reduce Eu^{3+} with low energy electrons and the ability of polyphosphate with a more depolymerized network compared to metaphosphate compositions to incorporate Eu^{2+} ions.

- The EPR and PL spectroscopy show the presence of two types of sites for divalent Eu^{2+} ions formed after irradiation in metaphosphate and polyphosphate glasses whatever the dose and electron energy.
- These studies associate generally the high symmetry site ($g=4.7$) to a strong crystal field that could correspond to 6-coordinated Eu^{3+} ions. The low-symmetry site ($g=6.3$) with a lower crystal field would rather deal with Eu^{2+} ions with a higher coordination number into a modifier position.
- It seems that the presence of Zn favors the formation of the high-symmetry site with a quasi-linear increase of both sites with increasing doses.
- When dose becomes higher than 10^9 Gy, we evidenced a predominance of modifier sites on network modifier sites linked to the migration of alkaline ions.
- 700 keV energy is much more efficient to reduce Eu^{3+} ions than 2.5 MeV and the generation of Eu^{2+} ions is more important in polyphosphate than in metaphosphate compositions.

From the results obtained in this chapter, it appears that the modifications of both the glassy network and the Eu^{3+} ions environment are dependent on the glass composition (e.g. insertion of Zn) and the irradiation parameters: particularly the integrated dose and the electron energy acting mostly on the reduction of Eu^{3+} ions.

In this section, we will try to present some assumptions for mechanisms leading to both local and medium range order variations under irradiation as well as establishing some connections.

In regards to glass composition, Table 2 shows the seven glass matrices which were studied. It is useful to remember some different ways that these can be classified. Firstly, metaphosphates are predominately Q^2 whereas polyphosphates are predominately Q^1 . Secondly, the glass matrices vary from highest alkali content in Meta-Na and Meta-Na-Li (noting that Li and Na have the highest mobility of the alkalis), to lowest alkali content in Meta-Zn. Another distinction concerns the modifier cationic field strength which decreases in the sequence $\text{Mg}^{2+} > \text{Li}^{1+} > \text{Na}^{1+} > \text{K}^{1+}$ (where Mg^{2+} and Zn^{2+} both have significantly higher cationic field strength than alkalis). In addition, two glass matrices have mixed alkalis, Meta-Na-Li and Poly-Zn-Na-K, and this might reduce the mobility of alkalis due to the mixed alkali effects.

In polyphosphate glasses under 2.5 MeV electron irradiation, the formation of POHC defect is detected by EPR spectroscopy at low doses until 10^7 Gy then a disappearance of this point defects following by the creation of peroxy point defects from dose 10^8 Gy corresponding to a trapped hole on oxygen atoms at the end of a short chain (P-O-O $^\circ$). These peroxy defects are very weakly formed in metaphosphate compositions. In parallel, we observed by Raman a massive increase of terminal P-O stretch motions of Q^1 in irradiated polyphosphate glasses from dose 10^8 Gy. It seems unreasonable that the peroxy radicals can be formed from preexisting P-O-O-P linkages in polyphosphates. We thus assume that peroxy defects could form from the recombination of an oxygen with terminal P-O bonds. The migration of a NBO could be associated with one alkaline ion migration. However, no polymerization increase occurs in polyphosphates glasses, we rather observe a small increase of Q^2 and Q^0 units that could be the result of a conversion of Q^1 units into Q^2+Q^0 species but the origin of migrating oxygen atom is not clear.

Concerning the network evolution, in Na metaphosphate glasses, it may be that irradiation effects primarily occurs with Na-NBO bonds which are plentiful and weak. Breaking and remaking these bonds will have an effect on the chains of Q^2 , causing them to 'twist' or 'bend'. But flexibility of Na makes it easier for Q^2 chains to rearrange, and this releases stress on Q^2 chains.

In Zn metaphosphate, irradiation effects could mainly occur with Zn-NBO bonds, which again causes some 'twists' or 'bends' in Q^2 chains. However, the Zn is less flexible, and the 'cross linking' role of Zn makes it harder for Q^2 chains to rearrange, so there is more stress on Q^2 chains compared to Na metaphosphate and a stronger disorder in the chains is represented by the observed variation in the Raman spectra.

We can suspect however that some coordination change around Eu^{3+} ions under irradiation may occur liberating some NBO and alkaline ions during reduction of Eu^{3+} to Eu^{2+} . This mechanism could explain the larger Eu^{3+} site dispersion after irradiation represented by the broadening of the ${}^5\text{D}_0 \rightarrow {}^7\text{F}_0$ emission band, considerable in zinc phosphate glass and weaker in alkali metaphosphate samples. Molecular dynamics simulation showed moreover that the presence of zinc increases the portion of Eu^{3+} ions under fivefold coordination explaining why this mixture of coordination number can be less sensitive to a Eu^{3+} site distortion represented by the slight increase of As in polyphosphates rather than in Na metaphosphate where 6 coordinated Eu^{3+} dominated (82 %) with a strong increase of As under irradiation.

The interstitial Na in alkali metaphosphate provides flexibility and this means that in the pristine glass the Eu are better able to take sites with dominant CN=6. According to the previous proposal, the flexibility provided by Na enables the phosphate chains to rearrange in response to irradiation effects on NBOs. However, these rearrangements of the phosphate chains will cause 'distortion' on Eu sites, hence a notable increase in As ratio. In addition, the MD model shows that it is common for Eu to have some NBO which are shared with Na (i.e. Eu-NBO-Na). This means that irradiation effects on Na-NBO bonds might cause the Na to move around, and this will also cause distortion of remaining Eu-NBO bonds.

Further, if we compare Zn metaphosphate and Na metaphosphate, it is obvious that Zn insertion favors effectively the reduction of Eu^{3+} to Eu^{2+} ions under irradiation. It is more difficult to evaluate the role of Zn in polyphosphate where the initial Eu^{3+} environment is different than in sodium metaphosphate glass with moreover a more depolymerized network. The lower initial average coordination number of Eu^{3+} as well as the charge equilibrium being modified by Zn^{2+} insertion could favor a greater production of divalent Eu under irradiation. As well, the reduction is more efficient under 700 keV compared to 2.5 MeV. We can suspect a more efficient alkali migration driven by the electrical field leading to a network reorganization more efficient to host Eu^{2+} ions with a larger NBO numbers.

- [1] R. A. B. Devine, « Macroscopic and microscopic effects of radiation in amorphous SiO₂ », *Nuclear Instruments and Methods in Physics Research Section B: Beam Interactions with Materials and Atoms*, vol. 91, n° 1-4, p. 378–390, 1994.
- [2] D. G. Howitt, H. W. Chan, J. F. DeNatale, et J. P. Heuer, « Mechanism for the radiolytically induced decomposition of soda–silicate glasses », *Journal of the American Ceramic Society*, vol. 74, n° 5, p. 1145–1147, 1991.
- [3] W. J. Weber *et al.*, « Radiation effects in glasses used for immobilization of high-level waste and plutonium disposition », *Journal of Materials Research*, vol. 12, n° 8, p. 1948–1978, 1997.
- [4] N. Ollier, G. Rizza, B. Boizot, et G. Petite, « Effects of temperature and flux on oxygen bubble formation in Li borosilicate glass under electron beam irradiation », *Journal of Applied Physics*, vol. 99, n° 7, p. 073511, avr. 2006.
- [5] C. Mendoza, S. Peugot, O. Bouty, R. Caraballo, et C. Jegou, « Simplified Nuclear Glasses Structure Behaviour Under Various Irradiation Conditions: A Raman Spectroscopy Study », *Procedia Chemistry*, vol. 7, p. 581-586, 2012.
- [6] B. Boizot, N. Ollier, F. Olivier, G. Petite, D. Ghaleb, et E. Malchukova, « Irradiation effects in simplified nuclear waste glasses », *Nuclear Instruments and Methods in Physics Research Section B: Beam Interactions with Materials and Atoms*, vol. 240, n° 1-2, p. 146-151, oct. 2005.
- [7] G. J. Exarhos, « Vibrational Raman studies of particle induced damage in oxide glasses », *Nuclear Instruments and Methods in Physics Research Section B: Beam Interactions with Materials and Atoms*, vol. 1, n° 2-3, p. 498-502, févr. 1984.
- [8] F. H. ElBatal, A. M. Abdelghany, et R. L. Elwan, « Structural characterization of gamma irradiated lithium phosphate glasses containing variable amounts of molybdenum », *Journal of Molecular Structure*, vol. 1000, n° 1-3, p. 103-108, août 2011.
- [9] V. N. Rai, B. N. R. Sekhar, P. Tiwari, R. J. Kshirsagar, et S. K. Deb, « Spectroscopic studies of gamma irradiated Nd doped phosphate glasses », *Journal of Non-Crystalline Solids*, vol. 357, n° 22-23, p. 3757-3764, nov. 2011.
- [10] V. Pukhkaya, F. Trompier, et N. Ollier, « New insights on P-related paramagnetic point defects in irradiated phosphate glasses: Impact of glass network type and irradiation dose », *Journal of Applied Physics*, vol. 116, n° 12, p. 123517, sept. 2014.
- [11] V. N. Rai, B. N. Raja Sekhar, S. Kher, et S. K. Deb, « Effect of gamma ray irradiation on optical properties of Nd doped phosphate glass », *Journal of Luminescence*, vol. 130, n° 4, p. 582-586, avr. 2010.
- [12] P. Ebeling, D. Ehrt, et M. Friedrich, « X-ray induced effects in phosphate glasses », *Optical Materials*, vol. 20, n° 2, p. 101-111, sept. 2002.
- [13] D. L. Griscom, E. J. Friebele, K. J. Long, et J. W. Fleming, « Fundamental defect centers in glass: Electron spin resonance and optical absorption studies of irradiated phosphorus-doped silica glass and optical fibers », *Journal of Applied Physics*, vol. 54, n° 7, p. 3743-3762, juill. 1983.
- [14] L. W. Hobbs, A. N. Sreeram, C. E. Jesurum, et B. A. Berger, « Structural freedom, topological disorder, and the irradiation-induced amorphization of ceramic structures », *Nuclear Instruments and Methods in Physics Research Section B: Beam Interactions with Materials and Atoms*, vol. 116, n° 1-4, p. 18–25, 1996.
- [15] R. K. Brow, C. C. Phifer, G. L. Turner, et R. J. Kirkpatrick, « Cation effects on ³¹P MAS NMR chemical shifts of metaphosphate glasses », *Journal of the American Ceramic Society*, vol. 74, n° 6, p. 1287–1290, 1991.
- [16] J. J. Hudgens, R. K. Brow, D. R. Tallant, et S. W. Martin, « Raman spectroscopy study of the structure of lithium and sodium ultraphosphate glasses », *Journal of Non-Crystalline Solids*, vol. 223, p. 21-31, janv. 1998.
- [17] G. B. Rouse Jr, P. J. Miller, et W. M. Risen Jr, « Mixed alkali glass spectra and structure », *Journal of Non-Crystalline Solids*, vol. 28, n° 2, p. 193–207, 1978.
- [18] J. Swenson, A. Matic, A. Brodin, L. Börjesson, et W. S. Howells, « Structure of mixed alkali phosphate glasses by neutron diffraction and Raman spectroscopy », *Phys. Rev. B*, vol. 58, n° 17, p. 11331-11337, nov. 1998.

- [19] R. K. Brow, D. R. Tallant, S. T. Myers, et C. C. Phifer, « The short-range structure of zinc polyphosphate glass », *Journal of Non-Crystalline Solids*, vol. 191, n° 1-2, p. 45-55, nov. 1995.
- [20] N. Ollier, R. Planchais, et B. Boizot, « EPR study of Yb-doped irradiated glasses », *Nuclear Instruments and Methods in Physics Research Section B: Beam Interactions with Materials and Atoms*, vol. 266, n° 12-13, p. 2854-2858, juin 2008.
- [21] S. Fan, C. Yu, D. He, X. Wang, et L. Hu, « Tunable white light emission from γ -irradiated Ag/Eu co-doped phosphate glass phosphor », *Optical Materials Express*, vol. 2, n° 6, p. 765, juin 2012.
- [22] E. Malchukova, B. Boizot, D. Ghaleb, et G. Petite, « Optical properties of pristine and γ -irradiated Sm doped borosilicate glasses », *Nuclear Instruments and Methods in Physics Research Section A: Accelerators, Spectrometers, Detectors and Associated Equipment*, vol. 537, n° 1-2, p. 411–414, 2005.
- [23] N. Ollier, B. Boizot, P. L'henoret, S. Guillous, et G. Petite, « Evidence of transient species occurring in the reduction process of trivalent lanthanides under 2.5 MeV electron irradiation by in situ cathodoluminescence and time-resolved photoluminescence », *Journal of Applied Physics*, vol. 105, n° 11, p. 113515, 2009.
- [24] J. de Bonfils, G. Panczer, D. de Ligny, S. Peugeot, et B. Champagnon, « Behaviour of simplified nuclear waste glasses under gold ions implantation: A microluminescence study », *Journal of Nuclear Materials*, vol. 362, n° 2-3, p. 480-484, mai 2007.
- [25] H. Ebendorff-Heidepriem et D. Ehrt, « Effect of europium ions on X-ray-induced defect formation in phosphate containing glasses », *Optical Materials*, vol. 19, n° 3, p. 351-363, mai 2002.
- [26] J. Qiu *et al.*, « Memorized polarization-dependent light scattering in rare-earth-ion-doped glass », *Applied Physics Letters*, vol. 77, n° 13, p. 1940-1942, sept. 2000.
- [27] J. Qiu, K. Kojima, K. Miura, T. Mitsuyu, et K. Hirao, « Infrared femtosecond laser pulse-induced permanent reduction of Eu^{3+} to Eu^{2+} in a fluorozirconate glass », *Optics Letters*, vol. 24, n° 11, p. 786, juin 1999.
- [28] J. Qiu, K. Miura, T. Suzuki, T. Mitsuyu, et K. Hirao, « Permanent photoreduction of Sm^{3+} to Sm^{2+} inside a sodium aluminoborate glass by an infrared femtosecond pulsed laser », *Applied physics letters*, vol. 74, n° 1, p. 10–12, 1999.
- [29] H. You et M. Nogami, « Optical Properties and Valence Change of Europium Ions in a Sol-Gel Al_2O_3 - B_2O_3 - SiO_2 Glass by Femtosecond Laser Pulses », *The Journal of Physical Chemistry B*, vol. 109, n° 29, p. 13980-13984, juill. 2005.
- [30] L. Yu et M. Nogami, « Upconversion luminescence properties of europium in ZnO-SiO_2 glasses by femtosecond laser excitation », *Materials Chemistry and Physics*, vol. 107, n° 2-3, p. 186-188, févr. 2008.
- [31] H. Rahimian, H. Mokhtari, et S. P. Shirmardi, « Improvement of Eu^{3+} emissions in oxyfluoride glass and nano glass-ceramic by electron beam irradiation », *Journal of Luminescence*, vol. 187, p. 535-539, juill. 2017.
- [32] E. Malchukova et B. Boizot, « Divalent Europium in β -Irradiated Aluminoborosilicate Glass: Rapid Communications of the American Ceramic Society », *Journal of the American Ceramic Society*, vol. 93, n° 12, p. 4005-4007, déc. 2010.
- [33] V. N. Rai, S. N. Thakur, et D. K. Rai, « Photoacoustic studies on neutron-irradiated rare earth oxide powers », *Applied spectroscopy*, vol. 40, n° 8, p. 1211–1214, 1986.
- [34] B. Babu *et al.*, « Radiation hardening in sol-gel derived Er^{3+} -doped silica glasses », *Journal of Applied Physics*, vol. 118, sept. 2015.
- [35] S. Baccaro *et al.*, « Radiation damage of silicate glasses doped with Tb^{3+} and Eu^{3+} », p. 5, 2003.
- [36] H. Ebendorff, Heidepriem et D. Ehrt, « Ultraviolet laser and x-ray induced valence changes and defect formation in europium and terbium doped glasses », *Physics and Chemistry of Glasses Proc. XIX Int. Congr. Glass, Edinburgh*, vol. 43, p. 10, 2002.
- [37] M. Mohapatra, R. M. Kadam, R. K. Mishra, C. P. Kaushik, B. S. Tomar, et S. V. Godbole, « Gamma radiation induced changes in nuclear waste glass containing Eu », *Physica B: Condensed Matter*, vol. 406, n° 20, p. 3980-3984, oct. 2011.

- [38] K. Jha et M. Jayasimhadri, « Structural and emission properties of Eu^{3+} -doped alkaline earth zinc-phosphate glasses for white LED applications », *Journal of the American Ceramic Society*, vol. 100, n° 4, p. 1402-1411, avr. 2017.
- [39] E. W. J. L. Oomen et A. M. A. van Dongen, « Europium (III) in oxide glasses », *Journal of Non-Crystalline Solids*, vol. 111, n° 2-3, p. 205-213, nov. 1989.
- [40] C. S. Rao, K. U. Kumar, et C. K. Jayasankar, « Luminescence properties of Eu^{3+} ions in phosphate-based bioactive glasses », *Solid State Sciences*, vol. 13, n° 6, p. 1309–1314, 2011.
- [41] M. Saad, W. Stambouli, S. A. Mohamed, et H. Elhouichet, « Ag nanoparticles induced luminescence enhancement of Eu^{3+} doped phosphate glasses », *Journal of Alloys and Compounds*, vol. 705, p. 550–558, 2017.
- [42] S. Nayab Rasool, L. Rama Moorthy, et C. Kulala Jayasankar, « Optical and luminescence properties of Eu^{3+} -doped phosphate based glasses », *Materials Express*, vol. 3, n° 3, p. 231–240, 2013.
- [43] C. R. Kesavulu, K. K. Kumar, N. Vijaya, K.-S. Lim, et C. K. Jayasankar, « Thermal, vibrational and optical properties of Eu^{3+} -doped lead fluorophosphate glasses for red laser applications », *Materials Chemistry and Physics*, vol. 141, n° 2-3, p. 903–911, 2013.
- [44] K. U. Kumar, S. S. Babu, C. S. Rao, et C. K. Jayasankar, « Optical and fluorescence spectroscopy of Eu^{3+} -doped $\text{P}_2\text{O}_5\text{-K}_2\text{O-KF-MO-Al}_2\text{O}_3$ (M= Mg, Sr and Ba) glasses », *Optics Communications*, vol. 284, n° 12, p. 2909–2914, 2011.
- [45] K. Linganna et C. K. Jayasankar, « Optical properties of Eu^{3+} ions in phosphate glasses », *Spectrochimica Acta Part A: Molecular and Biomolecular Spectroscopy*, vol. 97, p. 788–797, 2012.
- [46] U. Hoppe, G. Walter, G. Carl, J. Neufeind, et A. C. Hannon, « Structure of zinc phosphate glasses probed by neutron and X-ray diffraction of high resolving power and by reverse Monte Carlo simulations », *Journal of Non-Crystalline Solids*, vol. 351, n° 12-13, p. 1020-1031, mai 2005.
- [47] D. L. Griscom, E. J. Friebele, K. J. Long, et J. W. Fleming, « Fundamental defect centers in glass: Electron spin resonance and optical absorption studies of irradiated phosphorus-doped silica glass and optical fibers », *Journal of Applied Physics*, vol. 54, n° 7, p. 3743-3762, juill. 1983.
- [48] H. Ebendorff-Heidepriem et D. Ehrhart, « Spectroscopic properties of Eu^{3+} and Tb^{3+} ions for local structure investigations of fluoride phosphate and phosphate glasses », *Journal of Non-Crystalline Solids*, vol. 208, n° 3, p. 205-216, déc. 1996.
- [49] S. S. Babu, P. Babu, C. K. Jayasankar, W. Sievers, Th. Tröster, et G. Wortmann, « Optical absorption and photoluminescence studies of Eu^{3+} -doped phosphate and fluorophosphate glasses », *Journal of Luminescence*, vol. 126, n° 1, p. 109-120, sept. 2007.
- [50] G. H. Silva, V. Anjos, M. J. V. Bell, A. P. Carmo, A. S. Pinheiro, et N. O. Dantas, « Eu^{3+} emission in phosphate glasses with high UV transparency », *Journal of Luminescence*, vol. 154, p. 294-297, oct. 2014.
- [51] A. N. Meza-Rocha, A. Speghini, M. Bettinelli, et U. Caldiño, « Orange and reddish-orange light emitting phosphors: Sm^{3+} and $\text{Sm}^{3+}/\text{Eu}^{3+}$ doped zinc phosphate glasses », *Journal of Luminescence*, vol. 167, p. 305-309, nov. 2015.
- [52] V. Pukhkaya, P. Goldner, A. Ferrier, et N. Ollier, « Impact of rare earth element clusters on the excited state lifetime evolution under irradiation in oxide glasses », *Optics express*, vol. 23, n° 3, p. 3270–3281, 2015.
- [53] A. Ladaci *et al.*, « X-rays, γ -rays, electrons and protons radiation-induced changes on the lifetimes of Er^{3+} and Yb^{3+} ions in silica-based optical fibers », *Journal of Luminescence*, vol. 195, p. 402-407, mars 2018.
- [54] V. Pukhkaya, « Influence of Yb^{3+} and Er^{3+} ions environment on the evolution of its' luminescent properties in oxide glasses under ionizing irradiation », PhD Thesis, Ecole Polytechnique X, 2013.
- [55] M. Mahfoudhi et N. Ollier, « Tuning Eu^{2+} amount and site symmetry in phosphate glasses under irradiation by electron energy and integrated dose », *Optical Materials*, vol. 95, p. 109253, sept. 2019.
- [56] D. Ehrhart, « REVIEW: Phosphate and fluoride phosphate optical glasses — properties, structure and applications », *Physics and Chemistry of Glasses: European Journal of Glass Science and Technology Part B*, vol. 56, n° 6, p. 217-234, déc. 2015.

- [57] H. Ebendorff-Heidepriem et D. Ehrt, « Formation and UV absorption of cerium, europium and terbium ions in different valencies in glasses », *Optical Materials*, p. 19, 2000.
- [58] E. Malchukova et B. Boizot, « Reduction of Eu^{3+} to Eu^{2+} in aluminoborosilicate glasses under ionizing radiation », *Materials Research Bulletin*, vol. 45, n° 9, p. 1299-1303, sept. 2010.
- [59] M. Nogami, T. Yamazaki, et Y. Abe, « Fluorescence properties of Eu^{3+} and Eu^{2+} in $\text{Al}_2\text{O}_3\text{-SiO}_2$ glass », *Journal of Luminescence*, vol. 78, n° 1, p. 63-68, janv. 1998.
- [60] H. Ebendorff-Heidepriem et D. Ehrt, « Effect of europium ions on X-ray-induced defect formation in phosphate containing glasses », *Optical Materials*, vol. 19, n° 3, p. 351-363, mai 2002.
- [61] A. N. Trukhin, A. Antuzevics, K. Golant, et D. L. Griscom, « Luminescence of phosphorus doped silica glass », *Journal of Non-Crystalline Solids*, vol. 462, p. 10-16, avr. 2017.
- [62] P. Ebeling, D. Ehrt, et M. Friedrich, « Influence of modifier cations on the radiation-induced effects of metaphosphate glasses », *Glass science and technology*, vol. 76, n° 2, p. 56–61, 2003.
- [63] O. Gedeon, J. Zemek, et K. Jurek, « Changes in alkali-silicate glasses induced with electron irradiation », *Journal of Non-Crystalline Solids*, vol. 354, n° 12-13, p. 1169–1171, 2008.

List of Figures

FIGURE 1 SIRIUS ACCELERATOR IN LSI (A) CLOSE VIEW OF INSIDE – PELLETRON CHARGING SYSTEM, (B) ACCELERATOR CHAMBER, AND (C) IRRADIATION BEAM LINES.	112
FIGURE 2 COLOR CHANGE OF META-NA-EU GLASS AFTER 2.5 MEV ELECTRON IRRADIATION	113
FIGURE 3 RAMAN SPECTRA OF META-NA-EU IRRADIATED BY ELECTRON OF 2.5 MEV AT VARIOUS DOSE COMPARED TO PRISTINE GLASS, NORMALIZATION BY MAXIMUM	116
FIGURE 4 RAMAN SPECTRA OF META-NA-MG-EU IRRADIATED BY ELECTRON OF 2.5 MEV, NORMALIZATION BY MAXIMUM.....	117
FIGURE 5 RAMAN SPECTRA OF META-ZN-EU IRRADIATED BY ELECTRON OF 2.5 MEV AT VARIOUS DOSE COMPARED TO PRISTINE GLASS, NORMALIZATION BY MAXIMUM.	118
FIGURE 6 THE FULL WIDTH AT HALF MAXIMUM FWHM (LEFT) AND THE AREA (RIGHT) OF THE BAND AT 706 CM^{-1} DUE TO NS(POP) AS A FUNCTION OF DOSE LOGARITHM IN META-ZN-EU UNDER ELECTRON IRRADIATION.	118
FIGURE 7 THE FULL WIDTH AT HALF MAXIMUM FWHM OF THE BAND AT 1201 CM^{-1} DUE TO NS(PO ₂) AS A FUNCTION OF DOSE LOGARITHM IN META-ZN-EU UNDER ELECTRON IRRADIATION.....	119
FIGURE 8 RAMAN SPECTRA OF POLY-ZN-NA-EU IRRADIATED BY ELECTRON OF 2.5 MEV AT VARIOUS DOSE COMPARED TO PRISTINE GLASS, NORMALIZATION BY MAXIMUM	120
FIGURE 9 RAMAN SPECTRA OF POLY-ZN-K-EU (LEFT) AND POLY-ZN-NA-K-EU (RIGHT) IRRADIATED BY ELECTRON OF 2.5 MEV AT VARIOUS DOSE COMPARED TO PRISTINE GLASS, NORMALIZATION BY MAXIMUM	120
FIGURE 10 INTENSITY OF THE BANDS AT 1020 AND 1120 CM^{-1} DUE TO P-O STRETCH OF Q ¹ TERMINAL AS A FUNCTION OF DOSE LOGARITHM IN POLY-ZN-NA-EU UNDER 2.5 MEV ELECTRON IRRADIATION.	121
FIGURE 11 RAMAN SPECTRUM OF POLY-ZN-NA-EU UNDER 700 KEV ELECTRON IRRADIATION AT DOSE 10^9 GY IN THE LARGER VOLUME OF THE SAMPLE	122
FIGURE 12 RAMAN SPECTRUM OF META-ZN-EU UNDER 700 KEV ELECTRON IRRADIATION AT DOSE 2.5×10^8 GY IN THE LARGER VOLUME OF THE SAMPLE	122
FIGURE 13 LUMINESCENCE SPECTRA OF EU ³⁺ DOPED METAPHOSPHATE GLASS META-NA-EU BEFORE AND AFTER ELECTRON IRRADIATION ($\Delta\text{EXT} = 532$)	127
FIGURE 14 THE PL EMISSION SPECTRA OF EU-DOPED METAPHOSPHATE GLASS META-NA-EU.....	127
FIGURE 15 VARIATION OF THE ASYMMETRY RATIO AS OF EU ³⁺ IONS AFTER 2.5 MEV ELECTRON IRRADIATION AS A FUNCTION OF THE LOGARITHMIC DOSE IN (A) METAPHOSPHATE GLASSES: META-NA-EU, META-NA-LI-EU, META-NA-MG-EU AND META-ZN-EU. ($\Delta\text{EXT}=532$)	128
FIGURE 16 VARIATION OF THE ASYMMETRY RATIO AS OF EU ³⁺ IONS AFTER 2.5 MEV ELECTRON IRRADIATION AS A FUNCTION OF THE LOGARITHMIC DOSE IN POLYPHOSPHATE GLASSES (POLY-ZN-NA-EU, POLY-ZN-K-EU AND POLY-ZN-NA-K-EU) COMPARED TO METAPHOSPHATE GLASS META-NA-EU. ($\Delta\text{EXT}=532$)	129
FIGURE 17 VARIATION OF THE ASYMMETRY RATIO AS OF THE EU ³⁺ IONS AS A FUNCTION OF THE THICKNESS IN EU-DOPED METAPHOSPHATE GLASSES IRRADIATED BY ELECTRON OF 700 KEV AND COMPARED TO 2.5 MEV IRRADIATION (A) AT DOSE = 10^8 GY AND (B) AT DOSE = 10^9 GY. THE EMISSION SPECTRA WERE MEASURED UNDER 488 NM EXCITATION AND SAVED AT EVERY 200 μM IN ALL THE THICKNESS OF THE SAMPLE.	131
FIGURE 18 : VARIATION OF THE ASYMMETRY RATIO AS OF THE EU ³⁺ IONS AS A FUNCTION OF THE THICKNESS IN EU-DOPED POLYPHOSPHATE GLASSES IRRADIATED BY ELECTRON OF 700 KEV AND COMPARED TO 2.5 MEV IRRADIATION (A) AT DOSE = 10^8 GY AND (B) AT DOSE = 10^9 GY. THE EMISSION SPECTRA WERE MEASURED UNDER 488 NM EXCITATION AND SAVED AT EVERY 200 μM IN ALL THE THICKNESS OF THE SAMPLE	131
FIGURE 19 ZOOM OF THE NORMALIZED EMISSION BAND ATTRIBUTED TO THE $5D_0 \rightarrow 7F_0$ TRANSITION OF THE EU ³⁺ IONS IN (A) METAPHOSPHATE GLASS META-NA-EU AND (B) POLYPHOSPHATE GLASS POLY-ZN-NA-EU IRRADIATED BY ELECTRON OF 2.5 MEV AT VARIOUS DOSES.	134
FIGURE 20 VARIATION OF THE FULL WIDTH AT HALF MAXIMUM FWHM AFTER 2.5 MEV ELECTRON IRRADIATION AS A FUNCTION OF THE LOGARITHMIC DOSE IN (A) METAPHOSPHATE GLASSES: META-NA-EU, META-NA-LI-EU AND META-NA-MG-EU AND (B) IN POLYPHOSPHATE GLASS POLY-ZN-NA-EU, POLY-ZN-K-EU AND POLY-ZN-NA-K-EU	135

FIGURE 21 ZOOM OF THE NORMALIZED EMISSION BAND ATTRIBUTED TO THE $5D_0 \rightarrow 7F_0$ TRANSITION OF THE Eu^{3+} IONS IN (A) META-NA-EU AND (B) POLY-ZN-NA-EU AFTER 700 KEV ELECTRON IRRADIATION AT DOSE = 10^8 GY. THE EMISSION SPECTRA WERE MEASURED UNDER 488 NM EXCITATION AND SAVED AT EVERY 200 μ M IN ALL THE THICKNESS OF THE SAMPLE.....	137
FIGURE 22 VARIATION OF THE FULL WIDTH AT HALF MAXIMUM FWHM AS A FUNCTION OF THE THICKNESS UNDER IRRADIATION BY ELECTRON OF 700 KEV AT DOSE = 10^8 GY IN META-NA-EU, META-ZN-EU, POLY-ZN-NA-EU AND POLY-EU-50-50. (THE EMISSION SPECTRUM WERE MEASURED UNDER 488 NM EXCITATION AND SAVED AT EVERY 200 μ M IN ALL THE THICKNESS OF THE SAMPLE)	138
FIGURE 23 THE PL EMISSION SPECTRA OF (A) EU-DOPED METAPHOSPHATE GLASS META-NA-EU AND (B) EU-DOPED POLYPHOSPHATE GLASS POLY-ZN-NA-EU AFTER 2.5 MEV ELECTRON IRRADIATION AT VARIOUS DOSES FROM 10^5 TO OVER 10^9 GY. ($\lambda_{EXT}=355$ NM).....	142
FIGURE 24 THE PL EMISSION SPECTRA OF (A) EU-DOPED METAPHOSPHATE GLASS (META-NA-EU) AND (B) EU-DOPED POLYPHOSPHATE GLASS (POLY-ZN-NA-EU) AFTER 700 KEV AND 2.5 MEV ELECTRON IRRADIATION AT 10^8 AND 10^9 GY DOSES. ($\lambda_{EXT}=355$ NM)	143
FIGURE 25 A FIT OF THE EMISSION SPECTRA OF THE Eu^{2+} IONS IN (A) EU-DOPED METAPHOSPHATE GLASS (META-NA-EU) AND (B) EU-DOPED POLYPHOSPHATE GLASS (POLY-ZN-NA-EU) AFTER 700 KEV ELECTRON IRRADIATION AT 10^9 GY DOSE. TWO COMPONENTS AT NEAR 450 AND 500 NM IN BOTH GLASSES ATTESTING THE PRESENCE OF 2 SITES FOR Eu^{2+} IONS.	144
FIGURE 26 EPR SPECTRA NORMALIZED BY MASS AND GAIN OF POLY-ZN-NA-EU GLASS IRRADIATED BY ELECTRON OF 2.5 MEV AT VARIOUS DOSES.....	145
FIGURE 27 THE PL EMISSION SPECTRA OF EU-DOPED META AND POLYPHOSPHATE GLASSES (META-NA-EU, META-NA-MG-EU, META-ZN-EU AND POLY-ZN-NA-EU) AFTER 700 KEV AT DOSE 10^9 GY. ($\lambda_{EXT}=355$)	146
FIGURE 28 VARIATION OF THE EPR SIGNAL INTENSITY (A) $I_{G=6.3}$ AND (B) $I_{G=4.7}$ ATTRIBUTED RESPECTIVELY TO LOW AND HIGH SITE SYMMETRY OF Eu^{2+} ION IN META-NA-EU, META-ZN-EU, POLY-ZN-NA-EU AND POLY-ZN-NA-EU-($Q^1/Q^2:50/50$) GLASSES IRRADIATED BY 2.5 MEV AT VARIOUS DOSES: FROM 10^5 GY TO OVER 10^9 GY.	147
FIGURE 29 THE RATIO BETWEEN Eu^{2+} LOW-SYMMETRY SITE AND HIGH-SYMMETRY SITE FOR POLY-ZN-NA-EU GLASS UNDER 2.5 MEV IRRADIATIONS AS A FUNCTION OF DOSE LOGARITHM.	148
FIGURE 30 COMPARISON BETWEEN 2.5 MEV AND 700 KEV ELECTRON IRRADIATION OF THE EPR SIGNAL INTENSITY (A) $I_{G=6.3}$ AND (B) $I_{G=4.7}$ ATTRIBUTED RESPECTIVELY TO LOW AND HIGH SYMMETRY SITE OF Eu^{2+} ION IN META AND POLYPHOSPHATE GLASSES FOR 10^8 AND 10^9 GY DOSES.....	149

List of Tables

TABLE 1 ELECTRON IRRADIATION CONDITIONS.....	113
TABLE 2 ASYMMETRY RATIO OF Eu^{3+} IONS IN UNIRRADIATED PHOSPHATE GLASSES.	126
TABLE 3 THE $Eu^{3+} \ ^5D_0$ ENERGY LEVEL LIFETIME EVOLUTION T UNDER 2.5 MEV ELECTRON IRRADIATION FOR VARIOUS DOSE IN METAPHOSPHATE AND POLYPHOSPHATE GLASSES.	139
TABLE 4 RATIO BETWEEN LOW-SYMMETRY SITE (G=6.3) AND HIGH-SYMMETRY SITE (G=4.7) FOR DIFFERENT PHOSPHATE GLASSES IRRADIATED BY 700 KEV AT 10^9 GY DOSE.	145

Chapter 5

Study of phosphate glasses under IR femtosecond laser irradiation

Chapter 5: Study of phosphate glasses under IR femtosecond laser irradiation

1	Experimental methods	162
2	Glass modifications induced by fs-laser (bibliographic part)	164
2.1	Interaction of femtosecond laser pulses with glass materials	164
2.1.1	Photoionization processes	165
2.1.2	Energy relaxation processes	165
2.2	Generality on silica:	166
3	Phosphate glass structure under fs laser irradiation at low repetition rate (10 kHz)	169
3.1	Alkali Metaphosphate glasses	169
3.1.1	Eu-doped Na metaphosphate glass (4 μ J)	169
3.1.2	Non-doped and Er doped Na metaphosphate glasses:	175
3.2	Eu doped zinc metaphosphate glasses	176
3.3	Polyphosphate glasses	179
3.3.1	Eu-doped Zinc sodium polyphosphate glass (Poly-Na-Eu-4 μ J)	179
3.3.2	Non-doped and Er-doped zinc sodium polyphosphate glasses:	182
4	Phosphate glass structure under fs laser irradiation at high repetition rate (500 kHz)	183
5	Refractive index changes and optical birefringence at low repetition rate	185
5.1	Birefringence:	185
5.2	Refractive index changes	185
5.2.1	Generality:	186
5.2.2	Study of refractive index kinetics in Metaphosphate glasses	188
5.2.3	Study of refractive index kinetics in Zinc Polyphosphate glasses:	189
5.2.4	Correlation between defect centers and refractive index changes	191
6	Rare earth environment under fs laser irradiation at low repetition rate	194
6.1	Rare earth environment under fs laser irradiation (Bibliographic part)	194
6.2	Photo-Emission micro-spectroscopy:	195
6.2.1	Metaphosphate glasses (Meta-Na-Eu and Meta-Zn-Eu)	195
6.2.2	Polyphosphate glasses (Poly-Zn-Na-Eu)	196
6.3	Asymmetry ratio between ${}^5D_0-{}^7F_2$ and ${}^5D_0-{}^7F_1$	197
6.4	${}^5D_0-{}^7F_0$ transition:	198
6.5	Divalent europium:	200

1 Experimental methods

To study phosphates glasses and rare earth (RE) environment evolution in phosphate glasses under irradiation, we used in this thesis chapter a femtosecond fiber laser writing system in collaboration with MAP (Advanced Material for Photonics) group at ICMMO (Institut de Chimie Moléculaire et des Matériaux d'Orsay) from Orsay University. A photo of the dedicated FLAG platform is shown in figure 1.



Figure 1 FLAG laser platform

The femtosecond fiber laser system used for the modifications of our bulk phosphate glasses consists of a directly diode-pumped Ytterbium fiber laser (Satsuma HP from Amplitude Systemes, France), with a central wavelength of 1030 nm. The typical pulse duration is 250 fs and the repetition rate can be adjusted from single pulse up to 2MHz. In this work single lines or set of lines have been inscribed at 300 μm below the surface glass for various pulse energies ranging in 0.01-5 μJ as explained in figure 2. In this view, the sample was moved or scanned along a chosen direction, let's say y-axis, at a constant speed to imprint some lines. In this study the laser polarization was linear and oriented parallel to the written lines.

Then we analyzed the RE environment modifications and the structural modifications by focusing the Raman and PL laser approximatively in the center of the lines inscribed at 300 μm below the surface (as seen in fig. 2). However, we observed no significant variation compared to unmodified glass. We suggested that this method (even in confocal mode) was not accurate enough with a potential integration of the pristine glass part also averaging the observed modification of the Raman and PL spectra. Therefore, we repeated, in a second step, the work in the cross-section configuration (index b fig. 2). In this regards, we analyzed the structure and the RE environment variation in different region of the laser tracks cross-sections.

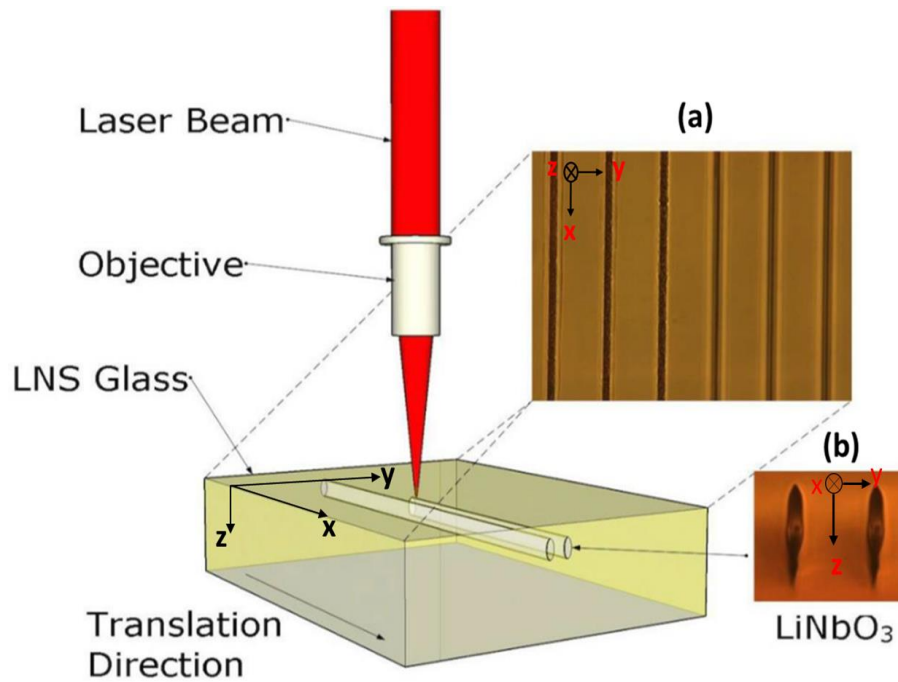


Figure 2 Explanation of the geometry used for "laser lines" writing in the optical materials. In this example the glass was $\text{Li}_2\text{O-Nb}_2\text{O}_5\text{-SiO}_2$.

Two different repetition rates were used in this work:

- a low repetition rate of 10 kHz, which allows to investigate a repetitive regime since the heat generated by the laser pulse has enough time to diffuse out (typ. It needs a few microseconds) before the next pulse resulting in no heat accumulation from pulse to pulse. This regime allows to generate micro-quenching like melting for a few microseconds followed but a quite high quenching rate (typ. up to 10^9 °C/s in oxide glasses)
- a high repetition rate of 500 kHz that leads to a pulse to pulse heat accumulation process. This allows reaching the melting temperature or crystallization for a significant time up to 100'µs depending on the scanning speed and to cool down "slowly" the sample. The key characteristics of laser parameters used in this thesis are summarized in table.

Table 1 Typical data for writing lines by irradiation with the energy of each line.

	Low repetition rate = 10 kHz	High repetition rate = 500 kHz
Scanning speed (mm/s)	0.01	0.1
Numerical aperture	0.6	
Pulse duration (fs)	250	
Wavelength (nm)	1030	
Depth of focus (μm)	300	
Pulse energy (μJ)	0.05-4.5	0.01-1
Line number		
1	4.5	1
2	4	0.8
3	3	0.6
4	2	0.5
5	1	0.4
6	0.5	0.3
7	0.4	0.2
8	0.3	0.1
9	0.2	0.05
10	0.1	0.01
11	4.5	-

2 Glass modifications induced by fs-laser (bibliographic part)

2.1 Interaction of femtosecond laser pulses with glass materials

In order to introduce the interest of femtosecond lasers for the laser-matter interaction, the mechanisms leading to permanent modifications induced by ultrashort irradiation are schematically illustrated on the timescales chart in fig 3. First, we will present the mechanisms of photoionization, responsible for the creation of a plasma of free electrons, then we will see the different relaxation processes contributing to the local modification of the refractive index.

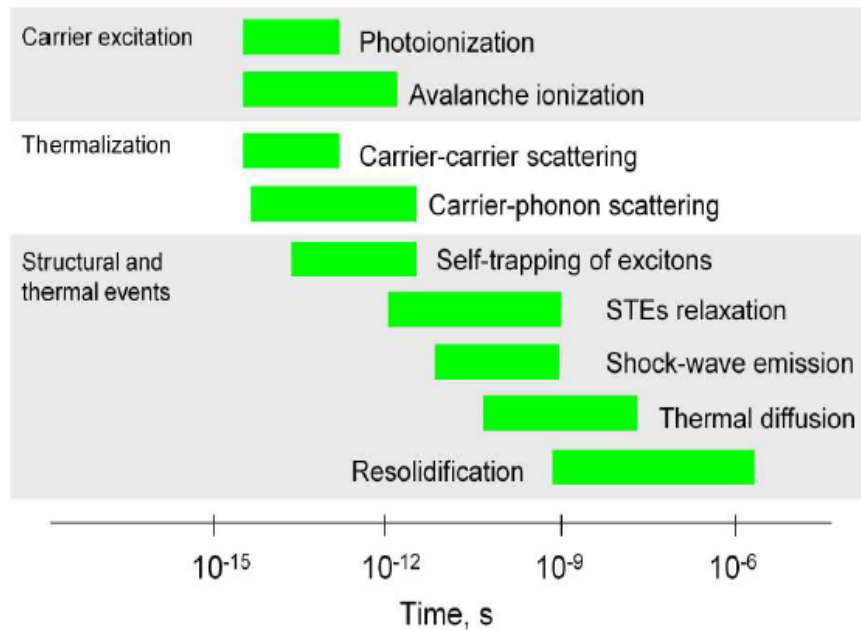


Figure 3 Timescales of the physical phenomena associated with the interaction of a femtosecond laser with glass materials [1]

2.1.1 Photoionization processes

It is well-known that the interaction between the material and visible and near infrared light takes place via the electronic subsystem. In dielectrics electrons are strongly coupled to the ions, resulting in a wide gap appearing between the valence and conduction bands. Since the photon energy is small compared to the material band gap, no linear absorption takes place. This defines the transparency of dielectrics in the considered spectral range. However, the use of focused femtosecond pulses allows reaching laser intensities sufficiently high (around 10 TW/cm^2). This condition allows the creation of nonlinear optical absorption (leading to photoionization processes), leading to generation of free electrons in the conduction band. Thus, the exponential increase of this density causes the creation of an ionized gas: plasma, which can be described according to the assumptions of the Drude model. This model makes it possible to estimate the contribution of this plasma on the dielectric function ϵ and by extension on the changes in optical properties of the material subjected to a pulsed laser.

2.1.2 Energy relaxation processes

The ionization mechanisms are conditioned by the presence of the electric field of the laser and occur accordingly on a time scale comparable to the pulse duration. In this section, we give an overview of the relaxation phenomena (during which the energy of the plasma is transferred to the matrix, after the passage of the pulse) which plays an important role in describing the mechanisms of modification of the material. Note that the different processes involved do not occur sequentially but overlap in time, as shown in figure 3, thus forming a chain of more or less complex events spread over a wide range of time ranging from femtosecond to microsecond for dielectrics.

In general, a solid can be seen as a network of ions surrounded by electrons more or less linked thus defining the insulating or conductive nature of the material. The energy absorbed by the

electrons during the ionization step is transferred to the ion network after the passage of the pulse. During the relaxation process, the free electrons composing the plasma transfer their energy to the matrix ions by non-radiative recombination (emission of phonons which correspond to a quantum of vibration energy). From a more general point of view, the relaxation process can be obtained from the two temperatures model valid for both dielectrics and metals describing the temporal evolution of the temperature of the electronic gas T_e on the one hand and the ionic temperature T_i on the other hand. In the context of an interaction with a femtosecond laser, an electronic heating phase takes place during the passage of the pulse while the network of ions is only slightly disturbed leaving the material in a situation of very strong imbalance ($T_e \gg T_i$). Once the pulse is complete, a process of thermalisation between electrons and ions occurs for which T_i increases until reaching the thermal equilibrium $T_e = T_i$. Energy relaxation and electron-matrix coupling therefore imply local structural changes that can modify the refractive index [2].

2.2 Generality on silica:

Since 1970's, many investigation of the effects of femtosecond laser radiation in various bulk glasses have been completed with the objective of producing new optical devices used in telecommunication, optical sensing and optical signal processing domains [3]. Thus, indeed the fs laser can act in a wide variety of properties including refractive index, absorption properties, non-linear optical susceptibility, structure, morphology with the possibility to write 3D optical circuits in bulk glasses.

In silica, three structural modification regimes are observed (as seen in figure 4): a positive refractive index change (usually denoted as type I), a self-arranged nanoscale layered structures resulting in form of birefringence (type II) and micro-explosion leading to voids (type III) [4]. These structural modifications depend on the regime of laser interaction, particularly on the energetic dose, pulse duration, laser repetition rate and focusing conditions as well as to the properties of materials like viscosity, density, electronic polarizability, absorption coefficient, reflectivity, and thermal conductivity, etc.

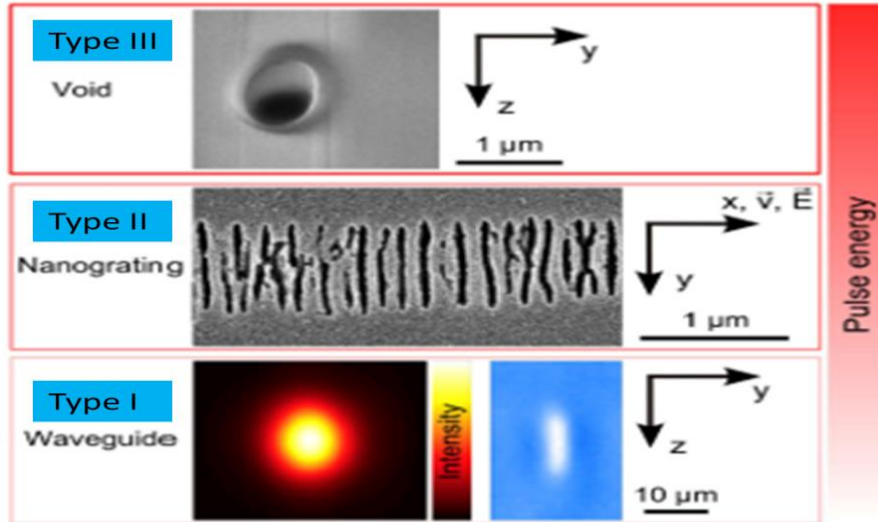


Figure 4 Three structural modification regimes created by femtosecond laser writing in silica

The characteristics of these different regimes and modifications are detailed below.

- **Isotropic index changes based modifications (Type I)**

The first observation of a threshold that we can report under a sufficiently intense irradiation is the reduction of the optical transmission. It is observed over a wide range of wavelengths from infrared to blue [5], [6]. This indicates that the glass is modified in its structure. The corresponding threshold energy is defined by the relation [7] :

$$E_{th} = \frac{I_{th} \Delta t \lambda^2}{\pi (NA)^2 + I_{th} \frac{\lambda^2}{P_{cr}}}$$

Where I_{th} is the intensity; Δt is the pulse duration; λ is the wavelength; NA is the numerical aperture of the focusing lens and P_{cr} is the critical power.

At low energy, an increase (from 10^{-4} up to $3-6 \cdot 10^{-3}$) of the refractive index is observed in the silica. It is attributed to a permanent densification due to a rapid cooling of the initially very hot focal volume [8], [9]. In addition, the focusing of the femtosecond laser pulses gives rise to a constraint that plays a role in this densification under certain conditions [10]. Defects centers (also called color centers) induced by femtosecond laser irradiation may be responsible for a portion of the refractive index change through the Kramers-Kronig relationship (a change in absorption leads to a refractive index change since these two quantities are conjugate complexes of the dielectric constant) [11]. Although color centers induced in femtosecond laser irradiated glasses have been observed [8], [12], there has been no experimental evidence so far of a strong link between their formation and induced index change. Waveguides formed in silica with an infrared femtosecond laser [13] showed photo-induced absorption peaks at 213 nm and 260 nm corresponding to the respective center defects E' and NBOHC. However, the two defects were completely erased after annealing at 400°C, although it retained its guiding properties up to 900°C. As a result, color centers are unlikely to have played a strong role in the refractive index change [13]. Other results lead to the conclusion that the thermal stability of the colour centers produced in borosilicate and

silica glasses is not compatible with that of the change in refractive index [12]. It has recently been shown, in pure silica glasses for the realization of waveguides, that colour centers contribute to the refractive index changes for only 20% [2] whereas the major part has been attributed to defects-assisted densification by the authors.

In an extremely simplistic view of the free electron plasma relaxation created by laser irradiation, it can be said that the transfer of energy from free electrons to the glass network leads to very high local temperature. The temperature can reach several thousand degrees [14] at the focal point limited by thermal conduction [15] (and high pressures), up to the local melting of the glass, inducing densification (or expansion as a function of the relationship between the density and the fictive temperature for example) after the rapid cooling of the glass [16]. This results, for example, in a lower average Si-O-Si angle and thus some changes in some infrared bands (for example, the antisymmetric elongation vibration centered at 1120 cm^{-1}) and a change in the D_1 and D_2 bands observed in Raman spectroscopy [16], [17], D_1 and D_2 being respectively associated with the vibrations of cycles with 4 and 3 tetrahedra. In silica, these structural modifications are correlated with an increase in the refractive index, of the order of a few 10^{-3} in writing conditions close to ours. The hypothesis of local densification of glass as a contribution to the increase of the refractive index was already advanced during the first publications on this subject [3], [11], [12], [15], [18] following atomic force microscopic observation of the depression of the surface by a few tens of nanometers at the level of the irradiated zone.

- **Anisotropic refractive index changes based modifications (Type II)**

For higher energy pulses, a second threshold is observed which is based on the appearance of nanostructures (Fig. 4) caused for example by the interference between the laser field and the electron plasma wave according to the first model that was proposed in 2003 [19].

Y. Shimotsuma and P. Kazansky made this discovery in 2003. It remained to determine the nature of these nanoplanes. Some saw fractures, others oxygen depletions [19]. In 2011 Lancry et al [15] revealed that nanogratings are formed by a decomposition of silica (nanoporous silica formation). This decomposition of silica into porous nanolayers can be done, contrary to the fictive temperature modification, only by a pulse-to-pulse accumulation. As the material cooled down completely between pulses, we initially proposed an accumulation of point defects. We then explain the variations with doping by production of defects that vary greatly. This production is favored by the addition of germanium or conversely, it can be inhibited to observe only isotropic index change by adding fluorine in silica, which provide interesting results depending on the type of application envisaged.

- **Voids (Type III)**

For even higher energy pulses giving rise to peak intensities greater than 10^{14} W/cm^2 , holes in volume (so-called voids) are achievable by femtosecond laser irradiation. They are at the origin of a mechanism called the Coulomb micro-explosion. A first model was proposed by Fleischer's team [20] and also reported later by Schaffer [21]. The mechanism at the base of void formation was briefly the following: when the density of excitations at a point in the material is very large, the Coulombian force between ions can overcome their binding energy. In this case, ions are also moved to interstitial positions around the starting point. This results

in cavity formation surrounded by a high-density shell. The mechanism was then revisited as follows: the energy is absorbed in a small volume producing a pressure which subsequently drives a shock wave and stress exceeding the Young modulus of the material. The strong spherical shock wave starts to propagate outside the center of symmetry of the absorbed energy region compressing the material. At the same time, a rarefaction wave propagates to the center of symmetry decreasing the density in the area of the energy deposition. The shock wave stops when the pressure behind the shock front becomes comparable with the Young modulus. Such voids can be exploited for 3D storage of information[22].

3 Phosphate glass structure under fs laser irradiation at low repetition rate (10 kHz)

We studied in this part the structural modifications in phosphate glasses under femtosecond laser writing with low repetition rate of 10 kHz that is a non-cumulative heating regime. Thus, we analyzed the structure variation in different region of the laser trace cross-section.

3.1 Alkali Metaphosphate glasses

3.1.1 Eu-doped Na metaphosphate glass

Figure 5a exhibits the white light optical microscope images of the lines written by fs laser with different pulse energy ranging from 0.05 μJ to 5 μJ . The laser parameters were fixed as follow: 1030 nm, 250 fs, 10 kHz, 10 $\mu\text{m/s}$, linear polarization. The parallel lines are inscribed at 300 μm below the surface of Eu doped sodium metaphosphate glass using a 0.6 NA aspheric lens. The written lines present different optical contrast in transmission and width linked to the increasing pulse energy. We note that permanent modifications appear from pulse energy of 0.5 μJ as observed in figure 5a.

Figure 5b displayed the cross-section of the irradiated lines. Thus, as noted before, when we look at the cross-section of the laser lines, we should see that the modified area has the shape of a kind of drop mostly due to the focusing conditions. The drop is better confirmed at low pulse energy ($E = 0.5 \mu\text{J}$) and its length (the laser trace along z-direction) expanded with increasing pulse energy from 20 μm at $E = 0.5 \mu\text{J}$ to around 100 μm at energy of 4.5 μJ (Figure 6). Even more, white trace is observed at low pulse energy ($E = 0.5, 1 \mu\text{J}$) then voids and bubbles appear along the “waveguide” cross-section at higher energy from 2 μJ . We also note that the width (typ. 1-5 microns) of the laser trace in the cross-section are in the same order than the laser spot confirming the non-cumulative heating regime.

As displayed in figure 5c, the drop of the laser trace can be divided in 3 different zones:

- The tip
- The spot center with dark zone (negative refractive index variation)
- The tail with white zone (with a positive refractive index variation)

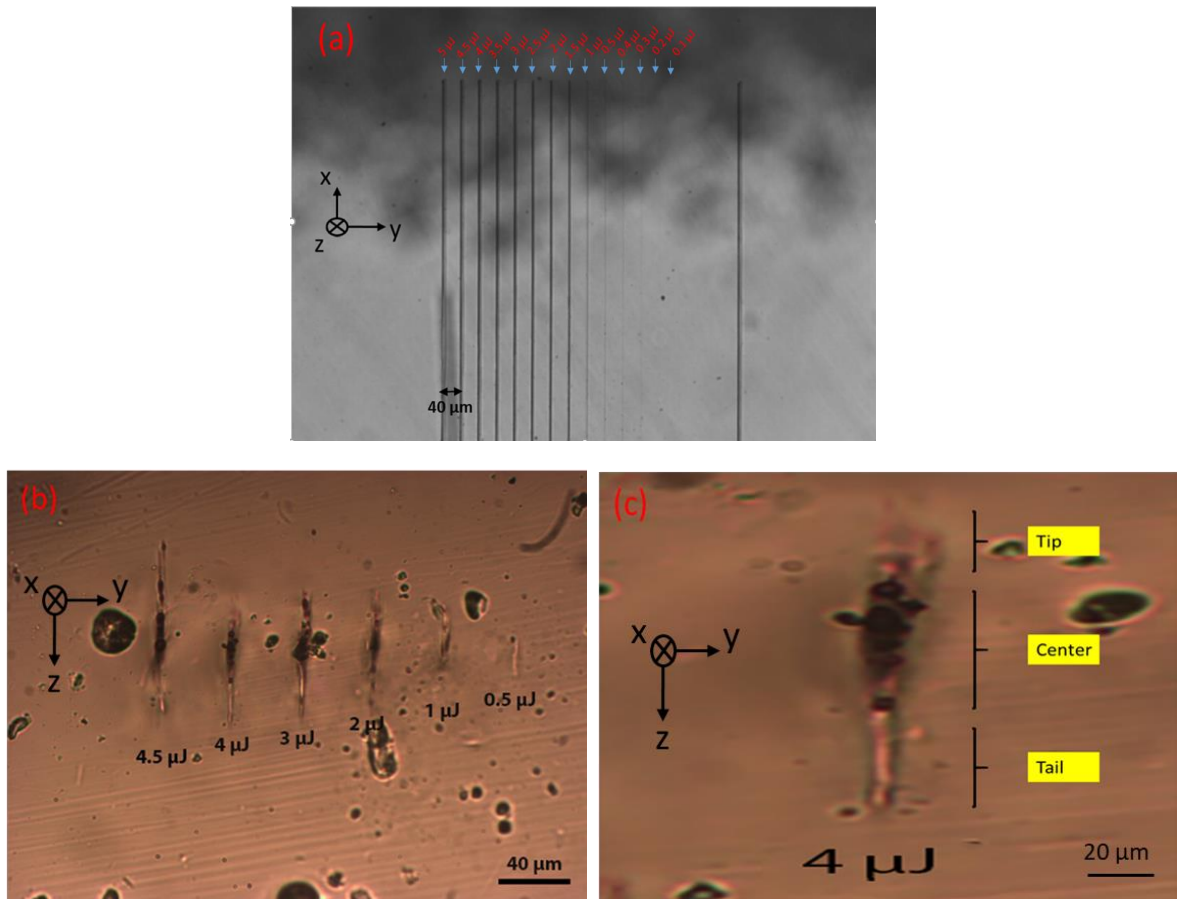


Figure 5 (a) White light microscopic image of lines written by femtosecond laser with repetition rate of 10 kHz and different pulse energies inside Meta-Na-Eu glass at 300 μm below the surface through a 10× objective, (b) Microscopic image of a series of lines along the z axis (cross-section of the laser spot) inscribed by pulse energy ranging in 5-0.5 μJ through 20× objective (c) Zoom of the profile of the line inscribe by 4 μJ pulse energy along the z axis.

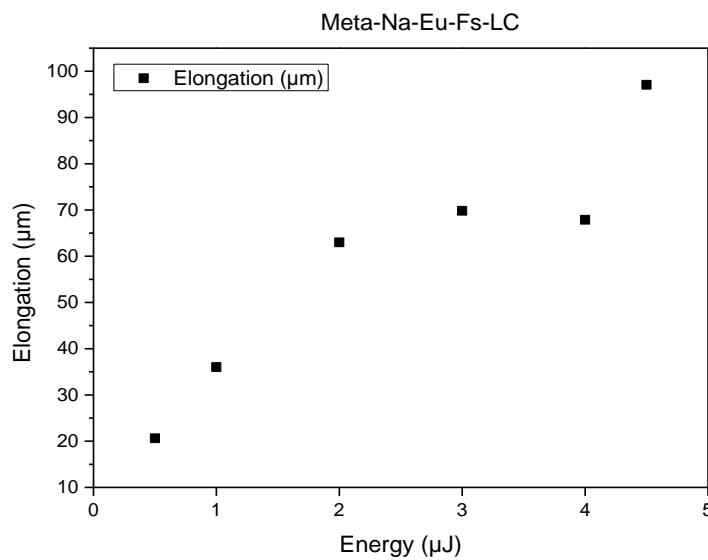


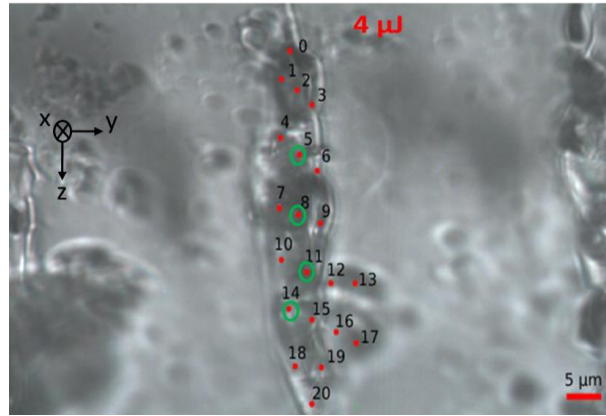
Figure 6 The longitudinal laser spot elongation (in the laser propagation direction) as a function of pulse energy in Meta-Na-Eu glass.

3.1.1.1 Center and tip of the transversal laser trace

Figure 7a presents the microscopic image of the transversal laser line irradiated with 4 μJ pulse energy in Meta-Na-Eu glass through a 100 \times objective. In this connection, figure 7b displays the Raman cartography of the different positions in the center and the tip of the laser trace cross-section as indicated by the red dots in the microscopic image.

The dots circled in green (fig 8a) undergo a drastic variation in the Raman spectra. Therefore, we note that the center of the laser trace suffers an important modification of the Na metaphosphate glass structure compared to unmodified region as described below:

- Thus, Raman spectra exhibited an increase of the intensity in the region 300-500 cm^{-1} correspond to the bending vibration $\delta(\text{P-O})$. Further, we note two new peaks at 725 and 740 cm^{-1} that are likely due to a beginning of crystallization.
- As well, a new band occurs at around 890 cm^{-1} due to the asymmetric stretching mode $\nu_{\text{as}}(\text{POP})$ of Q^2 units [23], [24].
- Regarding to the region 900-1400 cm^{-1} , fs laser irradiation affects an important increase in the intensity of the band at 1016 cm^{-1} attributed to the P-O stretch of Q^1 chain terminator [25].
- Further, an additional contribution of the band at around 1106 cm^{-1} due to the asymmetric stretching mode $\nu_{\text{as}}(\text{PO}_3^{2-})$ of the Q^1 units. This drastic change in the green circle regions suggests an important decrease in the network polymerization of the laser spot center in europium doped sodium metaphosphate glass whereas, there is no clear change of the structure in the tip and the contrast of the laser trace.
- Even more, the huge band at 1166 cm^{-1} due to the symmetric stretching modes of NBO $\nu_{\text{s}}(\text{PO}_2)$ in Q^2 units [23], [24], [26], [27] displays a shift of about 6 cm^{-1} towards lower wavenumber in the center of laser trace cross-section suggesting an increase of the O-P-O angle and/or variation in the local cationic environment. Rouse et al. [28] indicated that as the $\nu_{\text{s}}(\text{PO}_2)$ decrease in the frequency as phosphate chains length is longer, indicative of the increase in the average PO2 bond angle.



Meta-Na-Eu-Raman-LC-carto-4 μJ

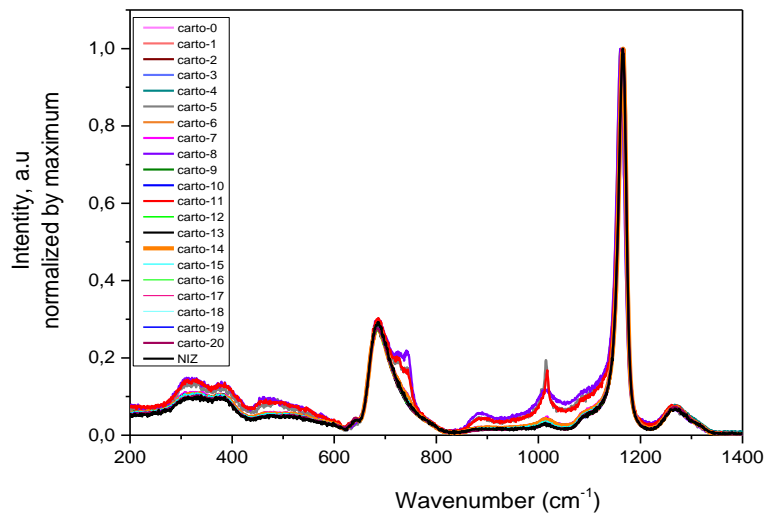
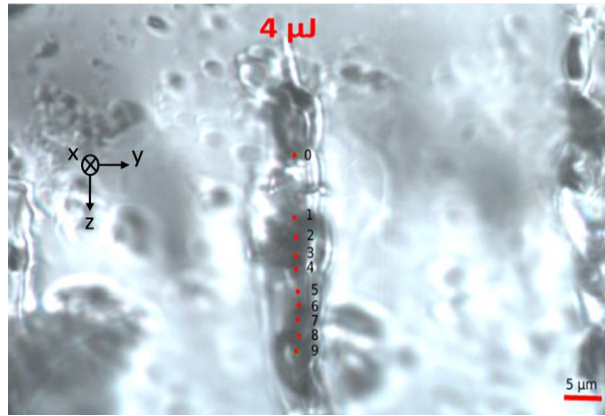


Figure 9 (a) Microscopic image of **the center and the tip** of the laser line cross-section irradiated at 4 μJ pulse energy in **Meta-Na-Eu** glass through a 100 \times objective. The red dots positions associated to the Raman cartography. (b) The Raman cartography of the different red dots positions in the center and the tip of the transversal laser trace.

3.1.1.2 Black region in the center of the transversal laser trace

To better understand the structure variation, we have recorded the Raman spectrum cartography in a series of points in the transversal center line characterized by a black region as indicated by the microscopic image (Figure 8a). The Raman spectra (figure 8b) confirmed the previous results that the glass suffers a drastic variation in the structure after fs laser irradiation in the center spot laser.



Meta-Na-Eu-Raman-LC-carto-4 μJ

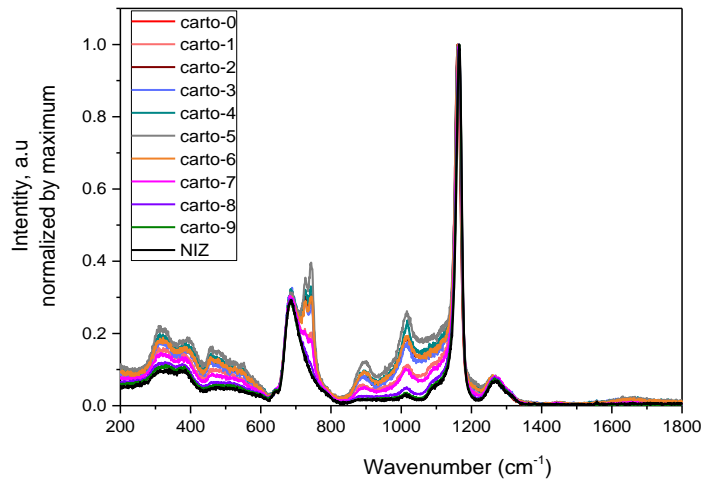
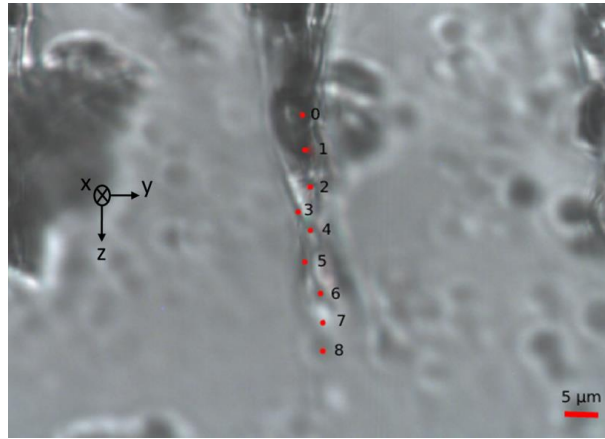


Figure 8 (a) Microscopic image of the **center** of the cross-section laser line irradiated at $4 \mu\text{J}$ pulse energy in Meta-Na-Eu glass through a $100\times$ objective which the red dots positions associated to the Raman cartography. (b) The Raman cartography of **the black region in the center** of the transversal laser trace as shown by the red dots in the microscopic image.

3.1.1.3 Tail of the transversal laser trace

Now, let's look at the structure change in the tail region. The Raman cartography displayed in figure 9 illustrates the structure of the different red dots positions in the tail of the laser line cross section inscribed by $4 \mu\text{J}$ pulse energy in Meta-Na-Eu glass. Thus, we observe a lower change in the structure in the white region of the tail as seen in the microscopic image (fig 10a).



Meta-Na-Eu-LC-Tail-4 μJ

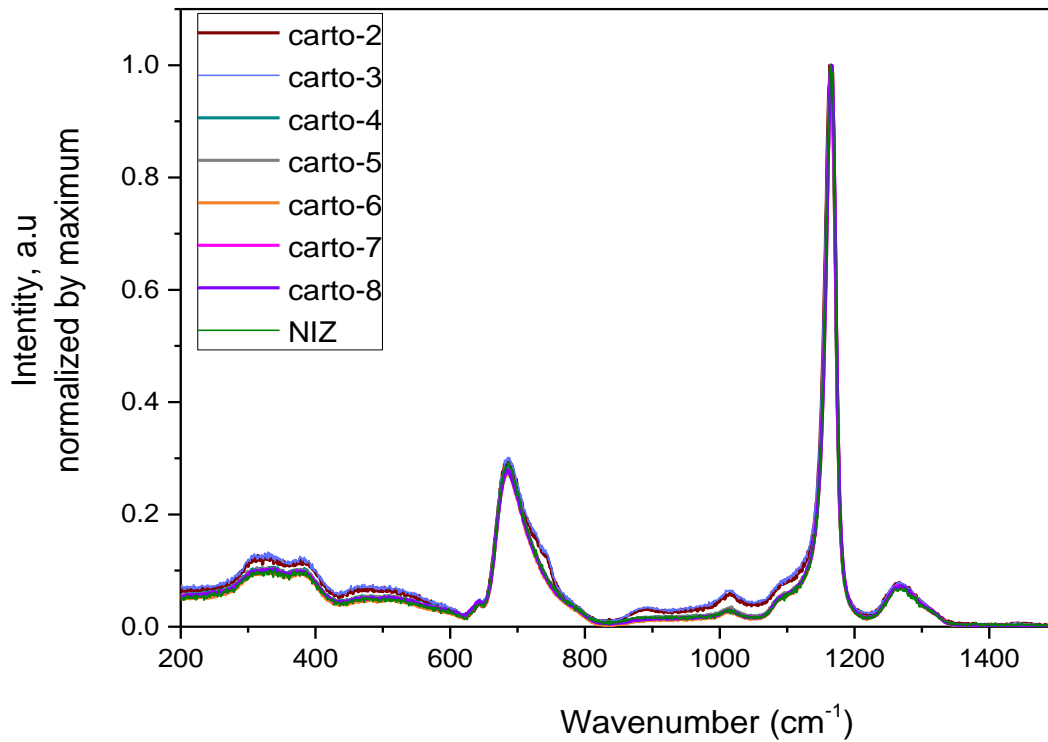


Figure 9 (a) Microscopic image of **the tail** of the cross-section laser line irradiated at 4 μJ pulse energy in Meta-Na-Eu glass through a 100× objective which the red dots positions associated to the Raman cartography. (b) The Raman cartography of the red dots positions in the tail of the transversal laser trace compared to unmodified region.

3.1.1.4 Pulse energy effect

Figures 10a and 10b exhibit the Raman spectra of the center of the transversal laser spot in Meta-Na-Eu glass irradiated at respectively 3 μJ and 1 μJ compared to pristine glass. We observe the same behavior as under 4μJ pulse and this result confirm the drastic change of

the structure in the center of the transversal laser spot whatever the pulse energy in the 1 μ J-4 μ J range. On the other hand, for low pulse energy, 0.5 μ J (not shown), we did not observe any change in the Raman spectra compared to pristine glass whereas we can observe some refractive index changes by optical microscopy.

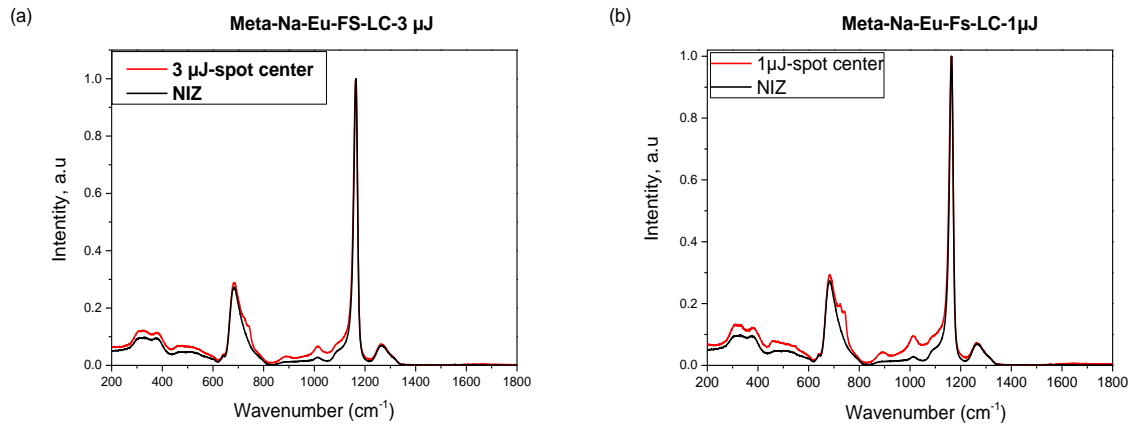


Figure 10 Raman spectra of the center of the cross-section laser line in Meta-Na-Eu inscribed by pulse energy of (a) 3 μ J and (b) 1 μ J compared to pristine glass

3.1.2 Non-doped and Er doped Na metaphosphate glasses:

We performed the same analysis for non-doped and Er doped metaphosphate glasses (fig. 11 and 12). Raman spectra showed no significant structure change in the Meta-Na under fs laser with pulse energy of 4 μ J (fig. 11b). On the contrary, we observed a slight change of the Raman spectra in Er doped metaphosphate under pulse energy of 3 μ J (fig. 12b). The choice of 3 μ J is due to the fact that the laser trace cross-section with pulse energy of 4 μ J presented a crack and white zone in the center. We observe the formation of a small shoulder at 740 cm^{-1} . Further, a more contribution of the bands at 1016 cm^{-1} and 1106 cm^{-1} are observed attributed respectively to the symmetric and asymmetric $\nu_s(\text{PO}_3^{2-})$ and $\nu_{as}(\text{PO}_3^{2-})$ of the end group of Q^1 unit measuring more Q^1 species.

These results suggest no significant change of the structure in Meta-Na glass, a tendency for a slight decrease in the network polymerization in Meta-Na-Er and a drastic variation in the vitreous network of Meta-Na-Eu glass. As a first suggestions, the rare earth (RE) ions play a central role in the change of the structure under fs laser irradiation in metaphosphate glass and in particular the Eu-doped metaphosphate glass undergoes the important decrease in network polymerization compared to Er-doped glasses. We have to underline that Meta-Na-Eu glass remains stable under electron irradiation and there is no significant change in the vitreous network whatever the dose (chapter 4) identically to meta Na glass.

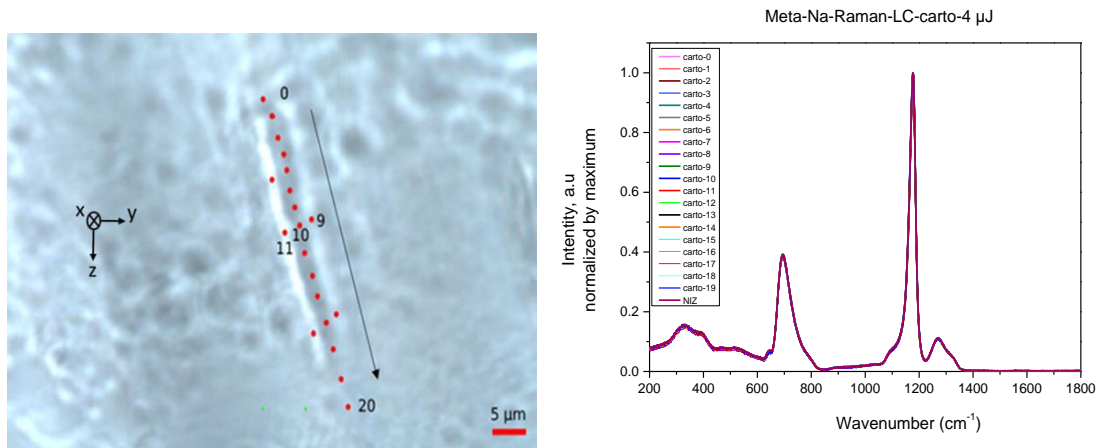


Figure 11 (a) Microscopic image of the cross-section laser line irradiated at $4 \mu\text{J}$ pulse energy in **Meta-Na glass** through a $100\times$ objective. The red dots positions associated to the Raman cartography. (b) The Raman cartography of all-region of the transversal laser trace as shown by the red dots in the microscopic image compared to unmodified region.

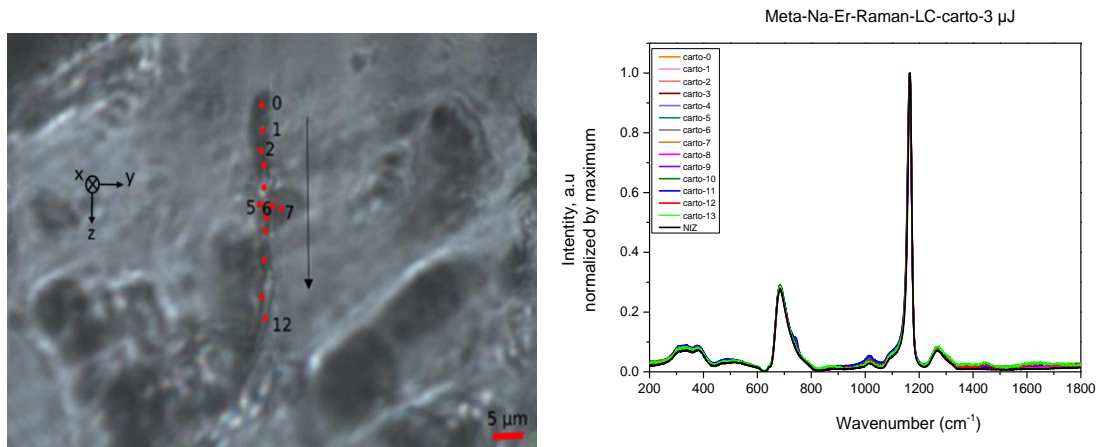


Figure 12 (a) Microscopic image of the cross-section laser line irradiated at $3 \mu\text{J}$ pulse energy in **Meta-Na-Er glass** through a $100\times$ objective. The red dots positions associated to the Raman cartography. (b) The Raman cartography of all-region of the transversal laser trace as shown by the red dots in the microscopic image compared to the unmodified region.

3.2 Eu doped zinc metaphosphate glasses

Figure 13 displays the microscopic image of the transversal laser lines inscribed with various pulse energies in Meta-Zn-Eu glass which presents a much wider traces compared to as shown in Na metaphosphate glasses. Thus, the Raman cartography (associated to red points of Fig. 14a) presented in figure 14b showed that the center under fs laser irradiation with pulse energy of $4 \mu\text{J}$ undergoes a radical structural change. The occurrence of different thin peaks in the $300\text{-}1400 \text{ cm}^{-1}$ range suggests a crystallization in the center of the irradiated region. On the other side, the red dots circled in green provided no change in the Raman spectra compared to the unmodified zone. It confirmed that the structural changes appear in the center of the line only. In this regards, we remind that a remarkable change of the Raman

spectra was observed in Meta-Zn-Eu glass under electron irradiation from integrated dose of 10^8 Gy demonstrating an increase of the P-O-P bond angle, variation in the cationic environment as well a growth of the disorder. However, we did not detect any crystallization and this variation remain lower compared to what is observed under fs laser writing.

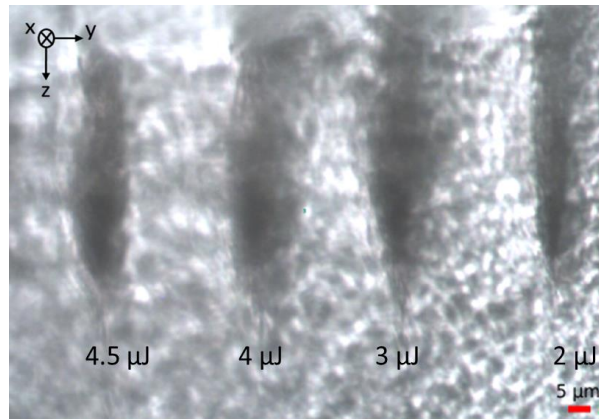


Figure 13 Microscopic image of a series of lines along the z axis (cross-section of the laser spot) inscribed at various pulse energy ranging through 50× objective in **Meta-Zn-Eu** glass.

Center of the transversal laser trace (pulse energy of 4 μJ)

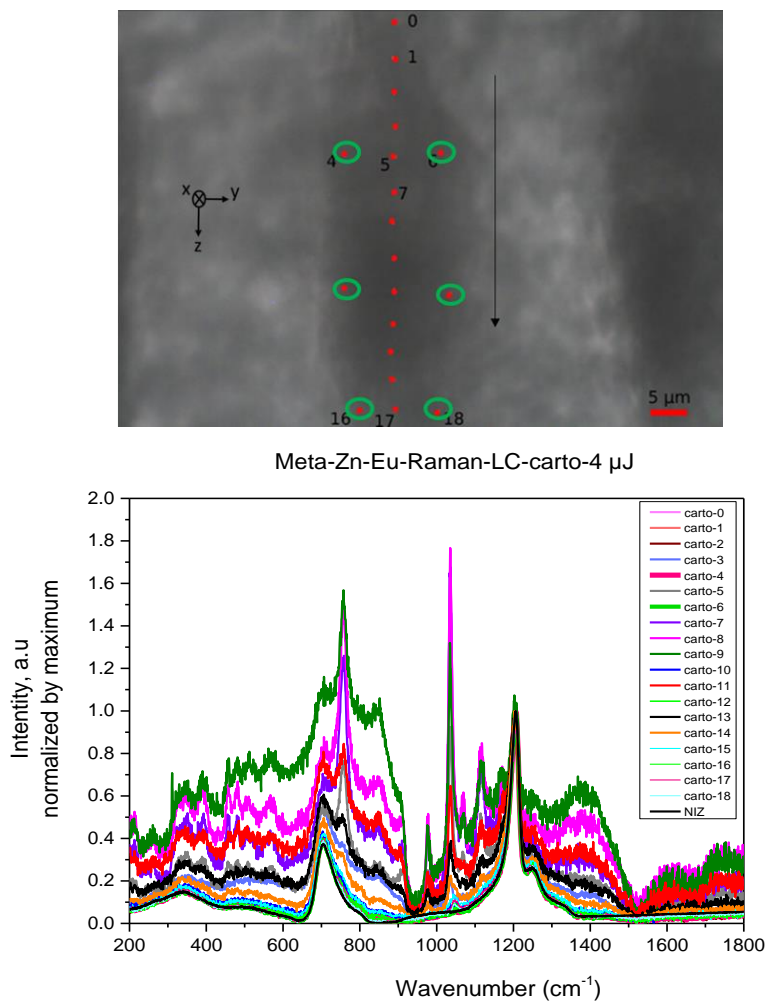


Figure 14 (a) Microscopic image of the cross-section laser line irradiated at 4 μJ pulse energy in **Meta-Zn-Eu glass** through a 100 \times objective. The red dots positions associated to the Raman cartography. (b) The Raman cartography of **the center** of the transversal laser trace as shown by the red dots in the microscopic image compared to the unmodified region.

Figure 15 displays the microscopic image and the Raman cartography of the tail in the laser line cross-section irradiated at 4 μJ pulse energy in Meta-Zn-Eu glass. As for Meta-Na-Eu sample, the tail sustains a lower structural variation compared to as shown in the center.

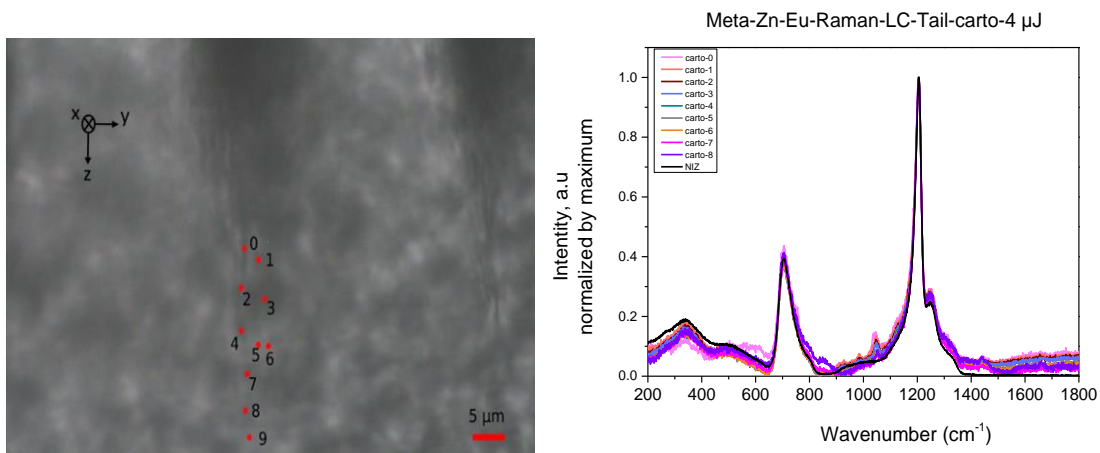


Figure 15 (a) Microscopic image of the cross-section laser line irradiated at $4 \mu\text{J}$ pulse energy in **Meta-Zn-Eu glass** through a $100\times$ objective. The red dots positions associated to the Raman cartography. (b) The Raman cartography of **the tail** of the transversal laser trace as shown by the red dots in the microscopic image compared to the unmodified region.

These results demonstrate an important decrease of the network polymerization in the center of laser line cross section with beginning of crystallization and more precisely in the black region of the center in Meta-Na-Eu glass for laser E pulse $\geq 1\mu\text{J}$. Whereas, there is no significant change of the Raman spectra in the tip, the tail and the contrast and the structure remain stable in these zones. A strong crystallization of the Zn-Eu metaphosphate glass is obtained for $E > 0.5 \mu\text{J}$. On the contrary, non doped metaphosphate glasses or Er doped Nametaphosphate glass show a stability of their glassy network

3.3 Polyphosphate glasses

3.3.1 Eu-doped Zinc sodium polyphosphate glass (Poly-Na-Eu- $4\mu\text{J}$)

Figure (16a) displays the microscopic image of the laser lines cross section inscribed with 10 kHz repetition rate at $300 \mu\text{m}$ under the surface of Poly-Zn-Na-Eu glass. The lines are produced by different energy pulse (4.5 to $0.05 \mu\text{J}$) and are distant of $40 \mu\text{m}$ from each other as described before. Figure (16b) exhibit the zoom of the laser lines cross section inscribed at $2 \mu\text{J}$ that the laser spot behaves very well like a drop and we clearly distinguished three zones:

- The tip with white zone
- The spot center characterized by a black region. This zone suffer a negative refractive index change.
- The tail with white zone, which likely refers to a positive refractive index change.

As observed for metaphosphate composition, the laser spot elongation increase with increasing pulse energy from $20 \mu\text{m}$ at $1\mu\text{J}$ energy to around $65 \mu\text{m}$ at $4 \mu\text{J}$ pulse energy (Fig. 17).

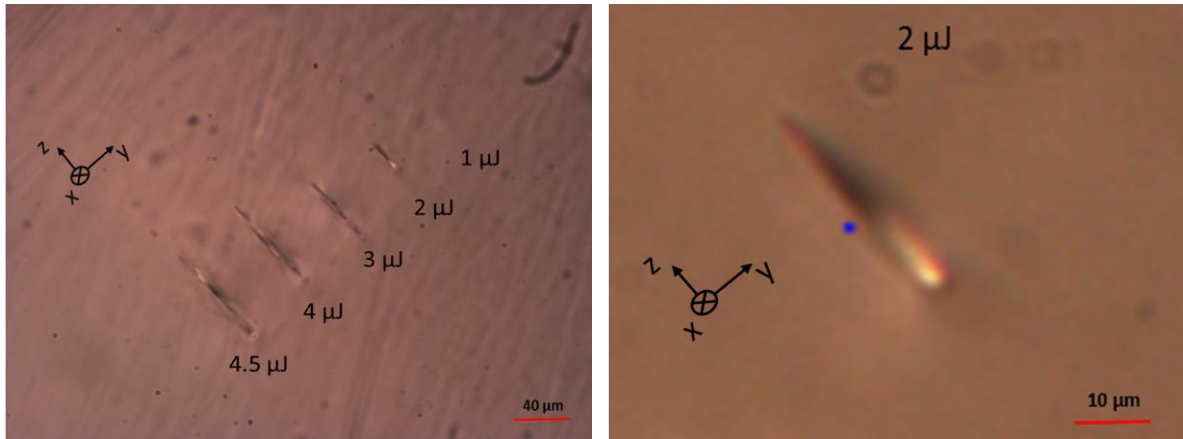


Figure 16 (a) Microscopic image of the laser lines cross section written with repetition rate of 10 kHz and different pulse energies at 300 μm below the surface of Poly-Zn-Na-Eu glass through a 10 \times objective (b) A zoom of the microscopic image of the laser trace cross section inscribed at 2 μJ pulse energy in Poly-Zn-Na-Eu.

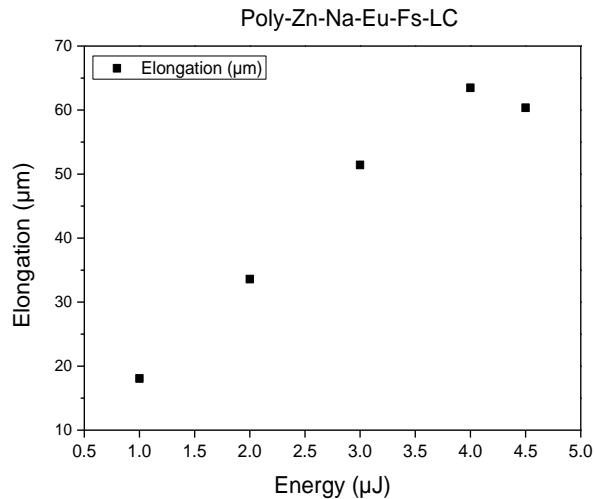


Figure 17 The longitudinal laser spot elongation (along the laser propagation direction) as a function of pulse energy in Poly-Zn-Na-Eu glass.

3.3.1.1 Center of the transversal laser trace

Figure 18 displayed the microscopic image as well as the associated Raman cartography in the center (red dots) of the laser traces cross sections produced at pulse energy of 4 μJ in Poly-Zn-Na-Eu glass. Therefore, when we examined the Raman spectra in the center compared to unmodified region, a slight structure variation is detected with a similar behavior as observed under electron irradiation. The shoulder at 708 cm^{-1} is attributed to the symmetric stretching of bridging oxygen $\nu_s(\text{P-O-P})$ in Q^2 units. Further, in the 900-1400 cm^{-1} range we observe additional contributions at around 915 cm^{-1} and 1009 cm^{-1} . The bond at 915 cm^{-1} due to symmetric stretching modes $\nu_s(\text{PO}_4)$ of Q^0 species [25].

As well, Brow et al. [25] assigned the band at near 1008 cm^{-1} to the P-O stretch of Q^1 chain terminator. As well, the increase in the intensity at 1125 cm^{-1} attributed to the P-O stretching of Q^1 chain terminator. These results suggested bond breaking with the creation of Q^1

terminators in Poly-Zn-Na-Eu glass under fs laser irradiation at low repetition rate. We note a similar structural change in polyphosphate samples as under electron irradiation but with a lower efficiency of fs laser compared to electrons. As well, we mention no structural change at low pulse energy until $1 \mu\text{J}$ whereas a similar compoment in the Raman spectra evolution are observed for higher pulse energy from $2 \mu\text{J}$.

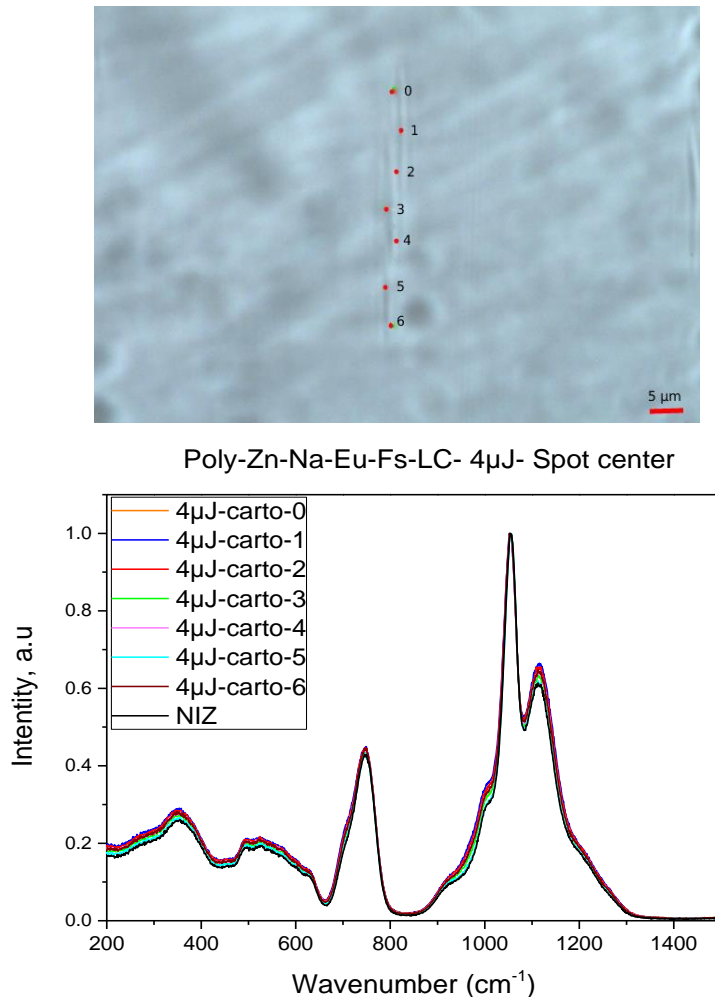


Figure 18 (a) Microscopic image of **the center and the tip** of the cross-section laser line irradiated at $4 \mu\text{J}$ pulse energy in **Poly-Zn-Na-Eu** glass through a $100\times$ objective. The red dots positions associated to the Raman cartography. (b) The Raman cartography of **the center** in the transversal laser trace as shown by the red dots in the microscopic image compared to the unmodified region.

3.3.1.2 Tail of the transversal laser trace

On the other hand, we examined the structure evolution in the tail region. The Raman cartography associated to the red points positions in the microscopic image (fig 19) showed a slight structure evolution in the red points circled in green, which belong the intermediate zone between the tail and the center whereas it remains stable in the other region of the tail. These results confirmed the previous results obtained for metaphosphate composition that there is no measurable change of the vibrational structure in the tail characterized by a white

light zone and may be a positive refractive index change. So, it is interesting to associate the structural change with the negative refractive index change.

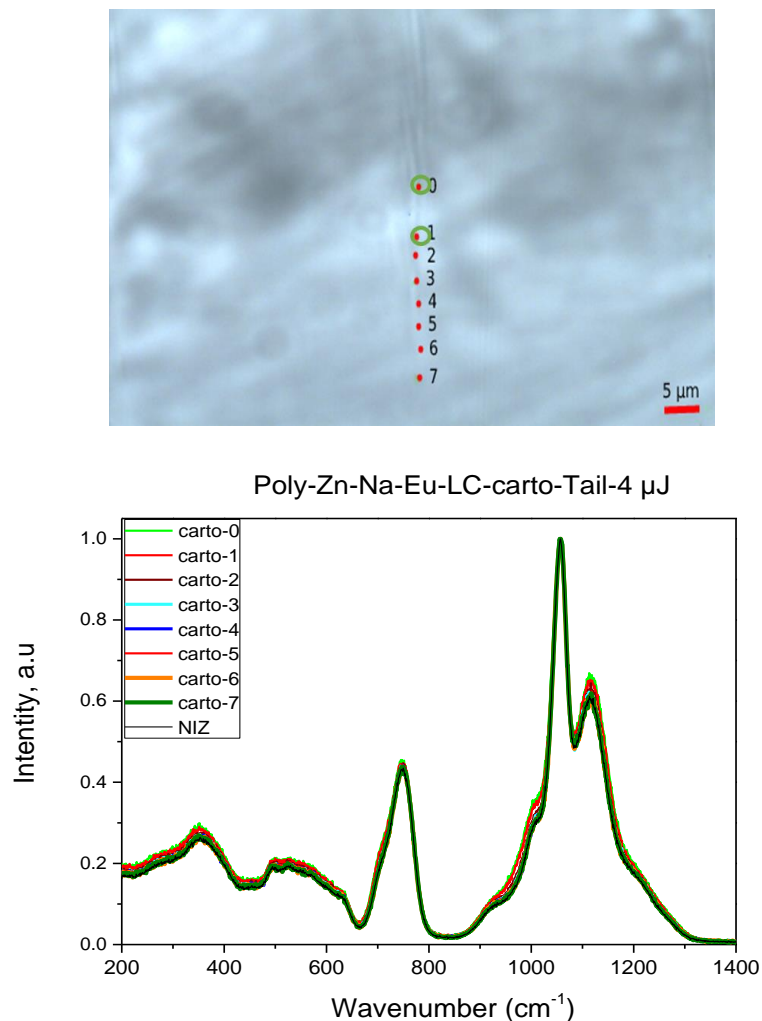


Figure 19 (a) Microscopic image of **the tail** of the cross-section laser line irradiated at $4 \mu\text{J}$ pulse energy in **Poly-Zn-Na-Eu** glass through a $100\times$ objective. The red dots positions associated to the Raman cartography. (b) The Raman cartography of **the tail** of the transversal laser trace as shown by the red dots in the microscopic image compared to the unmodified region.

3.3.2 Non-doped and Er-doped zinc sodium polyphosphate glasses:

Figure 20 and 21 present the microscopic image and the Raman cartography along the laser trace cross section in successively Poly-Zn-Na and Poly-Zn-Na-Er glasses irradiated by fs laser with $4 \mu\text{J}$ pulse energy. We observe the same behavior in the Raman spectra evolution as for Eu-doped polyphosphate glasses for both glasses. It means that there is no obviously rare earth ions doping effect on the structure evolution under fs laser irradiation contrary to what was found for metaphosphate samples. This result can be explained by the fact that the incorporation of Eu ion in polyphosphate network which is depolymerized may affect less the glass structure than in metaphosphate.

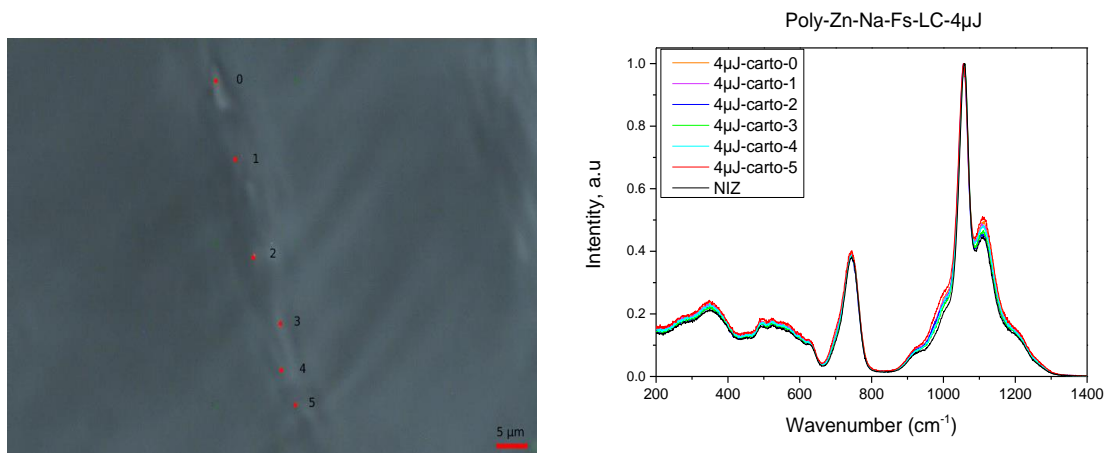


Figure 20 (a) Microscopic image of the cross-section laser line irradiated at $4 \mu\text{J}$ pulse energy in **Poly-Zn-Na glass** through a $100\times$ objective. The red dots positions associated to the Raman cartography. (b) The Raman cartography of all-region of the transversal laser trace as shown by the red dots in the microscopic image compared to unmodified region.

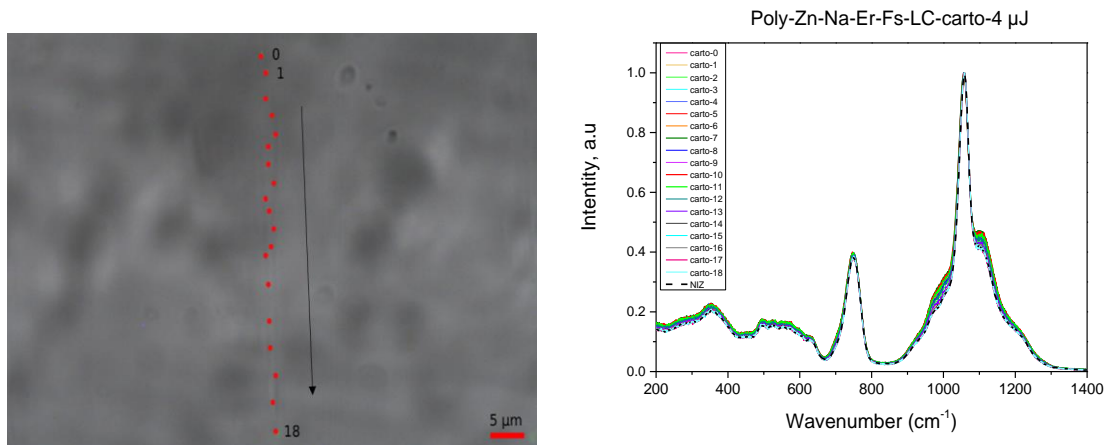
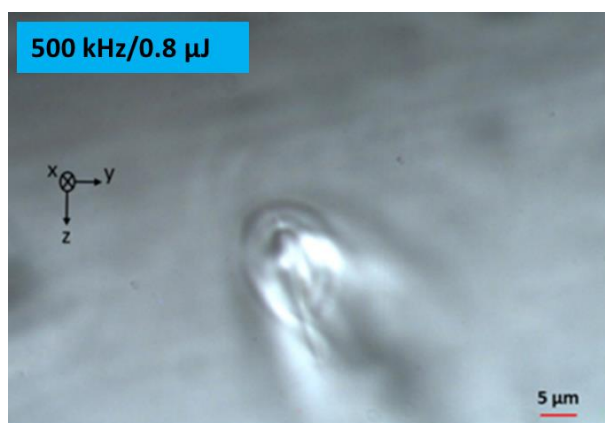


Figure 21 (a) Microscopic image of the cross-section laser line irradiated at $4 \mu\text{J}$ pulse energy in **Poly-Zn-Na-Er glass** through a $100\times$ objective. The red dots positions associated to the Raman cartography. (b) The Raman cartography of all-region of the transversal laser trace as shown by the red dots in the microscopic image compared to unmodified region.

4 Phosphate glass structure under fs laser irradiation at high repetition rate (500 kHz)

Unfortunately, the lines written at high repetition rate (500 kHz) were not visible enough in metaphosphate so the results given in this part concern only polyphosphate glasses. Only traces in polyphosphate glasses at energies of 1, 0.8 and $0.6 \mu\text{J}$ could be analyzed by Raman spectroscopy.

An example of the microscopic image as well as the associated Raman cartography in the transversal laser trace produced under high repetition rate of 500 kHz and pulse energy of $0.8 \mu\text{J}$ in Poly-Zn-Na glass was displayed in figure 22.



Poly-Zn-Na-Fs-500 kHz-0.8μJ

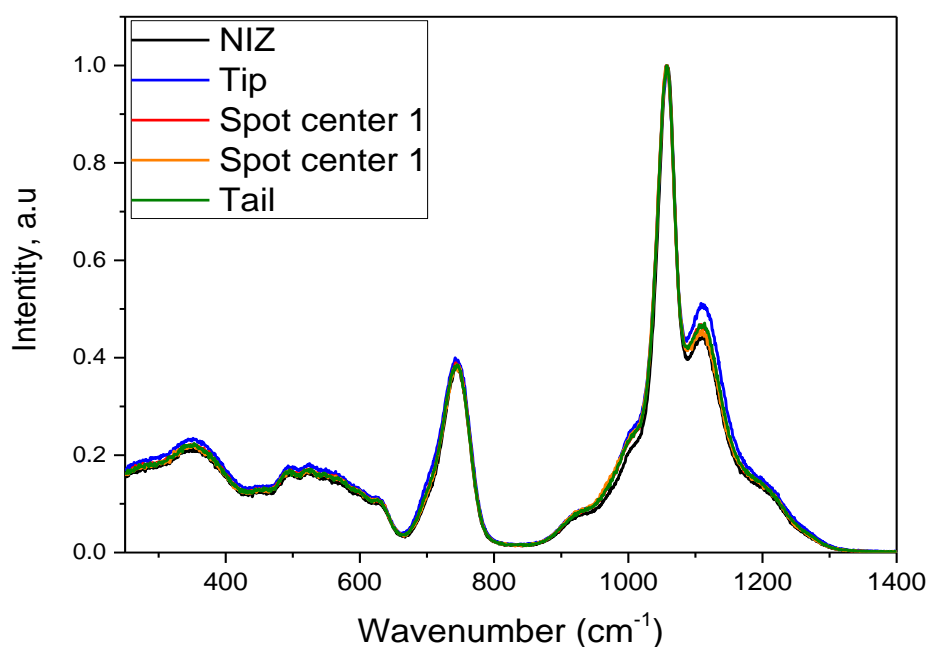


Figure 22 (a) Microscopic image of the cross-section laser trace irradiated at **high repetition rate (500 kHz)** and $0.8 \mu\text{J}$ pulse energy in Poly-Zn-Na glass through a $100\times$ objective. The red dots positions associated to the Raman cartography. (b) The Raman cartography of the different position of the transversal laser trace in the tip, the spot center and the tail.

We derive from these analyzes that in heat accumulation regime, the effects are comparable and of the same order of magnitude with those obtained at low repetition rate (10 kHz) for Poly-Zn-Na and Poly-Zn-Na-Eu glasses, ie an increase in the number of Q^1 terminals. On the other hand, Poly-Zn-Na-K-Eu glass is more stable at 500 kHz than at 10 kHz. A migration of the glass elements in this regime is expected. It was shown in particular that single valent ions like (Na^+ , K^+ ...) could migrate in the opposition direction than multivalent element such as Zn^{2+} . It is thus a bit surprising to observe similar modifications of the Raman spectra with 500 kHz and 10 kHz.

5 Refractive index changes and optical birefringence at low repetition rate

5.1 Birefringence:

We used in this part the polarized microscopy to determine qualitatively the birefringence of the transversal section of irradiated lines. As example, figure 23 displayed the image of irradiated lines cross section in Poly-Zn-Na-Eu glass taken in the diagonal position between two crossed polarizers. As a result, we report a slight birefringence in some parts of the trace, presumably due to constraints in RE doped and non-doped alkali metaphosphate glasses (Na and NaLi). In contrast, zinc phosphate glasses undergoes a significant laser-induced birefringence and a strong scattering wavy patterns obtained mostly in the tip of the transversal laser traces at high pulse energy from 2 μJ (as seen in figure 23b). Note that the non-irradiated area is isotropic i.e. totally dark between crossed polarizers.

This strong birefringence is the signature of a strong change in the specific volume of the glass (for example expansion): a permanent tension which is accompanied by an elastic response in and of the laser tracks leading to the formation of a stress field and thus stress-induced birefringence.

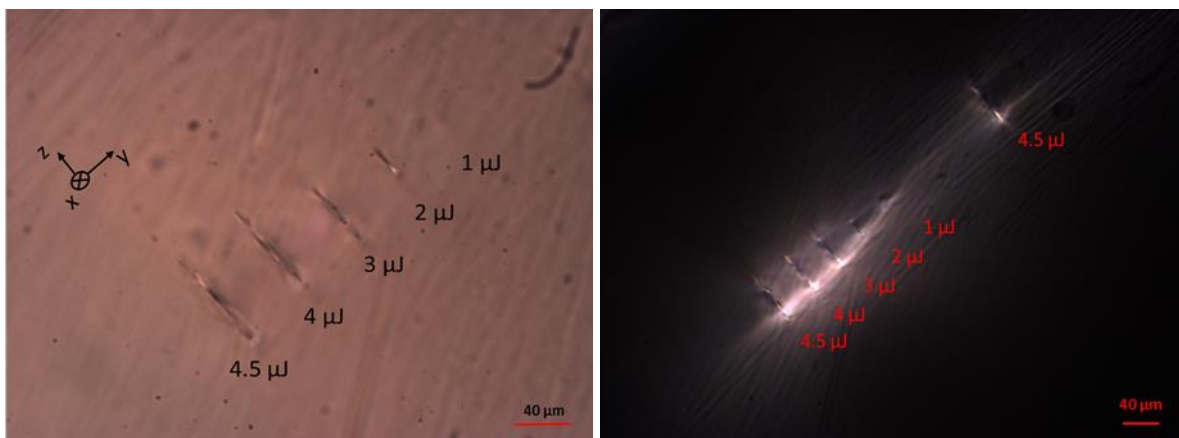


Figure 23 Image of the cross section irradiated lines in Poly-Zn-Na-Eu taken (a) without and (b) with polarizers (diagonal position with respect to the polarizers). Distance between each line is 40 μm , pulse energy ranging in 4.5-0.5 μJ .

5.2 Refractive index changes

In this part, we studied the refractive index changes after fs laser irradiation with low repetition rate of 10 kHz and various pulse energy. The investigated samples are both RE doped and non-doped (for sake of comparison) phosphates glasses, which can be subdivided in two categories, namely meta and polyphosphate glasses. We note that the measurement are made directly in the lines (xy plan) inscribed by the fs laser below the surface in contrast to the Raman and luminescence studies where we did the experiments in the laser line cross

section (xz plan) so unfortunately we cannot directly compare the results obtained on the refractive index with those by Raman spectroscopy.

5.2.1 Generality:

The quantitative phase measurement (QPM) in ICMMO was used to determine the phase-shift $\Delta\phi$ expressed in radians. There is relation of proportionality between the phase shift $\Delta\phi$ and the refractive index change Δn , which is explained in the following relation:

$$\Delta n = \frac{\Delta\phi \times \lambda}{2\pi d}$$

With λ is the wavelength used for the measurement (546 nm) and d is the transversal laser spot elongation or more accurately the thickness of the written laser track. So if $\Delta\phi > 0$ then the average $\Delta n > 0$. In this framework, we can thus investigate the Δn behavior with the sign and the amplitude of $\Delta\phi$ according the pulse energy and the glass chemical composition. This experiment contains a dedicated transmission optical microscope that has sensitivity on the phase-shift measurement thanks to a piezo-controlled microscope objective. The principle is to adjust the focal plane on the written structures of the glass, locate the mark indicating the location of the lines then adjust the “wheel of the z-axis” (depth of the focus) to see appear the photo-inscribed lines in the depth. We must then focus on the lines that we want to measure. Then the QPM software is recording 3 images at different focus (typically with a 3 microns step) and computes the images to get a quantitative phase image.

When a zone is white, it corresponds to a positive phase-shift. For a dark zone, we obtain a negative peak due to a negative phase shift. The zero of the image corresponds to the unmodified region. In this connection, here is an example to illustrate the complexity of the measured profiles but low energy cases reveal more simple profiles (Fig. 24).

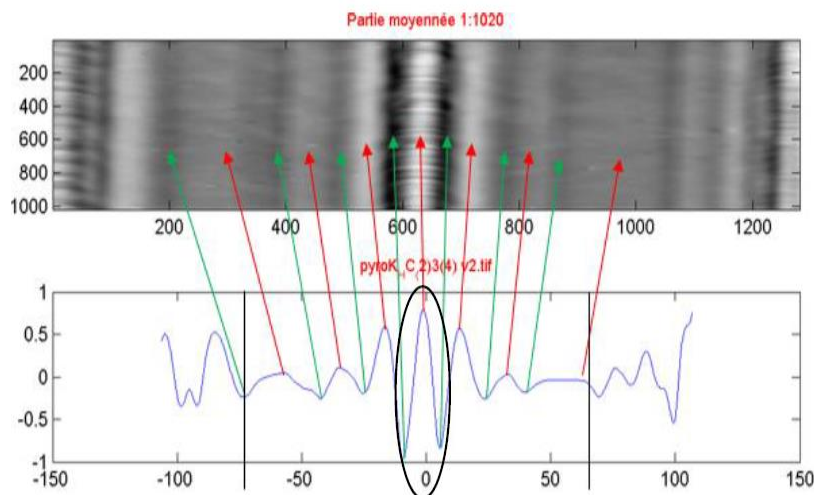


Figure 24 Illustrations of the profiles of the averaged phase difference between the glass matrix and irradiated lines along the scanning direction.

Figure 25 exhibited an example of a QPM image of the irradiated lines in Meta-Na-Li-Eu that we used to analyze data. So we can extract the profiles of the averaged phase variation along a line as well as the profiles of the averaged phase difference between the unmodified region

and irradiated lines along the scanning direction at different pulse energy (4.5, 4, 3.5, 3 and 2.5 μJ).

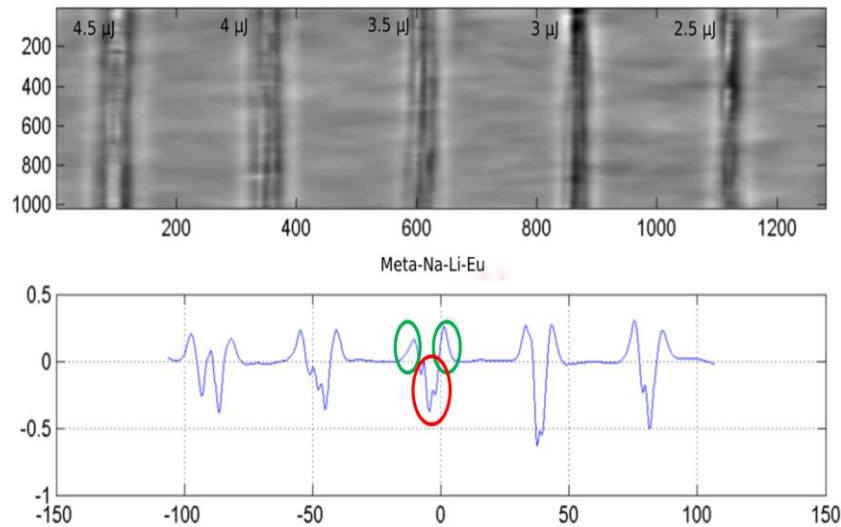


Figure 25 The microscopic image of the irradiated lines in Meta-Na-Li-Eu used to analyze data and extract the profiles of the averaged phase variation (above). The profiles of the averaged phase difference between the unmodified region and irradiated lines along the scanning direction at different pulse energy (4.5, 4, 3.5, 3 and 2.5 μJ) (below)

Let's choose the lines behavior inscribed by high energy pulse (3.5 μJ) in Meta-Na-Li-Eu to highlight more precisely the typical features of such a profile. So we can observe two behaviors as shown in figure 25 for the region surrounded by a green and red circle:

- A negative phase variation is mainly observed in the center of the irradiated zone (zone circled with red) with presence of spatial fluctuations of the phase amplitude.
- On both side of the central irradiated region, we can mention the presence of two symmetric and positive shoulders (zone circled in green) whose amplitude decrease exponentially when getting away from irradiated zone.

Central zone:

The central zone presents a negative refractive index change. It can be explained by the fact that there is a local expansion of the glass in this irradiated zone. This expansion is linked by the local melting of the glass in this central zone following by a very fast quenching inducing a permanent modification in the volume. This can be described through the fictive temperature approach where a higher quenching rate leads to a higher fictive temperature. In most glasses (apart silica) this higher quenching rate leads to an increase of the glass specific volume.

The presence of fluctuation in the center of irradiated zone is detected only under high pulse energy from 1 μJ and we notice more fluctuations in the center zone with increasing pulse energy. These fluctuations are more important under high pulse energy, which correlate with longer elongation and stronger index changes. These fluctuations are likely due to the fact that the irradiated zone is inhomogeneous along the z-axis (i.e. the light propagation direction).

As we can see in the laser line cross-section along the z-axis in Meta-Na-Eu, the laser trace has a shape of a drop as explained in the previous part. The tail zone of the drop present a behavior with $\Delta n > 0$. In contrast, the tip and the center zone of the drop present a dark region with $\Delta n < 0$. This observation confirms the inhomogeneity along the z-axis and explain the occurrence of strong fluctuations in the center zone of the line.

Contrast zone

For the positive shoulder that appear around the line center named as “the contrast zone”, it can be explained by an elastic response of the material to the expansion in the irradiated zone and these surroundings.

From these results we found that the shape of the refractive index change profile is complex and exhibit a negative peak with strong fluctuation in the line center surrounded by a positive index change in the contrast zone. Therefore, we also need in the future to measure the average phase variation $\Delta\phi$ in the cross section to get a global idea in the refractive index change in the laser writing region.

5.2.2 Study of refractive index kinetics in Metaphosphate glasses

Figure 26 compares the average phase difference $\Delta\phi$ in the central irradiated zone as a function of the pulse energy ranging in 0.05-5 μ J in non-doped, Eu and Er doped sodium metaphosphate glasses. These measurements confirm that a strong negative refractive index change occurs in the center of the irradiated lines. As well, we note a non-monotonous trend according to the pulse energy. Thus, for the three glasses, the $\Delta\phi$ reaches the strongest negative changes for 1.5-2 μ J/pulse and then the phase shift amplitude decreases for higher pulse energies to reach around 0.1 rad at 5 μ J.

In this connection, we calculated roughly the refractive index change Δn at 2 μ J energy for Meta-Na-Eu and Meta-Na-Er glasses with respectively a value of -0.9×10^{-3} and -1.8×10^{-3} . The Meta-Na undergoes a maximum change at 1.5 μ J pulse energy with a value of -0.7×10^{-3} (The transversal laser spot elongation are around 65 μ m for these pulse energy)

From these results, we revealed a decrease of the Δn in the order Meta-Na-Er > Meta-Na-Eu > Meta-Na, which indicate the contribution of the RE ions in the refractive index change under fs laser irradiation. However, we can notice that no link can be surprisingly be made between the tendency of the glass to crystallize shown by Raman spectroscopy and the amplitude of the refractive index variation.

Many phosphate glasses in literature typically exhibit or favor negative index changes inside the fs-laser irradiated region. As an example, Fletcher et al. [29]–[31] reported a negative changes in the index of refraction inside the fs-laser irradiated region at 1 kHz repetition rate in a series of phosphate glasses resulting in a poor guiding characteristics with the exception of 60ZnO-40P₂O₅ polyphosphate sample where a positive change in the refractive index was obtained. In [32], The strong value of refractive index is due to the migration of ion during the heat accumulation regime, leading to a high local concentration of lanthanum La in phosphate glasses after the action of the writing laser pulses at 500 kHz repetition rate which exhibited a positive and negative change Δn in the range $[-1.6 \times 10^{-3}, 1.6 \times 10^{-3}]$. Ehrt et al. [33] reported a

positive or negative refractive index in fluoride phosphate glasses depending on the glass composition and laser writing condition with a maximum change of -1×10^{-3} under 1 kHz repetition rate and varying energy of 1-10 μJ . Other glasses as silicate or borosilicate reported a negative refractive index change in the order of 10^{-4} - 10^{-3} [34],[35].

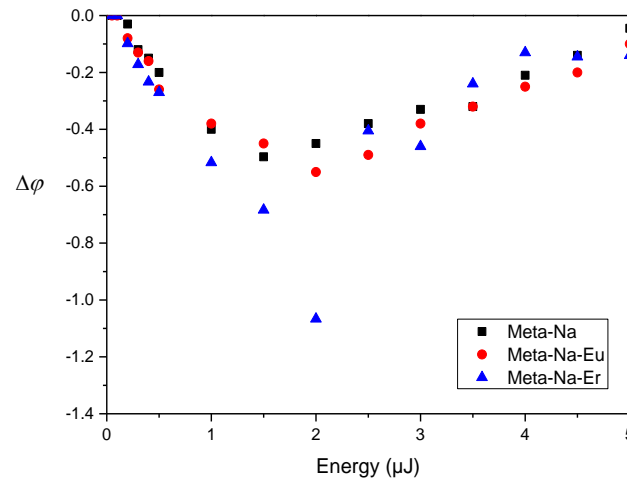


Figure 26 The average phase difference $\Delta\phi$ between the unmodified region and irradiated center lines as a function of the pulse energy ranging in 5 μJ - 0.05 μJ in Meta-Na, Meta-Na-Eu and Meta-Na-Er glasses.

5.2.3 Study of refractive index kinetics in Zinc Polyphosphate glasses:

Figure 27a compared the phase variation $\Delta\phi$ in the line center as a function of the pulse energy in non-doped and Eu doped zinc sodium polyphosphate glasses (Poly-Zn-Na, Poly-Zn-Na-Eu). In the same manner, Figure 27b displayed the $\Delta\phi$ in the zinc mixed sodium potassium polyphosphate glasses (Poly-Zn-Na-K, Poly-Zn-Na-K-Eu). This experiment confirms the previous results in metaphosphate glasses that the RE ions insertion in the network increases the refractive index change. While the energy corresponding to the maximum (negative amplitude) index change is between 1.5 and 2 μJ for metaphosphate, it is higher 3.5-4 μJ for polyphosphate glasses. Accordingly, Raman spectra reported a remarkable structural variation at high pulse energy from 2 μJ that could explain the strong $\Delta\phi$ in the 3.5-4 μJ pulse range. Even more, these measurements confirm the previous results in metaphosphate composition that the presence of RE ions in the glass lead to the raise of the index change. We notice a stronger effect of the europium ions doping in poly compared to metaphosphate glasses where the maximum refractive index change goes from -3.7×10^{-3} to -1.7×10^{-3} in Poly-Zn-Na whereas the maximum change increases from -0.7×10^{-3} to -0.9×10^{-3} in successively Meta-Na and Meta-Na-Eu. Here again, this is difficult to correlate the results with the Raman trends where the effect of RE doping even if it initially depolymerizes the glass network does not seem to impact much the structural evolution driven by fs laser interaction.

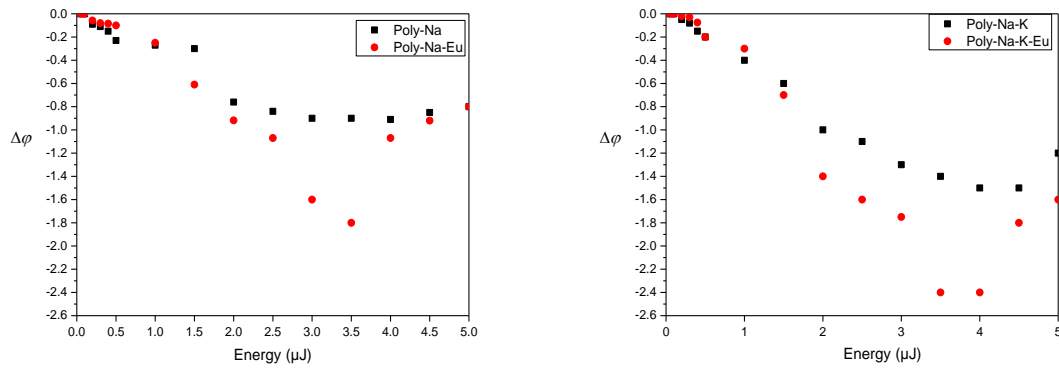


Figure 27 The average phase difference $\Delta\phi$ between the unmodified region and irradiated center lines as a function of the pulse energy ranging in $5 \mu\text{J} - 0.05 \mu\text{J}$ in (a) non-doped and Eu doped zinc sodium polyphosphate (Poly-Zn-Na and Poly-Zn-Na-Eu) and (b) non-doped and Eu doped zinc mixed sodium potassium polyphosphate glasses (Poly-Zn-Na-K and Poly-Zn-Na-K-Eu).

Alkali effect

Figure 28 exhibited the phase-shift variation $\Delta\phi$ as a function of the pulse energy in respectively non-doped (fig 28a) and Eu-doped metaphosphate glasses (fig 28b). In the same context, figure 29 displayed the $\Delta\phi$ in non-doped (fig 29a) and Eu-doped polyphosphate glasses (fig 29b). For metaphosphate glasses, both non-doped and Eu-doped mixed lithium sodium suffers an important decrease of the phase changes compared to the single sodium metaphosphate glasses. As well, it showed the maximum phase change in the order $\text{K} > \text{Na} + \text{K} > \text{Na}$ in both Eu-doped and non-doped polyphosphate glasses. These results suggest the effect of the nature of alkali ion in the refractive index change under fs writing.

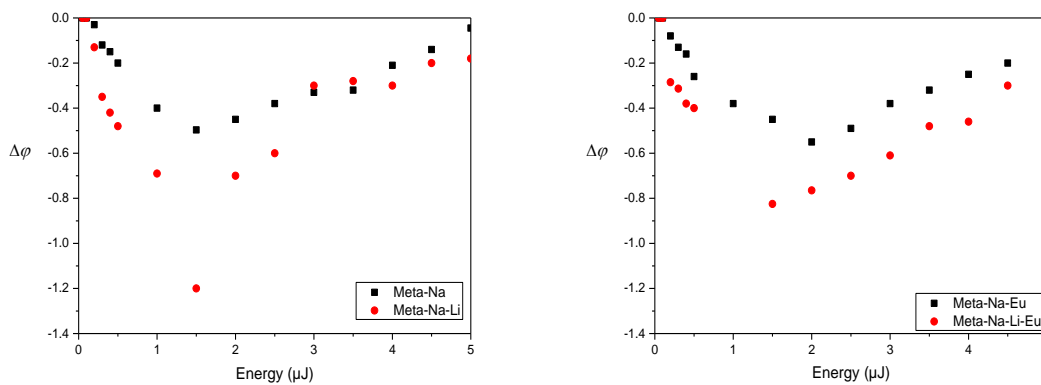


Figure 28 The average phase difference $\Delta\phi$ between the unmodified region and irradiated center lines as a function of the pulse energy ranging in $5 \mu\text{J} - 0.05 \mu\text{J}$ in (a) non-doped (Meta-Na and Meta-Na-Li) and (b) Eu doped metaphosphate glasses (Meta-Na-Eu and Meta-Na-Li-Eu).

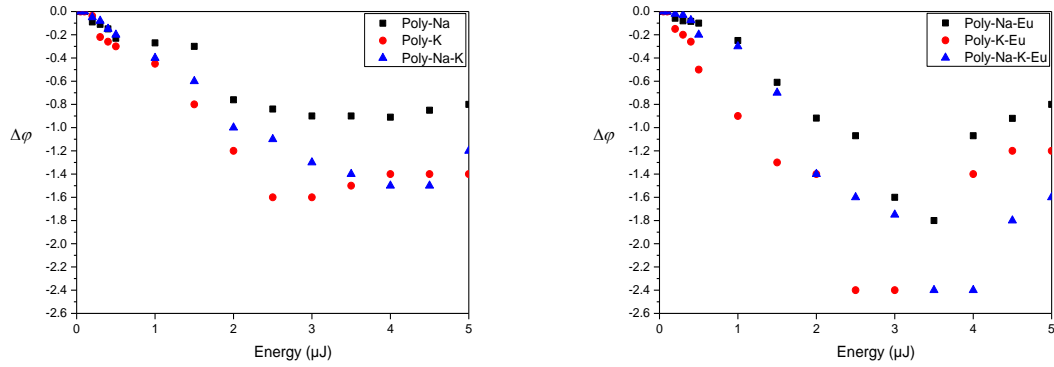


Figure 29 The average phase difference $\Delta\phi$ between the unmodified region and irradiated center lines as a function of the pulse energy ranging in $5 \mu\text{J} - 0.05 \mu\text{J}$ in (a) non-doped zinc polyphosphate (Poly-Zn-Na, Poly-Zn-K and Poly-Zn-Na-K) and (b) Eu doped zinc polyphosphate (Poly-Zn-Na-Eu, Poly-Zn-K-Eu and Poly-Zn-Na-K-Eu)

5.2.4 Correlation between defect centers and refractive index changes

In order to try to interpret the refractive index variation, we identified and quantify the point defects by PL and EPR. First, we have measured the fluorescence spectra of fs laser modified Na metaphosphate glasses at various pulse energy (figure 30). A broad noticeable photoluminescence band centered at 590 nm was observed. This emission band has been attributed to Phosphorus Oxygen Hole Center (POHC) defect in analogy with NBOHC in silica glass even if there is no demonstration of such attribution [29]. In this defect, phosphorus atom is linked to 2 non-bridging oxygen NBO and one hole is delocalized on both of them. Fletcher et al. [29] correlated the greater fluorescence intensities of this defect to the higher shifts in the $\nu_s(\text{PO}_2)$ modes Raman peak frequency. It indicates that the mechanism of glass network expansion caused by the absorption of fs-laser pulses results in broken P-O bonds and a lower glass density. This suggestion is not consistent with our results where Raman spectra displaying no significant shift of the band at 1167 cm^{-1} due to $\nu_s(\text{PO}_2)$ modes in irradiated lines of non-doped Meta-Na glass, whereas we observe a higher intensity of the POHC emission band. The maximum change in intensity of the POHC fluorescence as a function of the pulse energy in Meta-Na glass is presented in figure 31a. The intensity of this defect reaches a maximum at pulse energy of $2 \mu\text{J}$. This results correlates with the average phase difference $\Delta\phi$ which reaches a maximum change at the same pulse energy (Fig 31a and 31b). As a first suggestions, the POHC defect formation is correlated to the refractive index changes under fs laser writing in alkali metaphosphate glasses.

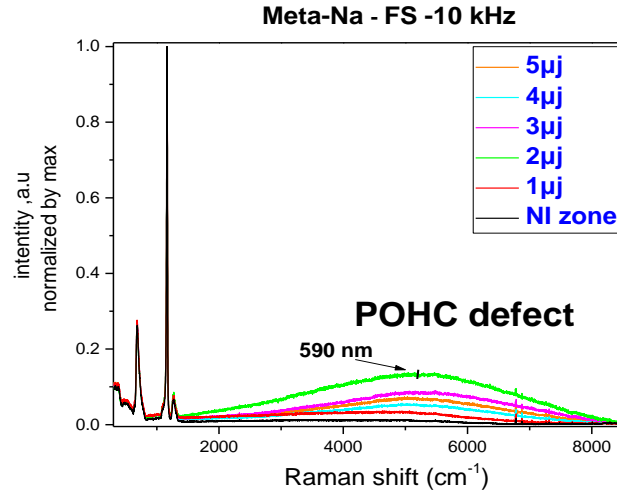


Figure 30 The photoluminescence spectra of modified and unmodified Meta-Na glass for various fs laser pulse energy ranging in 1-5 μJ ($\lambda_{\text{ext}}=458\text{ nm}$).

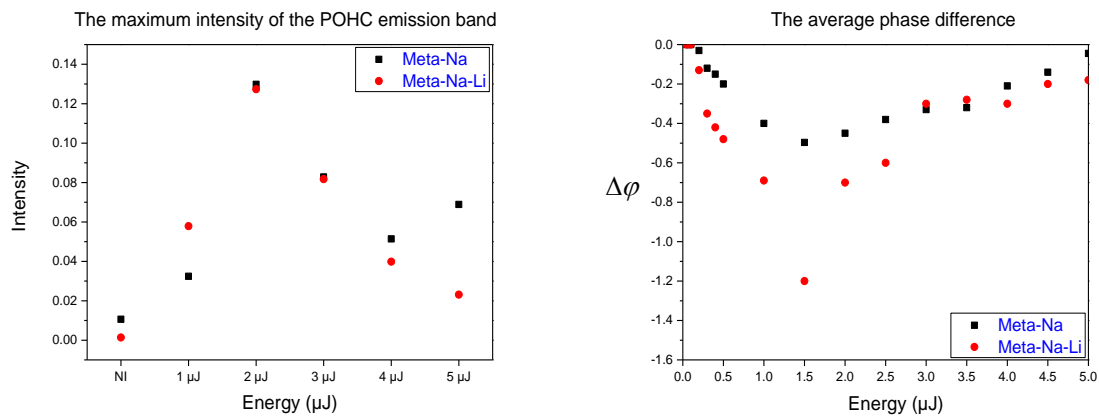


Figure 31 The maximum intensity of the POHC emission band (a) and the average phase difference $\Delta\phi$ between the unmodified region and irradiated center lines (b) as a function of the pulse energy ranging in 5 μJ - 0.05 μJ in non-doped alkali (Na and NaLi) metaphosphate glasses.

For increasing the number of point defects to be able to be detected by EPR spectroscopy, 200 lines of 3 mm long and 10 μm distant from each other were written in each samples at the energy corresponding to max $\Delta\phi$. In this framework, figure 32 exhibits the EPR spectrum of POHC defects created under several writing lines at pulse energy of 2 μJ in non-doped and Eu doped Na metaphosphate. These results are in agreement with the PL measurements and reported a dominant strong signal under a doublet form in the range 3475-3515 Gauss attributed to the POHC defect in alkali metaphosphate glasses.

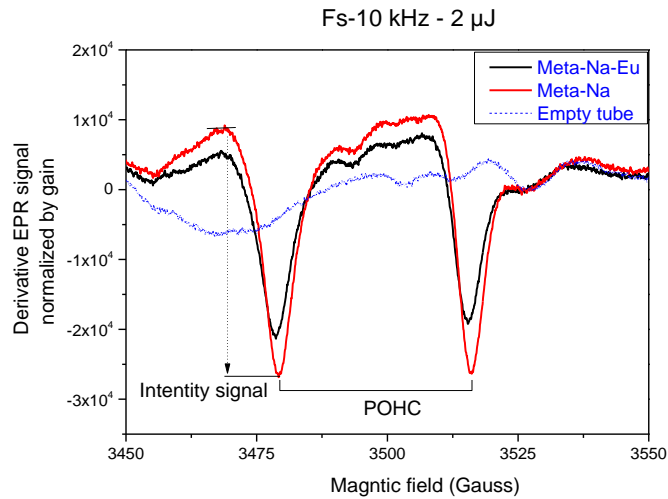


Figure 32 EPR spectrum of POHC defects created under 200 lines of 3 mm long written at 300 μm below the surface using fs laser at 10 kHz repetition rate and pulse energy of 2 μJ in non-doped and Eu doped Na metaphosphate glasses.

The EPR signal of non-doped and especially of Eu doped Poly-Zn-Na glasses under fs laser writing at pulse energy of 3.5 μJ (Figure 33) are more complex implying the occurrence of a new signal. This signal is similar to the Peroxy defect in silica and is due to one hole trapped on a peroxy linkage P-O-O (two bonded oxygen to a phosphorus atom) [36]. These results are in agreement with electron irradiation where Peroxy defect strongly dominated the EPR spectra in zinc polyphosphate glasses after the extinction of the POHC signal at high dose from 10^7 Gy dose. To quantify the point defects formation, table 3 reported the type and the peak to peak intensity of the EPR signal comparing with the $\Delta\phi$ in different Eu doped and non-doped metaphosphate and polyphosphate glasses under several writing lines.

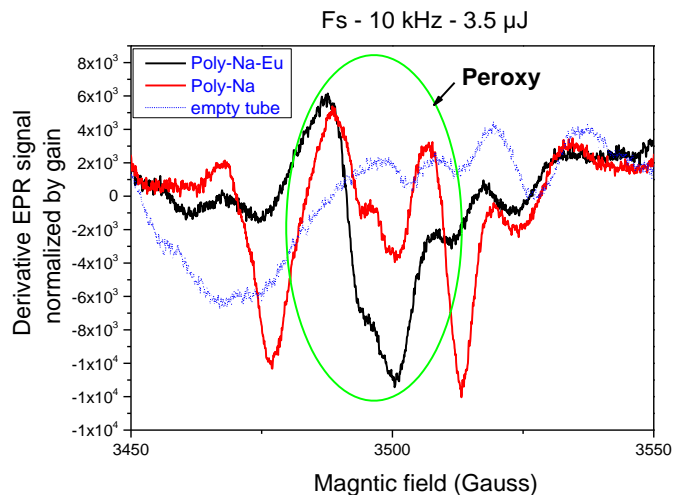


Figure 33 EPR spectrum of POHC and Peroxy defects created under 200 lines of 3 mm long written at 300 μm below the surface using fs laser at 10 kHz repetition rate and pulse energy of 3.5 μJ in non-doped and Eu doped Na zinc polyphosphate glasses.

Table 2 Type of defect, average phase difference and intensity peak to peak of the EPR signal of POHC and Peroxy defects created in metaphosphate and polyphosphate glasses under fs writing.

	Pulse energy	Type of defect	$\Delta\phi$	Intensity of the EPR Signal
Meta-Na	2 μ J	POHC	-0.45	35218
Meta-Na-Eu	2 μ J	POHC	-0.55	24808
Poly-Na	3.5 μ J	POHC-Peroxy	-0.9	17310
Poly-Na-Eu	3.5 μ J	Peroxy	-1.8	13900
Poly-Na-K	3.5 μ J	Peroxy	-1.4	5134
Poly-Na-K-Eu	3.5 μ J	-	-	-

We can see in table 2 that contrary to refractive index variation, the Eu doping leads to a decrease of the point defect amount in agreement with what was observed with electrons in general for several types of RE [37] From these results, there is no apparent correlation between the refractive index change and the EPR signal of POHC and Peroxy defects. This indicates that the contribution of these points defects to the refractive index changes remain quite limited. So there is at least one other mechanism leading to the observed changes, which is a likely permanent volume change accompanied by the formation of a stress field. It is interesting to underline that in part we emphasized that the negative refractive index variation (visible in the center of the laser spot), can be connected to structural changes

6 Rare earth environment under fs laser irradiation at low repetition rate

6.1 Rare earth environment under fs laser irradiation (Bibliographic part)

Let us remember, the objective of this thesis is comparing and controlling the rare earth environment modification under fs laser and electron irradiation in phosphate glasses. In previous research, fs laser has been used as a powerful tool to generate microscopic modification in transparent material. In comparison with other irradiation source, fs laser has many advantages such as high electric field intensity which is sufficient for inducing non-linear optical effects in materials [38], ultrashort interaction times as well as the capability of modifying the internal structure without destroying the integrity of the glass and to be able to localize the modification spatially on a microscopic scale [39]. Therefore, few work in literature reported the rare earth environment modification under femtosecond writing in glasses that are attractive material in optic such as optical waveguides, waveguides amplifiers and 3D optical memory [40].

Reduction of RE³⁺ to RE²⁺:

As known, some RE³⁺ ions such as Sm³⁺ and Eu³⁺ [38], [40]–[42] exist under a stable divalent form. Thus, reduced rare earth ions doped glasses exhibit a larger Faraday effect long lasting phosphorescence, photo-stimulated luminescence, photochemical spectral hole burning memory and other important properties [41]. In this framework, Qiu et al. [43] reported a permanent photo-reduction of Sm³⁺ to Sm²⁺ inside a Sm doped sodium aluminoborate glass after 800 nm focused fs laser irradiation with repetition rate of 200 kHz, pulse time of 120 fs and average power of 400 mW. In another work and using similar laser parameter, Qiu et al.

[38] confirmed the photoreduction of Eu^{3+} to Eu^{2+} ions in Eu doped fluorozirconate glasses under fs laser irradiation using the difference absorption and electron paramagnetic resonance spectroscopy. It is suggested that Eu^{3+} act as electron trapping center whereas active sites in the glass matrix act as hole trapping centers leading to the formation of Eu^{2+} ions.

Likewise, You and Nogami et al. [40] proved the valence change of Eu^{3+} ion in aluminoborosilicate glasses under 800 nm fs laser pulses with repetition rate of 1kHz, pulse duration of 130 fs and average power of 600 mW. They explained the photoreduction as a redistribution of electron and holes thrownra out the conduction and valence bands via multiphoton excitation which lead to the formation of Eu^{2+} ions in glass. Moreover, Lim et al. [42] declared the photoreduction of Eu^{3+} to Eu^{2+} in sodium borate glasses using 800 nm fs laser with 1kHz repetition rate and 100 fs pulse duration. So we observed in conclusion that reduction of Eu^{3+} is mainly observed at low cadency.

Other modification in the RE environment under fs laser irradiation in glasses were reported in literature. Yu and Nogami et al. [24],[29] reported an increase of the relative intensity of $^5\text{D}_0\text{-}^7\text{F}_0$ transition as well as a rise in the asymmetry ratio ($^5\text{D}_0\text{-}^7\text{F}_2 / ^5\text{D}_0\text{-}^7\text{F}_1$) because of the change of the local structure around Eu^{3+} ions in silicate glasses.

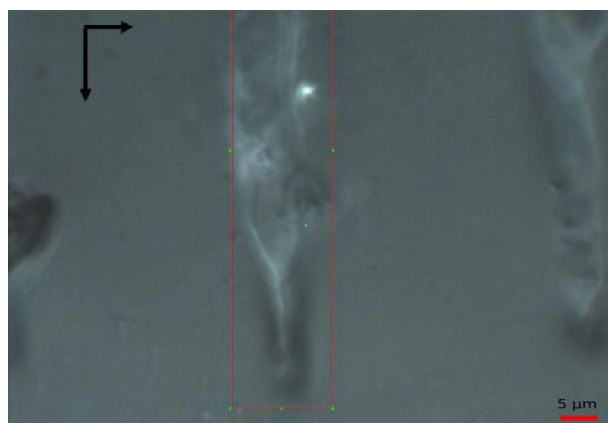
Ferrer and Troy et al. [45], [46] studied the local Er and Yb environment in Er-Yb codoped phosphate glass under 1030 fs laser irradiation with high repetition rate of 1MHz and energy ranging in 315-630 nJ. They found an increase in the 555 nm Er^{3+} fluorescence in the fs laser modified region, which was attributed to the reduced energy transfer from Er^{3+} to Yb^{3+} due to the expansion of the network.

6.2 Photo-Emission micro-spectroscopy:

6.2.1 Metaphosphate glasses (Meta-Na-Eu and Meta-Zn-Eu)

Figure 34 exhibits the microscopic image as well as the associated emission cartography of the Eu^{3+} ions in the laser trace cross-section in Meta-Na-Eu glass compared to unmodified regions. The laser writing parameters are 1030 nm, 250 fs, 10 kHz, 10 $\mu\text{m/s}$, linear polarization. As shown in the microscopic image (figure 34a), the emission cartography was recorded in the red boxed zone each 4 μm along the y-axis and each 10 μm along the y-axis. We note that the boxed area contain both the tail and the center of the transversal laser line.

The emission spectra were recorded under the 458 nm line excitation of an Ar laser and it displays the emission bands corresponding to $^5\text{D}_0\text{-}^7\text{F}_j$ ($j=0,1$ and 2) transition. We notice a crucial variation of the emission intensity in the irradiated zone. As well, we note that the spot center undergoes a decrease in the emission intensity contrary to the tail region that suffer an increase in the emission intensity. The formation of POHC point defect with 2 absorption bands at 410 and 540 nm [47] could explain the decrease of the Eu^{3+} emission. Same results are showed for Meta-Zn-Eu glass.



Meta-Na-Eu-PL-LC-carto-4 μJ

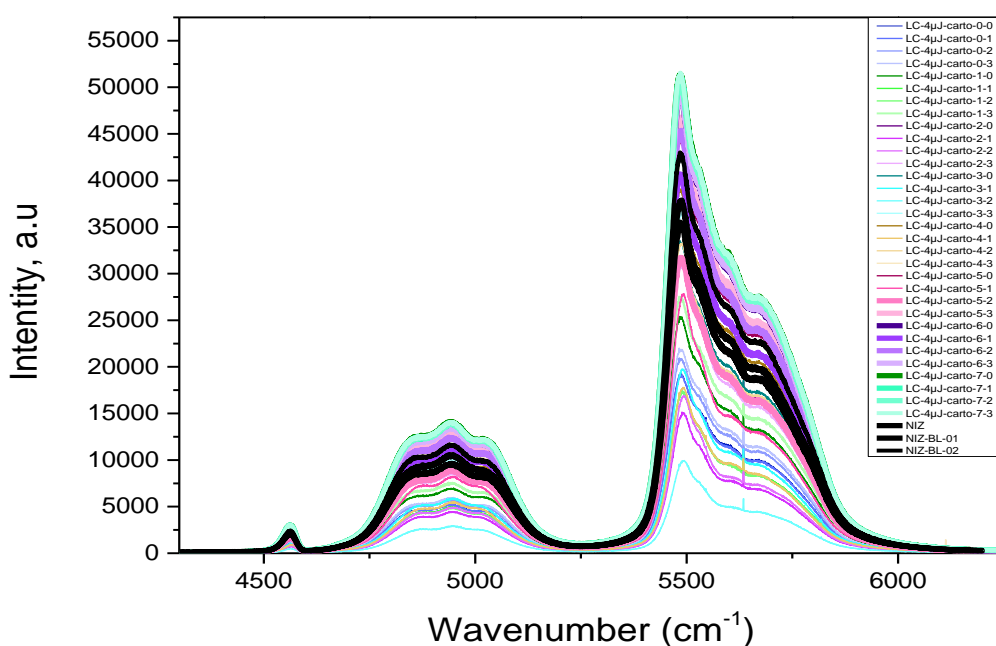


Figure 34 (a) Microscopic image of the laser line cross-section irradiated at 4 μJ pulse energy in **Meta-Na-Eu glass** through a 100× objective. (b) The corresponding emission cartography of the Eu^{3+} ions in the red boxed area as displayed in the microscopic image. The PL spectra were recorded in the red boxed region each 4 μm along the x axis and each 10 μm along the y axis.

6.2.2 Polyphosphate glasses (Poly-Zn-Na-Eu)

Further, we studied the luminescence properties of the Eu^{3+} ions under fs laser irradiation in polyphosphate compositions. Figure 35 exhibited the luminescence cartography of the Eu^{3+} ions in the transversal laser line inscribed with 10 kHz repetition rate and 4 μJ pulse energy. Compared to unmodified region, we observe no variation of the emission intensity contrary to as shown in metaphosphate composition. As noted before, EPR spectra (Fig 33) showed no formation of POHC defect in Poly-Zn-Na-Eu under fs laser irradiation but some peroxy radicals point defects P-O-O^\bullet . So, this very weak change confirms the suggestion that the emission intensity decrease is related to the formation of POHC defects.

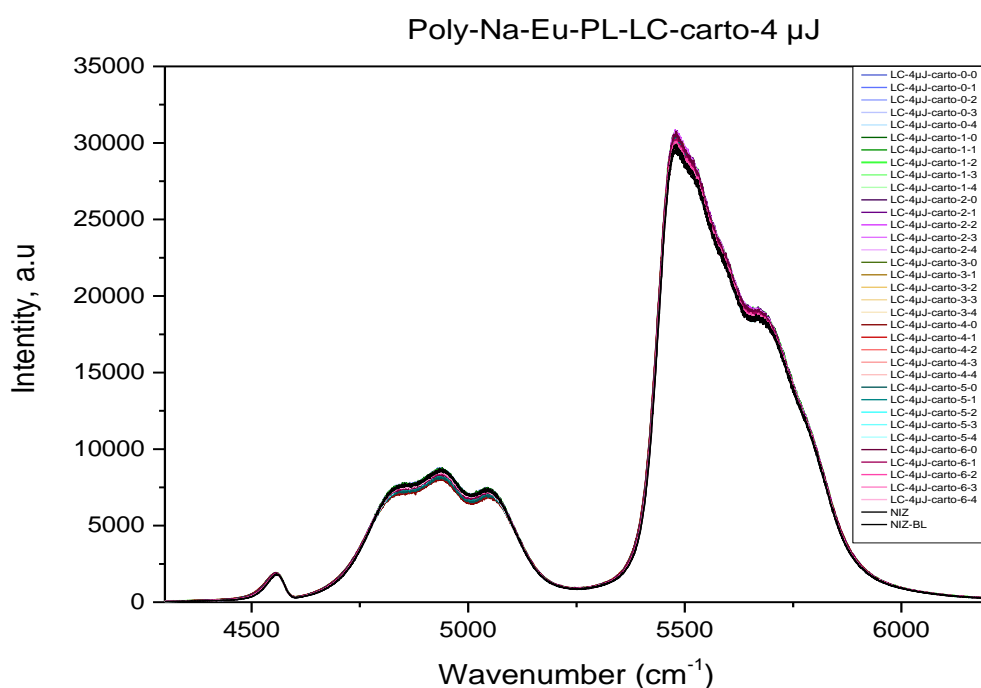
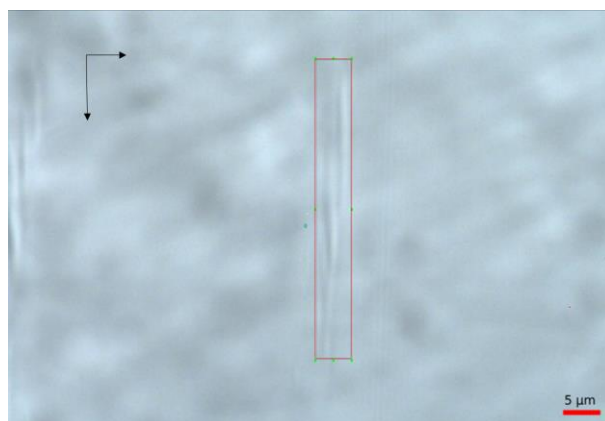


Figure 35 (a) Microscopic image of the laser line cross-section irradiated at 10 kHz repetition rate and **4 μJ** pulse energy in **Poly-Zn-Na-Eu glass** through a 100× objective. (b) The corresponding emission cartography of the Eu^{3+} ions in the red boxed area as displayed in the microscopic image. The PL spectra were recorded in the red boxed region each 1.5 μm along the x axis and each 7.5 μm along the y axis.

6.3 Asymmetry ratio between ${}^5\text{D}_0\text{-}{}^7\text{F}_2$ and ${}^5\text{D}_0\text{-}{}^7\text{F}_1$

Using the emission cartography (Fig. 34 and 35) of the Eu^{3+} ions in the laser trace, we calculated the integrated emission band ratio between ${}^5\text{D}_0\text{-}{}^7\text{F}_2$ and ${}^5\text{D}_0\text{-}{}^7\text{F}_1$ known as the asymmetry ratio (as explained in the chapter 4). Figures 36a and 36b exhibited the asymmetry ratio variation under fs laser irradiation in the tail and the center of the drop in respectively Meta-Na-Eu and Poly-Zn-Na-Eu.

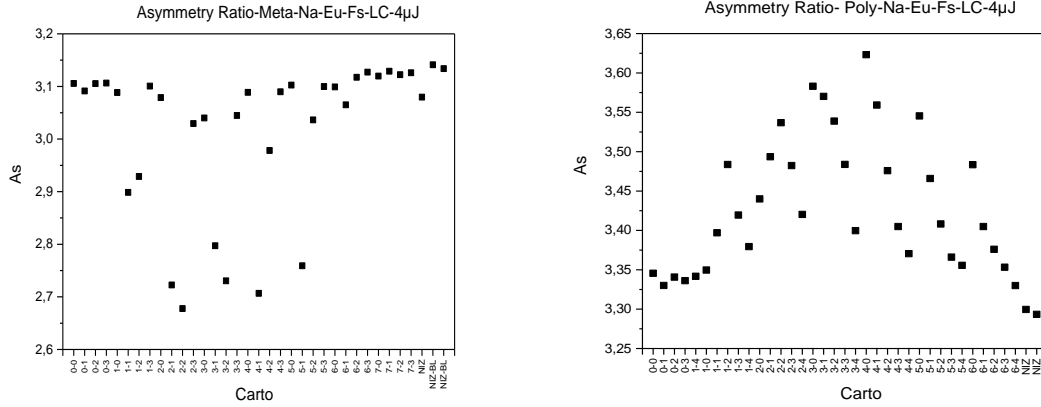


Figure 36 The asymmetry ratio (A_s) variation (${}^5D_{0-7}F_2 / {}^5D_{0-7}F_1$) correspond to the emission cartography of the Eu^{3+} ions in the laser line cross-section irradiated at 10 kHz repetition rate and $4 \mu\text{J}$ pulse energy in (a) Meta-Na-Eu and (b) Poly-Zn-Na-Eu glasses compared to unmodified region and pristine glasses.

This measure indicates insignificant change of the asymmetry ratio (noted A_s) in the tip and the tail of the drop compared to the unmodified region in both Meta-Na-Eu and Poly-Zn-Na-Eu glasses. Whereas, there is a meaningful change in the center of the laser trace. Thus, we observe a decrease of the A_s value from around 3.15 in pristine glass to near 2.75 in the center of the transversal laser trace in Meta-Na-Eu whereas for Poly-Zn-Na-Eu glass, the A_s ratio suffer an increase from 3.3 in unmodified region to 3.63 in the trace center irradiated at $4 \mu\text{J}$ pulse energy. In this connection and in previous work in literature, Yu and Nogami et al. [29] reported an increase of this ratio from 3.41 to 4.15 in irradiated zinc silicate glass by fs laser. The increase of the A_s ratio is also seen under different irradiation as gold ions, gamma and electron irradiation [35]–[37]. We also reported an important increase of this ratio especially in metaphosphate glasses under electron irradiation as reported in the previous chapter of this work. This increase is explained by a reduction of the site symmetry of the Eu^{3+} ions. Therefore, differently to as reported under electron irradiation that A_s strongly increased in metaphosphate composition, the A_s ratio suffer a decrease under fs laser writing in Meta-Na-Eu after fs laser writing. This decrease may be related to an increase of the site symmetry of the Eu^{3+} ions in agreement with the tendency of those glasses to crystallized evidenced by Raman spectroscopy in the center of the laser trace

6.4 ${}^5D_{0-7}F_0$ transition:

Another information about the europium environment evolution under fs laser pulse can be extracted from the ${}^5D_{0-7}F_0$ emission band. In this framework, figure 37a and 37b displayed the ${}^5D_{0-7}F_0$ emission for different points of the mapping in the tail and the center of the laser trace cross section in respectively Meta-Na-Eu and Poly-Zn-Na-Eu glasses.

We notice a small shift of the maximum of the emission band of the ${}^5D_{0-7}F_0$ transition towards higher wavenumber in the laser spot center of Meta-Na-Eu glass whereas it suffer a shift towards lower wavenumber compared to unmodified region in Poly-Zn-Na-Eu glass.

Moreover, we notice a sharpening of the emission band of the ${}^5D_0-{}^7F_0$ transition in Meta-Na-Eu sample. On the contrary, we observed a broadening of this band in the transversal laser trace of Poly-Zn-Na-Eu glass.

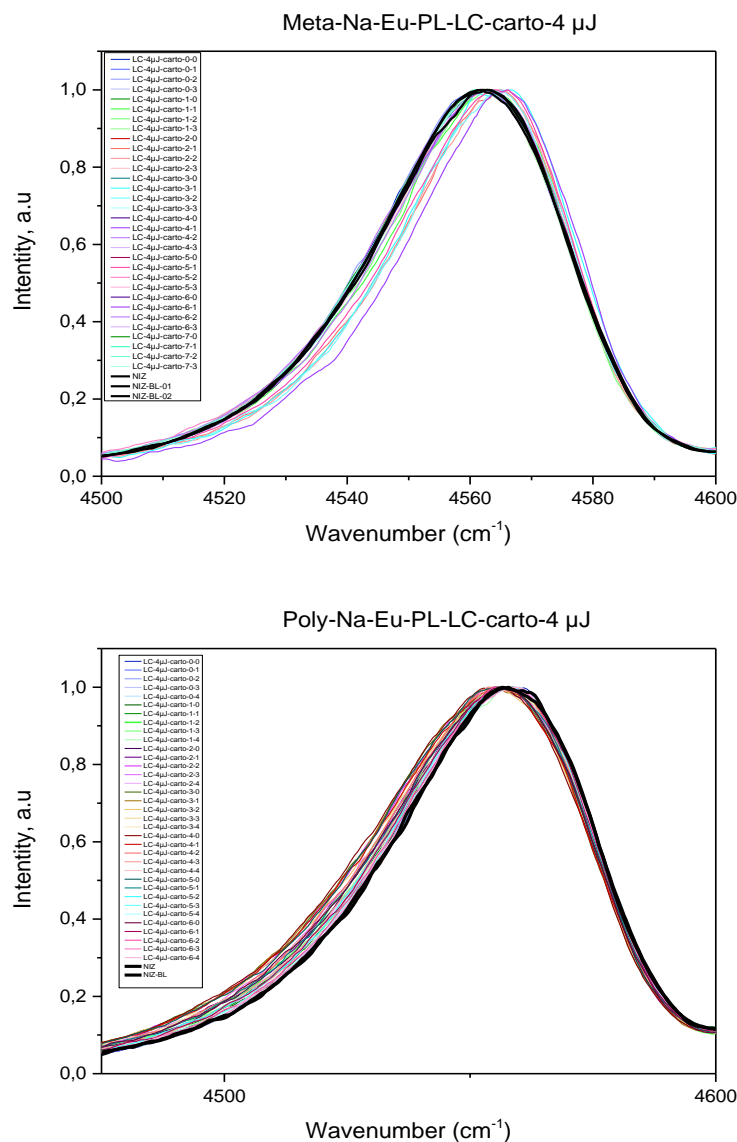


Figure 37 Zoom of the emission cartography of the Eu^{3+} ions attributed to the ${}^5D_0-{}^7F_0$ transition in the laser line cross-section irradiated at 10 kHz repetition rate and $4 \mu\text{J}$ pulse energy in (a) Meta-Na-Eu and (b) Poly-Zn-Na-Eu glasses. (Zoom of the PL cartography correspond to fig 34 and 35)

To quantify this compression and broadening in respectively Meta-Na-Eu and Poly-Zn-Na-Eu, we determined the full width at half maximum (FWHM) of the ${}^5D_0-{}^7F_0$ emission bands. Figure 38a and 38b exhibited the FWHM of the ${}^5D_0-{}^7F_0$ emission band in the tail and the center of the longitudinal laser trace compared to unmodified region in successively Meta-Na-Eu and Poly-Zn-Na-Eu glasses. We notice a decrease of the FWHM from around 38 cm^{-1} in unmodified region to near 34 cm^{-1} in the center trace with a reduction of about 4 cm^{-1} in Meta-Na-Eu. In contrast, the FWHM increase from 49 cm^{-1} to around 54 cm^{-1} with a broadening of 5 cm^{-1} in Poly-Zn-Na-Eu indicating a larger sites dispersion of Eu^{3+} ions under irradiation at $4 \mu\text{J}$ pulse

energy. The reduction of the site distribution and the ${}^5D_0 \rightarrow {}^7F_0$ energy in meta can be associated to a beginning of crystallization of the glass.

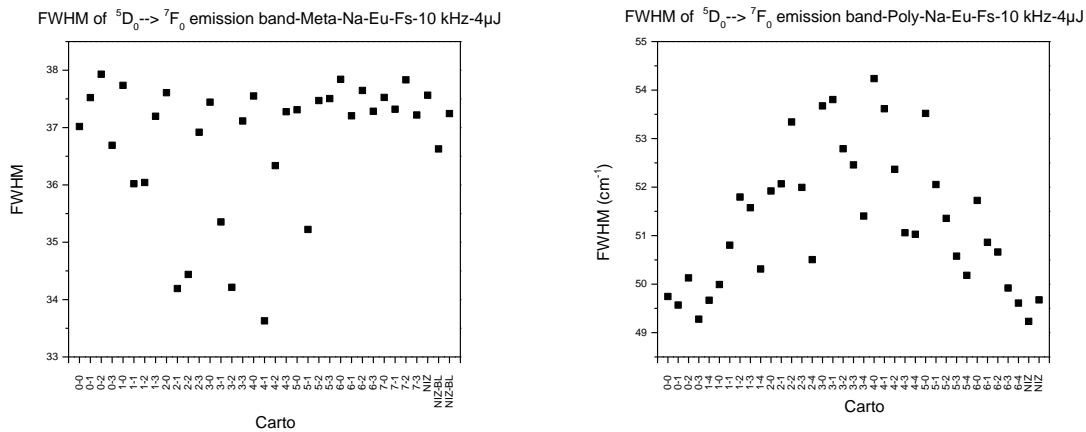


Figure 38 The full width at half maximum (FWHM) of the ${}^5D_0 \rightarrow {}^7F_0$ emission band in the tail and the center of the transversal laser trace inscribed at $4 \mu\text{J}$ pulse energy compared to unmodified region in (a) Meta-Na-Eu and (b) Poly-Zn-Na-Eu glasses.

6.5 Divalent europium:

No signal corresponding to Eu^{2+} ions are visible on the EPR spectra displayed in figure 39 after 200 lines writing in different meta and poly phosphate glasses as. The absence of divalent formation under fs laser contrasts with electron irradiation experiments (N 4) in which we detected a strong reduction from Eu^{3+} to Eu^{2+} ions whatever the dose under 2.5 MeV and 700 keV. As well, these results are contradictory to as reported in literature. Thus, Qiu et al. [38] reported the photo-reduction of Eu^{3+} to Eu^{2+} ions in Eu doped fluorozirconate glasses under fs laser irradiation (800 nm 150 fs, 200 kHz and focused laser of 1 and 10s) using the difference of optical absorption and electron paramagnetic resonance spectroscopy. Likewise, You and Nogami et al. [40] proved the valence change of Eu^{3+} ion in aluminoborosilicate glasses under 800 nm fs laser pulses with repetition rate of 1 kHz, pulse duration of 130 fs, average power of 600 mW and speed of 1 mm/s. In [42], they reported a photo-reduction of Eu^{3+} to Eu^{2+} in sodium borate glasses using 800 nm fs laser with 1 kHz repetition rate and 100 fs pulse duration. We can notice that the glass matrix were different and the scanning speed was very weak in our work (0.01 mm/s). A more detailed study should be carried out by the laser parameters to evidence the condition leading to Eu^{2+} formation in those glass matrix.

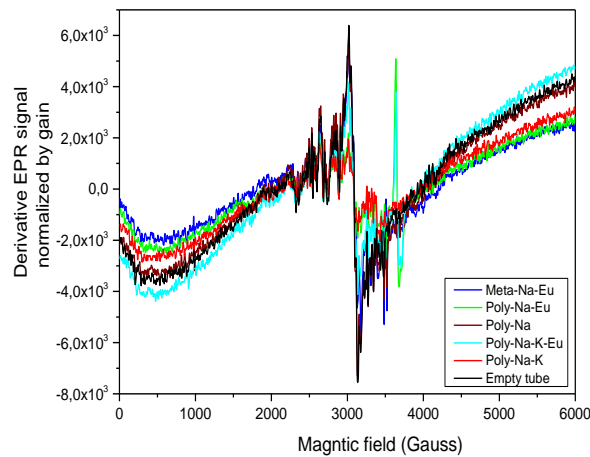


Figure 39 EPR spectra normalized by gain of Eu doped meta and polyphosphate glasses inscribed by femtosecond laser with 200 lines of 3 mm long written at 300 μm below the surface at repetition rate of 10 kHz.

Adding europium leads to the crystallization of metaphosphate glasses after femtosecond laser writing at low repetition rate of 10 kHz. Crystallization may be related to thermal effect introduced by the fs laser because it does not appear under electron irradiation. Thus, Eu doped glasses have a higher glass transition temperature T_g compared to non-doped glass (for example $T_g = 251$ and 291°C in respectively non-doped and Eu doped sodium metaphosphate glasses).

Therefore, crystallization explains the slight decrease of the asymmetry ratio in the center of the transversal laser trace in Eu doped metaphosphate glasses that increase the order and causes the growth of Eu^{3+} site symmetry.

Although electron irradiation does not cause crystallization in metaphosphate glasses, it is observed that electron irradiation has a bigger effect on the phosphate network in Zn metaphosphate glass compared to Na. It appears similar that femtosecond laser irradiation produces more pronounced crystallization in Eu-doped Zn metaphosphate glass compared to Na.

In Zn-Na-Eu polyphosphate glass there is no crystallization under femtosecond laser irradiation, and the changes to the phosphate network in Raman cartography are quite similar to those seen under electron irradiation.

Under femtosecond laser there is no formation of divalent europium in alkali and zinc phosphate glasses in contrast to as reported in literature [2–5]. This stability of the Eu^{3+} ions can be related to the laser parameters especially to the scanning speed or to the insufficient number of lines inscribed below the surface.

It is interesting that in metaphosphate glasses femtosecond laser irradiation is capable of producing crystallization but not Eu^{2+} , whereas electron irradiation is capable of producing Eu^{2+} but not crystallization. This might highlight the different features of the irradiation

events, for example the different length scale, expected to be of order Angstrom for electron collisions, and of the order 100 nm for laser heating.

It is interesting to notice a refractive index change with a structural evolution occurring only in the center of the drop (evidenced by Raman). However, no real link between the amplitude of the Δn variation and the structural evolution can be established. We show moreover a strong effect of the glass composition (alkali nature, RE doping) on the Δn value. This could be due to a migration of those elements but at these low repetition rate 10 KHz, no such effect was evidenced, and they appear when it is higher than 200 KHz [6].

As well, the contribution of the point defects to the refractive index change is quite limited. So no clear origin of the Δn variation can be proposed after our study. Moreover, a global Δn averaged on the whole drop will be important to be measured (as we evidenced opposite signs) to compare to the literature values and to better understand the role of the glass composition on the refractive index variation.

- [1] R. R. Gattass et E. Mazur, « Femtosecond laser micromachining in transparent materials », *Nature photonics*, vol. 2, n° 4, p. 219, 2008.
- [2] M. Royon, « Ingénierie de verres de silice : influence de pré-traitements sur la variation d'indice de réfraction de guides d'ondes photo-inscrits par laser femtoseconde ».
- [3] K. M. Davis, K. Miura, N. Sugimoto, et K. Hirao, « Writing waveguides in glass with a femtosecond laser », *Opt. Lett.*, vol. 21, n° 21, p. 1729, nov. 1996.
- [4] K. Mishchik, « Ultrafast laser-induced modification of optical glasses: a spectroscopy insight into the microscopic mechanisms », PhD Thesis, 2012.
- [5] A. Couairon, L. Sudrie, M. Franco, B. Prade, et A. Mysyrowicz, « Filamentation and damage in fused silica induced by tightly focused femtosecond laser pulses », *Physical Review B*, vol. 71, n° 12, p. 125435, 2005.
- [6] L. Sudrie, « Propagation non-linéaire des impulsions laser femtosecondes dans la silice », PhD Thesis, 2002.
- [7] C. B. Schaffer, A. Brodeur, J. F. García, et E. Mazur, « Micromachining bulk glass by use of femtosecond laser pulses with nanojoule energy », *Optics letters*, vol. 26, n° 2, p. 93–95, 2001.
- [8] J. W. Chan, T. R. Huser, S. H. Risbud, et D. M. Krol, « Modification of the fused silica glass network associated with waveguide fabrication using femtosecond laser pulses », *Applied Physics A: Materials Science & Processing*, vol. 76, n° 3, p. 367–372, mars 2003.
- [9] R. Brueckner, « Properties and structure of vitreous silica. I », *Journal of non-crystalline solids*, vol. 5, n° 2, p. 123–175, 1970.
- [10] M. Sakakura, M. Shimizu, Y. Shimotsuma, K. Miura, et K. Hirao, « Temperature distribution and modification mechanism inside glass with heat accumulation during 250 kHz irradiation of femtosecond laser pulses », *Applied Physics Letters*, vol. 93, n° 23, p. 231112, 2008.
- [11] K. Hirao et K. Miura, « Writing waveguides and gratings in silica and related materials by a femtosecond laser », *Journal of non-crystalline solids*, vol. 239, n° 1-3, p. 91–95, 1998.
- [12] A. M. Streltsov et N. F. Borrelli, « Study of femtosecond-laser-written waveguides in glasses », *JOSA B*, vol. 19, n° 10, p. 2496–2504, 2002.
- [13] A. Saliminia, R. Vallee, et S. L. Chin, « Waveguide writing in silica glass with femtosecond pulses from an optical parametric amplifier at 1.5 μm », *Optics communications*, vol. 256, n° 4-6, p. 422–427, 2005.
- [14] S. M. Eaton *et al.*, « Heat accumulation effects in femtosecond laser-written waveguides with variable repetition rate », *Optics Express*, vol. 13, n° 12, p. 4708–4716, 2005.
- [15] M. Lancry, B. Poumellec, A. Chahid-Erraji, M. Beresna, et P. G. Kazansky, « Dependence of the femtosecond laser refractive index change thresholds on the chemical composition of doped-silica glasses », *Optical Materials Express*, vol. 1, n° 4, p. 711–723, 2011.
- [16] L. Bressel *et al.*, « Femtosecond laser induced density changes in GeO₂ and SiO₂ glasses: fictive temperature effect », *Optical materials express*, vol. 1, n° 4, p. 605–613, 2011.
- [17] J. W. Chan, T. Huser, S. Risbud, et D. M. Krol, « Structural changes in fused silica after exposure to focused femtosecond laser pulses », *Optics letters*, vol. 26, n° 21, p. 1726–1728, 2001.
- [18] K. Miura, J. Qiu, H. Inouye, T. Mitsuyu, et K. Hirao, « Photowritten optical waveguides in various glasses with ultrashort pulse laser », *Applied Physics Letters*, vol. 71, n° 23, p. 3329–3331, déc. 1997.
- [19] Y. Shimotsuma, P. G. Kazansky, J. Qiu, et K. Hirao, « Self-organized nanogratings in glass irradiated by ultrashort light pulses », *Physical review letters*, vol. 91, n° 24, p. 247405, 2003.
- [20] R. L. Fleischer, P. B. Price, et R. M. Walker, « Solid-state track detectors: applications to nuclear science and geophysics », *Annual Review of Nuclear Science*, vol. 15, n° 1, p. 1–28, 1965.
- [21] C. B. Schaffer, A. Brodeur, N. Nishimura, et E. Mazur, « Laser-induced microexplosions in transparent materials: microstructuring with nanojoules », in *Commercial and Biomedical Applications of Ultrafast Lasers*, 1999, vol. 3616, p. 143–147.
- [22] E. N. Glezer *et al.*, « Three-dimensional optical storage inside transparent materials », *Opt. Lett., OL*, vol. 21, n° 24, p. 2023–2025, déc. 1996.

- [23] J. J. Hudgens, R. K. Brow, D. R. Tallant, et S. W. Martin, « Raman spectroscopy study of the structure of lithium and sodium ultraphosphate glasses », *Journal of Non-Crystalline Solids*, vol. 223, p. 21-31, janv. 1998.
- [24] A. M. Efimov, « IR fundamental spectra and structure of pyrophosphate glasses along the $2\text{ZnO} \cdot x\text{P}_2\text{O}_5 - (2-x)\text{Me}_2\text{O} \cdot y\text{P}_2\text{O}_5$ join with Me being Na and Li/ », p. 18, 1997.
- [25] R. K. Brow, D. R. Tallant, S. T. Myers, et C. C. Phifer, « The short-range structure of zinc polyphosphate glass », *Journal of Non-Crystalline Solids*, vol. 191, n° 1-2, p. 45-55, nov. 1995.
- [26] R. K. Brow, D. R. Tallant, J. J. Hudgens, S. W. Martin, et A. D. Irwin, « The short-range structure of sodium ultraphosphate glasses », *Journal of Non-Crystalline Solids*, vol. 177, p. 221-228, nov. 1994.
- [27] L. L. Velli, C. P. E. Varsamis, E. I. Kamitsos, D. Möncke, et D. Ehrhart, « Structural investigation of metaphosphate glasses », vol. 46, n° 2, p. 5, 2005.
- [28] G. B. Rouse Jr, P. J. Miller, et W. M. Risen Jr, « Mixed alkali glass spectra and structure », *Journal of Non-Crystalline Solids*, vol. 28, n° 2, p. 193–207, 1978.
- [29] L. B. Fletcher, J. J. Witcher, N. Troy, S. T. Reis, R. K. Brow, et D. M. Krol, « Direct femtosecond laser waveguide writing inside zinc phosphate glass », *Optics Express*, vol. 19, n° 9, p. 7929, avr. 2011.
- [30] L. B. Fletcher *et al.*, « Femtosecond laser writing of waveguides in zinc phosphate glasses [Invited] », *Optical Materials Express*, vol. 1, n° 5, p. 845, sept. 2011.
- [31] L. B. Fletcher, J. J. Witcher, N. Troy, R. K. Brow, et D. M. Krol, « Single-pass waveguide amplifiers in Er-Yb doped zinc polyphosphate glass fabricated with femtosecond laser pulses », *Optics Letters*, vol. 37, n° 7, p. 1148, avr. 2012.
- [32] J. del Hoyo *et al.*, « Control of waveguide properties by tuning femtosecond laser induced compositional changes », *Applied Physics Letters*, vol. 105, n° 13, p. 131101, sept. 2014.
- [33] D. Ehrhart, T. Kittel, M. Will, S. Nolte, et A. Tünnermann, « Femtosecond-laser-writing in various glasses », *Journal of Non-Crystalline Solids*, vol. 345-346, p. 332-337, oct. 2004.
- [34] J. Cao, B. Poumellec, F. Brisset, et M. Lancry, « Pulse energy dependence of refractive index change in lithium niobium silicate glass during femtosecond laser direct writing », *Optics express*, vol. 26, n° 6, p. 7460–7474, 2018.
- [35] V. R. Bhardwaj *et al.*, « Femtosecond laser-induced refractive index modification in multicomponent glasses », *Journal of Applied Physics*, vol. 97, n° 8, p. 083102, avr. 2005.
- [36] M. E. Archidi, M. Haddad, A. Nadiri, F. Benyaïch, et R. Berger, « Defect centers in X-irradiated alkali phosphate glasses: EPR studies », *Nuclear Instruments and Methods in Physics Research Section B: Beam Interactions with Materials and Atoms*, vol. 116, n° 1, p. 145-149, août 1996.
- [37] N. Ollier, R. Planchais, et B. Boizot, « EPR study of Yb-doped irradiated glasses », *Nuclear Instruments and Methods in Physics Research Section B: Beam Interactions with Materials and Atoms*, vol. 266, n° 12-13, p. 2854-2858, juin 2008.
- [38] J. Qiu, K. Kojima, K. Miura, T. Mitsuyu, et K. Hirao, « Infrared femtosecond laser pulse-induced permanent reduction of Eu^{3+} to Eu^{2+} in a fluorozirconate glass », *Optics Letters*, vol. 24, n° 11, p. 786, juin 1999.
- [39] L. Yu et M. Nogami, « Upconversion luminescence properties of europium in ZnO-SiO_2 glasses by femtosecond laser excitation », *Materials Chemistry and Physics*, vol. 107, n° 2-3, p. 186-188, févr. 2008.
- [40] H. You et M. Nogami, « Optical Properties and Valence Change of Europium Ions in a Sol-Gel $\text{Al}_2\text{O}_3\text{-B}_2\text{O}_3\text{-SiO}_2$ Glass by Femtosecond Laser Pulses », *The Journal of Physical Chemistry B*, vol. 109, n° 29, p. 13980-13984, juill. 2005.
- [41] J. Qiu, K. Miura, T. Suzuki, T. Mitsuyu, et K. Hirao, « Permanent photoreduction of Sm^{3+} to Sm^{2+} inside a sodium aluminoborate glass by an infrared femtosecond pulsed laser », *Applied physics letters*, vol. 74, n° 1, p. 10–12, 1999.
- [42] K.-S. Lim *et al.*, « Femtosecond laser-induced reduction in Eu-doped sodium borate glasses », *Journal of Luminescence*, vol. 122-123, p. 14-16, janv. 2007.

- [43] J. Qiu, K. Miura, H. Inouye, Y. Kondo, T. Mitsuyu, et K. Hirao, « Femtosecond laser-induced three-dimensional bright and long-lasting phosphorescence inside calcium aluminosilicate glasses doped with rare earth ions », *Applied Physics Letters*, vol. 73, n° 13, p. 1763-1765, sept. 1998.
- [44] L. Yu et M. Nogami, « Photoluminescent changes of Eu³⁺ in ZnO–SiO₂ glasses induced by femtosecond laser », *Journal of Alloys and Compounds*, vol. 462, n° 1-2, p. 187-191, août 2008.
- [45] A. Ferrer, D. Jaque, J. Siegel, A. R. de la Cruz, et J. Solís, « Origin of the refractive index modification of femtosecond laser processed doped phosphate glass », *Journal of Applied Physics*, vol. 109, n° 9, p. 093107, mai 2011.
- [46] N. Troy *et al.*, « Structural modification in Er-Yb doped zinc phosphate glasses with megahertz repetition rate femtosecond pulses », présenté à SPIE LASE, San Francisco, California, USA, 2012, p. 82470U.
- [47] D. L. Griscom, E. J. Friebele, K. J. Long, et J. W. Fleming, « Fundamental defect centers in glass: Electron spin resonance and optical absorption studies of irradiated phosphorus-doped silica glass and optical fibers », *Journal of Applied Physics*, vol. 54, n° 7, p. 3743-3762, juill. 1983.
- [48] J. de Bonfils, G. Panczer, D. de Ligny, S. Peugeot, et B. Champagnon, « Behaviour of simplified nuclear waste glasses under gold ions implantation: A microluminescence study », *Journal of Nuclear Materials*, vol. 362, n° 2-3, p. 480-484, mai 2007.
- [49] H. Rahimian, H. Mokhtari, et S. P. Shirmardi, « Improvement of Eu³⁺ emissions in oxyfluoride glass and nano glass-ceramic by electron beam irradiation », *Journal of Luminescence*, vol. 187, p. 535-539, juill. 2017.
- [50] M. Mohapatra, R. M. Kadam, R. K. Mishra, C. P. Kaushik, B. S. Tomar, et S. V. Godbole, « Gamma radiation induced changes in nuclear waste glass containing Eu », *Physica B: Condensed Matter*, vol. 406, n° 20, p. 3980-3984, oct. 2011.

List of Figures

FIGURE 1 FLAG LASER PLATFORM.....	162
FIGURE 2 EXPLANATION OF THE GEOMETRY USED FOR "LASER LINES" WRITING IN THE OPTICAL MATERIALS. IN THIS EXAMPLE THE GLASS WAS $\text{Li}_2\text{O-Nb}_2\text{O}_5\text{-SiO}_2$	163
FIGURE 3 TIMESCALES OF THE PHYSICAL PHENOMENA ASSOCIATED WITH THE INTERACTION.....	165
FIGURE 4 THREE STRUCTURAL MODIFICATION REGIMES CREATED BY FEMTOSECOND LASER WRITING IN SILICA.....	167
FIGURE 5 (A) WHITE LIGHT MICROSCOPIC IMAGE OF LINES WRITTEN BY FEMTOSECOND LASER WITH REPETITION RATE OF 10 KHZ AND DIFFERENT PULSE ENERGIES INSIDE META-NA-EU GLASS AT 300 μM BELOW THE SURFACE THROUGH A 10 \times OBJECTIVE, (B) MICROSCOPIC IMAGE OF A SERIES OF LINES ALONG THE Z AXIS (CROSS-SECTION OF THE LASER SPOT) INSCRIBED BY PULSE ENERGY RANGING IN 5-0.5 μJ THROUGH 20 \times OBJECTIVE (C) ZOOM OF THE PROFILE OF THE LINE INSCRIBE BY 4 μJ PULSE ENERGY ALONG THE Z AXIS.....	170
FIGURE 6 THE LONGITUDINAL LASER SPOT ELONGATION (IN THE LASER PROPAGATION DIRECTION) AS A FUNCTION OF PULSE ENERGY IN META-NA-EU GLASS.....	170
FIGURE 7 (A) MICROSCOPIC IMAGE OF THE CENTER AND THE TIP OF THE LASER LINE CROSS-SECTION IRRADIATED AT 4 μJ PULSE ENERGY IN META-NA-EU GLASS THROUGH A 100 \times OBJECTIVE. THE RED DOTS POSITIONS ASSOCIATED TO THE RAMAN CARTOGRAPHY. (B) THE RAMAN CARTOGRAPHY OF THE DIFFERENT RED DOTS POSITIONS IN THE CENTER AND THE TIP OF THE TRANSVERSAL LASER TRACE.....	172
FIGURE 8 (A) MICROSCOPIC IMAGE OF THE CENTER OF THE CROSS-SECTION LASER LINE IRRADIATED AT 4 μJ PULSE ENERGY IN META-NA-EU GLASS THROUGH A 100 \times OBJECTIVE WHICH THE RED DOTS POSITIONS ASSOCIATED TO THE RAMAN CARTOGRAPHY. (B) THE RAMAN CARTOGRAPHY OF THE BLACK REGION IN THE CENTER OF THE TRANSVERSAL LASER TRACE AS SHOWN BY THE RED DOTS IN THE MICROSCOPIC IMAGE.....	173
FIGURE 9 (A) MICROSCOPIC IMAGE OF THE TAIL OF THE CROSS-SECTION LASER LINE IRRADIATED AT 4 μJ PULSE ENERGY IN META-NA-EU GLASS THROUGH A 100 \times OBJECTIVE WHICH THE RED DOTS POSITIONS ASSOCIATED TO THE RAMAN CARTOGRAPHY. (B) THE RAMAN CARTOGRAPHY OF THE RED DOTS POSITIONS IN THE TAIL OF THE TRANSVERSAL LASER TRACE COMPARED TO UNMODIFIED REGION.....	174
FIGURE 10 RAMAN SPECTRA OF THE CENTER OF THE CROSS-SECTION LASER LINE IN META-NA-EU INSCRIBED BY PULSE ENERGY OF (A) 3 μJ AND (B) 1 μJ COMPARED TO PRISTINE GLASS.....	175
FIGURE 11 (A) MICROSCOPIC IMAGE OF THE CROSS-SECTION LASER LINE IRRADIATED AT 4 μJ PULSE ENERGY IN META-NA GLASS THROUGH A 100 \times OBJECTIVE. THE RED DOTS POSITIONS ASSOCIATED TO THE RAMAN CARTOGRAPHY. (B) THE RAMAN CARTOGRAPHY OF ALL-REGION OF THE TRANSVERSAL LASER TRACE AS SHOWN BY THE RED DOTS IN THE MICROSCOPIC IMAGE COMPARED TO UNMODIFIED REGION.....	176
FIGURE 12 (A) MICROSCOPIC IMAGE OF THE CROSS-SECTION LASER LINE IRRADIATED AT 3 μJ PULSE ENERGY IN META-NA-ER GLASS THROUGH A 100 \times OBJECTIVE. THE RED DOTS POSITIONS ASSOCIATED TO THE RAMAN CARTOGRAPHY. (B) THE RAMAN CARTOGRAPHY OF ALL-REGION OF THE TRANSVERSAL LASER TRACE AS SHOWN BY THE RED DOTS IN THE MICROSCOPIC IMAGE COMPARED TO THE UNMODIFIED REGION.....	176
FIGURE 13 MICROSCOPIC IMAGE OF A SERIES OF LINES ALONG THE Z AXIS (CROSS-SECTION OF THE LASER SPOT) INSCRIBED AT VARIOUS PULSE ENERGY RANGING THROUGH 50 \times OBJECTIVE IN META-ZN-EU GLASS.....	177
FIGURE 14 (A) MICROSCOPIC IMAGE OF THE CROSS-SECTION LASER LINE IRRADIATED AT 4 μJ PULSE ENERGY IN META-ZN-EU GLASS THROUGH A 100 \times OBJECTIVE. THE RED DOTS POSITIONS ASSOCIATED TO THE RAMAN CARTOGRAPHY. (B) THE RAMAN CARTOGRAPHY OF THE CENTER OF THE TRANSVERSAL LASER TRACE AS SHOWN BY THE RED DOTS IN THE MICROSCOPIC IMAGE COMPARED TO THE UNMODIFIED REGION.....	178
FIGURE 15 (A) MICROSCOPIC IMAGE OF THE CROSS-SECTION LASER LINE IRRADIATED AT 4 μJ PULSE ENERGY IN META-ZN-EU GLASS THROUGH A 100 \times OBJECTIVE. THE RED DOTS POSITIONS ASSOCIATED TO THE RAMAN CARTOGRAPHY. (B) THE RAMAN CARTOGRAPHY OF THE TAIL OF THE TRANSVERSAL LASER TRACE AS SHOWN BY THE RED DOTS IN THE MICROSCOPIC IMAGE COMPARED TO THE UNMODIFIED REGION.....	179
FIGURE 16 (A) MICROSCOPIC IMAGE OF THE LASER LINES CROSS SECTION WRITTEN WITH REPETITION RATE OF 10 KHZ AND DIFFERENT PULSE ENERGIES AT 300 μM BELOW THE SURFACE OF POLY-ZN-NA-EU GLASS THROUGH A 10 \times OBJECTIVE (B) A ZOOM OF THE MICROSCOPIC IMAGE OF THE LASER TRACE CROSS SECTION INSCRIBED AT 2 μJ PULSE ENERGY IN POLY-ZN-NA-EU.....	180

FIGURE 17 THE LONGITUDINAL LASER SPOT ELONGATION (ALONG THE LASER PROPAGATION DIRECTION) AS A FUNCTION OF PULSE ENERGY IN POLY-ZN-NA-EU GLASS.	180
FIGURE 18 (A) MICROSCOPIC IMAGE OF THE CENTER AND THE TIP OF THE CROSS-SECTION LASER LINE IRRADIATED AT 4 μJ PULSE ENERGY IN POLY-ZN-NA-EU GLASS THROUGH A 100 \times OBJECTIVE. THE RED DOTS POSITIONS ASSOCIATED TO THE RAMAN CARTOGRAPHY. (B) THE RAMAN CARTOGRAPHY OF THE CENTER IN THE TRANSVERSAL LASER TRACE AS SHOWN BY THE RED DOTS IN THE MICROSCOPIC IMAGE COMPARED TO THE UNMODIFIED REGION.....	181
FIGURE 19 (A) MICROSCOPIC IMAGE OF THE TAIL OF THE CROSS-SECTION LASER LINE IRRADIATED AT 4 μJ PULSE ENERGY IN POLY-ZN-NA-EU GLASS THROUGH A 100 \times OBJECTIVE. THE RED DOTS POSITIONS ASSOCIATED TO THE RAMAN CARTOGRAPHY. (B) THE RAMAN CARTOGRAPHY OF THE TAIL OF THE TRANSVERSAL LASER TRACE AS SHOWN BY THE RED DOTS IN THE MICROSCOPIC IMAGE COMPARED TO THE UNMODIFIED REGION.....	182
FIGURE 20 (A) MICROSCOPIC IMAGE OF THE CROSS-SECTION LASER LINE IRRADIATED AT 4 μJ PULSE ENERGY IN POLY-ZN-NA GLASS THROUGH A 100 \times OBJECTIVE. THE RED DOTS POSITIONS ASSOCIATED TO THE RAMAN CARTOGRAPHY. (B) THE RAMAN CARTOGRAPHY OF ALL-REGION OF THE TRANSVERSAL LASER TRACE AS SHOWN BY THE RED DOTS IN THE MICROSCOPIC IMAGE COMPARED TO UNMODIFIED REGION.	183
FIGURE 21 (A) MICROSCOPIC IMAGE OF THE CROSS-SECTION LASER LINE IRRADIATED AT 4 μJ PULSE ENERGY IN POLY-ZN-NA-ER GLASS THROUGH A 100 \times OBJECTIVE. THE RED DOTS POSITIONS ASSOCIATED TO THE RAMAN CARTOGRAPHY. (B) THE RAMAN CARTOGRAPHY OF ALL-REGION OF THE TRANSVERSAL LASER TRACE AS SHOWN BY THE RED DOTS IN THE MICROSCOPIC IMAGE COMPARED TO UNMODIFIED REGION.	183
FIGURE 22 (A) MICROSCOPIC IMAGE OF THE CROSS-SECTION LASER TRACE IRRADIATED AT HIGH REPETITION RATE (500 KHZ) AND 0.8 μJ PULSE ENERGY IN POLY-ZN-NA GLASS THROUGH A 100 \times OBJECTIVE. THE RED DOTS POSITIONS ASSOCIATED TO THE RAMAN CARTOGRAPHY. (B) THE RAMAN CARTOGRAPHY OF THE DIFFERENT POSITION OF THE TRANSVERSAL LASER TRACE IN THE TIP, THE SPOT CENTER AND THE TAIL.	184
FIGURE 23 IMAGE OF THE CROSS SECTION IRRADIATED LINES IN POLY-ZN-NA-EU TAKEN (A) WITHOUT AND (B) WITH POLARIZERS (DIAGONAL POSITION WITH RESPECT TO THE POLARIZERS). DISTANCE BETWEEN EACH LINE IS 40 μM , PULSE ENERGY RANGING IN 4.5-0.5 μJ	185
FIGURE 24 ILLUSTRATIONS OF THE PROFILES OF THE AVERAGED PHASE DIFFERENCE BETWEEN THE GLASS MATRIX AND IRRADIATED LINES ALONG THE SCANNING DIRECTION.	186
FIGURE 25 THE MICROSCOPIC IMAGE OF THE IRRADIATED LINES IN META-NA-LI-EU USED TO ANALYZE DATA AND EXTRACT THE PROFILES OF THE AVERAGED PHASE VARIATION (ABOVE).THE PROFILES OF THE AVERAGED PHASE DIFFERENCE BETWEEN THE UNMODIFIED REGION AND IRRADIATED LINES ALONG THE SCANNING DIRECTION AT DIFFERENT PULSE ENERGY (4.5, 4, 3.5, 3 AND 2.5 μJ) (BELOW).....	187
FIGURE 26 THE AVERAGE PHASE DIFFERENCE $\Delta\Phi$ BETWEEN THE UNMODIFIED REGION AND IRRADIATED CENTER LINES AS A FUNCTION OF THE PULSE ENERGY RANGING IN 5 μJ - 0.05 μJ IN META-NA, META-NA-EU AND META-NA-ER GLASSES.	189
FIGURE 27 THE AVERAGE PHASE DIFFERENCE $\Delta\Phi$ BETWEEN THE UNMODIFIED REGION AND IRRADIATED CENTER LINES AS A FUNCTION OF THE PULSE ENERGY RANGING IN 5 μJ - 0.05 μJ IN (A) NON-DOPED AND EU DOPED ZINC SODIUM POLYPHOSPHATE (POLY-ZN-NA AND POLY-ZN-NA-EU) AND (B) NON-DOPED AND EU DOPED ZINC MIXED SODIUM POTASSIUM POLYPHOSPHATE GLASSES (POLY-ZN-NA-K AND POLY-ZN-NA-K-EU).	190
FIGURE 28 THE AVERAGE PHASE DIFFERENCE $\Delta\Phi$ BETWEEN THE UNMODIFIED REGION AND IRRADIATED CENTER LINES AS A FUNCTION OF THE PULSE ENERGY RANGING IN 5 μJ - 0.05 μJ IN (A) NON-DOPED (META-NA AND META-NA-LI) AND (B) EU DOPED METAPHOSPHATE GLASSES (META-NA-EU AND META-NA-LI-EU).	190
FIGURE 29 THE AVERAGE PHASE DIFFERENCE $\Delta\Phi$ BETWEEN THE UNMODIFIED REGION AND IRRADIATED CENTER LINES AS A FUNCTION OF THE PULSE ENERGY RANGING IN 5 μJ - 0.05 μJ IN (A) NON-DOPED ZINC POLYPHOSPHATE (POLY-ZN-NA, POLY-ZN-K AND POLY-ZN-NA-K) AND (B) EU DOPED ZINC POLYPHOSPHATE (POLY-ZN-NA-EU, POLY-ZN-K-EU AND POLY-ZN-NA-K-EU).....	191
FIGURE 30 THE PHOTOLUMINESCENCE SPECTRA OF MODIFIED AND UNMODIFIED META-NA GLASS FOR VARIOUS FS LASER PULSE ENERGY RANGING IN 1-5 μJ ($\lambda_{\text{EXT}}=458 \text{ NM}$).....	192

FIGURE 31 THE MAXIMUM INTENSITY OF THE POHC EMISSION BAND (A) AND THE AVERAGE PHASE DIFFERENCE $\Delta\Phi$ BETWEEN THE UNMODIFIED REGION AND IRRADIATED CENTER LINES (B) AS A FUNCTION OF THE PULSE ENERGY RANGING IN $5\ \mu\text{J}$ - $0.05\ \mu\text{J}$ IN NON-DOPED ALKALI (NA AND NALI) METAPHOSPHATE GLASSES. 192	192
FIGURE 32 EPR SPECTRUM OF POHC DEFECTS CREATED UNDER 200 LINES OF 3 MM LONG WRITTEN AT $300\ \mu\text{M}$ BELOW THE SURFACE USING FS LASER AT 10 KHZ REPETITION RATE AND PULSE ENERGY OF $2\ \mu\text{J}$ IN NON-DOPED AND EU DOPED NA METAPHOSPHATE GLASSES 193	193
FIGURE 33 EPR SPECTRUM OF POHC AND PEROXY DEFECTS CREATED UNDER 200 LINES OF 3 MM LONG WRITTEN AT $300\ \mu\text{M}$ BELOW THE SURFACE USING FS LASER AT 10 KHZ REPETITION RATE AND PULSE ENERGY OF $3.5\ \mu\text{J}$ IN NON-DOPED AND EU DOPED NA ZINC POLYPHOSPHATE GLASSES 193	193
FIGURE 34 (A) MICROSCOPIC IMAGE OF THE LASER LINE CROSS-SECTION IRRADIATED AT $4\ \mu\text{J}$ PULSE ENERGY IN META-NA-EU GLASS THROUGH A $100\times$ OBJECTIVE. (B) THE CORRESPONDING EMISSION CARTOGRAPHY OF THE Eu^{3+} IONS IN THE RED BOXED AREA AS DISPLAYED IN THE MICROSCOPIC IMAGE. THE PL SPECTRA WERE RECORDED IN THE RED BOXED REGION EACH $4\ \mu\text{M}$ ALONG THE X AXIS AND EACH $10\ \mu\text{M}$ ALONG THE Y AXIS. 196	196
FIGURE 35 (A) MICROSCOPIC IMAGE OF THE LASER LINE CROSS-SECTION IRRADIATED AT 10 KHZ REPETITION RATE AND $4\ \mu\text{J}$ PULSE ENERGY IN POLY-ZN-NA-EU GLASS THROUGH A $100\times$ OBJECTIVE. (B) THE CORRESPONDING EMISSION CARTOGRAPHY OF THE Eu^{3+} IONS IN THE RED BOXED AREA AS DISPLAYED IN THE MICROSCOPIC IMAGE. THE PL SPECTRA WERE RECORDED IN THE RED BOXED REGION EACH $1.5\ \mu\text{M}$ ALONG THE X AXIS AND EACH $7.5\ \mu\text{M}$ ALONG THE Y AXIS. 197	197
FIGURE 36 THE ASYMMETRY RATIO (AS) VARIATION (${}^5\text{D}_0\text{-}{}^7\text{F}_2 / {}^5\text{D}_0\text{-}{}^7\text{F}_1$) CORRESPOND TO THE EMISSION CARTOGRAPHY OF THE Eu^{3+} IONS IN THE LASER LINE CROSS-SECTION IRRADIATED AT 10 KHZ REPETITION RATE AND $4\ \mu\text{J}$ PULSE ENERGY IN (A) META-NA-EU AND (B) POLY-ZN-NA-EU GLASSES COMPARED TO UNMODIFIED REGION AND PRISTINE GLASSES. 198	198
FIGURE 37 ZOOM OF THE EMISSION CARTOGRAPHY OF THE Eu^{3+} IONS ATTRIBUTED TO THE ${}^5\text{D}_0\text{-}{}^7\text{F}_0$ TRANSITION IN THE LASER LINE CROSS-SECTION IRRADIATED AT 10 KHZ REPETITION RATE AND $4\ \mu\text{J}$ PULSE ENERGY IN (A) META-NA-EU AND (B) POLY-ZN-NA-EU GLASSES. (ZOOM OF THE PL CARTOGRAPHY CORRESPOND TO FIG 34 AND 35) 199	199
FIGURE 38 THE FULL WIDTH AT HALF MAXIMUM (FWHM) OF THE ${}^5\text{D}_0\text{-}{}^7\text{F}_0$ EMISSION BAND IN THE TAIL AND THE CENTER OF THE TRANSVERSAL LASER TRACE INSCRIBED AT $4\ \mu\text{J}$ PULSE ENERGY COMPARED TO UNMODIFIED REGION IN (A) META-NA-EU AND (B) POLY-ZN-NA-EU GLASSES. 200	200
FIGURE 39 EPR SPECTRA NORMALIZED BY GAIN OF EU DOPED META AND POLYPHOSPHATE GLASSES INSCRIBED BY FEMTOSECOND LASER WITH 200 LINES OF 3 MM LONG WRITTEN AT $300\ \mu\text{M}$ BELOW THE SURFACE AT REPETITION RATE OF 10 KHZ. 201	201

List of Tables

TABLE 1 TYPICAL DATA FOR WRITING LINES BY IRRADIATION WITH THE ENERGY OF EACH LINE. 164	164
TABLE 2 TYPE OF DEFECT, AVERAGE PHASE DIFFERENCE AND INTENSITY PEAK TO PEAK OF THE EPR SIGNAL OF POHC AND PEROXY DEFECTS CREATED IN METAPHOSPHATE AND POLYPHOSPHATE GLASSES UNDER FS WRITING. 194	194

Conclusions
and
Perspectives

Conclusions and Perspectives

In this thesis, we were interested in understanding the mechanisms leading to the structural modifications of Zn polyphosphate and metaphosphate glasses under various radiation types: electrons and photons (femtosecond laser) in order to study and control the RE doping ions environment via almost the resulting luminescence properties.

The study has been carried out by looking for the impact of some factors such as glass chemical composition and irradiation conditions. The glasses were thus synthesized with different alkaline and alkali-earth ions (Na, Li, K and Mg) and different polymerization degree and the influence of electron energy, and integrated dose, pulse laser energy and repetition rate) was examined.

In addition to experimental measurements (photoluminescence, Raman and EPR), molecular dynamics simulations on the unirradiated phosphate glass systems have been realized in order to determine in particular the coordination number of the Eu^{3+} ions and the distance of the nearest neighbors, and to interpret the results obtained after irradiation, in particular the role of ZnO.

We evidenced in this PhD that the glass composition and the irradiation conditions impact strongly the Eu^{3+} local environment evolution as well as the glass network changes. In particular, we highlighted that the site symmetry of Eu^{3+} is strongly affected in alkali metaphosphate whatever the dose. Eu^{2+} is more efficiently produced under 700 keV irradiation and it is striking to notice that we can control the ratio between them by changing dose and energy. We also proved that some crystallization occurs in metaphosphate glasses under 10 KHz fs-laser.

More precisely, the main results of this thesis were obtained by using electron irradiation with electron energy of 700 keV and 2.5 MeV. Studying the structure evolution under 2.5 MeV electron irradiation, we demonstrate no significant network evolution of the Na metaphosphate glass whatever the integrated dose whereas there is a slight variation of the vitreous network in mixed Na/Li,Na/Mg and Zn metaphosphate glasses at high dose from 10^8 Gy traduced by an increase of the O-P-O bond angle, a variation in the local cationic environment and a growth of the disorder that may be due to change in the distribution of the Q^2 P-O bond length and bond angles.. In polyphosphate glasses, there is a significant

variation of the structure under 2.5 MeV irradiation and the bond breaking occurs at high dose from 10^8 Gy dose with the massive creation of Q^1 terminators. The same behavior of the structure evolution is observed under 700 keV for Zn metaphosphate and polyphosphate. As well, the structure appears to be changed in a larger volume than the penetration depth of electron especially in polyphosphate glass.

Examining the local environment of the Eu^{3+} ions, we have shown an important increase of the asymmetry ratio (As) from 3.1-3.3 in pristine glasses to 5.6-6 at high dose (1.5×10^9 Gy) indicating a significant decrease of the site symmetry of the Eu^{3+} as well as/or a higher Eu-O covalency. This effect is strong in alkali metaphosphate glasses whereas the variation of the asymmetry ratio is less pronounced in phosphate glasses containing ZnO, meaning that the local variation of the Eu^{3+} symmetry is decorrelated from the network variation. We explained those results by considering the MD calculations based on the fact that the Na metaphosphate glasses exhibit an average coordination number for Eu^{3+} ions close to 6 contrary to Zn glasses where it is lower.

Concerning the impact of the energy and dose For a 10^9 Gy dose, we observe a similar modification of the site symmetry under both energies irradiation in all kinds of phosphate glasses. Even more, at 10^9 Gy under 700 keV irradiation, the mixed alkali Na/Li metaphosphate and Na/K polyphosphate glasses support a larger reduction of the Eu^{3+} site symmetry. All these results demonstrate that the alkali ion migration operating under 700 keV and 2.5 MeV (doses $> 10^9$ Gy) are involved in the local Eu^{3+} environment variation showing a larger site dispersion after irradiation whatever the conditions

The EPR and PL spectroscopy show the presence of two types of sites for divalent Eu^{2+} ions formed in metaphosphate and polyphosphate glasses whatever the dose and electron energy. Based on molecular dynamics calculation and literature, we tentatively associated the high symmetry site ($g=4.7$) to a strong crystal field that could correspond to 6-coordinated Eu^{3+} ions. The low-symmetry site ($g=6.3$) with a lower crystal field would rather deal with Eu^{2+} ions under a higher coordination number into a modifier position. We evidenced that the presence of Zn favors the formation of the high-symmetry site with a quasi-linear increase of both sites with increasing doses. When dose becomes higher than 10^9 Gy, we observed a predominance of modifier sites onto network former sites linked to the migration of alkaline ions. In the other hand, 700 keV energy is much more efficient to reduce Eu^{3+} ions than 2.5

MeV and the generation of Eu^{2+} ions is more important in polyphosphate than in metaphosphate compositions.

Concerning the structural modifications under femtosecond laser writing with low repetition rate of 10 kHz, some evidence of crystallization in the center of the transversal laser traces of the Eu-doped Na and Zn metaphosphate were observed whatever the pulse energy in the $1\mu\text{J}$ - $4\mu\text{J}$ range. Note that the Eu doping is needed for the crystallization of the glass. In contrast, zinc polyphosphate glasses display similar structural evolution as observed under electron irradiation when pulse energies are higher than $1\mu\text{J}$.

The refractive index measurement in irradiated alkali and alkali earth metaphosphate glasses (Na, Na+Li and Na+Mg) showed two behaviors: a strong negative refractive index change ($\text{max} = -3.7 \times 10^{-3}$) occur in the center of the fs laser irradiated lines and a positive change on both sides of the central irradiated region. Concerning the center of irradiated lines, we note a non-monotonous trend according to the pulse energy with a strongest negative changes for $1.5\text{-}2\mu\text{J/pulse}$

Moreover, we have shown an increase of Δn variation in the order Meta-Na-Er > Meta-Na-Eu > Meta-Na, which reveals the positive contribution of the RE ions in the refractive index change value under fs laser irradiation.

For zinc polyphosphate glasses, the maximum (negative amplitude) index change is obtained for higher energy ($3.5\text{-}4\mu\text{J}$). As well, these measurements confirm that the presence of RE ions in the glass lead to the raise of the index change.

Regarding the RE environment evolution, we measured a crucial decrease of the emission intensity of the Eu^{3+} ions in the transversal laser trace of Na and Zn metaphosphate glasses in the center and increase in the tail region. However, we observed no variation of the emission intensity for zinc polyphosphate composition where no formation of POHC defect was evidenced suggesting the impact of POHC defects which present 2 absorption bands at 410 and 540 nm [3].

The asymmetry ratio variation after fs laser writing in Eu-doped glasses behaves differently to those reported under electron irradiation. Thus, the decrease of As value to 2.75 in the center of the transversal laser trace in Meta-Na-Eu is in agreement with the tendency of this glass to crystallize, Eu^{3+} ion belonging to crystallized phases. This effect is inferred by

sharpening of the emission band of the ${}^5D_0\text{-}{}^7F_0$. However, for Poly-Zn-Na-Eu glass, the As ratio suffers a slight increase from 3.3 in unmodified region to 3.63 in the center of the transversal laser trace irradiated at 4 μJ pulse energy as well as a broadening of the ${}^5D_0\rightarrow{}^7F_0$ emission band, identically to electron irradiation effects. In contrast to electron irradiation, there is no formation of divalent europium in the different phosphate glasses under fs laser writing at low repetition rate.

From this work, we can say that it is possible to manage the europium environment in phosphate glasses under irradiation by electron and femtosecond laser by playing on the glass composition as well as irradiation condition like energy, dose, scanning speed and repetition rate.

However this study should be followed by some other because there are still other questions to solve.

The results concerning the Eu environment modification under electron irradiation are not interpreted clearly due to the limitations of PL and EPR spectroscopy. The use of XAS (XANES and EXAFS) definer acronym experiments in non-irradiated and irradiated glasses to study the Eu^{3+} environment variation in term of coordination number and Eu-O distances would help to better characterize the site distribution and symmetry evolutions of the Eu^{3+} sites as well as understand the mechanisms leading to the reduction of Eu^{3+} to Eu^{2+} ions after irradiation (what about the exact Eu^{2+} environment).

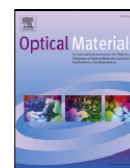
The part dedicated to fs-laser study was limited in this work, many complementary measurements could be done. It will be interesting to purchase the analysis at high repetition rate of 500 kHz in a cumulative-heating regime on all samples including the Er-doped phosphate glasses to understand better the role of RE ions in the refractive index change and the glass structure evolution. Moreover, in this regime we know that ion migration occurs and it will help to cartography those elements by SEM and to compare the structural evolutions and chemical elements repartitions under both repetition rates. The mapping of point defects in the laser trace as well as potential divalent Eu^{2+} could also be performed by EPR spectroscopy.

- [1] A. Ladaci, S. Girard, L. Mescia, T. Robin, A. Laurent, B. Cadier, M. Boutillier, A. Morana, D. Di Francesca, Y. Ouerdane, A. Boukenter, X-rays, γ -rays, electrons and protons radiation-induced changes on the lifetimes of Er $3+$ and Yb $3+$ ions in silica-based optical fibers, *Journal of Luminescence*. 195 (2018) 402–407.
doi:10.1016/j.jlumin.2017.11.061.
- [2] V. Pukhkaya, P. Goldner, A. Ferrier, N. Ollier, Impact of rare earth element clusters on the excited state lifetime evolution under irradiation in oxide glasses, *Optics Express*. 23 (2015) 3270–3281.
- [3] D.L. Griscom, E.J. Friebele, K.J. Long, J.W. Fleming, Fundamental defect centers in glass: Electron spin resonance and optical absorption studies of irradiated phosphorus-doped silica glass and optical fibers, *Journal of Applied Physics*. 54 (1983) 3743–3762.
doi:10.1063/1.332591.



Contents lists available at ScienceDirect

Optical Materials

journal homepage: www.elsevier.com/locate/optmat

Tuning Eu^{2+} amount and site symmetry in phosphate glasses under irradiation by electron energy and integrated dose

Mohamed Mahfoudhi^{*}, Nadège Ollier

Laboratoire des Solides Irradiés (LSI), CEA-DRF-IRAMIS, Ecole Polytechnique, CNRS Institut Polytechnique de Paris, F-91128, Palaiseau, France



ARTICLE INFO

Keywords:

Electron irradiation
Divalent europium
Phosphate glasses
Photoluminescence
Electron paramagnetic resonance (EPR)

ABSTRACT

This paper relates the formation of Eu^{2+} under 700 keV and 2.5 MeV irradiation in meta and polyphosphate glasses. EPR and photoluminescence measurements evidenced the presence of two sites for Eu^{2+} ions corresponding to low-symmetry and high-symmetry sites. We highlighted that the glass composition and in particular the presence of ZnO favors the formation of high-symmetry sites. Moreover, we found out that 700 keV electron energy is much more efficient to produce Eu^{2+} ions compared to 2.5 MeV. This is probably linked to an enhancement of the alkaline migration generated under the charge depletion induced by the 700 keV electrons implantation. This migration depolymerizes the network structure and tends to favor the formation of Eu^{2+} . The same tendency is observed at 2.5 MeV when the dose is higher than 1 GGy.

1. Introduction

Phosphate glasses are known as suitable matrix to incorporate large amount of Rare Earth Element (REE) and limiting clustering effect contrary to silica. P atoms in silica fibers were also proved to be powerful in the Yb cluster dissolution [1]. Moreover, their low T_g (lower than 450 °C) makes them interesting for industrial applications such as optics, biomedicine, data storage and energy applications [2–8]. Rare earth element doped glasses are commonly used in optics as amplifier, laser materials ...

Many recent papers [10–13] show the interest of Eu-doped glasses (aluminosilicate, fluoro-aluminoborate, tellurite, lead phosphate) for phosphors and luminophore applications.

Eu^{2+} is one of the REE used in phosphor materials by emitting light in a broad blue range due to $4f \rightarrow 5d$ transitions, while Eu^{3+} ions exhibit lines narrower in the red range.

From the applicative point of view, it can be very attractive to adjust the emission spectra of Eu-doped phosphors by modifying $\text{Eu}^{2+}/\text{Eu}^{3+}$ relative concentration and site symmetry of each valence state. Different solutions exist to reach this goal: the first one is to produce glasses under reduced atmosphere that mostly affects the $\text{Eu}^{2+}/\text{Eu}^{3+}$ ratio. Some papers report a heat treatment or play on the glass composition to reduce the Eu^{3+} into Eu^{2+} ions. As an example, Bouchouicha et al. [13] investigated the luminescence properties of Eu^{2+} ions in calcium aluminosilicate glass-ceramics after annealing and they reported a remarkable increase of the emission intensity and a shift

towards lower wavelength with increasing time-heat treatment. This phenomenon is interpreted by the incorporation of Eu^{2+} ions into crystalline phases after the reduction of Eu^{3+} ions.

The second one resides on the use of irradiation. The reduction of Eu^{3+} into divalent Eu^{2+} was demonstrated in literature by using electrons in borosilicate by Mougnaud et al. [14] and in aluminoborosilicate glasses by Malchukova et al. [15] or by UV laser and X-ray by Ehrt et al. [16,17] in phosphate. Furthermore, the reduction of the Eu^{3+} to Eu^{2+} ions under femtosecond laser irradiation has been also observed in aluminoborosilicate glasses [18] or borate glasses [19]. Qiu et al. [20] were the first to evidence electron trapping on Eu^{3+} under fs laser in fluorozirconate type glass. We also evidenced strong modification of the Eu^{3+} site symmetry depending on the dose and glass composition in agreement with the few works in literature that reported a Eu^{3+} ions environment variation under electron in oxyfluoride glass [21] and in borosilicate glasses under gamma [22] and gold ion irradiation [23]. Our results will be published in a coming article.

In the present study, we will show how it is possible to impact both the site symmetry and the amount of produced Eu^{2+} by optimizing the electron energy (700 keV vs 2.5 MeV) and the integrated dose from 10^5 to 4×10^9 Gy in phosphate glass types (metaphosphate and polyphosphate). The site dependence versus the nature of the glass additionally will be also analyzed.

^{*} Corresponding author.

E-mail address: mohamed.mahfoudhi@polytechnique.edu (M. Mahfoudhi).

<https://doi.org/10.1016/j.optmat.2019.109253>

Received 29 May 2019; Received in revised form 2 July 2019; Accepted 15 July 2019
0925-3467/© 2019 Published by Elsevier B.V.

Table 1
Nominal glass composition (mol%).

Samples	Mol. %						
	P ₂ O ₅	Na ₂ O	Li ₂ O	K ₂ O	ZnO	MgO	Eu ₂ O ₃
Metaphosphate glasses							
Meta-Na-Eu	49.40	49.40					1.20
Meta-Na-Li-Eu	49.40	24.70	24.70				1.20
Meta-Na-Mg-Eu	49.40	32.90				16.50	1.20
Meta-Zn-Eu	49.40				49.40		1.20
Polyphosphate glasses							
Poly-Zn-Na-Eu	33.00	19.80			46.00		1.20
Poly-Zn-K-Eu	33.00			19.80	46.00		1.20
Poly-Zn-K-Na-Eu	33.00	9.90		9.90	46.00		1.20
Poly-Zn-Na-Eu (Q ₁ /Q ₂ :50/50)	39.52	38.52			19.76		1.20

2. Experimental part

Various undoped and Eu-doped phosphate glasses were prepared by the standard melt-quenching method. Appropriate amounts of (NH₄)₂HPO₄, Na₂CO₃, Li₂CO₃, K₂CO₃, MgO, ZnO and Eu₂O₃ were mixed and melted slowly in silica crucible up to 900–1200 °C depending on the composition using electric muffle furnace. The melted glass was quenched rapidly into Pt–Au crucible at 230 °C and then annealed immediately at 270 °C to release residual internal strains.

The nominal glass composition is presented in Table 1.

The glass samples were irradiated by SIRIUS electron accelerator (Laboratoire des Solides Irradiés, Palaiseau, France) with 2.5 MeV electron beam at various doses from 10⁵ Gy to 4.15 × 10⁹ Gy and with 700 keV electrons at 10⁸ and 10⁹ Gy. With 2.5 MeV electrons, the whole sample volume (4 × 4 × 0.8 mm) was homogeneously irradiated contrary to 700 keV energy where electrons are stopped in the glass at 600 μm depth (sample thickness ~1.2 mm).

Time-resolved photoluminescence (PL) spectra were recorded using Shamrock SR-303i spectrometer related to an ANDOR ICCD camera. The curves were measured the static photoluminescence emission spectra after excitation with 355 nm laser (pulsed Nd: YAG INDI laser) were used.

The electron paramagnetic resonance (EPR) spectra were carried out with Bruker X-band EMX spectrometer at 9.8 GHz frequency. All measurements were performed at room temperature and the derivative signals obtained are normalized by mass sample and gain.

3. Results

A zoom of the time-resolved photoluminescence emission spectra under 355 nm excitation in the 400–525 nm range is exhibited in Fig. 1a and b. They correspond respectively to metaphosphate glass (Meta-Na-Eu) and polyphosphate glass (Poly-Zn-Na-Eu) irradiated by electrons of 2.5 MeV at various doses from 10⁵ Gy to 4.15 × 10⁹ Gy (delay = 200 ns and gate width = 30 μs). It seems that the large emission band at 460 nm increases with dose in metaphosphate glasses (Fig. 1a) while the emission spectra in polyphosphate glasses show a new narrow band between 400 and 450 nm. The intensity of this band tends to decrease with dose as shown in Fig. 1b. Nevertheless, a large band centered at 490 nm is visible on those spectra.

Fig. 2a and b compare the emission spectra of Meta-Na-Eu and Poly-Zn-Na-Eu irradiated by electrons of 700 keV and 2.5 MeV respectively at similar doses 10⁸ and 10⁹ Gy. Fig. 2a shows that the intensity of the emission band centered at 450 nm and attributed to Eu²⁺ ion is strongly increased after 700 keV electron irradiation compared to 2.5 MeV energy. Moreover, a red shift of the broad emission band occurs when the dose increases from 10⁸ to 10⁹ Gy for 700 keV electrons in Na metaphosphate glass. This emission shape variation could be explained by the existence of two different Eu²⁺ sites and the ratio between both

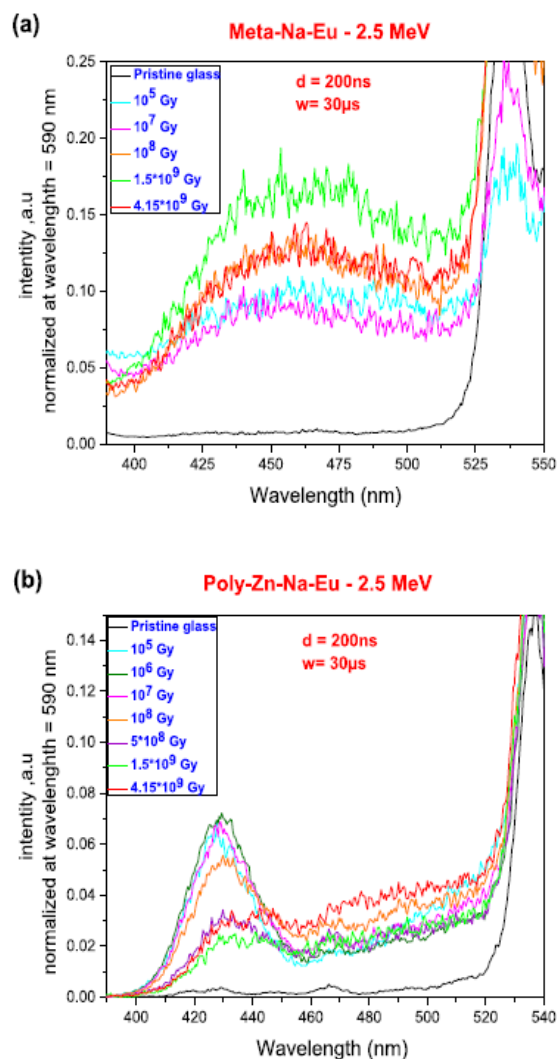


Fig. 1. The PL emission spectra of (a) Eu-doped metaphosphate glass Meta-Na-Eu and (b) Eu-doped polyphosphate glass Poly-Zn-Na-Eu after 2.5 MeV electron irradiation at various doses from 10⁵ to over 10⁹ Gy. ($\lambda_{exc} = 355$ nm).

sites depending on the dose. A careful fit of each emission spectra was performed, the results obtained for metaphosphate and polyphosphate at 700 keV and 10⁹ Gy are shown in Fig. 3. We observed 2 components at 450 and 500 nm in both glasses attesting the presence of 2 sites for Eu²⁺ ions. Fig. 2b displays as well a strong increase of the 500 nm band intensity after 700 keV electron irradiation compared to 2.5 MeV in polyphosphate glass.

Electronic paramagnetic resonance (EPR) spectroscopy is a powerful tool to obtain complementary quantitative data on Eu²⁺ formation under irradiation (indeed Eu²⁺ is a 4f⁷ paramagnetic ion). Fig. 4 displays the EPR spectra of Poly-Zn-Na-Eu glasses before and after 2.5 MeV irradiation for various doses. After irradiation, new signals at 1095 G ($g = 6.3$), 2466 G ($g = 2.8$) and 3500 G ($g = 2.0$) can be observed. These components are known as the “U” EPR signal and can be attributed to Eu²⁺ ions associated to a low-symmetry site whereas the signal at 1492 Gauss ($g = 4.7$) corresponds to a high-symmetry site of

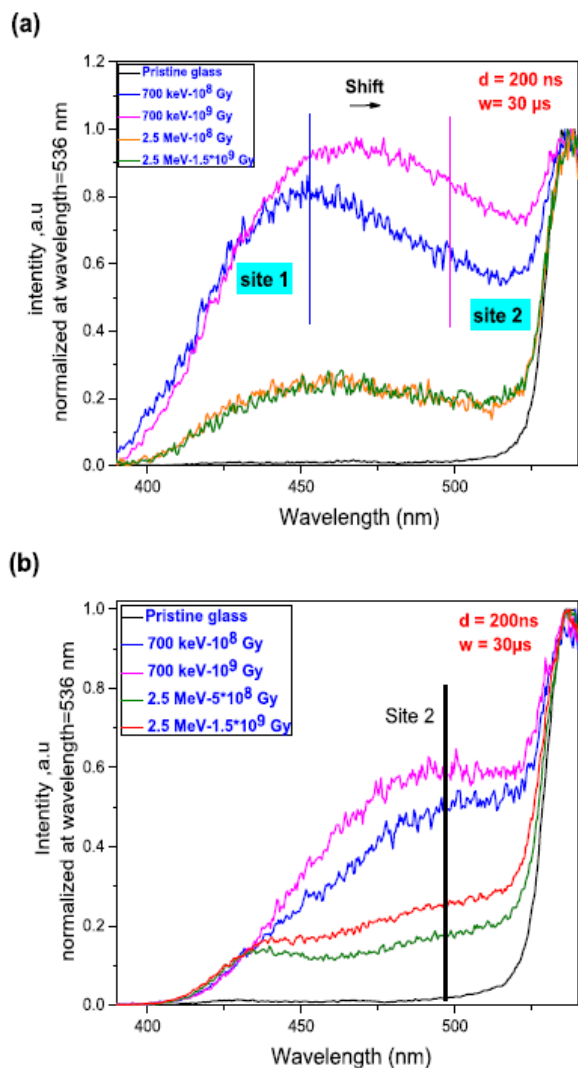


Fig. 2. The PL emission spectra of (a) Eu-doped metaphosphate glass (Meta-Na-Eu) and (b) Eu-doped polyphosphate glass (Poly-Zn-Na-Eu) after 700 keV and 2.5 MeV electron irradiation at 10^8 and 10^9 Gy doses. ($\lambda_{exc} = 355$ nm).

divalent europium [12]. We can observe at $g = 2$ a sharp saturated line that corresponds to the P-related point defects such as POHC (Phosphorus Oxygen Hole Centers). The detailed nature of point defects associated to P will not be described here. Furthermore, we can notice that all the signals associated to Eu^{2+} directly correlated to the Eu^{2+} amount increases with the irradiation dose.

Fig. 5a and b report the peak to peak intensity of the EPR signals at $g = 6.3$ and $g = 4.7$ of Meta-Na-Eu, Meta-Zn-Eu, Poly-Zn-Na-Eu and Poly-Zn-Na-Eu ($Q^1/Q^2:50/50$) corresponding to low and high symmetry sites of Eu^{2+} respectively as a function of the dose logarithm. We observe in Fig. 5a and b that both signals are weak and constant regardless of the dose in Meta-Na-Eu glass. In contrast, in presence of zinc oxide in the glasses, a quasi-linear increase of both lines at $g = 6.3$ and $g = 4.7$ occurs with the dose logarithm. The formation of Eu^{2+} is more efficient in Poly-Zn-Na-Eu ($Q^1/Q^2:50/50$) than in Poly-Zn-Na-Eu, while meta-Zn-Eu and Poly-Zn-Na-Eu exhibits quite similar efficiency of Eu^{3+} reduction under irradiation. Moreover, it can be notice that a lowest

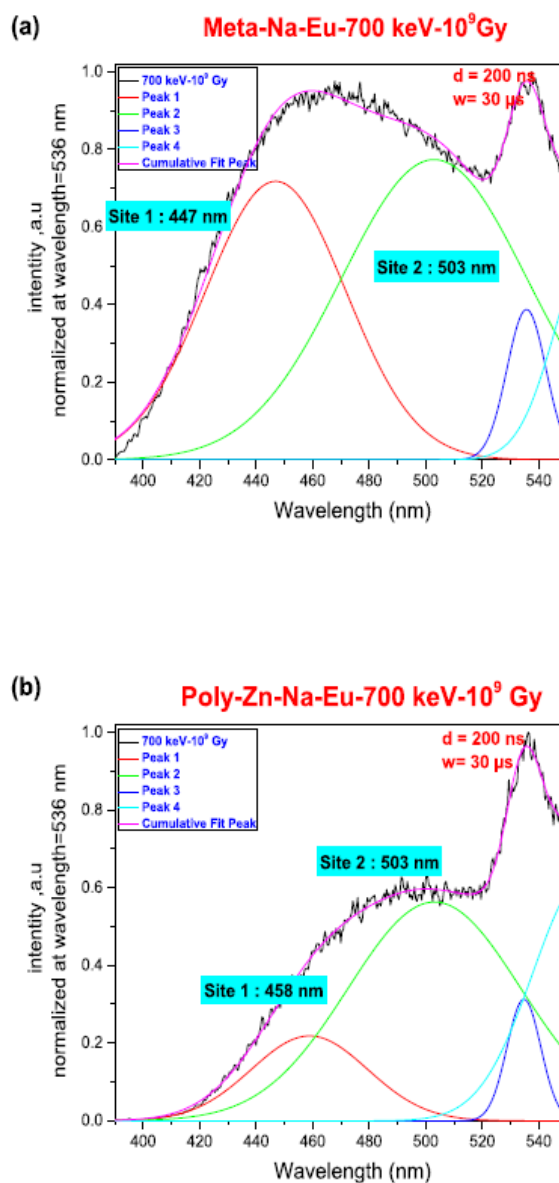


Fig. 3. A fit of the emission spectra of the Eu^{2+} ions in (a) Eu-doped metaphosphate glass (Meta-Na-Eu) and (b) Eu-doped polyphosphate glass (Poly-Zn-Na-Eu) after 700 keV electron irradiation at 10^9 Gy dose. Two components at near 450 and 500 nm in both glasses attesting the presence of 2 sites for Eu^{2+} ions.

amount of Eu^{2+} is formed under the high-symmetry site.

In Fig. 6, the intensity of $I_{g=6.3}$ signal corresponding to the low-symmetry Eu^{2+} site (Fig. 6a) and $I_{g=4.7}$ to the high-symmetry site (Fig. 6b) are reported for all glasses. It allows to compare the Eu^{3+} reduction efficiency between 2.5 MeV (empty symbols) and 700 keV (full symbols) at 10^8 Gy and 10^9 Gy doses. We observe a huge increase of the signal intensity under 700 keV irradiation compared to 2.5 MeV and the generation of Eu^{2+} ions is more important in polyphosphate than in metaphosphate compositions.

$I_{g=6.3}$ (corresponding to the low symmetry site) is increased from 1

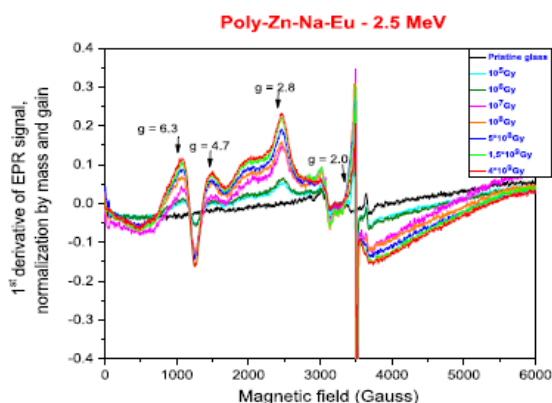


Fig. 4. EPR spectra normalized by mass and gain of Poly-Zn-Na-Eu glass irradiated by electron of 2.5 MeV at various doses.

(2.5 MeV at 10^9 Gy) to 16 (700 keV, 10^9 Gy) in Meta-Na-Eu while the intensity of high symmetry sites in the same conditions is multiplied by 20. In polyphosphate glasses, a larger amount of Eu^{2+} ions is produced under 700 keV compared to metaphosphate but the increase of Eu^{2+} reduced ions (expressed in percent) under both site symmetry shifting from 2.5 MeV to 700 keV energy is lower in Polyphosphate compared to Metaphosphate glasses. Thus, $I_{g=6.3}$ is multiplied by 8 from 700 keV to 2.5 MeV (at 10^9 Gy) (against 16 in Meta) and 11 for the signal at $g = 4.7$ (against 20 in Meta).

In addition, it is worth to notice that a mixed alkali effect occurs in Na/K polyphosphate glass for both energies 2.5 MeV and 700 keV, especially for the high symmetry site but also for the low symmetry site within 700 keV/ 10^9 Gy conditions. Actually, a non-linear variation (with either a maximum or a minimum) of Eu^{2+} amount can be observed in Fig. 6a and b.

Therefore, the mixed NaK zinc polyphosphate glass for the high-symmetry site exhibits the highest increase of Eu^{2+} amount from 2.5 MeV to 700 keV.

4. Discussion

The broad emission band around 450 nm occurring under irradiation can be attributed to the $4f^65d^1 \rightarrow 4f^7$ transition of Eu^{2+} ions. Actually, Eu^{2+} ions were detected in all irradiated phosphate glasses whatever the dose by EPR spectroscopy. Moreover, the lifetime of the blue emission band centered at 450 nm in different glasses displays a short lifetime from 150 ns (metaphosphate) to 2.76 μs (polyphosphate). These values are in agreement with literature examples reporting lifetimes of Eu^{2+} ions in glasses between 0.2 and 1.3 μs in fluoride phosphate glasses Ehrt et al. [16,17,24].

It can be deduced from photoluminescence (fit) and EPR experiments that two different sites of Eu^{2+} coexist in electron-irradiated phosphate glasses. The presence of two types of sites for divalent Eu^{2+} ions has already been mentioned in aluminoborosilicate [9,10], aluminosilicate [25], phosphate and fluoride-phosphate glasses [11,12]. These studies associate generally the high symmetry site ($g = 4.7$) to a strong crystal field that could correspond to 6-coordinated Eu^{2+} ions. The low-symmetry site ($g = 6.3$) with a lower crystal field would rather deal with Eu^{2+} ions with a higher coordination number into a modifier position. The shift of the $5d \rightarrow 4f$ emission band of Eu^{2+} to higher wavelengths in literature was attributed to an increase of crystal field or to a higher covalency [26]. We therefore assign the high symmetry site to the emission at 500 nm and the low-symmetry one to the emission at 450 nm. Nevertheless, there is no clear evidence from our spectroscopic measurements that (Eu^{3+}) ions occurred from a direct trapping

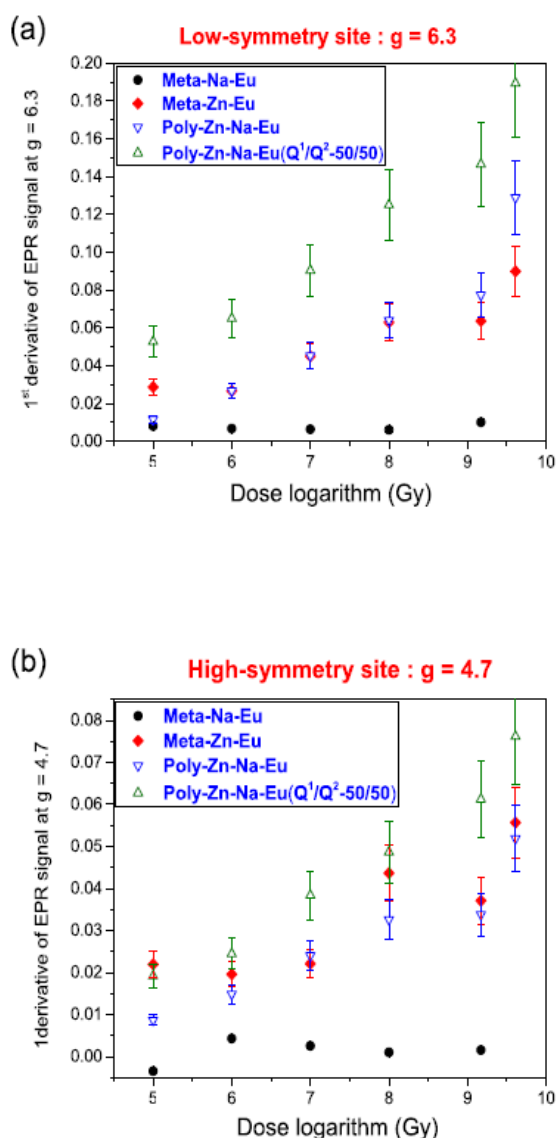


Fig. 5. Variation of the EPR signal intensity (a) $I_{g=6.3}$ and (b) $I_{g=4.7}$ attributed respectively to low and high site symmetry of Eu^{2+} ion in Meta-Na-Eu, Meta-Zn-Eu, Poly-Zn-Na-Eu and Poly-Zn-Na-Eu ($Q^1/Q^2=50/50$) glasses irradiated by 2.5 MeV at various doses: from 10^5 to over 10^9 Gy.

on two original Eu^{3+} sites already existing in the pristine glasses.

At first, it can be seen that the glass composition and the glass polymerization impact the nature of the Eu^{2+} sites. The ratio between both sites from one composition to another one can be extracted from EPR measurements. Table 2 reports the ratio between low-symmetry site and high-symmetry site for 4 glass compositions (700 keV, 10^9 Gy). It seems that the presence of Zn favors the formation of the high-symmetry site. Fig. 7 confirms the predominance of site 2 (500 nm) in polyphosphate by the red shift of the emission band. This result is supported by Table 2 where we can notice the huge intensity of the high symmetry site in polyphosphate compared to metaphosphate glasses (factor 7). This result is moreover in agreement with [26] based on the

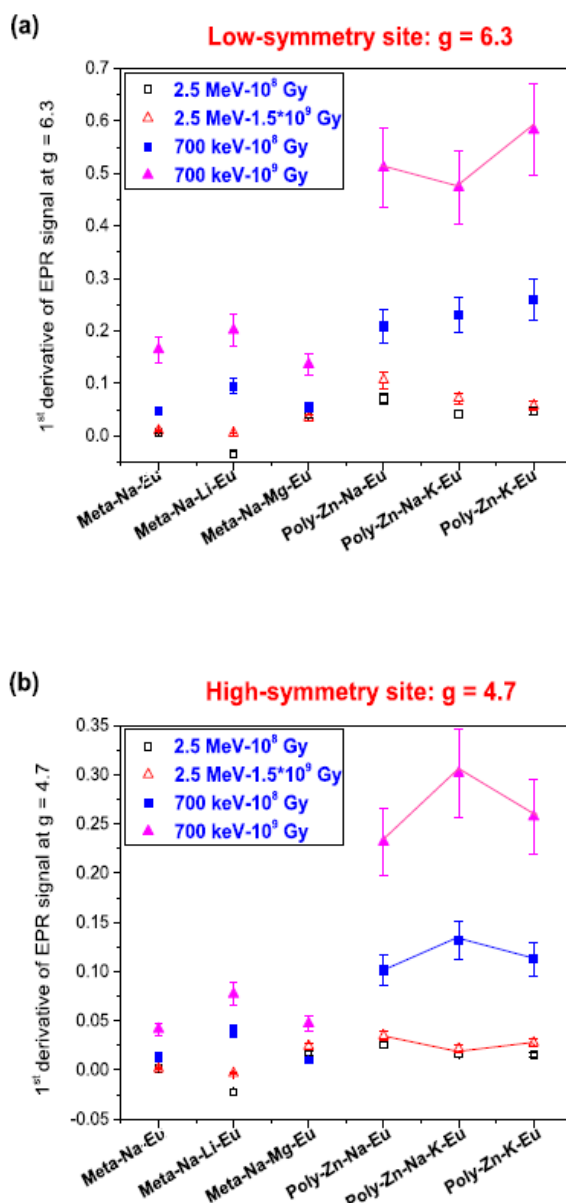


Fig. 6. Comparison between 2.5 MeV and 700 keV electron irradiation of the EPR signal intensity (a) $I_{g=6.3}$ and (b) $I_{g=4.7}$ attributed respectively to low and high symmetry site of Eu^{2+} ion in meta and polyphosphate glasses for 10^8 and 10^9 Gy doses.

Table 2

Ratio between low-symmetry site and high-symmetry site for different phosphate glasses irradiated by 700 keV at 10^9 Gy dose.

700 keV- 10^9 Gy				
	Low-symmetry site	High-symmetry site	Symmetry Ratio	ZnO (mol. %)
Meta-Na-Eu	0.16 ± 0.02	0.04 ± 0.01	3.92	–
Meta-Na-Mg-Eu	0.14 ± 0.02	0.05 ± 0.01	2.88	–
Poly-Zn-Na-Eu	0.51 ± 0.08	0.23 ± 0.03	2.20	49.40
Meta-Zn-Eu	0.08 ± 0.01	0.08 ± 0.01	1.06	46.00

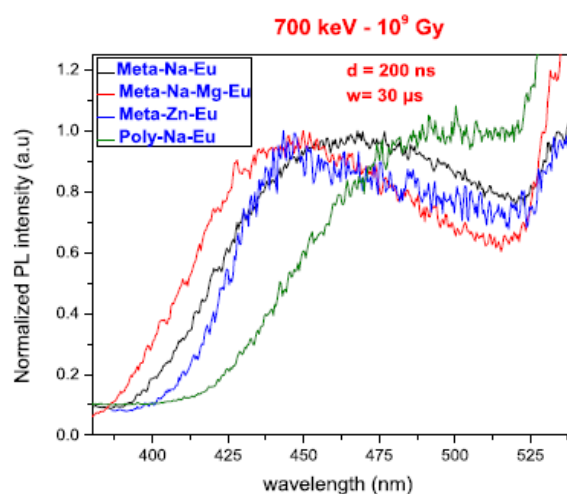


Fig. 7. The PL emission spectra of Eu-doped meta and polyphosphate glasses (Meta-Na-Eu, Meta-Na-Mg-Eu, Meta-Zn-Eu and Poly-Zn-Na-Eu) after 700 keV at dose 10^9 Gy. ($\lambda_{\text{exc}} = 355$).

fact that polyphosphate contain more NBO than metaphosphate glasses.

However, a direct comparison of the ratio between high and low symmetry sites obtained from EPR and PL is delicate. Indeed, PL method cannot deliver absolute quantitative ratio due to two main effects: first, the photobleaching occurring under the 355 nm laser excitation inducing a decrease of the Eu^{2+} emission intensity and secondly, a mismatching between PL and EPR measurements could be due to the interaction between Eu^{2+} and other luminescent species occurring under irradiation. Additional emission bands in the 400–600 nm region were detected like the emission of diamagnetic P-defects at 410 nm [27]. This band was observed in NaMg metaphosphate glasses [28] and Na metaphosphate. The P-defect emission band in presence of Zn is not visible anymore but a new band at 435 nm (see Fig. 1b) appears after irradiation. To the best of our knowledge, such an emission band was never reported yet in irradiated phosphate glasses but we deduced that it is directly correlated to the presence of Zn. Therefore it could be attributed to unusual Zn oxidation state like Zn^+ or to $(\text{Zn}^{2+})^- \text{EC}$. Ag = 1.99 EPR component in Zn metaphosphate glass was tentatively attributed to $(\text{Zn}^{2+})^- \text{EC}$ [29].

Zn doping gets a strong positive effect on the reduction efficiency of Eu^{3+} as it can be seen in Fig. 4. Indeed, the comparison between the Eu^{2+} amount produced in metaZn and metaNa (up to a factor 9) supports this result. The proportion of high symmetry site is increased by increasing the amount of Zn as attested by Table 2. This result could be explained by the fact that Zn^{2+} favors the insertion of sixfold coordinated Eu^{3+} ions in the system. Indeed, Eu^{3+} ions can be involved in the charge compensation of Zn^{2+} under tetrahedral environment [30].

If we compare now the emission shape of Eu^{2+} in Poly-Zn-Na-Eu, Poly-Zn-K-Eu and Poly-Zn-Na-K-Eu (not shown), there is clearly no impact here of the alkali type on the $5d \rightarrow 4f$ transition position contrary

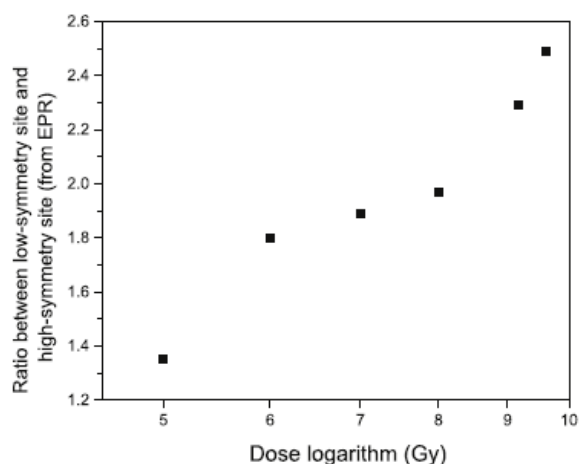


Fig. 8. The ratio between Eu^{2+} low-symmetry site and high-symmetry site for Poly-Zn-Na-Eu glass under 2.5 MeV irradiations as a function of dose logarithm.

to what was described by Cicconi et al. in Ref. [31] where the emission band shifts from 422 to 470 nm passing from Na to K. It can be noticed however that glasses in Ref. [31] were metaphosphate glasses and Eu^{2+} ions were reduced during the glass synthesis.

At 2.5 MeV, it seems that there is no dose effect on the ratio between site 1 and site 2. The existence of a “plateau” displayed in Fig. 8 supports this result as well as the stable shape of the photoluminescence spectra in 10^6 – 10^8 Gy range shown in Fig. 1. When dose becomes higher than 10^9 Gy, we can observe an increase of the ratio between both sites indicating a clear predominance of modifier sites on network modifier sites. We know from Ref. [32] that some alkali motion are involved in 2.5 MeV electron irradiated glasses when dose is higher $> 10^9$ Gy. In phosphate glasses, Raman spectra of polyphosphate glasses showed some depolymerization effects for doses $> 10^9$ Gy [28]. This network modification could induce a higher production of low-symmetry sites for Eu^{2+} ions. This hypothesis is supported by the nature of the low-symmetry site expected as “a modifier” site. The increase of the number of NBO under irradiation is in agreement with this scenario. The deviation from a linear behaviour visible in Fig. 4 was furthermore already observed for similar doses ($> 10^9$ Gy) in aluminoborosilicate glass [15].

From Fig. 5, by comparing same integrated dose, it is obvious to notice that 700 keV energy is much more efficient to reduce Eu^{3+} ions than 2.5 MeV. We observe in addition a real dependence on the alkali type in polyphosphate on the reduction efficiency at 700 keV and in particular the Na/Li metaphosphate and Na/K polyphosphate compositions exhibits a maximum of Eu^{2+} . It means that the reduction of Eu^{3+} ions (specially for the high symmetry site) is probably associated to a rearrangement of the Eu^{3+} initial site including the alkaline ions and O migration in the glass network. This result let us suspect that a direct reduction process for 2 Eu^{3+} preexisting sites is probably not the right scenario but one type of Eu^{2+} ions could be generated after modification of the Eu^{3+} environment.

We know that transport of alkaline ions is the dominant mechanism in low energy electron (typ. 50 keV) irradiated glasses with the creation of channels [33]. At 700 keV due to the thickness of the sample (larger than the penetration depth of the electrons), we expect also that migration of alkaline ions under the electrical field generated is effective. This difference with 2.5 MeV could explain the larger efficiency to reduce Eu^{3+} with low energy electrons and the ability of polyphosphate with a more depolymerized network compared to metaphosphate compositions to incorporate Eu^{2+} ions.

5. Conclusion

We demonstrated the high efficiency of electron irradiation to produce divalent Eu^{2+} in meta and polyphosphate ions under two types of sites. It is exacerbated under 700 keV at 10^9 Gy doses where alkaline motion is important. Moreover, the nature of the glass and the presence of Zn in the structure favors one type of site: the low symmetry sites Eu^{2+} into modifier position.

Declaration of competing interest

The authors declare that they have no known competing financial interests or personal relationships that could have appeared to influence the work reported in this paper.

Acknowledgments

We thank EMIR program for access to SIRIUS and we appreciate O. Cavani for running electron irradiation at Ecole Polytechnique (LSI, SIRIUS, France). This work is supported by “Investissements d’Avenir LabEx PALM (ANR-10-LABX-0039-PALM). As well, we thank G. Mountjoy for fruitful discussions of the results.

References

- [1] T. Deschamps, N. Ollier, H. Vezin, C. Gonnet, Clusters dissolution of Yb^{3+} in co-doped SiO_2 - Al_2O_3 - P_2O_5 glass fiber and its relevance to photodarkening, *J. Chem. Phys.* 136 (2012) 014503.
- [2] T.I. Suratwala, R.A. Steele, G.D. Wilke, J.H. Campbell, K. Takeuchi, Effects of OH content, water vapor pressure, and temperature on sub-critical crack growth in phosphate glass, *J. Non-Cryst. Solids* 263 (2000) 213–227.
- [3] J.H. Campbell, T.I. Suratwala, Nd-doped phosphate glasses for high-energy/high-peak-power lasers, *J. Non-Cryst. Solids* 263 (2000) 318–341.
- [4] C. Yamanaka, Y. Kato, Y. Izawa, K. Yoshida, T. Yamanaka, T. Sasaki, M. Nakatsuka, T. Mochizuki, J. Kuroda, S. Nakai, Nd-doped phosphate glass laser systems for laser-fusion research, *IEEE J. Quantum Electron.* 17 (1981) 1639–1649.
- [5] L. Canioni, M. Bellec, A. Royon, B. Bousquet, T. Cardinal, Three-dimensional optical data storage using third-harmonic generation in silver zinc phosphate glass, *Opt. Lett.* 33 (2008) 360–362.
- [6] J.C. Knowles, Phosphate based glasses for biomedical applications, *J. Mater. Chem.* 13 (2003) 2395–2401.
- [7] I. Ahmed, M. Lewis, I. Olsen, J.C. Knowles, Phosphate glasses for tissue engineering: Part 1. Processing and characterisation of a ternary-based P2O5-CaO-Na2O glass system, *Biomaterials* 25 (2004) 491–499.
- [8] B.C. Sales, L.A. Boatner, Lead-iron phosphate glass: a stable storage medium for high-level nuclear waste, *Science* 226 (1984) 45–48.
- [9] M.I. Ojovan, O.G. Balyukhova, Glasses for Nuclear Waste Immobilization, *WM*, 7 (2007), p. 15.
- [10] M. Soltys, J. Janek, L. Zur, J. Pisarska, W.A. Pisarski, Compositional-dependent europium-doped lead phosphate glasses and their spectroscopic properties, *Opt. Mater.* 40 (2015) 91–96.
- [11] M. Walas, A. Pastwa, T. Lewandowski, A. Synak, I. Gryczyński, W. Sadowski, B. Kościelna, Luminescent properties of Ln^{3+} doped tellurite glasses containing AlF_3 , *Opt. Mater.* 59 (2016) 70–75.
- [12] N.T. Thanh, V.X. Quang, V.P. Tuyen, N.V. Tam, T. Hayakawa, B.T. Huy, Role of charge transfer state and host matrix in Eu^{3+} -doped alkali and earth alkali fluoro-aluminoborate glasses, *Opt. Mater.* 34 (2012) 1477–1481.
- [13] H. Bouchouicha, G. Panczer, D. de Ligny, Y. Guyot, R. Ternane, Luminescent properties of Eu-doped calcium aluminosilicate glass-ceramics: a potential tunable luminophore, *Opt. Mater.* 85 (2018) 41–47.
- [14] S. Mognaud, M. Tribet, J.-P. Renault, P. Jollivet, G. Panczer, T. Charpentier, C. Jégou, Effect of low dose electron beam irradiation on the alteration layer formed during nuclear glass leaching, *J. Nucl. Mater.* 482 (2016) 53–62.
- [15] E. Makhukova, B. Boizot, Reduction of Eu^{3+} to Eu^{2+} in aluminoborosilicate glasses under ionizing radiation, *Mater. Res. Bull.* 45 (2010) 1299–1303.
- [16] H. Ebendorff-Heidepriem, D. Ehrhart, Ultraviolet laser and x-ray induced valence changes and defect formation in europium and terbium doped glasses, *Physics and Chemistry of Glasses Proc. XIX Int. Congr. Glass, Edinburgh*, vol. 43, 2002, p. 10.
- [17] H. Ebendorff-Heidepriem, D. Ehrhart, Effect of europium ions on X-ray-induced defect formation in phosphate containing glasses, *Opt. Mater.* 19 (2002) 351–363.
- [18] H. You, M. Nogami, Optical properties and valence change of europium ions in a $\text{Sol-Gel Al}_2\text{O}_3$ - B_2O_3 - SiO_2 glass by femtosecond laser pulses, *J. Phys. Chem. B* 109 (2005) 13980–13984.
- [19] K.-S. Lim, S. Lee, M.-T. Trinh, S.-H. Kim, M. Lee, D.S. Hamilton, G.N. Gibson, Femtosecond laser-induced reduction in Eu-doped sodium borate glasses, *J. Lumin.* 122–123 (2007) 14–16.
- [20] J. Qiu, K. Kojima, K. Miura, T. Mitsuoyu, K. Himo, Infrared femtosecond laser pulse-induced permanent reduction of Eu^{3+} to Eu^{2+} in a fluorozirconate glass, *Opt.*

- Lett. 24 (1999) 786.
- [21] H. Rahimian, H. Mokhtari, S.P. Shirmardi, Improvement of Eu^{3+} emissions in oxyfluoride glass and nano glass-ceramic by electron beam irradiation, *J. Lumin.* 187 (2017) 535–539.
- [22] M. Mohapatra, R.M. Kadam, R.K. Mishra, C.P. Kaushik, B.S. Tomar, S.V. Godbole, Gamma radiation induced changes in nuclear waste glass containing Eu, *Phys. B Condens. Matter* 406 (2011) 3980–3984.
- [23] J. de Bonfils, G. Panczer, D. de Ligny, S. Peugot, B. Champagnon, Behaviour of simplified nuclear waste glasses under gold ions implantation: a microluminescence study, *J. Nucl. Mater.* 362 (2007) 480–484.
- [24] D. Ehrhart, REVIEW: phosphate and fluoride phosphate optical glasses — properties, structure and applications, *Physics and Chemistry of Glasses, Eur. J. Glass Sci. Technol. B* 56 (2015) 217–234.
- [25] M. Nogami, T. Yamazaki, Y. Abe, Fluorescence properties of Eu^{3+} and Eu^{2+} in $\text{Al}_2\text{O}_3\text{-SiO}_2$ glass, *J. Lumin.* 78 (1998) 63–68.
- [26] H. Ebendorff-Heidepriem, D. Ehrhart, Formation and UV absorption of cerium, europium and terbium ions in different valencies in glasses, *Opt. Mater.* (2000) 19.
- [27] A.N. Trukhin, A. Antuzevics, K. Golant, D.L. Griscom, Luminescence of phosphorus doped silica glass, *J. Non-Cryst. Solids* 462 (2017) 10–16.
- [28] V. Pukhkaya, Influence of Yb^{3+} and Er^{3+} Ions Environment on the Evolution of its Luminescent Properties in Oxide Glasses under Ionizing Irradiation, PhD Thesis Ecole Polytechnique X, 2013.
- [29] P. Ebeling, D. Ehrhart, M. Friedrich, Influence of modifier cations on the radiation-induced effects of metaphosphate glasses, *Glass Sci. Technol.* 76 (2003) 56–61.
- [30] U. Hoppe, G. Walter, G. Carl, J. Neufeind, A.C. Hannon, Structure of zinc phosphate glasses probed by neutron and X-ray diffraction of high resolving power and by reverse Monte Carlo simulations, *J. Non-Cryst. Solids* 351 (2005) 1020–1031.
- [31] M.R. Cicconi, A. Veber, D. de Ligny, J. Rocherullé, R. Lebullenger, F. Tessier, Chemical tunability of europium emission in phosphate glasses, *J. Lumin.* 183 (2017) 53–61.
- [32] B. Boizot, N. Ollier, F. Olivier, G. Petite, D. Ghaleb, E. Makhukova, Irradiation effects in simplified nuclear waste glasses, *Nucl. Instrum. Methods Phys. Res. Sect. B Beam Interact. Mater. Atoms* 240 (2005) 146–151.
- [33] O. Gedeon, J. Zemek, K. Jurek, Changes in alkali-silicate glasses induced with electron irradiation, *J. Non-Cryst. Solids* 354 (2008) 1169–1171.

Titre : Modification de l'environnement de l'ion Eu^{3+} dans des verres métaphosphates et polyphosphates par irradiation aux électrons et laser femtoseconde

Mots clés : Europium, verre phosphate, Irradiation par électron, Laser femtoseconde, Simulation de dynamique moléculaire

Résumé : Les verres phosphates dopés terres rares (TR) sont des matériaux attractifs en optique en raison de leur basse température de transition vitreuse et de leur grande capacité à dissoudre les ions de terres rares par rapport aux verres silicates. Dans ce travail, nous sommes intéressés à comprendre les mécanismes conduisant à la modification structurale des verres polyphosphates de zinc et métaphosphates sous irradiation avec pour finalité de contrôler l'environnement des ions terres rares (ions Eu^{3+} en particulier) par l'irradiation. Nous avons comparé les effets obtenus sous irradiations aux électrons et par laser fs en faisant varier la dose et l'énergie des électrons (700 keV et 2.5 MeV), le taux de répétition du laser ainsi que les compositions de verre qui comportent différents

ions alcalins et alcalino-terreux (Na, Li, K et Mg) et teneurs en Zn. Nous avons mis en évidence la diminution de la symétrie du site Eu^{3+} , l'augmentation de la dispersion des sites ainsi qu'une réduction efficace des ions Eu^{3+} en Eu^{2+} sous irradiation électronique.

La présence de Zn atténue la variation de l'ordre local autour de la terre rare, alors que le réseau vitreux est moins stable sous irradiation. La formation d'ion Eu^{2+} (sous deux types d'environnement de haute et basse symétries est par ailleurs accrue en présence de Zn et en utilisant des électrons de 700 keV. Le laser femtoseconde à 10 KHz engendre une cristallisation des verres métaphosphates sans réduction des ions Eu^{3+} .

Title: Eu^{3+} ion environment modification by Electron and femtosecond laser irradiation in metaphosphate and polyphosphate glasses

Keywords : Europium, Phosphate glasses, Electron irradiation, femtosecond laser, Molecular Dynamics simulation

Abstract: Rare Earth (RE) doped phosphate glasses are attractive materials in optic due to their low glass transition temperature and their high ability to dissolve rare earth ions compared to silicate glasses. In this work, we are interested in understanding the mechanisms leading to the structural modification of zinc polyphosphate and metaphosphate glasses under irradiation with the aim of controlling the environment of rare earth ions (in particular Eu^{3+} ions) by irradiation. We compared the effects obtained under electron and femtosecond laser irradiation by varying the dose and electron energy (700 keV and 2.5 MeV), the laser repetition rate as well as the glass compositions that contain

different alkaline and alkaline earth ions (Na, Li, K and Mg) and Zn contents. We have demonstrated the decrease of the Eu^{3+} site symmetry, the increase of the sites dispersion as well as an effective reduction of Eu^{3+} to Eu^{2+} under electron irradiation. The presence of Zn attenuates the variation of the local order around the rare earth, while the vitreous network is less stable under irradiation. The formation of Eu^{2+} ions (under two types of high and low symmetry environments) is further enhanced in the presence of Zn and using 700 keV electrons. The femtosecond laser at 10 KHz gives causes crystallization of metaphosphate glasses without reduction of Eu^{3+} ions.